Faculty of Physics
Institute of Theoretical Physics

Indirect searches for the Standard Model extensions

Doctoral dissertation
In the field of Exact and Natural Sciences
In the discipline of Physical Sciences

Michał Ryczkowski

Written under the supervision of
Prof. dr hab. Janusz Rosiek
University of Warsaw, Faculty of Physics
Institute of Theoretical Physics

Warsaw, January 2025

Acknowledgments

This thesis is the result of more than four years of study and research conducted by its author (and his collaborators) as a PhD student at the Faculty of Physics, University of Warsaw. Counting my B.Sc. and M.Sc. studies, my journey in physics has lasted over ten year and continues to this day. During this time, I have continuously learned and grown, deepening my interest and fascination with physics each day.

Completion of this thesis would not have been possible without the help, guidance, and support of many people from the University of Warsaw. First and foremost, I am deeply grateful to my B.Sc., M.Sc. and Ph.D. supervisor, Prof. Janusz Rosiek, who has been an invaluable mentor throughout these years. I also wish to extend my gratitude to Prof. Stefan Pokorski and Prof. Marek Olechowski for their invaluable help and fruitful collaboration. I wish to further acknowledge the Cosmo UW Group — attending the meetings and discussions with its members has been a very valuable experience for me. I would also like to thank everyone associated with the Faculty of Physics, particularly those in the Institute of Theoretical Physics, whose hard work enables people like me to pursue research aligned with my deepest interests. Last but not least, I want to mention the RL Study Group. Beginning with our B.Sc. studies, over the years we have grown into a close group of friends sharing common interests and passions, engaging in endless discussions on topics closest to our hearts. You made this entire journey worthwhile.

Not less importantly, I am deeply grateful to my collaborators from the University of Ioannina, a beautiful place I was fortunate to visit numerous times over the years. My sincere thanks to Prof. Athanasios Dedes, Dr. Christos Suxho, and to my friends Dr. Lampros Trifyllis and Kostas Mantzaropoulos, and to for their collaboration, inspiring discussions, and warm hospitality.

Finally, I would like to thank the people closest to me — my family — for their constant love, support, and understanding. To my parents: Irena and Andrzej, my sister Ania, my grandparents Józefa, Alina, Antoni and Emil, and my love, my life partner, and my best friend — Zuzia: I am forever grateful. I would have never achieved any of this without you. Among other people who have shown their interest and support over the years, I want to mention the one and only FCN team, and my friends from the magnificent Mysiadło city — thank you all!

My Ph.D. studies, apart from the fellowship from the Doctoral School of Exact and Natural Sciences at the University of Warsaw, were partially funded by Narodowe Centrum Nauki under the grant DEC2019/35/B/ST2/02008.

Abstract

In this doctoral thesis, we investigate the effects of the experimental bounds (derived from the precision measurements of processes involving the Standard Model fields) and the theoretical constraints (arising from the consistency requirements of the considered model) on the prospects for indirect searches for physics beyond the Standard Model (BSM). This program can be realized within two distinct but complementary methods: the bottom-up and top-down approaches. The bottom-up approach focuses on studying discrepancies between experimental results and the Standard Model (SM) predictions without assuming the form of the underlying theory. With the lack of direct discoveries of new particles in our accelerator experiments and with the Large Hadron Collider (LHC) reaching its energy limit, this approach is becoming increasingly common for uncovering physics BSM. Conversely, the top-down approach is based on the specific Standard Model extensions proposed to address one or more of its shortcomings. In this work, we present three distinct, but complementary examples of studies based on these two approaches, providing a broader perspective on some current areas of interest in the field of particle physics. We first present two project that follow the bottom-up approach to searches for BSM physics. The first project, "`SmeftFR` v3 – Feynman rules generator for the Standard Model Effective Field Theory", resulted in a numerical tool designed for calculations in the Standard Model Effective Field Theory (SMEFT). The SMEFT allows the parametrization of BSM physics by higher-dimensional operators constructed from the SM fields, enabling the study of BSM phenomena in a model-independent way. Although very useful, the SMEFT is also a highly complicated framework, and tools like this one prove indispensable for efficient calculations. The second study, "Double Higgs boson production via vector-boson fusion (VBF) in SMEFT next-to-leading order (NLO) in the EFT expansion", provides a detailed calculation (with the use of the `SmeftFR` v3 package described in the previous chapter) of a specific process including effects of dimension-6 and dimension-8 bosonic operators. As a result, we obtain estimates of the maximal potential enhancement of this process within the SMEFT framework for the High Luminosity LHC (HL-LHC) accelerator experiment. The third and final study, "Vector-like fermions, real scalar and Higgs boson phenomenology", is a representative example of a top-down approach to new physics searches. Assuming specific BSM particle content — vector-like fermions (VLF) and a real scalar singlet — we work out theoretical constraints on the model parameters and calculate the possible impact of these BSM particles on the process of double Higgs boson production via gluon fusion, on electroweak precision observables, the electroweak phase transition and gauge couplings unification. Additionally, we presented a procedure of matching between the SMEFT and the considered VLF and scalar extensions, providing a bridge between the two approaches. While all three of these research projects serve as representative examples of high-standard research projects, their combination highlights and emphasizes indirect searches for BSM physics as a promising approach to new physics searches.

Streszczenie

W niniejszej rozprawie doktorskiej badamy wpływ ograniczeń eksperymentalnych (wynikających z pomiarów precyzyjnych procesów z udziałem pól modelu standardowego) oraz ograniczeń teoretycznych (wynikających z wymogów spójności rozważanego modelu) na perspektywy pośrednich poszukiwań fizyki spoza modelu standardowego. Ten program może to być realizowany w ramach dwóch różnych, ale komplementarnych podejść: oddolnego (ang. bottom-up) i odgórnego (ang. top-down). Podejście oddolne polega na badaniu różnic między danymi eksperymentalnymi a przewidywaniami modelu standardowego (SM), bez zakładania konkretnej formy bardziej fundamentalnej teorii. W obliczu braku bezpośrednich odkryć nowych cząstek w eksperymentach akceleratorowych oraz przy Wielkim Zderzaczu Hadronów (LHC) osiągającym swój limit energii, to podejście staje się coraz powszechniejsze przy poszukiwaniach nowej fizyki. Z kolei podejście odgórne opiera się na analizie konkretnych rozszerzeń modelu standardowego zaproponowanych w celu zaadresowania jednego lub wielu jego ograniczeń. W tej pracy prezentujemy trzy odrębne, ale uzupełniające się przykłady badań opartych na tych podejściach, oferujące szerszą perspektywę na niektóre z aktualnych obszarów zainteresowań w dziedzinie fizyki cząstek elementarnych. Na początek, prezentujemy dwa projekty podążające podejściem "oddolnym" w poszukiwaniach fizyki BSM. Wynikiem pracy nad pierwszym z nich, "`SmeftFR` v3 – generator reguł Feynmana dla efektywnego rozszerzenia modelu standardowego", jest narzędzie numeryczne zaprojektowane do obliczeń w efektywnym rozszerzeniu modelu standardowego (SMEFT). SMEFT pozwala na parametryzację fizyki BSM za pomocą operatorów wyższych wymiarów skonstruowanych z pól modelu standardowego (SM), dzięki czemu możliwe jest badanie fizyki BSM w sposób niezależny od konkretnego modelu. Choć bardzo użyteczny, SMEFT charakteryzuje się wysokim poziomem skomplikowania i tego rodzaju narzędzia okazują się niezbędne do efektywnych obliczeń w ramach SMEFT. Drugi projekt, "Produkcja pary bozonów Higgsa poprzez fuzję bozonów wektorowych (VBF) z uwzględnieniem wyższych wyrazów rozwinięcia (NLO) w SMEFT", prezentuje szczegółowe obliczenia (wykorzystując opisany wcześniej pakiet `SmeftFR` v3) dotyczące konkretnego procesu uwzględniając efekty operatorów bozonowych wyższych rzędów: wymiaru-6 i wymiaru-8. Jako wynik otrzymaliśmy oszacowanie maksymalnego wzmocnienia tego procesu w ramach SMEFT dla przyszłego eksperymentu akceleratorowego High Luminosity LHC (HL-LHC). Trzeci projekt badawczy, "Fermiony wektorowe, rzeczywisty skalar i fenomenologia bozonu Higgsa", jest reprezentatywnym przykładem podejścia "odgórnego" do poszukiwań nowej fizyki. Zakładając konkretny skład cząstek BSM — fermiony wektorowe (VLF) i rzeczywisty skalar — zdefiniowaliśmy teoretyczne ograniczenia dla parametrów tych modeli i oszacowaliśmy ich możliwy wpływ na proces produkcji pary bozonów Higgsa w fuzji gluonowej, na pomiary precyzyjnych obserwabli elektrosłabych, elektrosłabego przejścia fazowego oraz unifikacji stałych sprzężenia. Dodatkowo zaprezentowaliśmy przykład dopasowania (ang. matching) ze sobą SMEFT i rozważanych rozszerzeń modelu standardowego poprzez VLF i rzeczywisty skalar, zapewniając pomost między dwoma podejściami. Chociaż wszystkie trzy projekty badawcze osobno stanowią wartościowe przykłady jakościowych badań w fizyce wysokich energii, ich połączenie ujawnia i podkreśla pośrednie poszukiwania jako obiecujące podejście do poszukiwania nowej fizyki.

Contents

Chapter 1

Introduction

The question of the nature of reality has always drawn the attention of humanity and can be traced back thousands of years through the domains of religion and philosophy. Efforts to understand the basic rules governing our world led to a revolution that introduced a more systematic and rigorous approach to studying the fundamental laws of nature. This approach, rooted in observation and experiment, now known as the **scientific method**, revolutionized our understanding of fundamental principles and uncovered the laws governing the universe.

At the heart of these rapid developments lies the field of particle physics. Its most accurate description of elementary forces and particles, known as the **Standard Model** (SM), is one of humanity's greatest intellectual achievements. Despite its remarkable successes, the Standard Model falls short in explaining a range of phenomena — from the origin and composition of dark matter and dark energy, through the absence of a proper description of gravity, to the lack of a proper explanation of matter-antimatter asymmetry. Significant effort has been dedicated to provide an explanation of these phenomena by extending the Standard Model itself, with physicist all around the world trying to answer the question: *What lays beyond the Standard Model?* Unfortunately, no one has succeeded to this day.

This thesis provides a comprehensive overview of some main directions in contemporary particle physics. With the lack of direct discovery of new particles in current accelerator experiments, and with the Large Hadron Collider (LHC) reaching its energy limit, we focus mainly on the **indirect** approach to searches for new physics. This approach examines discrepancies between Standard Model predictions and precise experimental measurements, which may hint at the form of underlying, more fundamental theory. Researchers pursuing this method usually adopt one of the two strategies: the **bottom-up** or **top-down** approach. The former utilizes a model-independent approach to the new physics searches, while the latter assumes a specific form of model extending the SM, which modifies its predictions. This work presents representative examples of both methods: the bottom-up approach is demonstrated with the **Standard Model Effective Field Theory** (SMEFT) framework, which parametrizes heavy BSM physics through higher-dimensional operators constructed from SM fields in a model-independent way, while the top-down approach is presented through a beyond the Standard Model (BSM) scenario containing **vector-like fermions** (VLF) and a **real scalar singlet**.

This work is structured as follows. Chapter 1 - "Introduction" — sets the stage: Section 1.1 contains notations and conventions relevant to this work; Section 1.2 provides a broad overview of the current state of particle physics, including its main achievements and challenges; and Section 1.3 outlines strategies for searches for physics BSM. The main body of this thesis, titled "Three cases of indirect

searches for the Standard Model extensions", is presented in the subsequent three chapters. Chapters 2 and 3 present studies utilizing the bottom-up approach. The former is an example of numerical tool development: "`SmeftFR` v3 – Feynman rules generator for the Standard Model Effective Field Theory", while the latter focuses on the study of specific high-energy physics (HEP) process: "Double Higgs production via vector-boson fusion at next-to-leading order in SMEFT". Finally, Chapter 4, titled "Vector-like fermions, real scalar, and Higgs boson phenomenology", summarizes the top-down study, which evaluates the impact of a specific BSM model containing vector-like fermions and real scalar on chosen phenomena.

1.1 Notations and conventions

In this thesis, we use the notations for the metric tensor, position, and momentum four vectors in accordance with the standard textbooks (see e.g., [1–3]):

$$\begin{aligned} x^\mu &= (t, x^1, x^2, x^3) \equiv (t, \bar{x}), \\ p^\mu &= (E, p^1, p^2, p^3) \equiv (E, \bar{p}), \\ p^\mu &= i\frac{\partial}{\partial x^\mu} \equiv i\partial^\mu, \quad \bar{p} = -i\frac{\partial}{\partial \bar{x}}, \\ g^{\mu\nu} &= \mathrm{diag}(1, -1, -1, -1), \end{aligned} \tag{1.1}$$

which gives (Einstein's summation convention assumed):

$$p^2 = p^\mu p_\mu = E^2 - \bar{p}^2 = m^2 \geq 0. \tag{1.2}$$

Moreover, we set the fundamental constants as:

$$\begin{aligned} \text{speed of light:} \quad & c = 2.998 \times 10^8 \frac{\mathrm{m}}{\mathrm{s}} \equiv 1, \\ \text{Planck's constant:} \quad & \hbar = \frac{h}{2\pi} = 1.055 \times 10^{-34} \mathrm{J} \times \mathrm{s} \equiv 1. \end{aligned} \tag{1.3}$$

This leads to the assignment of mass (or energy) dimension to all considered quantities. For example:

$$\begin{aligned} [x] = [t] &= \mathrm{GeV}^{-1} \equiv -1, \\ [p] = [E] &= \mathrm{GeV} \equiv 1. \end{aligned} \tag{1.4}$$

Moreover, since the fundamental functional, action S, must be dimensionless quantity, we determine the mass dimension of the Lagrangian:

$$S = \int \mathcal{L} dx^4, \quad [S] = 0, \quad [dx^4] = -4, \quad [\mathcal{L}] = 4. \tag{1.5}$$

and the assignment of mass (or energy) dimensions to the fundamental fields:

$$\begin{aligned} &\text{scalar field:} \quad [\varphi] = 1, \\ &\text{vector field:} \quad [A^\mu] = 1, \\ &\text{fermion field:} \quad [\psi] = 3/2. \end{aligned} \tag{1.6}$$

The 4×4 gamma-matrices in Dirac representation are defined by the anticommutation relation:

$$\{\gamma^\mu, \gamma^\nu\} = 2g^{\mu\nu}, \quad \gamma^\mu = \{\gamma^0, \gamma^1, \gamma^2, \gamma^3\}, \tag{1.7}$$

with the following relations and definitions:

$$\begin{aligned} &\text{commutation relation:} \quad \sigma^{\mu\nu} = \frac{i}{2}\left[\gamma^{\mu}, \gamma^{\nu}\right], \\ &\gamma^5 \text{ matrix:} \quad \gamma^5 = i\gamma^0\gamma^1\gamma^2\gamma^3, \quad \left\{\gamma^5, \gamma^{\nu}\right\} = 0, \\ &\text{slash notation:} \quad \not{a} = a^{\mu}\gamma_{\mu}. \end{aligned} \tag{1.8}$$

1.2 Current state of particle physics

This section provides a general overview of particle physics as we understand it today. We begin with the most successful description of fundamental particles and interactions to date: the Standard Model. Developed and gradually verified over much of the XXth century, it was finally confirmed with the discovery of the Higgs boson in 2012 [4, 5]. Despite its tremendous success in explaining an incredibly wide range of phenomena, the Standard Model has many shortcomings in explaining other, which are discussed in the latter part of this section.

1.2.1 The Standard Model

General overview and a bit of history

The Standard Model of Elementary Particles is a gauge theory formulated in terms of fundamental quantum fields. Excitations of these fundamental entities are interpreted as particles that constitute the structure of our universe: fermions, which make up the visible matter content; gauge bosons, which mediate three of the four known fundamental interactions (electromagnetic, weak, and strong); and the Higgs boson, which is responsible for giving mass to other particles through the mechanism of spontaneous symmetry breaking. A brief graphical overview of this description is presented in Figure 1.1.

The beginning of the modern formulation of what we now call the Standard Model can be traced back to the first half of the XXth century, with the gradual development of quantum mechanics, quantum field theory and parallel discoveries of a plethora of new particles. Among the most important milestones leading to the final formulation of the SM, one can list:

- **Dirac equation** – introduced by Paul Dirac in 1928, it successfully combined quantum mechanics and special relativity, and predicted the existence of anti-particles.
- **Quantum Electrodynamics (QED)** – the first comprehensive quantum field theory, introduced in 1949 by Richard Feynman, Julian Schwinger, and Sin-Itiro Tomonaga, established the description of electromagnetic interactions through *gauge theory*.
- **Non-abelian gauge theories** – introduced by Chen-Ning Yang and Robert Mills in 1954, laying the groundwork for the future description of strong and weak interactions.
- **Electroweak theory** – developed by Sheldon Glashow in 1961, it unifies electromagnetic and weak interactions. Later expanded in 1967 to its modern form through the contributions of Abdus Salam and Steven Weinberg, who incorporated the **Higgs mechanism** — developed by François Englert, Robert Brout, Peter Higgs, Gerald Guralnik, C. R. Hagen, and Tom Kibble in 1964.

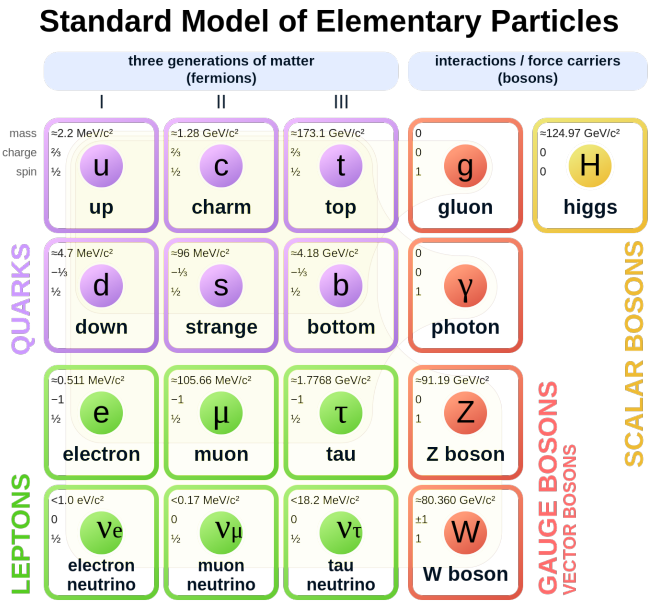

Figure 1.1: Particle content of the Standard Model.

- **Theory of quarks** – proposed in 1964 by Murray Gell-Mann and George Zweig, who introduced quarks as fundamental constituents of hadrons, such as protons and neutrons, later expanded by Oscar W. Greenberg who introduced the concept of color charge.

- **Quantum Chromodynamics (QCD)** – a non-abelian gauge theory describing the strong interactions that governs the behavior of quarks and gluons. Its final formulation from around 1973/74 builds on the work on the theory of quarks (Gell-Mann, Zweig, Greenberg); the work of William Bardeen, Harald Fritzsch, and Murray Gell-Mann on the gauge theory of the $SU(3)$ symmetry group in 1972; and the work of David Gross, Frank Wilczek, and H. David Politzer on asymptotic freedom in 1973.

- **Renormalization** – a crucial development, ensuring the mathematically consistency of the SM and allowing for interpretation of experimental data. One of the most important milestones was Gerard 't Hooft's and Martinus Veltman's proof in 1971 that the electroweak theory is renormalizable.

A slightly more formal introduction to the Standard Model

Setting out the notation, the Standard Model Lagrangian in the electroweak basis, invariant under the $SU(3)_C \times SU(2)_L \times U(1)_{Y_W}$ gauge group reads (where "primed" fields denote those in the electroweak basis, and "unprimed" denote those in the physical mass basis):

$$\begin{aligned}\mathcal{L}^{(4)}_{SM} = &-\frac{1}{4}G^A_{\mu\nu}G^{A\mu\nu} - \frac{1}{4}W^I_{\mu\nu}W^{I\mu\nu} - \frac{1}{4}B_{\mu\nu}B^{\mu\nu} + (D_\mu\varphi)^\dagger (D^\mu\varphi) + V_{SM}(\varphi) \\ &+ i\sum_\psi \overline{\psi}' \not{D}\psi' - \left(y^{e\prime}_{ij}\overline{l}'_{L,i}\varphi e'_{R,j} + y^{u\prime}_{ij}\overline{q}'_{L,i}\widetilde{\varphi}u'_{R,j} + y^{d\prime}_{ij}\overline{q}'_{L,i}\varphi d'_{R,j} + \text{h.c.}\right),\end{aligned} \tag{1.9}$$

ψ	$SU(3)_C$	$SU(2)_L$	Y_W	T_3	Q_{EM}
$q'_{L,j} = \begin{pmatrix} u'_{L,j} \\ d'_{L,j} \end{pmatrix}$	3	2	$+1/6$	$+1/2$ $-1/2$	$+2/3$ $-1/3$
$u'_{R,j}$	3	1	$+2/3$	0	$+2/3$
$d'_{R,j}$	3	1	$-1/3$	0	$-1/3$
$l'_{L,j} = \begin{pmatrix} \nu'_{L,j} \\ e'_{L,j} \end{pmatrix}$	1	2	$-1/2$	$+1/2$ $-1/2$	0 -1
$e'_{L,j}$	1	1	-1	0	-1

Table 1.1: The Standard Model matter field content. u and d denote "up" and "down" quark types, ν and e denote "up" and "down" lepton types (i.e., neutrinos and charged leptons). $j = 1, 2, 3$ denotes generation index.

where y'^{k}_{ij}, $k = e, u, d$ are complex 3×3 matrices of Yukawa couplings in flavor space, φ is a $SU(2)$ complex doublet with the weak hypercharge $Y_W = 1/2$, and $\tilde{\varphi} = i\tau_2\varphi^*$. The covariant derivative takes the form:

$$D_\mu = \partial_\mu + ig' B_\mu Y_W + i\frac{g}{2} W^I_\mu \tau^I + i\frac{g_s}{2} G^A_\mu \lambda^A, \tag{1.10}$$

with weak hypercharges $Y_W = Q_{EM} - T_3$ assigned in line with Table 1.1, τ^I, $I = 1, 2, 3$ representing the Pauli matrices and λ^A, $A = 1, \ldots, 8$ representing the Gell-Mann matrices. The field strength tensors read:

$$\begin{aligned} G^A_{\mu\nu} &= \partial_\mu G^A_\nu - \partial_\nu G^A_\mu - g_s f^{ABC} G^B_\mu G^C_\nu, \\ W^I_{\mu\nu} &= \partial_\mu W^I_\nu - \partial_\nu W^I_\mu - g\epsilon^{IJK} W^J_\mu W^K_\nu, \\ B_{\mu\nu} &= \partial_\mu B_\nu - \partial_\nu B_\mu, \end{aligned} \tag{1.11}$$

and the Standard Model potential written in terms of φ is given by:

$$V_{SM}(\varphi) = -\mu^2 \varphi^\dagger \varphi + \frac{\lambda}{2} (\varphi^\dagger \varphi)^2, \tag{1.12}$$

After the scalar φ acquires the vacuum expectation value (vev), defined as the minimum of the SM potential, we can expand Higgs doublet around it to obtain physical degree of freedom — the physical Higgs boson H:

$$\varphi = \begin{pmatrix} \Phi^+ \\ \frac{1}{\sqrt{2}} \left(v + H + i\Phi^0 \right) \end{pmatrix}, \quad v = \sqrt{\frac{2\mu^2}{\lambda}} = \frac{M_H}{\sqrt{\lambda}}, \tag{1.13}$$

where H represents the physical Higgs field, Φ^0 and Φ^+ are the Goldstone fields.

In order to identify physical degrees of freedom, one must perform various field redefinitions. In the case of the electroweak (EW) sector, for the physical charged $W^\pm$ bosons, we have:

$$W^{1/2}_\mu = \frac{1}{\sqrt{2}} (W^+_\mu \pm W^-_\mu), \quad M_W = \frac{1}{2} g v, \tag{1.14}$$

and for the photon A and heavy Z boson:

$$\begin{pmatrix} W_\mu^3 \\ B_\mu \end{pmatrix} = \begin{pmatrix} \cos\theta & \sin\theta \\ -\sin\theta & \cos\theta \end{pmatrix} \times \begin{pmatrix} Z_\mu \\ A_\mu \end{pmatrix}, \quad M_Z = \frac{1}{2}\sqrt{g^2 + g'^2}v, \quad M_A = 0. \tag{1.15}$$

For fermions, to obtain the physical basis, we have to diagonalize the general 3×3 mass matrices:

$$M_{ij}^{\prime,k} = y_{ij}^{\prime k} \frac{v}{\sqrt{2}}, \quad k = e, u, d. \tag{1.16}$$

We can again achieve it through proper field redefinitions of the fermion fields:

$$e'_{L/R} = V_{L/R}^e e_{L/R}, \quad u'_{L/R} = V_{L/R}^u u_{L/R}, \quad d'_{L/R} = V_{L/R}^d d_{L/R}, \tag{1.17}$$

where $V_{L/R}^k$ are 3×3 unitary rotation matrices. In case of quarks, the mass matrices read:

$$M_{ii}^p = \left(\left(V_L^p\right)^\dagger M^{\prime,p} V_R^p \right)_{ii}, \quad p = u, d, \tag{1.18}$$

where M_{ii}^p is now a diagonal 3×3 quark mass matrix. Finally, we can define the CKM quark mixing matrix as:

$$V_{CKM} = \left(V_L^u\right)^\dagger V_L^d. \tag{1.19}$$

In the absence of neutrinos, we can choose $V_L^e = V_R^e$, resulting in no corresponding mixing matrix for leptons. Thus, the weak and mass eigenstates for leptons remain the same. For a more detailed description, the reader can refer to one of the standard textbooks on the topic [1–3].

1.2.2 Open problems

Despite its enormous success, the Standard Model suffers from a limitations in its ability to explain a number of phenomena indicating the existence of the physics beyond the Standard Model. Among these, one can list:

1. **Hierarchy problem**
   The SM does not explain the small value of the Higgs boson mass $M_H = 125$ GeV, with quantum corrections making it extremely large (order of the Planck scale), implying a somewhat unnatural fine-tuning to secure this small value.

2. **Flavor problem**
   Neither the pattern of charged fermion masses (spanning many orders of magnitude) and their mixing, nor the magnitude of the observed CP violation can be explained within the SM and require building wider models, usually with new symmetries imposed.

3. **Neutrino masses**
   Within the SM framework, neutrinos are massless, left-handed particles. However, neutrino oscillation experiments indicate non-zero masses of these particles, which requires extending the SM by, e.g., including their right-handed counterparts to form Dirac mass terms or by postulating lepton-number violating Majorana mass terms.

4. **Matter-antimatter asymmetry**
   The dominance of matter over antimatter in the observable universe cannot be accounted for by the amount of CP-symmetry violation (which can be translated into matter-antimatter asymmetry) in the SM.

5. **Dark matter**
   Gravitational effects in galaxies, such as their rotation, motion, formation, or gravitational lensing, imply the existence of invisible matter responsible for roughly 27% of the mass-energy content of the universe, which cannot be explained by the SM alone.

6. **Dark energy**
   It is a hypothetical "force" driving the universe's accelerated expansion that cannot be explained within the framework of the SM.

7. **Gravity**
   The SM does not include one of the four fundamental forces — gravity — with no consistent and successful theory of quantum gravity established to this date.

1.3 Going beyond the Standard Model

Having outlined the limitations and issues related to the Standard Model, we can now turn our attention to searches for physics beyond the Standard Model. These searches aim to address and resolve one or more (preferably all) of the challenges discussed in the previous Section. There are several ways of categorizing various strategies for BSM searches. For the purpose of this work, the most useful is the one distinguishing the **bottom-up** and **top-down** approaches, which are described in detail in the following pages.

1.3.1 Bottom-up approach

The **bottom-up** approach to searches for physics beyond the Standard Model has been a major direction in particle physics research over the past few decades. This strategy is closely related to the experimental searches and real data and relies on identifying discrepancies between the theoretical predictions of the Standard Model and experimental results. Such differences, if observed, can provide crucial insights into the nature of underlying phenomena and help us develop more accurate models of the physical world.

There are a number of historical examples of the success of this approach, proving its utility. These include: the discovery of the 4th c quark, postulated to explain the rarity of certain kaon decays using the GIM mechanism [6]; and later precise predictions of the Higgs and top-quark masses from Large Electron–Positron Collider (LEP) collider electroweak precision tests before they were actually observed at Fermilab and LHC.

The bottom-up approach has always attracted researchers' attention, recently even more so due to the lack of direct evidence for new physics through the production of BSM particles in high-energy accelerator experiments. This methodology allows for model-independent studies of existing experimental data, in the hope that with sufficiently large numbers of anomalies and deviations from SM predictions eventually discovered, it will be possible to deduce — at least partially — the form of the underlying UV theory. Current notable examples of such discrepancies include: measurements of the muon anomalous magnetic moment $(g-2)$ (although recent lattice calculations [7] suggest agreement with SM predictions); anomalies in B-meson semileptonic decays suggesting (again, recent experimental results on the R_K ratio [8] did not confirm earlier reports of possible lepton flavor universality violation); or the W boson mass anomaly. Such anomalies often tend to fade away with time due to increased precision in measurements and calculations, and we have yet to find a truly convincing one in well-controlled Earth-based laboratories. On the other hand, the Standard Model

falls short in explaining a wide range of phenomena in cosmology, where the environment in which systems are investigated is far more complex and much less under control. It is therefore important to pursue both directions in the search for physics beyond the Standard Model.

Short introduction to the Effective Field Theories

The very important toolbox, that facilitates the bottom-up approach and allows its implementation in the model-independent searches for new physics, is known collectively as **Effective Field Theories** (EFTs) (see e.g., [9] for detailed introduction). The main idea behind EFTs is both simple and quite intuitive, and has been an ever-present concept in physics:

Low-energy phenomena can be accurately described without the detailed knowledge of the underlying, more fundamental theory.

Among the well-known examples of EFTs, one can list:

- **Newtonian gravity** — an effective description of General Relativity (GR) valid in the regime of small, non-relativistic velocities ($v \ll 1$) and weak gravitational fields $\frac{GM}{r} \ll 1$.
- **Non-relativistic quantum mechanics** — an effective low-energy limit of Quantum Electrodynamics, valid for photon energies much smaller than the electron mass $E_\gamma \ll m_e$. At low energies, relativistic effects, vacuum polarization, and loop corrections to photon scattering are suppressed. As a result, the Schrödinger equation can be used, e.g., to describe the hydrogen atom structure to a good accuracy. Higher order corrections can be then systematically included: first relativistic corrections from Dirac equation and later corrections from QED itself.
- **Quantum Electrodynamics** — a remarkably successful theory describing electromagnetic interactions established prior to the full development of the Standard Model and its structure. QED itself can be seen as an EFT of the Standard Model, valid at energies below the electroweak scale $E \ll \Lambda_{EW}$, $\Lambda_{EW} \approx 100$ GeV.

All of these examples have a common feature: at low energies, corrections to the more fundamental theory can be systematically organized as an expansion in a small parameter (or parameters), $\delta \ll 1$, arising due to the separation of scales between the low-energy and high-energy description. The leading-order terms in the expansion match the low energy description. This behavior is also known as decoupling. For the examples listed above, we can point out the following expansion parameters: $\delta^{(1)}_{GR} = v$ and $\delta^{(2)}_{GR} = \frac{GM}{r}$ for GR, $\delta_{QED/QM} = \frac{E_\gamma}{m_e}$ for QED and $\delta_{SM/QED} = \frac{E}{\Lambda_{EW}}$ for the Standard Model. In each case, the separation of scales allows the more fundamental theory to be expanded order-by-order, providing a well-defined and systematic procedure to describe it at low energies.

In the context of Quantum Field Theory, this approach has been formalized through the Appelquist-Carazzone decoupling theorem: [10]. The theorem states that if a renormalizable quantum gauge theory is embedded into a larger, renormalizable theory with particles at the mass scale Λ, the effects of a more fundamental theory at an energy scale $E \ll \Lambda$ are suppressed by the powers of the ratio $\frac{E}{\Lambda}$. In other words, the contributions from the heavy degrees of freedom — new particles — effectively decouple at energies below the scale Λ, and the theory at low energies can be systematically expanded around the small parameter $\delta = \frac{E}{\Lambda} \ll 1$[1]. In this way, we obtain Effective Field Theory description,

[1]Valid under the assumption that coupling constants in high energy theory are fixed; decoupling would not work if they grew together with the masses of heavy particles like e.g., for Yukawa couplings in the SM. In such case, effects of heavy fermions, like the top quark, may not decouple in the limit $m_t \to \infty$.

which is valid as long as $E \ll \Lambda$ is satisfied. Importantly, such EFT can be constructed and utilized even without the specific knowledge of the underlying fundamental theory, making it a powerful tool in the new physics searches.

As a consequence, this general model-independent framework allows us to describe and study a plethora of new physics models through a systematically defined EFT. It enables searches for indirect effects of heavy particles on the observables in our collider experiments. However, the price we pay for this generality lies in the technical complexity of EFTs. This is due to the fact, that the general EFT Lagrangian contains a very large number of terms and corresponding free parameters, especially for higher mass dimensions. Moreover, EFTs involve non-renormalizable interactions (although EFT can be renormalized order-by-order up to a given mass dimension), and several other theoretical issues, such as systematic inclusion of higher-order corrections.

Example of EFT – Fermi theory

In order to illustrate the utility of this approach and provide insight into its application, let us start with a well-known example: the Fermi theory of weak interactions. In the SM, the interactions between quarks and leptons are described through the following charged-current Lagrangian involving exchange of charged $W^{\pm}$ vector bosons:

$$\mathcal{L}_{CC} = -\frac{g}{\sqrt{2}} V_{CKM}^{ij} W_{\mu}^{+} \bar{u}_i \gamma^{\mu} P_L d_j - \frac{g}{\sqrt{2}} W_{\mu}^{+} \bar{\nu}_i \gamma^{\mu} P_L e_i + \text{h.c.}, \quad i,j = 1,2,3, \tag{1.20}$$

(we keep the same notation as in Section 1.2.1), while in Fermi theory they are parametrized by a set of effective four-fermion contact interactions.

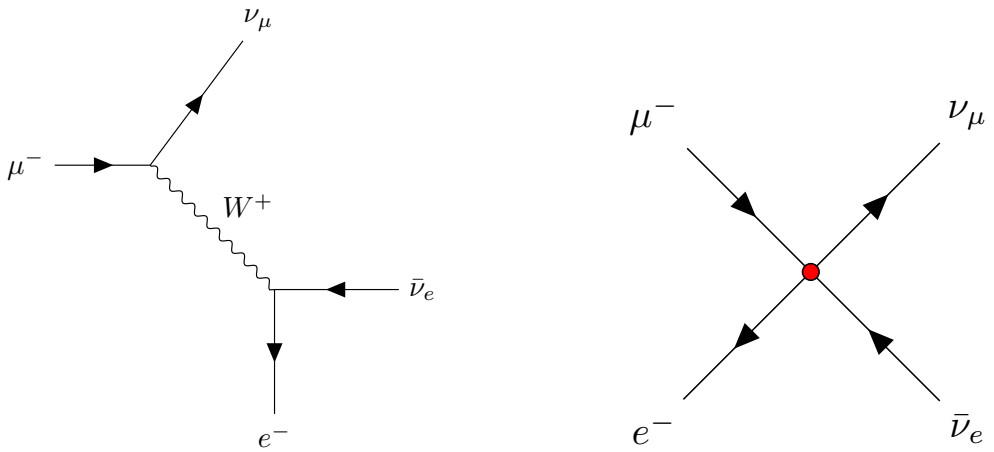

Figure 1.2: Muon decay in the Standard Model — left, and in the low-energy effective Fermi theory — right. The red dot indicates the effective Fermi interaction.

As a concrete example, consider the muon decay process ($\mu^- \to e^- \nu_\mu \bar{\nu}_e$) displayed in the left panel of Figure 1.2. The tree-level amplitude of this process in the SM reads:

$$i\mathcal{M}_{SM}^{\mu \to e\nu\bar{\nu}} = \left(\frac{-ig}{\sqrt{2}}\right)^2 (\bar{\nu}_\mu \gamma^{\mu} P_L \mu) \left(\frac{-ig_{\mu\nu}}{p_W^2 - M_W^2}\right) (\bar{e}\gamma^{\nu} P_L \nu_e). \tag{1.21}$$

At energy scales below the mass of W boson ($E \ll M_W$), the W propagator can be expanded as:

$$\frac{1}{p_W^2 - M_W^2} = -\frac{1}{M_W^2}\frac{1}{1-\frac{p_W^2}{M_W^2}} \xrightarrow[M_W >> p_W]{} -\frac{1}{M_W^2} + \mathcal{O}\left(\frac{1}{M_W^4}\right). \tag{1.22}$$

Substituting the leading-order term into Eq. (1.21), we obtain the amplitude in effective Fermi theory:

$$i\mathcal{M}_{Fermi}^{\mu\to e\nu\bar{\nu}} = -i\frac{g^2}{2M_W^2}(\bar{\nu}_\mu\gamma^\mu P_L\mu)(\bar{e}\gamma^\nu P_L\nu_e) = -i\frac{4G_F}{\sqrt{2}}(\bar{\nu}_\mu\gamma^\mu P_L\mu)(\bar{e}\gamma^\nu P_L\nu_e), \tag{1.23}$$

where G_F is the Fermi constant, which parametrizes the strength of this effective interaction. The effective dimension-6 four-fermion operator is then given by:

$$\mathcal{L}_{CC}^{eff} = -\frac{4G_F}{\sqrt{2}}(\bar{\nu}_\mu\gamma^\mu P_L\mu)(\bar{e}\gamma_\mu P_L\nu_e), \quad G_F = \frac{g^2}{8M_W^2}. \tag{1.24}$$

At low energies, only the effective interaction parametrized by the effective coupling G_F can be observed. Nevertheless, its value, extracted from the muon lifetime measurement, provides an estimate of the scale of the electroweak physics Λ_{EW} (or in other words, the $\frac{g^2}{M_W^2}$ ratio), with [11]:

$$G_F = \frac{1}{\Lambda_{EW}^2} = 1.66\times10^{-5}\frac{1}{\text{GeV}^2}, \quad \Lambda_{EW} \approx 290 \text{ GeV}. \tag{1.25}$$

EFT descriptions for the Standard Model

We are now in a situation similar to pre-electroweak times. The Standard Model is a well-established and highly successful framework, but we have reasons to believe that it is not a fundamental theory of nature (see the previous Section 1.2.1). In order to study and search for beyond the Standard Model physics in a model-independent way, we can follow Fermi's approach, and write down all possible higher-dimensional interaction involving the SM fields, forming the Effective Field Theory for the Standard Model. This description, valid to the scale of new physics Λ, can provide invaluable clues about the scale and structure of the more fundamental theory through the determination of the magnitudes and patterns of these effective interactions.

Depending on a particular set of assumptions, one can think of a number of different effective descriptions for the Standard Model. In the context of this work, we focus on the **Standard Model Effective Field Theory** (SMEFT) [12,13], where we assume the SM gauge group and particle content, including the Higgs as a $SU(2)$ doublet. The SMEFT Lagrangian can be written in the following form:

$$\mathcal{L}_{\text{SMEFT}} = \mathcal{L}_{\text{SM}} + \sum_i \frac{C_i\mathcal{O}_i}{\Lambda^{d_i-4}}, \tag{1.26}$$

with $\mathcal{L}_{\text{SM}}$ given by Eq. (1.9), Λ is the scale of new physics, and $\mathcal{O}_i$ denote higher-dimensional operators of dimension d_i invariant under the SM gauge group (note that the Lagrangian in Eq. (1.26) is defined in the unbroken phase of the theory, before identifying the physical Higgs field and other physical degrees of freedom).

Another framework — **Higgs Effective Field Theory** (HEFT) [14] — is also widely used in the context of new physics searches. It is more general than SMEFT, as it does not assume that the Higgs boson is a linear representation of SM symmetries (which also increases the number of free parameters

and diminishes the predictive power of HEFT), with its expansion parameter and region of validity $\frac{v}{\Lambda} \ll 1$.

Another class of Effective Field Theories for the Standard Model includes cases for which the SM itself is the more fundamental theory, but due to reasons such as calculational complexity, it's easier to work with its low-energy effective descriptions. Examples include:

- **Low Energy Effective Field Theory** (LEFT) [15] – which describes the SM at energies below the electroweak scale $E \ll \Lambda_{EW}$, $\Lambda_{EW} \approx 100$ GeV.
- **Heavy Quark Effective Theory** (HQEFT) [16, 17] – which provides a low-energy description of hadrons containing heavy quarks (b bottom or c charm), with one of the expansion parameters $\delta = \Lambda_{QCD}/m_Q$, where m_Q is the mass of $Q = b, c$ and $\Lambda_{QCD} \approx 200$ MeV is the energy scale of QCD.

As this thesis focuses on the applications of EFTs to searches for physics BSM, we will not discuss this class of EFTs further. Interested readers are referred to the provided references.

There are numerous examples of studies utilizing SMEFT (and more generally EFTs) that analyze specific processes in this model-independent framework, such as:

- Higgs boson decays [18–27],
- Higgs and multi-Higgs production [28–38]
- Vector-boson scattering and multiboson production [39–42],

and many others. These types of analyses are especially important from the point of view of determining the values of SMEFT Wilson coefficients through global SMEFT fits [43, 44]. By constraining WCs, such fits can provide invaluable insight into the form of the underlying UV theory.

In this thesis, we present two examples of the bottom-up approach applications. First, in Chapter 2, we present an example of development of a software tool designed specifically for automatizing calculations in the SMEFT framework: `SmeftFR` v3 – Feynman rules generator for the Standard Model Effective Field Theory. Such tools are indispensable for efficient computations within such a complicated framework as SMEFT. Then, in Chapter 3, we demonstrate an application of the code described in Chapter 2 by presenting calculations of one specific process: double Higgs boson production via vector-boson fusion in SMEFT, including terms $\mathcal{O}(1/\Lambda^2)$ (LO in the EFT expansion) and $\mathcal{O}(1/\Lambda^4)$ (NLO in the EFT expansion), with particular emphasis on predictions for the HL-LHC experiment.

1.3.2 Top-down approach

In the **top-down** approach to new physics searches, researchers begin with fundamental principles and symmetries to propose models that address specific issues. In practice, this often involves extending the Standard Model by introducing new particles and sectors of interactions designed to resolve one or more of its challenges. The impact of a given new physics model is uniquely determined by its specific particle content and allowed parameter space of their masses and couplings. The top-down approach has a long and successful history in particle physics, which justifies the significant research effort dedicated to it in the context of the quest for the discovery of beyond the Standard Model physics. Examples of such successes include the discovery of the Higgs boson, the discoveries of the weak W and Z bosons, all predicted by the unified theory of electroweak interactions, or the measurement of

neutrino oscillations. All these phenomena began as theoretical hypotheses and were later confirmed through experimental searches.

Over the past decades, numerous attempts have been made towards proposing a successful extension of the Standard Model that would not only address its theoretical limitations, but also have the potential to be verified experimentally. Without going into too much detail, in Table 1.2 we present an illustrative (and arbitrary) selection of such extensions to provide the reader with a general overview of chosen SM extensions with relevant references.

Model Class	**Model Examples**	**Key Features**	**Applications**
Supersymmetry	MSSM [45], NMSSM [46]	Introduces superpartners for each SM particle with spin differing by 1/2	Hierarchy problem Dark matter Unification
Scalar Extensions	Scalar singlet [47], Two Higgs doublet model (2HDM) [48]	Adds additional scalar multiplets to the SM field content	Dark matter CP violation Baryogenesis
Axions and Axion-like particles (ALPs)	Peccei-Quinn axion [49], DFSZ axion [50]	Introduces new particle, axion, emerging from the spontaneous breaking of a new global $U(1)_{PQ}$ symmetry	Strong CP problem Dark matter Anomaly cancellation
Z' Models	$U(1)_{B-L}$ models, E_6 models [51]	Introduces additional, heavy neutral gauge boson Z', arising from the breaking of an extended SM gauge symmetry	Dark matter Neutrino masses Anomaly cancellation

Table 1.2: A short overview of chosen widely studied Standard Model extensions.

In the context of this thesis, in Chapter 4 we present an example of a specific application of the top-down approach with a particular class of BSM models that involve heavy **vector-like fermion** (VLF) multiplets and a **real scalar singlet**. Basing on recent work [52], we use these model scenarios as a case study to illustrate the practical application of the top-down approach and demonstrate how this methodology can be used to deepen our understanding of BSM physics.

1.4 Three case studies of indirect searches for the Standard Model extensions

The two approaches to studying physics beyond the Standard Model introduced in the previous sections: **bottom-up** and **top-down**, should be viewed as complementary to one another, with their greatest utility arising when both are considered in parallel. Given the current lack of direct discoveries of new physics, and with the LHC approaching its energy limit, the primary means of measuring its effects may be through its indirect influence on precision measurements. Such potential deviations can be efficiently parametrized in a model-independent way using **Effective Field Theory** techniques (bottom-up approach). However, once such a deviation is detected, it is essential to interpret the

results through the lens of specific models to determine which extensions of the Standard Model are most viable. This is exactly the rationale behind the parallel model-independent and model-specific studies of various processes in high-energy physics, and is one of the main motivations behind the choice of specific research projects for the author's doctoral studies.

The first two chapters summarize studies focused on the bottom-up approach in indirect searches for the SM extensions. Both utilize the **Standard Model Effective Field Theory**, a common framework that allows for model-independent parameterization of BSM phenomena, and serve as important examples of this approach in modern particle physics. Chapter 2, "`SmeftFR` v3 – Feynman rules generator for the Standard Model Effective Field Theory", provides a comprehensive description of the numerical tool, `SmeftFR` v3. Due to the high level of complexity of calculations with SMEFT framework, this kind of programs are crucial for automatizing and enabling a broad range of analyses. Then, Chapter 3, "Double Higgs production via vector-boson fusion at next-to-leading order in SMEFT", provides an immediate `SmeftFR` v3 application. In it, we present a model-independent analysis of a specific process — double Higgs production via vector-boson fusion (VBF) in SMEFT — including higher-order therms in the EFT expansion. Our main result is the estimation of the maximal impact of BSM physics on this process for the HL-LHC collider experiment.

The third study, "Vector-like fermions, real scalar, and Higgs boson phenomenology", summarized in Chapter 4, is an example of application of the **top-down** approach in indirect searches for the SM extensions using two widely studied models: **vector-like fermions** and a **real scalar singlet**. We begin by exploiting the theoretical constraints to limit the parameter space of the models considered and combine them with experimental limits. We then apply these results to evaluate potential impact of these models on the processes of single and double Higgs boson production, electroweak precision observables, and the electroweak phase transition. The logic behind this program is that, if such impacts lead to detectable experimental signatures, they would **indirectly** support these models. Additionally, we present an example of the procedure for bridging the top-down and bottom-up approaches — matching between SMEFT operators and VLF and real scalar models.

The selection of these research projects was, apart from addressing several outstanding issues in high-energy physics, intended to ensure that, upon finishing his doctoral studies, the author would emerge as a competent researcher with wide expertise across this field.

Chapter 2

Tool development: SmeftFR v3 – Feynman rules generator for the Standard Model Effective Field Theory

2.1 Introduction and motivation

In this chapter, we present an example of a project dedicated to the numerical tool development facilitating the use of the bottom-up approach to new physics searches within the framework of the Standard Model Effective Field Theory. The increased interest in using the Effective Field Theory approach is closely related to the absence of direct evidence for new particles in collider experiments, which has shifted the focus of researchers towards searches for physics beyond the Standard Model in precision measurements. For this purpose, Effective Field Theory tools have become invaluable and have been commonly used in recent years for model-independent analyses of experimental data.

On the necessity for automation in SMEFT

Although universal and model-independent in parametrizing BSM phenomena, SMEFT is, at the same time, a very complex framework. The general form of its Lagrangian is presented in Eq. (1.26). The exact number of higher-dimensional operators for a given mass dimension d_i depends on particular assumptions, such as the number of fermion generations n_f [53], as shown in Table 2.1.

d_i	$n_f = 1$	$n_f = 3$
5	2	12
6	84	3045
8	993	44807
10	15456	2092441

Table 2.1: Numbers of higher-dimensional operators for a given mass dimension d_i and number of fermion generations n_f, as taken from [53].

The sheer number of these operators implies a high level of technical complexity involved in theoretical calculations for physical processes and observables in SMEFT. In addition, issues such as matching between UV models and SMEFT, renormalization group equations (RGE) in SMEFT, or fitting SMEFT Wilson coefficients to experimental data have proven that numerical tools are indispensable in efficient calculations within the SMEFT framework. In order to face this nontrivial matter, researchers around the world dedicated a significant amount of time and effort to develop numerical tools that address specific challenges related to SMEFT. Below, we present a short review of the most important tools currently available, divided by category [54, 55].

- **SMEFT matching to UV models and RGE running**
  `Matchete` [56], `Matchmakereft` [57], `MatchingTools` [58], `CoDeX` [59], `DsixTools` [60], `wilson` [61], `SOLD` [62], `RGESolver` [63],
- **SMEFT fitting to experimental data**
  `SMEFiT` [64], `smelli` [65], `HepFIT` [66], `match2fit` [67],
- **Feynman rules and physical observables**
  `SMEFTsim` [68, 69], `Dim6Top` [70], `SMEFT@NLO` [71] and `SmeftFR` [72].

This chapter is dedicated to the description of the code that falls into the last category: `SmeftFR` v3 — Feynman rules generator for the Standard Model Effective Field Theory [72, 73]. In Section 2.2,

we introduce SMEFT itself as the basis of this and the following Chapter, including its Lagrangian, operator basis, and description of input schemes. Then, in Section 2.3, we describe the main features of the `SmeftFR` v3 code. Section 2.4 contains details on the steps necessary to install and use the code, along with a description of the available options. Finally, Section 2.5, provides a detailed example of the applications of the code. We conclude in Section 2.6.

2.2 SMEFT – short overview

This section provides a short description of SMEFT and its most relevant features. We use the same notation as in Section 1.2.1 and follow [73, 74], whenever applicable. Some results are also discussed and presented in [75].

2.2.1 SMEFT Lagrangian and operator basis

In this work, we use the **Warsaw** basis [13] for the dimension-5 and dimension-6 SMEFT operators in the interaction basis, a standard choice now widely used in most research papers and tools on this topic. For the dimension-8 operators, we use the basis from [76] (with similar work published at the same time [77]). All SMEFT operators included in `SmeftFR` v3 are listed in Appendix A. In particular, the dimension-6 operators are listed in Table A.1, while all bosonic dimension-8 operators are listed in Tables A.2, A.3 and A.4. We neglect the dimension-7 and dimension-8 fermionic operators – see the discussion in Section 2.3. In `SmeftFR` v3, we excluded operators of the mass dimension higher than 8 — there are very rarely important and used in the existing interpretations of experimental data. Also, if such high-order operators were required to describe the BSM phenomena, the validity of the EFT expansions would become questionable. Therefore, we neglect them entirely. The initial SMEFT Lagrangian in this work reads:

$$\mathcal{L} = \mathcal{L}^{(4)}_{\mathrm{SM}} + \frac{1}{\Lambda} C_{\nu\nu} Q^{(5)}_{\nu\nu} + \frac{1}{\Lambda^2} \sum_{boson,fermion} C^{(6)}_{(b,f)} Q^{(6)}_{(b,f)} + \frac{1}{\Lambda^4} \sum_{boson} C^{(8)}_{b} Q^{(8)}_{b} \,. \tag{2.1}$$

Moving from the **interaction** to the **mass** basis in SMEFT after spontaneous symmetry breaking (SSB) — necessary for the calculation of physical observables — leads to a number of complications compared to the Standard Model alone. This involves more complex field and coupling redefinitions to ensure the canonical normalization of gauge, Higgs and fermion fields, as well as careful treatment of gauge fixing. This procedure, fully automated in `SmeftFR` v3, is detailed in this section, highlighting the importance of tools like `SmeftFR` v3.

Higgs sector

The parts of the SMEFT Lagrangian relevant to the Higgs mechanism and scalar bilinears, including relevant dimension-6 and dimension-8 operators in the unbroken phase, read:

$$\begin{aligned}
\mathcal{L}_H^{SMEFT} &= \left(D_\mu\varphi\right)^\dagger \left(D^\mu\varphi\right) - V(\varphi) \\
&\quad + C_{\varphi\Box} \left(\varphi^\dagger\varphi\right) \Box \left(\varphi^\dagger\varphi\right) + C_{\varphi 6\Box} \left(\varphi^\dagger\varphi\right)^2 \Box \left(\varphi^\dagger\varphi\right) \\
&\quad + C_{\varphi D} \left(\varphi^\dagger D_\mu\varphi\right)^* \left(\varphi^\dagger D^\mu\varphi\right) + C_{\varphi 6D} \left(\varphi^\dagger\varphi\right) \left(\varphi^\dagger D_\mu\varphi\right)^* \left(\varphi^\dagger D^\mu\varphi\right), \\
V(\varphi) &= -\mu^2 \left(\varphi^\dagger\varphi\right) + \frac{\lambda}{2} \left(\varphi^\dagger\varphi\right)^2 - C_\varphi \left(\varphi^\dagger\varphi\right)^3 - C_{\varphi^8} \left(\varphi^\dagger\varphi\right)^4 .
\end{aligned} \tag{2.2}$$

Minimization of the updated Higgs potential leads to the following relation between μ, λ and v, modified in comparison to the SM (see Eq. (1.13)):

$$\mu^2 = \frac{\lambda v^2}{2} - \frac{3}{4}v^4 C_\varphi - \frac{1}{2}v^6 C_{\varphi^8}, \tag{2.3}$$

with the covariant derivative of form:

$$D_\mu = \partial_\mu + ig' B_\mu Y_W + i\frac{g}{2}W_\mu^I \tau^I + i\frac{g_s}{2}G_\mu^A \lambda^A. \tag{2.4}$$

After SSB, we obtain the following form of scalar field bilinears:

$$\begin{aligned}\mathcal{L}_H^{\text{Bilinear}} &= \frac{1}{2}\left(1 + \frac{v^2}{2}C_{\varphi D} + \frac{v^4}{4}C_{\varphi 6D} - 2v^2 C_{\varphi\Box} - v^2 C_{\varphi 6\Box}\right)(\partial_\mu H)^2 \\ &+ \left(\frac{1}{2}\mu^2 - \frac{3}{2}\lambda v^2 + \frac{15}{8}v^4 C_\varphi + \frac{7}{4}v^6 C_{\varphi^8}\right)H^2 \\ &+ \frac{1}{2}\left(1 + \frac{v^2}{2}C_{\varphi D} + \frac{v^4}{4}C_{\varphi 6D}\right)\left(\partial_\mu \varphi^0\right)^2 + \left(\partial_\mu \varphi^-\right)\left(\partial^\mu \varphi^+\right).\end{aligned} \tag{2.5}$$

In order to retain the canonical normalization of kinetic terms (as we do not want to alter the form of propagators), we perform the following field redefinitions, with $(h, G^\pm, G^0)$ treated as fields in the physical, mass basis:

$$\begin{aligned} h = Z_h H, \quad G^0 = Z_{G^0}\varphi^0, \quad G^\pm = Z_{G^\pm}\varphi^\pm, \\ Z_{G^\pm}^2 = 1, \quad Z_{G^0}^2 = 1 + \frac{v^2}{2}C_{\varphi D} + \frac{v^4}{4}C_{\varphi 6D}, \\ Z_h^2 = 1 + \frac{v^2}{2}C_{\varphi D} + \frac{v^4}{4}C_{\varphi 6D} - 2v^2 C_{\varphi\Box} - v^2 C_{\varphi 6\Box}, \end{aligned} \tag{2.6}$$

leading to the Higgs mass-vev relation of form:

$$M_H^2 = \frac{1}{Z_h^2}\left(2\lambda v^2 - 6v^4 C_\varphi - 3v^6 C_{\varphi^8}\right). \tag{2.7}$$

Gauge sector

In the case of the gauge sector Lagrangian, the discussion again closely follows that of [74], with some differences arising from the inclusion of dimension-8 bosonic operators, which are additionally accounted for. The relevant terms in the interaction basis Lagrangian affecting gauge boson propagators and the field bilinears read:

$$\begin{aligned}\mathcal{L}_{\text{EW}} &= -\frac{1}{4}W_{\mu\nu}^I W^{I\mu\nu} - \frac{1}{4}B_{\mu\nu}B^{\mu\nu} + \left(D_\mu\varphi\right)^\dagger\left(D^\mu\varphi\right) \\ &+ C_{\varphi D}\left(\varphi^\dagger D_\mu\varphi\right)^*\left(\varphi^\dagger D^\mu\varphi\right) + C_{\varphi 6D}\left(\varphi^\dagger\varphi\right)\left(\varphi^\dagger D_\mu\varphi\right)^*\left(\varphi^\dagger D^\mu\varphi\right) \\ &+ C_{\varphi W}\left(\varphi^\dagger\varphi\right)W_{\mu\nu}^I W^{I\mu\nu} + C_{W^2\varphi^4}^{(1)}\left(\varphi^\dagger\varphi\right)^2 W_{\mu\nu}^I W^{I\mu\nu} + C_{W^2\varphi^4}^{(3)}\left(\varphi^\dagger\tau^I\varphi\right)\left(\varphi^\dagger\tau^J\varphi\right)W_{\mu\nu}^I W^{J\mu\nu} \\ &+ C_{\varphi B}\left(\varphi^\dagger\varphi\right)B_{\mu\nu}B^{\mu\nu} + C_{B^2\varphi^4}\left(\varphi^\dagger\varphi\right)^2 B_{\mu\nu}B^{\mu\nu} \\ &+ C_{\varphi WB}\left(\varphi^\dagger\tau^I\varphi\right)W_{\mu\nu}^I B^{\mu\nu} + C_{WB\varphi^4}\left(\varphi^\dagger\varphi\right)\left(\varphi^\dagger\tau^I\varphi\right)W_{\mu\nu}^I B^{\mu\nu} \\ \mathcal{L}_{\text{QCD}} &= -\frac{1}{4}G_{\mu\nu}^A G^{A\mu\nu} + C_{\varphi G}\left(\varphi^\dagger\varphi\right)G_{\mu\nu}^A G^{A\mu\nu} + C_{G^2\varphi^4}^{(1)}\left(\varphi^\dagger\varphi\right)^2 G_{\mu\nu}^A G^{A\mu\nu}\end{aligned} \tag{2.8}$$

After SSB this leads to the following gauge field bilinear terms:

$$\begin{aligned}
\mathcal{L}_{\text{EW}}^{\text{Bilinear}} =& -\frac{1}{4}\left(1-2v^2C_{\varphi W}-v^4C^{(1)}_{W^2\varphi^4}\right)\left(W^1_{\mu\nu}W^{1\mu\nu}+W^2_{\mu\nu}W^{2\mu\nu}\right)+\frac{g^2v^2}{8}\left(W^1_\mu W^{1\mu}+W^2_\mu W^{2\mu}\right)\\
&-\frac{1}{4}\left(1-2v^2C_{\varphi W}-v^4C^{(1)}_{W^2\varphi^4}-\frac{v^4}{4}C^{(3)}_{W^2\varphi^4}\right)W^3_{\mu\nu}W^{3\mu\nu}\\
&-\frac{1}{4}\left(1-2v^2C_{\varphi B}-v^4C^{(1)}_{B^2\varphi^4}\right)B_{\mu\nu}B^{\mu\nu}+\left(\frac{v^2}{2}C_{\varphi WB}+\frac{v^4}{4}C_{WB\varphi^4}\right)W^3_{\mu\nu}B^{\mu\nu}\\
&+\frac{v^2}{8}\left(1+\frac{v^2}{2}C_{\varphi D}+\frac{v^4}{4}C_{\varphi 6D}\right)\left(g'^2B_\mu B^\mu+g^2W^3_\mu W^{3\mu}-gg'(B_\mu W^{3\mu}+W^3_\mu B^\mu)\right),\\
\mathcal{L}_{\text{QCD}}^{\text{Bilinear}} =& -\frac{1}{4}\left(1-2v^2C_{\varphi G}-v^4C^{(1)}_{G^2\varphi^4}\right)G^A_{\mu\nu}G^{A\mu\nu}.
\end{aligned}\tag{2.9}$$

Canonical normalization of gauge fields $W^{1,2}_\mu$ and G^A_μ requires the following field redefinitions, where $W^\pm_\mu$ and g^A_μ are canonically normalized gauge fields in the mass basis:

$$G^A_\mu = Z_G g^A_\mu, \quad W^1_\mu = \frac{Z_W}{\sqrt{2}}\left(W^+_\mu+W^-_\mu\right), \quad W^2_\mu = \frac{iZ_W}{\sqrt{2}}\left(W^+_\mu-W^-_\mu\right), \tag{2.10}$$

with:

$$\begin{aligned}
Z_W &= \left(1-\frac{2v^2}{\Lambda^2}C_{\varphi W}-\frac{v^4}{\Lambda^4}C^{(1)}_{W2\varphi4}\right)^{-1/2},\\
Z_G &= \left(1-\frac{2v^2}{\Lambda^2}C_{\varphi G}-\frac{v^4}{\Lambda^4}C^{(1)}_{G2\varphi4}\right)^{-1/2}.
\end{aligned}\tag{2.11}$$

Canonical normalization of gauge fields W^3_μ and B_μ requires simultaneous diagonalization and normalization of the 2×2 "mixing" $\mathbb{X}$ matrix and the mass matrix:

$$\begin{aligned}
\mathcal{L}_{\text{EW}}^{\text{Bilinear}} \supset& -\frac{1}{4}\left(W^3_{\mu\nu},B_{\mu\nu}\right)\mathbb{X}\begin{pmatrix}W^{3\mu\nu}\\B^{\mu\nu}\end{pmatrix}+\frac{v^2}{8}Z_{G^0}\left(W^3_\mu,B_\mu\right)\begin{pmatrix}g^2 & -g\,g'\\ -g\,g' & g'^2\end{pmatrix}\begin{pmatrix}W^{3\mu}\\B^\mu\end{pmatrix},\\
\mathbb{X}_{11} &= 1-2v^2C_{\varphi W}-v^4C^{(1)}_{W^2\varphi^4}-\frac{v^4}{4}C^{(3)}_{W^2\varphi^4},\\
\mathbb{X}_{12} &= \mathbb{X}_{21} = \frac{v^2}{2}C_{\varphi WB}+\frac{v^4}{4}C_{WB\varphi^4},\\
\mathbb{X}_{22} &= 1-2v^2C_{\varphi B}-v^4C^{(1)}_{B^2\varphi^4}.
\end{aligned}\tag{2.12}$$

This can be achieved by the following transformation of W^3_μ and B_μ gauge fields, where Z_μ and A_μ are canonically normalized fields in the mass basis:

$$\begin{pmatrix}W^3_\mu\\B_\mu\end{pmatrix} = Z_{\gamma Z}\begin{pmatrix}Z_\mu\\A_\mu\end{pmatrix}. \tag{2.13}$$

The full analytical form of the $Z_{\gamma Z}$ matrix is calculated within the `SmeftFR` v3 code following the derivation described below. First, let us introduce intermediate "barred" fields:

$$\begin{pmatrix}W^3_\mu\\B_\mu\end{pmatrix} = \begin{pmatrix}Z_{W^3}\bar{W}^3_\mu\\Z_B\bar{B}_\mu\end{pmatrix}, \quad Z_3 = \mathbb{X}_{11}^{-1/2}, \quad Z_B = \mathbb{X}_{22}^{-1/2}. \tag{2.14}$$

Denoting $\epsilon = Z_3 Z_B \mathbb{X}_{21} \equiv Z_3 Z_B \mathbb{X}_{12}$, we get:

$$\begin{aligned}\mathcal{L}_{\text{EW}}^{\text{Bilinear}} \supset & -\frac{1}{4}\left(\bar{W}^3_{\mu\nu}, \bar{B}_{\mu\nu}\right)\begin{pmatrix}1 & \epsilon\\ \epsilon & 1\end{pmatrix}\begin{pmatrix}\bar{W}^{3\mu\nu}\\ \bar{B}^{\mu\nu}\end{pmatrix}\\ & + \frac{v^2}{8} Z^2_{G^0}\left(\bar{W}^3_{\mu}, \bar{B}_{\mu}\right)\begin{pmatrix}Z_3^2\, g^2 & -Z_3\, Z_B\, g\, g'\\ -Z_3\, Z_B\, g\, g' & Z_B^2\, g'^2\end{pmatrix}\begin{pmatrix}\bar{W}^{3\mu}\\ \bar{B}^{\mu}\end{pmatrix}.\end{aligned} \tag{2.15}$$

In order to simultaneously diagonalize these terms, $Z_{\gamma Z}$ should have the following form:

$$Z_{\gamma Z} = \begin{pmatrix}1 & -\frac{\epsilon}{2}\\ -\frac{\epsilon}{2} & 1\end{pmatrix}\begin{pmatrix}\cos\theta & \sin\theta\\ -\sin\theta & \cos\theta\end{pmatrix}. \tag{2.16}$$

The general formulas for ϵ and θ are complex and lengthy, and we choose to not display it here. After field redefinition by $Z_{\gamma Z}$ we get:

$$\mathcal{L}_{\text{EW}}^{\text{Bilinear}} \supset -\frac{1}{4}\left(Z_{\mu\nu}, A_{\mu\nu}\right)\begin{pmatrix}1 & 0\\ 0 & 1\end{pmatrix}\begin{pmatrix}Z^{\mu\nu}\\ A^{\mu\nu}\end{pmatrix} + \frac{1}{2}\left(Z_{\mu}, A_{\mu}\right)\begin{pmatrix}M_Z^2 & 0\\ 0 & 0\end{pmatrix}\begin{pmatrix}Z^{\mu}\\ A^{\mu}\end{pmatrix}. \tag{2.17}$$

Finally, in order to preserve the form of the covariant derivative, Eq. (2.4), we redefine gauge couplings in the following way:

$$g = Z_g \bar{g} \quad g' = Z_{g'}\bar{g}' \quad g_s = Z_{g_s}\bar{g}_s, \tag{2.18}$$

with:

$$\begin{aligned} Z_g = Z_W^{-1} &= \left(1 - \frac{2v^2}{\Lambda^2}C_{\varphi W} - \frac{v^4}{\Lambda^4}C^{(1)}_{W2\varphi 4}\right)^{1/2},\\ Z_{g_s} = Z_G^{-1} &= \left(1 - \frac{2v^2}{\Lambda^2}C_{\varphi G} - \frac{v^4}{\Lambda^4}C^{(1)}_{G2\varphi 4}\right)^{1/2},\\ Z_{g'} = Z_B^{-1} &= \left(1 - \frac{2v^2}{\Lambda^2}C_{\varphi B} - \frac{v^4}{\Lambda^4}C^{(1)}_{B2\varphi 4}\right)^{1/2}. \end{aligned} \tag{2.19}$$

The full electroweak bilinear Lagrangian in the mass basis has now the following form:

$$\begin{aligned}\mathcal{L}_{\text{EW}}^{\text{Bilinear}} =& -\frac{1}{4}\left(W^+_{\mu\nu}W^{+\mu\nu} + W^-_{\mu\nu}W^{-\mu\nu} + Z_{\mu\nu}Z^{\mu\nu} + A_{\mu\nu}A^{\mu\nu}\right) +\\ & + \frac{1}{2}M_W^2\left(W^+_{\mu}W^{+\mu} + W^-_{\mu}W^{-\mu}\right) + \frac{1}{2}M_Z^2 Z_\mu Z^\mu,\\ \mathcal{L}_{\text{QCD}}^{\text{Bilinear}} =& -\frac{1}{4}g^A_{\mu\nu}g^{A\mu\nu},\end{aligned} \tag{2.20}$$

with the physical masses of gauge bosons:

$$M_W^2 = \frac{\bar{g}^2 v^2}{4}, \quad M_A = 0, \quad M_Z^2 = \frac{v^2}{8}Z^2_{G^0}\left(\bar{g}'^2 + Z_3^2 Z_g^2 \bar{g}^2 + \frac{\epsilon^2}{4}(g'^2 + Z_3^2 Z_g^2 \bar{g}^2) + 2\epsilon Z_3 Z_g \bar{g}\bar{g}'\right). \tag{2.21}$$

As we have seen, the exact form of the above field normalization constants (including $Z_{\gamma Z}$ matrix), the relation for the corrected Higgs vev v, and the formulas for the Higgs and gauge boson masses M_H, M_W, M_Z, depend on the particular set of Wilson coefficients included in a given analysis, leading to potentially lengthy and complicated expressions. In `SmeftFR` v3, to speed up the calculations, such expressions are always calculated for the user-chosen subset of non-vanishing operators, not hard-coded in the full generality.

Gauge fixing

Finally, the adopted notation leads to the gauge fixing procedure that closely follows the one outlined in Section 5 of [74], with all the differences encoded in the form of the Z normalization constants that may now include dimension-8 contributions (the fully general procedure of gauge fixing in R_ξ gauge, for a generic EFT up to any order in the EFT expansion can be found in [78]).

Fermion sector

In the case of fermion sector, since we do not include dimension-7 and dimension-8 fermionic operators, we simply follow the procedure outlined in Section 3.4 of [74]. The fermion kinetic terms remain unaffected by the SSB, with the mass terms in the initial flavor (primed) basis given by:

$$\mathcal{L}_F \supset -\frac{1}{2}\nu'_L \mathbb{C} M'_\nu \nu'_L - \bar{e}'_L M'_e e'_R - \bar{u}'_L M'_u u'_R - \bar{d}'_L M'_d d'_R + \text{ H.c.}\,, \tag{2.22}$$

with 3×3 mass matrices of the following form:

$$\begin{aligned} M'_\nu &= -v^2 C_{\prescript{}{}{\prime}\nu\nu}\,, & M'_e &= \tfrac{v}{\sqrt{2}}\left(\Gamma_e - \tfrac{v^2}{2} C_{\prescript{}{}{\prime}e\varphi}\right), \\ M'_u &= \tfrac{v}{\sqrt{2}}\left(\Gamma_u - \tfrac{v^2}{2} C_{\prescript{}{}{\prime}u\varphi}\right), & M'_d &= \tfrac{v}{\sqrt{2}}\left(\Gamma_d - \tfrac{v^2}{2} C_{\prescript{}{}{\prime}d\varphi}\right). \end{aligned} \tag{2.23}$$

The mass (unprimed) basis is defined through a unitary rotation U_{ψ_X} from the initial flavor (primed) basis:

$$\psi'_X = U_{\psi_X}\, \psi_X\,, \tag{2.24}$$

with $\psi = \nu, e, u, d$ and $X = L, R$. This allows us to define mass eigenstates as ψ_X, with diagonal fermion mass matrices of the form:

$$\begin{aligned} U^\dagger_{e_L} M'_e U_{e_R} &= M_e = \text{diag}\,(m_e, m_\mu, m_\tau)\,, \\ U^\dagger_{u_L} M'_u U_{u_R} &= M_u = \text{diag}\,(m_u, m_c, m_t)\,, \\ U^\dagger_{d_L} M'_d U_{d_R} &= M_d = \text{diag}\,(m_d, m_s, m_b)\,, \\ U^T_{\nu_L} M'_\nu U_{\nu_L} &= M_\nu = \text{diag}\,(m_{\nu_1}, m_{\nu_2}, m_{\nu_3})\,. \end{aligned} \tag{2.25}$$

The final step to obtain the mass basis involves the redefinition of the fermionic Wilson coefficients in the initial basis to include rotation matrices. For example, we have the following relations (full list of relations can be found in Table 4 of [74]):

$$C_{e\varphi} = U^\dagger_{e_L} C_{\prescript{}{}{\prime}e\varphi} U_{e_R}, \quad (C_{ll})_{f_1 f_2 f_3 f_4} = (U_{e_L})_{g_2 f_2} (U_{e_L})_{g_4 f_4} (U_{e_L})^*_{g_1 f_1} (U_{e_L})^*_{g_3 f_3} (C_{\prescript{}{}{\prime}ll})_{g_1 g_2 g_3 g_4}\,. \tag{2.26}$$

2.2.2 Input schemes in SMEFT

So far, we have parametrized the SMEFT Lagrangian in terms of the same couplings as those normally used in the dimension-4 renormalizable SM Lagrangian, with the addition of Wilson coefficients of higher-order operators. This allows us to calculate observables in SMEFT in terms of the following set of "standard" parameters, which we will refer to from now on as the "SMEFT" input parameters:

$\bar{g}, \bar{g}', \bar{g}_s$	$SU(2), U(1), SU(3)$ gauge couplings,
v, λ	Higgs boson mass and quartic coupling,

$$
\begin{array}{rl}
m_q & \text{quark masses, } q = u, c, t, d, s, b, \\
K & \text{CKM quark mixing matrix,} \\
m_\ell, m_{\nu_\ell} & \text{charged lepton and neutrino masses, } \ell = e, \mu, \tau, \\
U & \text{PMNS lepton mixing matrix.}
\end{array}
\tag{2.27}
$$

However, parameters such as gauge couplings, the vacuum expectation value, Higgs quartic coupling, and mixing matrices are not directly measured in experiments. Deriving their values from experimental data depends on the Wilson coefficients of higher-dimension operators and they may not be identical between the SM and SMEFT. In order to determine their actual numerical values, one has to relate them to appropriate physical observables O_i - referred to as "input parameters" — and, in the case of SMEFT, to the Wilson coefficients. For example, for the electroweak sector we have:

$$
\begin{aligned}
\bar{g} &= \bar{g}(O_1, \ldots, O_n, C_1, \ldots, C_m), \\
\bar{g}' &= \bar{g}'(O_1, \ldots, O_n, C_1, \ldots, C_o), \\
v &= v(O_1, \ldots, O_n, C_1, \ldots, C_r), \\
\lambda &= \lambda(O_1, \ldots, O_n, C_1, \ldots, C_p).
\end{aligned}
\tag{2.28}
$$

Thus, the precise determination of $(\bar{g}, \bar{g}', v, \lambda)$ depends on the given set of input parameters, on the values of the Wilson coefficient, and on the order of the EFT expansion. This leads to further complications when calculating given observable $\mathcal{A}$ within SMEFT. Since we want to express $\mathcal{A}$ in terms of known (so directly measured) constants (and Wilson coefficients), it may not be sufficient to express the final result in terms of the initial "SMEFT" input parameters. Once we calculate $\mathcal{A}$ in terms of these initial model parameters, we must use expressions from Eq. (2.28), insert them back in the formulas for $\mathcal{A}$ and consistently re-expand the result up to the desired order in the $1/\Lambda$ expansion. This procedure can be summarized in the following manner:

$$
\begin{aligned}
\mathcal{A} &= \mathcal{A}_4(\bar{g}, \bar{g}', \ldots) + \frac{1}{\Lambda^2}\mathcal{A}_6^i(\bar{g}, \bar{g}', \ldots)C_6^i \\
&+ \frac{1}{\Lambda^4}\left(\mathcal{A}_8^{1ij}(\bar{g}, \bar{g}', \ldots)C_6^i C_6^j + \mathcal{A}_8^{2i}(\bar{g}, \bar{g}', \ldots)C_8^i\right) + \ldots \\
&= \mathcal{A}'_4(O_1, O_2, \ldots) + \frac{1}{\Lambda^2}\mathcal{A}'^i_6(O_1, O_2, \ldots)C_6^i \\
&+ \frac{1}{\Lambda^4}\left(\mathcal{A}'^{1ij}_8(O_1, O_2, \ldots)C_6^i C_6^j + \mathcal{A}'^{2i}_8(O_1, O_2, \ldots)C_8^i\right) + \ldots
\end{aligned}
\tag{2.29}
$$

As one might expect, such prescriptions quickly become highly complex and error-prone, especially at higher-orders of the EFT expansion. To make it more manifest, let us consider the derivation and application of the "G_F" electroweak input scheme up to dimension-6 in SMEFT. We want to express electroweak parameters $(\bar{g}, \bar{g}', v, \lambda)$ in terms of the set of physical observables: (G_F, M_Z, M_W, M_H). In order to do this, we first start from the relations between both sets of parameters:

$$
\begin{aligned}
M_W &= \frac{1}{2}\bar{g}v, \\
M_H &= \frac{1}{Z_h}\left(2\lambda v^2 - 6v^4 C_\varphi - 3v^6 C_{\varphi^8}\right)^{1/2}, \\
M_Z &= \frac{1}{2}\sqrt{\bar{g}^2 + \bar{g}'^2}v\left(1 + \frac{v^2\bar{g}\bar{g}'}{\bar{g}^2 + \bar{g}'^2}C_{\varphi WB}\right)Z_{G^0}, \\
v &= \frac{1}{2^{1/4}\sqrt{G_F}}\left(1 - \frac{C_{ll}^{2112} - C_{\varphi l3}^{11} - C_{\varphi l3}^{22}}{2\sqrt{2}G_F}\right),
\end{aligned}
\tag{2.30}
$$

where the first two relations for M_W and M_H appeared in the previous section, M_Z is the dimension-6 equivalent of Eq. (2.21), and the v - G_F relation is based on the calculation of muon decay in SMEFT, see e.g., [19]. One can immediately note, that although the relation for v is given, and the relation for $\bar{g}$ can be easily obtained:

$$\bar{g} \;=\; 2^{5/4}\sqrt{G_F}M_W\left(1+\frac{C_{ll}^{2112}-C_{\varphi l3}^{11}-C_{\varphi l3}^{22}}{2\sqrt{2}G_F}\right), \tag{2.31}$$

in order to derive formulas for λ and $\bar{g}'$, one has to solve a non-trivial system of equations. Thus, in order to facilitate SMEFT calculations directly in terms of a chosen set of input observables, `SmeftFR` v3 includes hard-coded relations between electroweak input parameters in "GF" and "AEM" input schemes up to dimension-8, see Appendix D.2).

The trade-off of model parameters required by the choice of "input scheme" also affects the derivation of interaction vertices generated by the higher-order operators. As an example, let us consider the hWW vertex in dimension-6 SMEFT. In terms of the initial, "SMEFT" parameters, it is given by Eq. (2.33). Plugging the relations from Eqs. (2.30), (2.31) back into the vertex expression and expanding up to the $\mathcal{O}(1/\Lambda^2)$ order in the EFT expansion, we obtain Eq. (2.34) - a corresponding formula in the "G_F" input scheme.

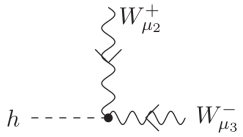

$$\begin{aligned} &+ \quad \frac{1}{2}i\bar{g}^2 v\eta_{\mu_2\mu_3}+\frac{1}{2}i\bar{g}^2v^3\eta_{\mu_2\mu_3}C_{\varphi\Box}-\frac{1}{8}i\bar{g}^2v^3\eta_{\mu_2\mu_3}C_{\varphi D} \\ &+ \quad 4ivC_{\varphi W}\left(p_2^{\mu_3}p_3^{\mu_2}-p_2\cdot p_3\eta_{\mu_2\mu_3}\right), \end{aligned} \tag{2.32}$$

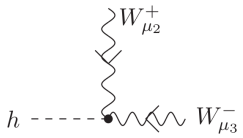

$$\begin{aligned} &+ \quad i2^{3/4}\sqrt{G_F}M_W^2\eta_{\mu_2\mu_3}+\frac{i2^{3/4}M_W^2}{\sqrt{G_F}}\eta_{\mu_2\mu_3}C_{\varphi\Box}-\frac{iM_W^2}{2^{3/4}\sqrt{G_F}}\eta_{\mu_2\mu_3}C_{\varphi D} \\ &- \quad \frac{iM_W^2}{2^{3/4}\sqrt{G_F}}\eta_{\mu_2\mu_3}C_{ll}^{2112}+\frac{iM_W^2}{2^{3/4}\sqrt{G_F}}\eta_{\mu_2\mu_3}\left(C_{\varphi l3}^{11}+C_{\varphi l3}^{22}\right) \\ &+ \quad \frac{i2^{7/4}}{\sqrt{G_F}}C_{\varphi W}\left(p_2^{\mu_3}p_3^{\mu_2}-p_2\cdot p_3\eta_{\mu_2\mu_3}\right). \end{aligned} \tag{2.33}$$

Even this relatively simple example demonstrates the complexity of such a procedure, particularly when terms $\mathcal{O}(1/\Lambda^4)$ are included in the analysis.

All the steps discussed in this section: the calculation and canonical normalization of the mass basis, gauge fixing, and consistent calculation of the vertices in terms of physical input parameters, are computationally highly complex and error-prone, emphasizing the necessity to automatize each of them. This highlights the rationale behind the development of `SmeftFR` v3, which is discussed in detail in the following Sections.

2.3 `SmeftFR` v3 – overview and main features

`SmeftFR` v3 is a `Mathematica` package written in symbolic `Wolfram Language` and based on the `FeynRules` [79, 80] package to produce Feynman rules in SMEFT. It is an extension and significant improvement over `SmeftFR` v2 [72], with its main features, alongside their description, listed below.

- `SmeftFR` v3 enables the production of Feynman rules in SMEFT including dimension-6 operators in the so-called Warsaw basis [13] (with numerical values initialized in the mass eigenstates "Warsaw mass" basis as defined for dimension-6 SMEFT in [74]), and **bosonic** dimension-8 operators in the basis of [76] — Eq. (2.34). he produced Feynman rules are expressed in terms of physical SM fields and normalized Goldstone and ghost fields. `SmeftFR` v3 novelty lies in the consistent inclusion of terms of order $\mathcal{O}(1/\Lambda^4)$ in the EFT expansion, including terms quadratic in dimension-6 and linear in dimension-8 Wilson coefficients. Higher-order terms are systematically truncated.

$$\mathcal{L} = \mathcal{L}^{(4)}_{\rm SM} + \frac{1}{\Lambda} C_{\nu\nu} Q^{(5)}_{\nu\nu} + \frac{1}{\Lambda^2} \sum_{boson, fermion} C^{(6)}_{(b,f)} Q^{(6)}_{(b,f)} + \frac{1}{\Lambda^4} \sum_{boson} C^{(8)}_{b} Q^{(8)}_{b} \ . \tag{2.34}$$

  We decided to exclude all the dimension-7 and fermionic dimension-8 operators for both theoretical and practical reasons. The former are always lepton or baryon number violating and therefore strongly constrained by experiments. The dimension-8 operators are generally strongly suppressed and require strong enhancement to have any significant effect. That is the case, e.g., in processes involving vector-boson scattering, where the effects of extra terms grow quickly with process energy [40, 81–84], see also Section 2.5. This justifies the inclusion of only purely bosonic operators in `SmeftFR` v3. Another reason for not including fermionic operators is more practical, namely their very high number, which makes their consistent inclusion very CPU time-consuming. However, users can follow the instructions detailed in Section 2.4 to include any additional fermionic dimension-8 operators they require for a given analysis.

- Neutrinos can be treated in `SmeftFR` v3 in two different ways. First, in the absence of the L-flavor violating dimension-5 operator $Q_{\nu\nu}$, neutrinos are treated as massless Weyl spinors, whereas the inclusion of $Q_{\nu\nu}$ leads to their treatment as massive Majorana spinors. Although this choice does not have any impact on the standard gauge-neutrino interactions, it may affect non-standard interactions arising from higher-dimensional operators (for discussion, see e.g., [85, 86]).

- `SmeftFR` v3 allows users to express Feynman rules directly in terms of a set of input parameters that are chosen to be physical observables. `SmeftFR` v3 users can define their own preferred set of input parameters (see Section 2.3.2), or use those predefined by the authors of the code (see Section 2.3.1). They include two input schemes for the electroweak sector, with all terms up to $\mathcal{O}(1/\Lambda^4)$ order in the EFT expansion taken into account:

  – "G_F" scheme with input parameters: (G_F, M_Z, M_W, M_H),
  – "α_{em}" scheme with input parameters: $(\alpha_{em}, M_Z, M_W, M_H)$.

  Moreover, following [87], `SmeftFR` v3 includes a predefined input scheme for the CKM matrix, including terms up to $\mathcal{O}(1/\Lambda^2)$ order in the EFT expansion.

- Since `SmeftFR` v3 generates `FeynRules` "model files" automatically, users can include a subset of Wilson coefficients relevant for a given analysis. This not only simplifies the results and the analysis itself, but also significantly speeds up calculations. For a given set of dimension-6 Wilson coefficients, `SmeftFR` v3 is about an order of magnitude faster than the previous version, `SmeftFR` v2 [72].

- Depending on a given analysis, `SmeftFR` v3 can generate Feynman rules in the *unitary* gauge or in the linear R_ξ gauge (including all relevant ghost and Goldstone vertices, a procedure thoroughly described in [74], see also [78]).

- Feynman rules obtained using `SmeftFR` v3 are produced in the `FeynRules` format. Users can then decide to further export results into various formats, suitable for a different kind of analyses, including:
  - `UFO` (Universal FeynRules Output) [88] – a format for automated matrix-element generators, including: `MadGraph5_aMC@NLO 5` [89], `Sherpa` [90], `CalcHEP` [91], `WHIZARD` [92, 93],
  - `FeynArts` [94] – a format that can be treated as an input for analytical amplitude calculations using `FormCalc` [95] or `FeynCalc` [96],
  - LaTeX– `SmeftFR` v3 provides a dedicated LaTeXgenerator producing clear and readable vertices and expressions for Feynman rules,
  - `WCxf` [97] – a standardized format for Wilson coefficients aimed at compatibility and consistency across different tools designed for calculations in SMEFT.

`SmeftFR` v3 has been thoroughly tested and validated utilizing various analytical and numerical tests, detailed in Section 2.4.5.

2.3.1 Predefined input schemes in `SmeftFR` v3

EW sector

`SmeftFR` v3 includes two predefined input schemes for the electroweak sector, in which we express $(\bar{g}, \bar{g}', \lambda, v)$ parameters in terms of the masses of physical SM particles — Higgs and gauge bosons, and low-energy observables — Fermi's constant G_F and the fine structure constant α_{em}:

- (G_F, M_Z, M_W, M_H) - "G_F" input scheme,
- $(\alpha_{em}, M_Z, M_W, M_H)$ - "α_{em}" input scheme.

These particular input schemes are widely used by the community and have several advantages, including the lack of WCs in particle propagators, which would make calculations and the EFT expansion in $1/\Lambda$ significantly more difficult. Detailed expressions, including the dimension-6, dimension-6^2 and dimension-8 terms, can be found in Appendix D.2. The strong coupling constant is defined as $\bar{g}_s = \sqrt{4\pi\alpha_s(M_Z)}$, with no additional SMEFT contributions to $\alpha_s(M_Z)$ assumed.

Fermion sector

- Quarks – quark masses are assumed to be equal to their physical masses, while corrections to the CKM matrix K are evaluated following [87], and include terms linear in WCs of dimension-6 operators.
- Leptons – charged lepton masses are assumed to be equal to their physical masses, while neutrino masses are proportional to dimension-5 Weinberg operator's WC $m_{\nu_i} = v^2|C^i_{\nu\nu}|$. PMNS matrix mixing angles are assumed to be equal to ones in the SM, without any SMEFT contributions.

2.3.2 User-defined input schemes in `SmeftFR` v3

Apart from these predefined input schemes, users can choose their own set of input parameters and include them in `SmeftFR` v3, provided that they are defined in the correct format and in relation to

the SmeftFR v3 "default" parameters listed in Table 2.2. Below, we present requirements to properly include a user-defined input parameter scheme.

1. Input parameters are assumed to be measurable physical observables or quantities without any contributions from SMEFT WCs, and should be real scalar numbers, without any flavor or gauge indices.

2. Names of user-defined input parameters should not overlap with the names of variables already used by the code (SmeftFR executes automatic checks for overlapping names).

3. User-defined input parameters and relations between them and "default" input parameters should be defined in the file code/smeft_input_scheme.m, following the standard format of FeynRules model definition files. A detailed example of such a scheme can be found in the file code/smeft_input_scheme.m provided with the SmeftFR v3 distribution.

4. User has to provide analytical expressions for all variables listed in Table 2.2, relating them to the chosen set of input parameters and WCs of higher dimensional operators. A detailed example using predefined "G_F" and "α_{em}" SMEFT input schemes can be found in the file code/smeft_input_scheme.m (see routine SMEFTInputScheme).

Gauge and Higgs sector		Quark sector		Lepton sector	
UserInput$vev	v	UserInput$MQU	m_u	UserInput$MLE	m_e
UserInput$GW	$\bar{g}$	UserInput$MQC	m_c	UserInput$MLM	m_μ
UserInput$G1	$\bar{g}'$	UserInput$MQT	m_t	UserInput$MLT	m_τ
UserInput$GS	$\bar{g}_s$	UserInput$MQD	m_d	UserInput$MVE	m_{ν_e}
UserInput$hlambda	λ	UserInput$MQS	m_s	UserInput$MVM	m_{ν_μ}
UserInput$MZ	M_Z	UserInput$MQB	m_b	UserInput$MVT	m_{ν_τ}
UserInput$MW	M_W	UserInput$CKM	K	UserInput$PMNS	U
UserInput$MH	M_H				

Table 2.2: Variables and their names in SmeftFR v3 that should be determined to properly define input scheme.

2.4 Using SmeftFR v3

2.4.1 Installation

SmeftFR v3 utilizes the FeynRules package to derive Feynman rules. To ensure proper functioning of SmeftFR , it is essential to ensure that the latter is installed properly. The most recent version of FeynRules , along with detailed installation and usage instructions, can be found at the following address:

https://feynrules.irmp.ucl.ac.be

Once this requirement is satisfied, SmeftFR v3 can be downloaded from the following address:

https://www.fuw.edu.pl/smeft/

One can find there the latest SmeftFR version, with all necessary files, the manual, news, and information regarding the package and its usage. To ensure proper functioning of SmeftFR v3, one should use it with Mathematica v12.1 and FeynRules 2.3.49 or newer. To install the package, one should download the .zip file containing the latest SmeftFR version (currently it is v3.02) and unpack it into the following FeynRules directory:

Models/SMEFT_N_NN

where _N_NN refers to the SmeftFR package version. Once unpacked, the main $FeynRulesPath has to be set properly in the smeft_fr_init.m and smeft_fr_interfaces.m files, corresponding to the main FeynRules installation directory. For non-standard installations (not advised!), the variable SMEFT$Path also has to be updated accordingly.

2.4.2 Code structure

The full general SMEFT Lagrangian, which includes the dimension-5, -6 and bosonic -8 operators is very complicated, and leads to lengthy and CPU time-consuming numerical calculations that may last for hours or even days on a standard PC. However, in most cases, we are interested in the effects of the subset of all higher-dimensional operators on the studied phenomena (although one has to be careful here, as in general operators may mix under renormalisation [98–100]). For this reason, SmeftFR v3 can dynamically calculate the Feynman rules for a chosen subset of SMEFT WCs, which significantly speeds up the calculations.

The structure of the code and its flow are illustrated graphically in Figure 2.1 and can be divided into three main steps:

1. First, the routine relating "default" and "predefined"/"user-defined" input parameters and WCs is executed, assigning the correct numerical values to them. Then, two FeynRules model files — one for the gauge and one for the mass basis — are dynamically generated, including all the information required to describe interactions in various input parametrizations.

2. Second, the SMEFT Lagrangian in the gauge basis is initialized, transformed analytically to the mass basis, and used to generate the Feynman rules in the mass basis. This procedure also generates relations for the Z_X normalization constants in terms of the "default" and "predefined"/"user-defined" input parameters, without inserting those relations back into the Lagrangian (which saves a significant amount of computation time). The resulting mass basis Lagrangian and Feynman rules are written in terms of Z_X constants. The expressions for the Z_X are also derived up to the desired $1/\Lambda$ order of the EFT expansion (with maximal $1/\Lambda^4$). It is important to keep in mind that for a consistent $1/\Lambda$ expansion, one has to once again truncate the higher-order terms once explicit formulas for the Z_X factors are inserted into the Lagrangian and Feynman rules. The resulting mass basis Lagrangian, Feynman rules, and Z_X expressions are saved locally on disk.

3. Finally, one can use the previously generated mass basis SMEFT Lagrangian to export the generated Feynman rules to one of the formats supported by FeynRules through SmeftFR v3

built-in interfaces. As listed above, this includes: LaTeX, `WCxF`, `UFO` and `FeynArts` formats, with various options for output parametrization (in terms of Z_X constants, "default" SMEFT parameters, or "predefined"/"user-defined" input parameters) available.

2.4.3 Feynman rules calculation

Model initialization

Once `SmeftFR` v3 is properly installed, one can proceed with the first step in the Feynman rules calculation: generate the `FeynRules` model files. This is done by executing the following command, preceded by the selection of the relevant SMEFT operators and the initialization of numerical values of WCs:

```
SMEFTInitializeModel[Option1→Value1, Option2→Value2, ...];
```

The full set of available options is listed in Table C.2 and includes the choice of: SMEFT operators, gauge, EFT expansion order, parameter input scheme, and neutrino treatment. This command sets the stage for the Feynman rules calculation. A full list of dimension-5, dimension-6, and bosonic dimension-8 SMEFT operators available in the `SmeftFR` v3 distribution — along with the assumed naming convention — is presented in Section A. Several comments are in place here:

- To optimize `SmeftFR` v3 performance, users should select only the subset of Wilson coefficients relevant for a given analysis.
- To ensure compatibility with other SMEFT-related codes compliant with the `WCxf` format [97], the user should initialize numerical values of the SMEFT Wilson coefficients through a `WCxf` input file.
- `MajoranaNeutrino` and `Correct4Fermion` options are used to modify the analytical expressions for the Feynman rules as calculated by `FeynRules` . This is because certain `FeynRules` interfaces, such as UFO, intentionally leave the relative sign of four-fermion interactions uncorrected[1], as it is later corrected by Monte Carlo generators like MadGraph5. On the other hand, for manual or symbolic computations it is convenient to correct the form of the Feynman rules from the start, obtained when options are set to their default values.
- The current implementation of the input scheme for the CKM matrix is based on [87]. It may lead to numerically very large corrections to the CKM matrix, usually suggesting a violation of experimental bounds on flavor transitions and the need to modify the WCs. In such a case, the relevant warning is displayed and corrections are not included (this can be overwritten by setting the option `ForceCKMInput` → `True`). The maximal allowed correction to any of the CKM elements is set by the variable `SMEFT$CKMTreshold` in the `code/smeft_variables.m` file (by default set to `SMEFT$CKMTreshold=0.2`, can be modified by the user).

After execution, the `SMEFTInitializeModel` command creates two parameter model files in the `output` subdirectory:

- `smeft_par_WB.fr`: SMEFT parameter file with Wilson coefficients in gauge basis (defined as ''`Internal`'' parameters with no numerical values assigned).

[1] B. Fuks, private communication.

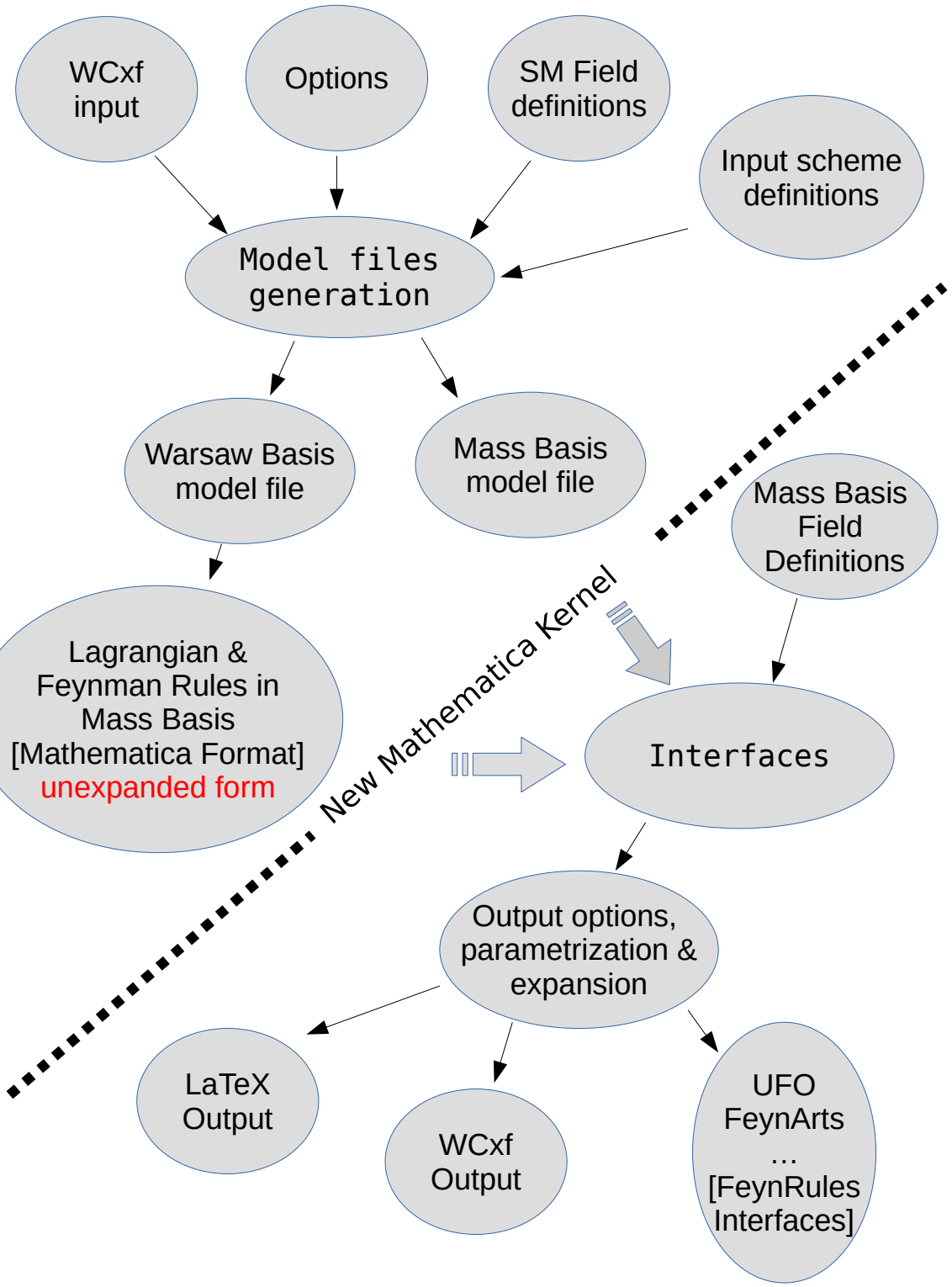

Figure 2.1: Structure of the `SmeftFR` v3 code.

- `smeft_par_MB.fr`: SMEFT parameter file with Wilson coefficients in the mass basis (defined as `"External"` parameters with numerical values of WCs imported from the input file in WCxf format).

These model files contain definitions of the "default" SMEFT parameters (i.e., SM parameters such as g, g', λ), copied from the `smeft_par_SM.fr`, `smeft_par_head_WB.fr`, and `smeft_par_head_MB.fr` files in the `definitions` subdirectory. Additionally, they contain a list of "user-defined" input parameters from the header of the `code/smeft_input_scheme.m` file. Only later values of "user-defined" parameters are copied to the model files and numerical values of parameters can be updated to include corrections from higher-order operators (thus, hand-made modifications to files in the `definitions` subdirectory are not advised and will be overwritten by the code). Field definitions used by `SmeftFR` v3 are not generated dynamically but are taken from fixed files named `smeft_fields_WB.fr` and `smeft_fields_MB.fr` in `definitions` subdirectory.

Finally, in order to manage the EFT expansion and ensure truncation of terms of higher than $\mathcal{O}\left(1/\Lambda^{2\,\mathrm{ExpansionOrder}}\right)$ order in the EFT expansion, `SmeftFR` v3 assigns an "interaction order" parameter to the SMEFT Wilson coefficients: `NP=1` for dimension-6 and `NP=2` for dimension-8 WCs. The corresponding `ExpansionOrder` parameter is also passed to the model files `smeft_par_WB.fr` and`smeft_par_MB.fr` as:

```
M$InteractionOrderLimit = {
  {QCD,99},
  {NP,ExpansionOrder},
  {QED,99}
 }
```

Lagrangian and Feynman rules in the mass basis

In the next step, we can calculate the Lagrangian and Feynman rules in the mass basis by executing the following chain of commands:

`SMEFTLoadModel[ ]`	Loads the `output/smeft_par_WB.par` model file and imports the SMEFT Lagrangian in the gauge basis for the chosen subset of bosonic operators.
`SMEFTFindMassBasis[ ]`	Finds field bilinears and analytical transformations diagonalizing the mass matrices. It also calculates the expressions for Z_X normalization constants.
`SMEFTFeynmanRules[ ]`	Analytically evaluates the SMEFT Lagrangian and Feynman rules in the mass basis to the required order in $\mathcal{O}(1/\Lambda)$, *without substituting explicit expressions for Z_X constants* (see example in Figure 2.2).
`SMEFTOutput[` *Options* `]`	By default, stores the SMEFT model file with parameters in the mass basis as `output/smeft_par_MB.m` and the mass basis Lagrangian and vertices in `output/smeft_feynman_rules.m`. To generate output in different locations, use options *ModelFile* → *filename1* and *TargetFile* → *filename2*.

Constant	Variable	Constant	Variable
Z_{g_s}	`gsnorm`	Z_G	`Gnorm`
Z_g	`gwnorm`	Z_W	`Wnorm`
$Z_{g'}$	`g1norm`	$Z_{\gamma Z}^{ij}$	`AZnorm[i,j]`
Z_h	`Hnorm`	Z_{G^0}	`G0norm`
Z_{G^+}	`GPnorm`		

Table 2.3: Names of normalization constants and corresponding internal `SmeftFR` v3 variables.

Depending on the particular choice of SMEFT parameters, the order of the EFT expansion and the options specified during the execution of the `SMEFTInitializeModel` command, these steps of the calculation may be CPU time-consuming. The user is advised to select only a subset of operators relevant for a given analysis. In a number of cases, such as treating neutrinos as Majorana particles with the dimension-5 Weinberg operator, or the inclusion of baryon and lepton number violating four-fermion operators, `FeynRules` produces warnings of the following form:

QN::NonConserv: Warning: non quantum number conserving vertex encountered!
Quantum number LeptonNumber not conserved in vertex ...

In these specific cases, such warnings should be ignored.

The results of the calculations, including the mass basis Lagrangian and the corresponding Feynman rules, are by default saved in the file `output/smeft_feynman_rules.m`. The Feynman rules and parts of the mass basis Lagrangian for various classes of interactions are organized into variables with self-explanatory names, as listed in Table C.7. Additionally, the file `output/smeft_feynman_rules.m` contains expressions for the normalization factors Z_X relating Higgs, gauge fields and their couplings in the Warsaw and the mass bases, presented in both the "default" and "user" parametrizations (see Table 2.3 for the corresponding names of code variables). In addition, formulas for tree-level corrections to the Standard Model mass parameters and Yukawa couplings are stored in variables `SMEFT$vev`, `SMEFT$MH`, `SMEFT$MW`, `SMEFT$MZ`, `SMEFT$YL[i,j]`, `SMEFT$YD[i,j]` and `SMEFT$YU[i,j]`, alongside the selected user-defined program options.

Once the calculations are finished, the expressions for the Lagrangian and vertices stored in the variables listed in Table C.7 are written in terms of the Z_X constants in unexpanded form, as presented in Figure 2.2. To generate fully expanded formulas up to the required order of the $1/\Lambda$ expansion, the routine `SMEFTExpandVertices` should be executed. For example, to expand vertices in the "default" parametrization up to the $1/\Lambda^4$ terms in the EFT expansion, one should use:

```
SMEFTExpandVertices[Input -> "smeft", ExpOrder -> 2]
```

and, for vertices in the "user" parametrization up to terms $1/\Lambda^2$:

```
SMEFTExpandVertices[Input -> "user", ExpOrder -> 1]
```

The expanded versions of the vertices are stored in variables with names ending with "Exp" (`LeptonGaugeVerticesExp, QuarkGaugeVerticesExp` etc.) and can be displayed or used in further calculations using the standard `FeynRules` format.

The evaluation of Feynman rules for vertices involving more than two fermions may be problematic for FeynRules , with possible warnings displayed. However, in most cases, these vertices are calculated correctly despite these warnings (apart from the issue of the relative sign of four-fermion diagrams mentioned earlier). In cases where this issue persists — such as the correct automatic derivation of quartic interactions involving four Majorana neutrinos — SmeftFR overwrites the FeynRules result with the correct manually calculated formulas encoded in Mathematica format.

Another remark concerns the hermicity property of the SMEFT Lagrangian. For certain types of interactions - such as four-fermion vertices involving two quarks and two leptons - the FeynRules function CheckHermicity reports non-hermicity of terms in the Lagrangian. However, such terms are indeed Hermitian if the permutation symmetries of the indices of the relevant Wilson coefficients are properly taken into account. These symmetries are automatically imposed if the numerical values of Wilson coefficients are initialized using the SMEFTInitializeMB or SMEFTToWCXF routines (see the following Section 2.4.4).

The Feynman rules for the mass basis Lagrangian are now calculated; however, the definitions of fields and parameters used to initialize the SMEFT model in FeynRules are still expressed in the gauge basis. To avoid inconsistencies, before exporting the calculated expressions to other formats in the smeft_fr_interfaces.m notebook, one should quit the current Mathematica kernel, and start a new one to load the mass basis Lagrangian along with the compatible model files, as described in next Section 2.4.4. All further calculations should be performed within this new kernel (routine SMEFTExpandVertices can also be used within this new kernel in the same way as described earlier).

2.4.4 Interfaces to various formats

Having obtained the Feynman rules in the mass basis, we can now export them (alongside corresponding values of WCs) into other formats supported by FeynRules and SmeftFR , more specifically: WCxf, LaTeX, UFO, and FeynArts. In order to do this, we have to start by opening the smeft_fr_interfaces.m notebook in a new Mathematica kernel (see comment above) and reload FeynRules , SmeftFR and the mass basis Lagrangian by calling the following routine:

SMEFTInitializeMB[*Options*]

with the allowed options provided in Table C.3. After executing SMEFTInitializeMB, the mass basis model files are loaded, and the mass basis Lagrangian is stored in a global variable named MEFT$MBLagrangian for further use by the interface routines. This step may be CPU time-consuming, depending on the specific choice of options and SMEFT operators.

WCxf output

There are two standalone SmeftFR v3 routines translating values of WCs between the WCxf and FeynRules formats that can be used independently of FeynRules and the mass basis Lagrangian initialization:

1. FeynRules → WCxf

   SMEFTToWCXF[SMEFT_Parameter_File, WCXF_File, *FirstLetter* → *SMEFT$MB*]

   where SMEFT_Parameter_File, WCXF_File define the input FeynRules and output WCxf files in the JSON format, respectively. The latter can be used to provide numerical values of WCs to

other codes compatible with the `WCxf` format (the *FirstLetter* option is only relevant if the first letter of WCs differs from that specified in the `MBFirstLetter` option of the `SMEFTInitializeModel` routine).

2. `WCxf` → `FeynRules`

   `ReadWCXFInput[ WCXF_File,` *Options* `]`
   `WCXFToSMEFT[ SMEFT_Parameter_File,` *Options*`]`

   `ReadWCXFInput` extracts the values of WCs from a `WCxf` format file, and `WCXFToSMEFT` creates `FeynRules` parameter model file including, apart from WCs, definitions and numerical values of all input parameters. All allowed options are presented in Table C.4.

LaTeX output

`SmeftFR` v3 provides a dedicated LaTeX output generator distinct from the generic `FeynRules` one. The output can be produced by executing the following command, with the full list of *Options* presented in Table C.5:

`SMEFTToLatex[` *Options* `]`

The generated LaTeX output is saved in the `output/latex` directory and contains, for the sake of clarity, only terms up to the $\mathcal{O}(1/\Lambda^2)$ order in the EFT expansion. Additionally, it omits expressions for five- and six-gluon vertices due to their high level of complexity. `SmeftFR` v3 utilizes the "axodraw.sty" style [101] to draw Feynman diagrams in the LaTeX output, which requires compilation through an intermediate *Postscript* file. Thus, instead of "standard" compilation through e.g., *pdflatex*, it is necessary to go through the following (or equivalent) set of commands:

```
latex smeft_feynman_rules.tex
dvips smeft_feynman_rules.dvi
ps2pdf smeft_feynman_rules.ps
```

For the conventions used in the `SmeftFR` LaTeX output, see Appendices A1–A3 of ref. [74].

`FeynArts` output

The mass basis Lagrangian, stored in the `SMEFT$MBLagrangian` variable, can be used to generate `FeynArts` model files by executing the following routine:

`WriteFeynArtsOutput[ SMEFT$MBLagrangian,` *Output* → *"output/FeynArts", ...*`]`

The resulting `FeynArts` model files are stored in the *"output/FeynArts"* sub-directory and can be used for further analytical calculations with programs such as `FeynCalc` or `FormCalc`.

`UFO` output

In `SmeftFR` v3, the `UFO` output format model files can be generated by calling the following routine, with all of the available options defined in Table C.6:

`SMEFTToUFO[ Lagrangian,` *Options* `]`

By default, the argument `Lagrangian` should be set to the variable storing the mass basis Lagrangian, `SMEFT$MBLagrangian`, unless the user prefers to generate vertices for a specific sub-sector of the theory. This can be done by specifying instead one of the variables defined in Table C.7, with obvious name replacements like `LeptonGaugeVertices` → `LeptonGaugeLagrangian`, etc. One can note that the `SMEFTToUFO` command is distinct from the `FeynRules` built-in `WriteUFO` command due to the following reason. The `UFO` format requires an additional parameter — "interaction order" (IO) — to be assigned to all couplings. This helps Monte Carlo generators, such as `MadGraph5`, to handle the maximal order of diagrams included in a process under consideration. By default, the standard `FeynRules UFO` interface assigns QED IO= -1 to the Higgs boson vev, v, as it is numerically large and can effectively cancel the suppression from smaller Yukawa or gauge couplings. In the SM, such procedure never leads to a total negative IO for any vertex. However, in the case of SMEFT, vertices proportional to higher powers of v may have a negative total "QED" IO. This leads to warnings and termination when such a model is imported to `MadGraph5`. Fortunately SMEFT vertices have an additional type of IO assigned, "NP=0,1,2", defining their EFT order (which is $1/\Lambda^{2\,\mathrm{NP}}$). This labeling is sufficient for MC generators to truncate amplitudes correctly. For this reason, `SMEFTToUFO` command removes "QED" IO from all vertices proportional to WCs of higher-dimension operators (this can be switched off by setting the relevant option).

It is important to note that some Monte Carlo generators, such as `MadGraph 5`, support only real values for input parameters. Thus, to ensure that the `UFO` output is working properly, one should set the option `RealParameters` → `True` when calling the `SMEFTInitializeMB` routine. Additionally, `MadGraph5` uses hard-coded names for the QED and QCD coupling constants (`ee, aEWM1, aS`). For compatibility, `SmeftFR` v3 preserves these names, copying them into `UFO` model files independently of how the "user-defined" input parameters are named. If necessary for compatibility with other codes, additional "special" variable names can be added to `SmeftFR` by updating the routine `UpdateSpecialParameters` in the file `smeft_parameters.m`.

If four-fermion vertices are included in the SMEFT Lagrangian, the `UFO` model files generator prints the following warning (similar warnings may also appear when using other `FeynRules` output routines):

Warning: Multi-Fermion operators are not yet fully supported!

Although, in our experience, the `UFO` output seems to work properly also for four-fermion interactions despite the warning, it should be treated with care and limited trust - performing appropriate checks is left to the user.

The inclusion of baryon and lepton number violating (BLV) four-fermion interactions leads to additional problems in the `UFO` model files, with `MadGraph5` displaying warnings that these interactions are not yet supported and aborting process generation. For this reason, such terms are, by default, not included in the `SMEFT$MBLagrangian` variable, unless the option `IncludeBL4Fermion` in the `SMEFTInitializeMB` routine is explicitly set to `True`. When this option is enabled, the `FeynArts` output seems to work properly.

Finally, one should note that the `FeynRules` interfaces sometimes appear to be "non-commuting". For example, calling the `FeynArts` output routine first may lead to errors in the subsequent execution of the `UFO` interface, such as signaling problems with the incorrect handling of vertices containing explicit $\sigma^{\mu\nu}$ Dirac matrices or issues with the color indices of the $SU(3)$ group structure constants, while the routines called in the opposite order are both working properly. Therefore, it is safer to generate one type of output at a time and reinitialize the model in the mass basis. The WCxf and

LaTeX generators do not suffer from such issues and can be used safely together with others.

Forms of output

`SmeftFR` v3 can calculate and export interaction vertices in three forms, among which users can choose by selecting a particular version of the `Expansion` option in `Output` routines:

1. `Expansion` → `"none"`
   Interaction vertices are given in terms of "default" parameters, WCs and Z_X normalization constants. Such output is compact and fast to produce. Also, it is the most universal one — adding additional higher-order operators (e.g., fermionic $d = 8$ operators or even higher EFT orders), apart from directly appearing in new vertices relevant to a given operator, can be accommodated by adding new contributions to expressions for Z_X constants. In this form, however, consistent expansion to a given EFT order is not clearly defined, as it can be done only after substituting explicit expressions for Z_X. All normalization constants with corresponding internal variables are presented in Table 2.3. Sample vertices in this parametrization are displayed in Figure 2.2.

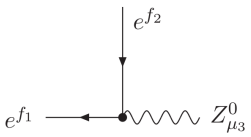

$$
\begin{aligned}
&+ \quad \frac{i}{2}\delta_{f_1 f_2}\left(\bar{g}' Z_{g'} Z^{21}_{\gamma Z}\left(\gamma^{\mu_3} P_L + 2\gamma^{\mu_3} P_R\right) + \bar{g} Z_g Z^{11}_{\gamma Z}\gamma^{\mu_3} P_L\right)\\
&- \quad \sqrt{2} v Z^{21}_{\gamma Z} p_3^{\nu}\left(C^{f_2 f_1}_{eB*}\sigma^{\mu_3\nu} P_L + C^{f_1 f_2}_{eB}\sigma^{\mu_3\nu} P_R\right)\\
&+ \quad \sqrt{2} v Z^{11}_{\gamma Z} p_3^{\nu}\left(C^{f_2 f_1}_{eW*}\sigma^{\mu_3\nu} P_L + C^{f_1 f_2}_{eW}\sigma^{\mu_3\nu} P_R\right)\\
&+ \quad \frac{iv^2}{2}\gamma^{\mu_3} P_R\left(\bar{g} Z_g Z^{11}_{\gamma Z} - \bar{g}' Z_{g'} Z^{21}_{\gamma Z}\right) C^{f_1 f_2}_{\varphi e}\\
&+ \quad \frac{iv^2}{2}\gamma^{\mu_3} P_L\left(\bar{g} Z_g Z^{11}_{\gamma Z} - \bar{g}' Z_{g'} Z^{21}_{\gamma Z}\right) C^{f_1 f_2}_{\varphi l 1}\\
&+ \quad \frac{iv^2}{2}\gamma^{\mu_3} P_L\left(\bar{g} Z_g Z^{11}_{\gamma Z} - \bar{g}' Z_{g'} Z^{21}_{\gamma Z}\right) C^{f_1 f_2}_{\varphi l 3}
\end{aligned}
$$

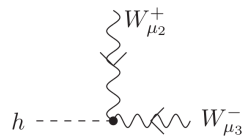

$$
+\frac{i\bar{g}^2 v}{2Z_h}\eta_{\mu_2\mu_3} + \frac{4iv}{Z_g^2 Z_h}\left(p_2^{\mu_3} p_3^{\mu_2} - p_2 \cdot p_3 \eta_{\mu_2\mu_3}\right) C_{\varphi W}
$$

Figure 2.2: $Z\ell^+\ell^-$ and hW^+W^- vertices in terms of of Z_X couplings (including a sample list of operators up to the dimension-6). $C_{\varphi W} \to C_{\varphi W}/\Lambda^2$ convention is assumed.

2. `Expansion` → `"smeft"`
   The "default" SMEFT parametrization, with vertices given in terms of "default" parameters and WCs, and with shifts of SM fields and normalization couplings expanded accordingly. The result is expanded to the desired EFT order ($d = 4$, 6 or 8). Sample vertices in this parametrization are presented in Figure 2.3.

3. `Expansion` → `"user"`
   Interaction vertices are given directly in terms of user-defined input parameters and WCs, again with shifts of SM fields and couplings expanded accordingly. The result is expanded up to the desired EFT order ($d = 4$, 6 or 8). Sample vertices for the (G_F, M_Z, M_W, M_H) input scheme in the electroweak sector (see the discussion in Section 2.3.1) are presented in Figure 2.4.

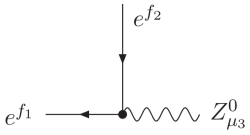

$$
\begin{aligned}
&- \frac{i}{2\sqrt{\bar{g}'^2+\bar{g}^2}}\delta_{f_1f_2}\left(\left(\bar{g}'^2-\bar{g}^2\right)\gamma^{\mu_3}P_L+2\bar{g}'^2\gamma^{\mu_3}P_R\right)\\
&+ \frac{i\bar{g}'\bar{g}v^2}{2\left(\bar{g}'^2+\bar{g}^2\right)^{3/2}}\delta_{f_1f_2}\left(\left(\bar{g}'^2-\bar{g}^2\right)\gamma^{\mu_3}P_L-2\bar{g}^2\gamma^{\mu_3}P_R\right)C_{\varphi WB}\\
&+ \frac{\sqrt{2}\bar{g}'v}{\sqrt{\bar{g}'^2+\bar{g}^2}}p_3^{\nu}\left(C_{eB*}^{f_2f_1}\sigma^{\mu_3\nu}P_L+C_{eB}^{f_1f_2}\sigma^{\mu_3\nu}P_R\right)\\
&+ \frac{\sqrt{2}\bar{g}v}{\sqrt{\bar{g}'^2+\bar{g}^2}}p_3^{\nu}\left(C_{eW*}^{f_2f_1}\sigma^{\mu_3\nu}P_L+C_{eW}^{f_1f_2}\sigma^{\mu_3\nu}P_R\right)\\
&+ \frac{1}{2}iv^2\sqrt{\bar{g}'^2+\bar{g}^2}C_{\varphi e}^{f_1f_2}\gamma^{\mu_3}P_R+\frac{1}{2}iv^2\sqrt{\bar{g}'^2+\bar{g}^2}C_{\varphi l1}^{f_1f_2}\gamma^{\mu_3}P_L\\
&+ \frac{1}{2}iv^2\sqrt{\bar{g}'^2+\bar{g}^2}C_{\varphi l3}^{f_1f_2}\gamma^{\mu_3}P_L
\end{aligned}
$$

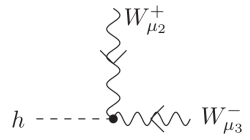

$$
\begin{aligned}
&+ \frac{1}{2}i\bar{g}^2v\eta_{\mu_2\mu_3}+\frac{1}{2}i\bar{g}^2v^3\eta_{\mu_2\mu_3}C_{\varphi\Box}-\frac{1}{8}i\bar{g}^2v^3\eta_{\mu_2\mu_3}C_{\varphi D}\\
&+ 4ivC_{\varphi W}\left(p_2^{\mu_3}p_3^{\mu_2}-p_2\cdot p_3\eta_{\mu_2\mu_3}\right)
\end{aligned}
$$

Figure 2.3: Same as in Figure 2.2 but in default ($\bar{g}'$, $\bar{g}$, v) parametrization scheme (the Z_X couplings are expanded up to the dimension-6 terms).

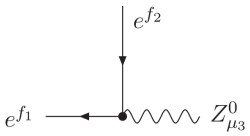

$$
\begin{aligned}
&- \frac{i2^{1/4}\sqrt{G_F}}{M_Z}\delta_{f_1f_2}\left(\left(M_Z^2-2M_W^2\right)\gamma^{\mu_3}P_L+2\left(M_Z^2-M_W^2\right)\gamma^{\mu_3}P_R\right)\\
&+ \frac{i2^{3/4}M_W\sqrt{M_Z^2-M_W^2}}{M_Z\sqrt{G_F}}\delta_{f_1f_2}C_{\varphi WB}\gamma^{\mu_3}\\
&+ \frac{2^{1/4}\sqrt{M_Z^2-M_W^2}}{\sqrt{G_F}M_Z}p_3^{\nu}\left(C_{eB*}^{f_2f_1}\sigma^{\mu_3\nu}P_L+C_{eB}^{f_1f_2}\sigma^{\mu_3\nu}P_R\right)\\
&+ \frac{2^{1/4}M_W}{\sqrt{G_F}M_Z}p_3^{\nu}\left(C_{eW*}^{f_2f_1}\sigma^{\mu_3\nu}P_L+C_{eW}^{f_1f_2}\sigma^{\mu_3\nu}P_R\right)\\
&+ \frac{i\,\delta_{f_1f_2}}{2^{9/4}\sqrt{G_F}M_Z}C_{\varphi D}\left(\left(2M_W^2+M_Z^2\right)\gamma^{\mu_3}P_L+2\left(M_W^2+M_Z^2\right)\gamma^{\mu_3}P_R\right)\\
&+ \frac{iM_Z}{2^{1/4}\sqrt{G_F}}C_{\varphi e}^{f_1f_2}\gamma^{\mu_3}P_R+\frac{iM_Z}{2^{1/4}\sqrt{G_F}}C_{\varphi l1}^{f_1f_2}\gamma^{\mu_3}P_L+\frac{iM_Z}{2^{1/4}\sqrt{G_F}}C_{\varphi l3}^{f_1f_2}\gamma^{\mu_3}P_L\\
&+ \frac{i\,\delta_{f_1f_2}}{2^{9/4}\sqrt{G_F}M_Z}C_{ll}^{2112}\left(\left(M_Z^2-2M_W^2\right)\gamma^{\mu_3}P_L+2\left(M_Z^2-M_W^2\right)\gamma^{\mu_3}P_R\right)\\
&+ \frac{i\,\delta_{f_1f_2}}{2^{9/4}\sqrt{G_F}M_Z}\left(C_{\varphi l3}^{11}+C_{\varphi l3}^{22}\right)\left(\left(2M_W^2-M_Z^2\right)\gamma^{\mu_3}P_L+2\left(M_W^2-M_Z^2\right)\gamma^{\mu_3}P_R\right)
\end{aligned}
$$

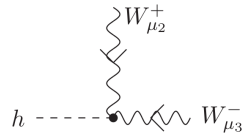

$$
\begin{aligned}
&+ i2^{3/4}\sqrt{G_F}M_W^2\eta_{\mu_2\mu_3}+\frac{i2^{3/4}M_W^2}{\sqrt{G_F}}\eta_{\mu_2\mu_3}C_{\varphi\Box}-\frac{iM_W^2}{2^{3/4}\sqrt{G_F}}\eta_{\mu_2\mu_3}C_{\varphi D}\\
\alpha_{em}\ &- \frac{iM_W^2}{2^{3/4}\sqrt{G_F}}\eta_{\mu_2\mu_3}C_{ll}^{2112}+\frac{iM_W^2}{2^{3/4}\sqrt{G_F}}\eta_{\mu_2\mu_3}\left(C_{\varphi l3}^{11}+C_{\varphi l3}^{22}\right)\\
&+ \frac{i2^{7/4}}{\sqrt{G_F}}C_{\varphi W}\left(p_2^{\mu_3}p_3^{\mu_2}-p_2\cdot p_3\eta_{\mu_2\mu_3}\right)
\end{aligned}
$$

Figure 2.4: Same as in Figure 2.2 but in the (G_F, M_Z, M_W, M_H) input scheme (the Z_X couplings are expanded up to the dimension-6 terms).

Further extensions

At this point, one can think of many possible further extensions of SmeftFR , beyond version 3. We list a number of potential future directions.

1. **Inclusion of fermionic dimension-7 and dimension-8 operators**
   As we pointed out in Section 2.2.1, we decided not to include fermionic dimension-7 and -8 operators due to their potential limited impact on studied phenomena and their very high number that makes this endeavor very time- and effort-consuming. However, users who are interested in extending SmeftFR v3 with a particular set of fermionic dimension-7 or -8 operators can follow the detailed prescription describing this procedure, that can be found in Appendix D or at the following address:

   https://www.fuw.edu.pl/smeft/FermionDim8Operators.pdf

2. **Inclusion of dimension-higher-than-8 operators**
   Inclusion of dimension-higher-than-8 operators would require several minor changes in the code and could be done with a finite amount of time and effort. However, as mentioned at the beginning of this chapter for most of the applications that we can think of, dimension-8 should be sufficient and dimension-9 and -10 (or higher) contributions should be negligible. Also, non-negligible dimension-9 or -10 contributions would suggest problems with the validity of the EFT expansion.

3. **Additional input schemes**
   As described in Section 2.3.1, the user can define their own input parameter schemes that will be compatible with SmeftFR v3 if this procedure is followed. On the side of the authors of the code, we decided to include two of the most popular electroweak input schemes, and we leave users with the task of including their own, if necessary. As for other sectors, apart from the CKM matrix K input scheme, we are not aware of any other parameter schemes that could be included (but this may change in the future).

2.4.5 Tests and validation

SmeftFR v3 has been thoroughly validated by the authors of this code through various analytical and numerical tests, always finding very good or almost perfect agreement with other corresponding publicly available software packages.

Analytical tests

For analytical tests, we have used SmeftFR v3 FeynArts output and utilized the following chain of programs:

SmeftFR $\rightarrow$ FeynArts $\rightarrow$ FormCalc/FeynCalc

to perform the following set of analytical tests.

1. **Goldstone-Boson-Equivalence-Theorem (GBET)**
   According to the GBET [102–105], matrix elements of longitudinal polarizations for tree level

vector-boson scattering processes should be equal to matrix elements for the same process, but with vector bosons replaced by Goldstone bosons:

$$\mathcal{M}\left(V_L V_L \to V_L V_L\right) \xrightarrow{s \gg M} \mathcal{M}\left(GG \to GG\right), \quad V = (W^{\pm}, Z), \quad G = (G^0, G^{\pm}). \tag{2.35}$$

We checked explicitly that this identity holds up in SMEFT up to the $\mathcal{O}(1/\Lambda^4)$ order in the EFT expansion, and that this result is independent of the input scheme choice. An example of such amplitude is presented in Section 2.5, Eq. (2.41).

2. **Positivity bounds**
   Another interesting test of `SmeftFR` v3 output for dimension-8 SMEFT operators comes from the positivity constraints on WCs [106, 107]. Analyticity of the amplitude, the optical theorem and the Froissart bound lead to the conclusion, that for any 2-2 elastic scattering amplitude of SM particles, the following identity should hold:

$$\frac{d^2}{ds^2}\,\mathcal{M}(ij \to ij)(s, t = 0) \;\geq 0\,, \tag{2.36}$$

   where i, j are the SM fields, and s, t are the Mandelstam variables. $Q^{(1,2,3)}_{\varphi^4 D^4}$ dimension-8 operators can potentially affect the scattering matrix elements between Higgs and longitudinal components of vector bosons, leading to the corrections $\propto s^2/\Lambda^4$, and can therefore be subjugated to the condition (2.36). Indeed, using the `SmeftFR` v3 `FeynArts` output, we checked that these matrix elements lead to the following set of conditions:

$$hh \to hh \qquad \Longrightarrow \quad C^{(1)}_{\varphi^4 D^4} + C^{(2)}_{\varphi^4 D^4} + C^{(3)}_{\varphi^4 D^4} \geq 0\,, \tag{2.37}$$

$$Z_L h \to Z_L h \qquad \Longrightarrow \quad C^{(2)}_{\varphi^4 D^4} \geq 0\,, \tag{2.38}$$

$$W^+_L h \to W^+_L h \qquad \Longrightarrow \quad C^{(1)}_{\varphi^4 D^4} + C^{(2)}_{\varphi^4 D^4} \geq 0\,. \tag{2.39}$$

   All other longitudinal vector bosons scattering amplitudes satisfy these inequalities, e.g., $W^+_L W^+_L \to W^+_L W^+_L$ amplitude gives:

$$W^+_L W^+_L \to W^+_L W^+_L \quad \Longrightarrow \quad C^{(1)}_{\varphi^4 D^4} + C^{(2)}_{\varphi^4 D^4} + C^{(3)}_{\varphi^4 D^4} \geq 0\,, \tag{2.40}$$

   already satisfied by (2.37). Results obtained by us are in agreement with [106] and are again independent of input scheme.

3. **Ward identities**
   Finally, we used the Feynman rules generated by `SmeftFR` v3 to check various Ward identities, always finding very good agreement.

Numerical tests

In order to test the validity of `SmeftFR` , we performed several types of numerical crosschecks against already existing codes using the `SmeftFR` v3 `UFO` outputs.

1. We compared **cross-sections** for various processes obtained with `SmeftFR` v3 against the results obtained with the `SMEFT@NLO` [71] package up to terms of order $\mathcal{O}(1/\Lambda^2)$ in the EFT expansion – Table E.1 in Appendix E (note that `SMEFT@NLO`, `Dim6Top` [70] and `SMEFTsim` [68] have been formally validated up to this order [108], so it is sufficient to compare with only one of these codes).

2. We compared **matrix elements** for various processes obtained with `SmeftFR` against the results obtained with the `SMEFTsim` package up to terms of order $\mathcal{O}(1/\Lambda^2)$ in the EFT expansion, testing all implemented dimension-6 operators (apart from the B- and L- violating ones) — Tables E.2, E.3 in Appendix E.

3. We compared matrix elements for various processes obtained with `SmeftFR` against the results obtained with the code described in ref. [109] (available at `https://feynrules.irmp.ucl.ac.be/wiki/AnomalousGaugeCoupling`) up to terms of order $\mathcal{O}(1/\Lambda^4)$ in the EFT expansion, testing all operators considered in [109] — Table E.5 in Appendix E.

For the purpose of these comparisons, we used the default predefined "G_F" input parameter scheme, with numerical values of parameters initialized as central values from [110]. Moreover, the CKM and PMNS mixing matrices were assumed to be equal to identity matrices. More details, including comparison tables containing specific processes and WCs, can be found under in Appendix E, or at the following link:

`https://www.fuw.edu.pl/smeft/Validation.pdf`

2.5 `SmeftFR` v3 by an example

Having described the features of `SmeftFR` v3, it is very instructive to provide a step-by-step example of its application to give a deeper insight into the program's working and capabilities. For this purpose, we decided to present a calculation of a vector-boson scattering (VBS) process at the LHC (first presented in [55]). An example of such a process is shown in Figure 2.5 (W bosons can be alternatively replaced by Z bosons). This class of processes is particularly interesting due to its importance in probing the electroweak sector and its potential sensitivity to BSM physics (see, e.g. [40]).

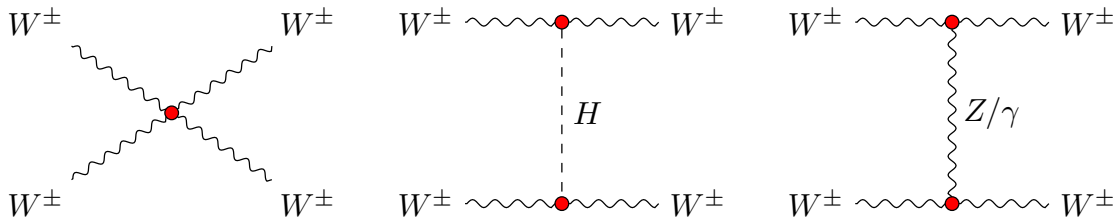

Figure 2.5: Diagrams of the same-sign $W^\pm$ vector-boson scattering process. The red dots indicate vertices where the SMEFT corrections can be inserted.

2.5.1 Model initialization and Feynman rules calculation

After loading the `FeynRules` and `SmeftFR` v3 codes in the `Mathematica` `SmeftFR_init.nb` notebook included with the `SmeftFR` distribution, the first step is to define the set of operators in the gauge basis. In this case, we choose the following dimension-6 and dimension-8 operators, which may have a significant impact on vector-boson scattering processes (the naming convention is described in appendix A).

```
In[1]:= OpList6={"phi","phiBox","phiD","phiW","phiWB","phiB","W"};
        OpList8={"phi8","phi6Box","phi6D2","phi4n1","phi4n2","phi4n3"};
```

One can identify these operators with the φ^6, $\varphi^4 D^2$ and $X^2\varphi^2$ classes for dimension-6 (Table A.1) and φ^8, $\varphi^6 D^2$ and $\varphi^4 D^4$ classes for dimension-8 operators (Table A.2). In the next step, we initialize the SMEFT Lagrangian with the chosen set of available options:

```
In[2]:= SMEFTInitializeModel[Operators→OpList,
        Gauge→Rxi,
        ExpansionOrder→2,
        WCXFInitFile→WCXFInput,
        InputScheme→"GF",
        CKMInput→"no",
        RealParameters→True,
        MaxParticles→4];
```

We chose to generate the Feynman rules in the R_ξ gauge up to the $\mathcal{O}(1/\Lambda^4)$ order in the EFT expansion, including vertices with the maximal number of four external legs. The numerical values for the Wilson coefficients were provided in the `WCXFInput` file. We selected the "G_F" input parameter scheme for the electroweak sector, and neglected SMEFT corrections to the CKM matrix. With this setup, we can execute the chain of commands described in Section 2.4.3 to produce model files, calculate the Lagrangian in the gauge basis, identify field bilinears and analytical transformations to diagonalize mass matrices, and finally obtain the Lagrangian the in mass basis with the corresponding Feynman rules up to the $\mathcal{O}(1/\Lambda^4)$ order in the EFT expansion. At this stage, field normalization constants are not expanded. This whole chain takes ~ 7 minutes on a typical laptop.[2] The obtained vertices in this form are stored in the `"/output/smeft_feynman_rules.m"` file.

Once the calculation is finished, we can display the vertex expression, e.g. $h\gamma\gamma$ in the previously adopted "G_F" input scheme by executing the following command:

```
In[3]:= SMEFTExpandVertices[Input→"user",ExpOrder→2];

        SelectVertices[GaugeHiggsVerticesExp,SelectParticles→{H,A,A}]
```

$$
\begin{aligned}
\text{Out[3]}= \{\{\{A,1\},\{A,2\},\{H,3\}\},\ & \left(\frac{1}{\Lambda^2}\right)^2 \frac{i}{2^{3/4}\ G_F^{3/2}\ M_Z^2\ (M_W^2-M_Z^2)} \\
& \Big(-C^{\varphi D}\ C^{\varphi W}\ M_W^4-8\ (C^{\varphi W})^2\ M_W^4+4\ (C^{\varphi WB})^2\ M_W^4+16\ (C^{\varphi W})^2\ M_W^2\ M_Z^2-4\ (C^{\varphi WB})^2\ M_W^2\ M_Z^2+C^{\varphi D}\ C^{\varphi W}\ M_Z^4 \\
& -8\ (C^{\varphi W})^2\ M_Z^4-C^{\varphi D}\ C^{\varphi WB}\ M_W^3\ \sqrt{-M_W^2+M_Z^2}-12\ C^{\varphi W}\ C^{\varphi WB}\ M_W^3\ \sqrt{-M_W^2+M_Z^2}+12\ C^{\varphi W}\ C^{\varphi WB}\ M_W\ M_Z^2\ \sqrt{-M_W^2+M_Z^2} \\
& +8\ (C^{\varphi B})^2\ (M_W^4-M_W^2\ M_Z^2)+C^{\varphi B}\ M_W\ (M_W^2-M_Z^2)\ (4\ C^{\varphi Box}\ M_W+C^{\varphi D}\ M_W-4\ C^{\varphi WB}\ \sqrt{-M_W^2+M_Z^2}) \\
& -4\ C^{\varphi Box}\ (M_W^2-M_Z^2)\ (C^{\varphi W}\ M_W^2-C^{\varphi W}\ M_Z^2+C^{\varphi WB}\ M_W\ \sqrt{-M_W^2+M_Z^2})\Big)(p_1^{\mu_2}\ p_2^{\mu_1}-\eta_{\mu_1,\mu_2}\ p_1\cdot p_2) \\
& +\frac{1}{\Lambda^2}\frac{2\ i\ 2^{3/4}}{\sqrt{G_F}\ M_Z^2}\left(C^{\varphi B}\ M_W^2-C^{\varphi WB}\ M_W\ \sqrt{-M_W^2+M_Z^2}+C^{\varphi W}\ (-M_W^2+M_Z^2)\right)(p_1^{\mu_2}\ p_2^{\mu_1}-\eta_{\mu_1,\mu_2}\ p_1\cdot p_2)\}\}
\end{aligned}
$$

One can easily identify the dimension-6 and dimension-6^2 contributions. Note that the whole expression is proportional to the $(p_1^{\mu_2}p_2^{\mu_1} - g^{\mu_1\mu_2}p_1\cdot p_2)$ Lorentz factor, as expected from the requirement of gauge invariance. Purely dimension-8 contributions can be displayed by printing other expressions,

[2] Running times throughout are referring to a `i7,2.8GHz,16GB-RAM` computer with `Linux Ubuntu 22.04`.

e.g., for the $ZZZZ$ vertex. This vertex is first generated at this level of the EFT expansion, with contributions from the $Q_{\varphi^4 D^4}^{(1),(2),(3)}$ dimension-8 operators:

```
In[4]:= SMEFTExpandVertices[Input→"user",ExpOrder→2];
```

```
Out[4]= {{{{Z,1},{Z,2},{Z,3},{Z,4}},
   2 i (C^φ4n1+C^φ4n2+C^φ4n3) (1/Λ^2)^2 M_Z^4 (η_μ1,μ4 η_μ2,μ3+η_μ1,μ3 η_μ2,μ4+η_μ1,μ2 η_μ3,μ4)}}
```

At this stage, the user can export the chosen vertices in one of the available output formats: using the "G_F" parameter input scheme with the **''user''** option, in the default parameter scheme with the **''smeft''** option, or in the unexpanded version by selecting **''none''**.

2.5.2 Interfaces and output generation

We can now generate the chosen outputs using the built-in `SmeftFR` v3 interfaces to LaTeX, `UFO`, `FeynArts` or `WCxf` formats. In order to achieve this (following steps detailed in Section 2.4.4), we have to `Quit[]` the current *Mathematica* kernel and open the `SmeftFR_interfaces.nb` notebook. Then, after loading the `FeynRules` and `SmeftFR` codes, the mass basis Lagrangian can be reloaded by executing the following command:

```
In[5]:= SMEFTInitializeMB[Expansion→"user", Include4Fermion→False];
```

After the calculation is completed, the entire SMEFT Lagrangian in the mass basis is stored in the variable `SMEFT$MBLagrangian` for further use by interface routines. This Lagrangian is expressed in the "user", "G_F" predefined input scheme, and includes terms up to $\mathcal{O}(1/\Lambda^4)$ order in the EFT expansion.

At this point, we can export Wilson coefficients from `FeynRules` to `WCxf` or LaTeX(only dimension-6 terms) formats. In case of this calculation, we further focus on `FeynArts` and `UFO` outputs.

`FeynArts` output

`SmeftFR` v3 can generate `FeynArts` output by running the following `FeynRules` command:

```
In[6]:= WriteFeynArtsOutput[SMEFT$MBLagrangian,
        Output→FileNameJoin[{SMEFT$Path,"output","FeynArts","FeynArts"}]];
```

This calculation, depending on the complexity of the model, can take several hours to complete (in this case, approximately 3 hours). Once finished, the `SmeftFR` v3 model files can be used with external tools, like `FormCalc` or `FeynCalc`, to compute quantities of interest, such as helicity amplitudes for specific processes. In this case, we calculated helicity amplitudes for the VBS process $W^+W^+ \to W^+W^+$. Isolating the longitudinal polarizations, we were able to arrive at relatively compact expressions for the amplitudes at high energies, $s \gg M_W^2$:

$$\mathcal{M}_{W_L^+W_L^+\to W_L^+W_L^+}(s,\theta) = -2\sqrt{2}G_F M_H^2\left[1-\frac{M_Z^2}{M_H^2}\left(1-\frac{4}{\sin^2\theta}\right)\right] \qquad (\mathbf{SM})$$

$$+ \quad (2C_{\varphi\Box}+C_{\varphi D})\,\frac{s}{\Lambda^2} \qquad (\mathbf{dim-6})$$

$$
\begin{aligned}
&+ \quad \Big[8C_{\varphi^6\Box} + 2C_{\varphi^6 D^2} + 16(C_{\varphi\Box})^2 + (C_{\varphi D})^2 - 8C_{\varphi\Box}\, C_{\varphi D} \\
&- \quad 16(C^{(1)}_{\varphi^4 D^4} + 2C^{(2)}_{\varphi^4 D^4} + C^{(3)}_{\varphi^4 D^4}) G_F M_W^2 \Big] \frac{\sqrt{2}}{8\, G_F \Lambda^2} \frac{s}{\Lambda^2} \qquad (\mathbf{dim-6})^{\mathbf{2}} \\
&+ \quad \Big[(3+\cos 2\theta)(C^{(1)}_{\varphi^4 D^4} + C^{(3)}_{\varphi^4 D^4}) + 8C^{(2)}_{\varphi^4 D^4}\Big] \frac{s^2}{8\Lambda^4} \qquad (\mathbf{dim-8}) \qquad (2.41)
\end{aligned}
$$

This result is consistent with [40] up to the $\mathcal{O}(1/\Lambda^2)$ order in the EFT expansion, while the $\mathcal{O}(1/\Lambda^4)$ terms are presented here for the first time. This amplitude was also used for the GBET validation discussed in Section 2.4.5.

`UFO` output and `MadGraph5`

`SmeftFR` v3 `UFO` model files can serve as input for running realistic Monte Carlo simulations, and can be generated by executing the following command:

```
In[7]:= SMEFTToUFO[ SMEFT$MBLagrangian, CorrectIO→True ];
```

where the `CorrectIO` option ensures correct interaction order assignment for MC generators. The generation of the `UFO` output can be quite time consuming and may take up to several hours (in this case it was approximately 2 hours), leading to lengthy calculations by Monte Carlo generators (here we used `MadGraph5`). An important comment is in place here. Very often, the goal of the calculation is to examine the impact of a single SMEFT operator on the process of interest. To achieve this, the user has two options:

1. Generate a single, complex model containing many WCs and manually set only one of them to a non-zero value using `MadGraph5` built-in `set` command.

2. Generate separate `UFO` models, each with one non-zero WC, and load a separate model for each run.

The latter approach can significantly speed up calculations and may be particularly attractive for users with limited CPU resources. To our knowledge, among currently available software, only `SmeftFR` v3 is able to generate such "individual" model files for one operator at a time.

Once the `SmeftFR` v3 successfully generated the `UFO` model files, we can use them to compute matrix elements and cross-sections with `MadGraph5`. Table 2.4 presents the results of such cross-section calculation for our example of a VBS process at the LHC. We divided the results by orders of the EFT expansion (SM, $\mathcal{O}(1/\Lambda^2)$ and $\mathcal{O}(1/\Lambda^4)$) to highlight the potential importance of higher-order SMEFT corrections. As one can note, the quadratic effects of $(C_W)^2$ enhance the cross-section by a factor of 4400, the impact of $C^2_{\varphi\Box}$ depends on the overall sign of the WC, while the dimension-8 WC $C^{(i)}_{\varphi^4 D^4}$ enhances the cross-section by the factor of $\times 100$. All of these effects can be understood by following the analytic amplitude presented in (2.41).

2.6 Summary and conclusions

In this Chapter, we presented `SmeftFR` v3, a software package for efficient calculations within the Effective Field Theory framework, which is an important direction of research in modern particle

	SmeftFR $\mathcal{O}(1/\Lambda^2)$	SmeftFR $\mathcal{O}(1/\Lambda^4)$
p p > w+ w+ j j QCD=0		
SM	0.12456 ± 0.00029	
C_W	8.564 ± 0.020	37161 ± 83
$+C_{\varphi\Box}$	0.13387 ± 0.00032	0.20981 ± 0.00059
$-C_{\varphi\Box}$	0.14670 ± 0.00043	0.12511 ± 0.00035
$C_{\varphi 6\Box}$	-	0.12868 ± 0.00031
$C^{(i)}_{\varphi^4 D^4}$	-	10.891 ± 0.024

Table 2.4: Cross-sections (in pb) obtained using MadGraph5 v3.4.1 with UFO models provided by SmeftFR v3 at the orders $\mathcal{O}(1/\Lambda^2)$ and $\mathcal{O}(1/\Lambda^4)$ in the EFT expansion for the p p > w+ w+ j j QCD=0 process at the LHC with $\sqrt{s} = 13$ TeV and cuts: $\Delta\eta_{jj} > 2.5$, $m_{jj} > 500$ GeV. Simulations are performed in the default "G_F" electroweak input scheme with the default numerical values of input parameters. For each run, only one of the WCs has non-zero value assigned, equal to $\frac{C_i}{\Lambda^2} = \frac{4\pi}{\text{TeV}^2}$ for dim-6 and $\frac{C_i}{\Lambda^4} = \frac{(4\pi)^2}{\text{TeV}^4}$ for dim-8 operators.

physics, and a part of the broader bottom-up approach. SmeftFR v3 is a specialized tool designed as a Feynman rules generator for the Standard Model Effective Field Theory, a commonly used framework for model-independent studies of heavy physics beyond the Standard Model.

We began by emphasizing the necessity for the automation of calculations within the SMEFT. The sheer number of higher-dimensional operators rapidly growing with the EFT mass dimension, makes even the typically straightforward procedure of Feynman rules derivation highly complex. We provided a short overview of the SMEFT and its key features, including dimension-5 and -6 operators in the "Warsaw" basis, as well as bosonic dimension-8 operators. This discussion covered topics such as the mass basis derivation, canonical normalization of kinetic terms, and expressing SMEFT observables in terms of experimental inputs like G_F, α_{em}, and Higgs and gauge boson masses. These examples further highlight the importance of automation in managing the complexity of SMEFT analyses. To give readers a broader perspective, we also surveyed other publicly available numerical tools designed to address various SMEFT-related challenges.

Having justified the need for such a tool, we proceeded to describe the main features of SmeftFR v3, a new version of a well-established code, now improved with a number of new and important capabilities in comparison to its predecessors. SmeftFR v3 – "Feynman rules generator for the Standard Model Effective Field Theory", enables users to consistently produce SMEFT interaction vertices up to the $\mathcal{O}(1/\Lambda^4)$ order in the EFT expansion. These vertices can be expressed in terms of predefined or used-defined set of observable input parameters, encompassing not only the electroweak sector, but also the flavor sector through the inclusion of SMEFT corrections to the CKM matrix. The code dynamically generates FeynRules model files only for the operators corresponding to user-selected Wilson coefficients only, significantly improving the speed the calculations. SmeftFR v3 can calculate Feynman rules in unitary and R_ξ-gauges, with all other available options detailed in the main text of this Chapter. The obtained vertices and can also be exported to various formats, such as LaTeX, UFO and FeynArts, for further analyses.

A detailed description of the code's installation, usage and some additional aspects follows, including analytical and numerical consistency tests performed to ensure its correctness. Among the analytical tests, we include the Goldstone-Boson-Equivalence-Theorem, positivity bounds, and Ward

identities. On the numerical side, we found very good agreement between SmeftFR v3 UFO output and other corresponding publicly available codes, such as SMEFTsim and SMEFT@NLO, which are commonly used for Monte Carlo simulations in SMEFT analyses. Although similar in some aspects, SmeftFR offers several unique features that make it particularly suited for certain types of analyses.

Finally, we presented a detailed step-by-step example demonstrating the practical use and capabilities of the SmeftFR v3 code through an analysis of the Vector Boson Fusion process. In this example $\mathcal{O}(1/\Lambda^4)$ terms in the EFT expansion were incorporated and included both in the analytical calculation of helicity amplitudes and in the Monte Carlo simulations. We showed here that NLO effects may be significant and should not be overlooked in such studies.

The current version of SmeftFR v3 code and its manual can be downloaded from

www.fuw.edu.pl/smeft

We believe that SmeftFR v3 is a valuable tool that streamlines calculations in SMEFT, from the theoretical Lagrangian level to the amplitude calculations required for experimental analyses in BSM physics. By combining the bottom-up approach to BSM studies with the development of advanced numerical tools, it aligns very well with the scope of this thesis, and is a great example of a high-quality, ambitious research study that is in line with the current trends in modern particle physics.

Chapter 3

Bottom-up approach: Double Higgs production via vector boson fusion at next-to-leading order in SMEFT

3.1 Introduction: double Higgs production in the Standard Model and beyond

In this chapter, we present another example of an analysis utilizing the bottom-up approach in the searches for beyond the Standard Model physics. It is focused on a model-independent study of a specific process, namely double Higgs boson production, within the framework of Standard Model Effective Field Theory. The process of double Higgs boson production is one of the most promising directions in the searches for the physics BSM. Current experimental bounds from the LHC read:

$$\begin{aligned} \sigma(pp \to HH) &< 2.4 \times \sigma^{SM}(pp \to HH), \text{ ATLAS [111]}, \\ \sigma(pp \to HH) &< 3.4 \times \sigma^{SM}(pp \to HH), \text{ CMS [112]}, \end{aligned} \tag{3.1}$$

and indicate significant potential for new physics to affect this process by enhancing its cross-section compared to the SM prediction. Moreover, double-Higgs production is very important because it is relevant in understanding the mechanism of the electroweak symmetry breaking (EWSB) and the determination of the Higgs trilinear self-coupling, which is essential in exploring the nature of the Higgs potential or the stability of the electroweak vacuum.

In the Standard Model, the main production channel of a pair of Higgs bosons occurs via one-loop gluon fusion (ggF) contributions — triangle and box diagrams displayed in Figure 3.1 — and has been widely studied in the literature [113–125]. The cancellation between these two contributions leads to a significant suppression of the final predicted cross-section (in comparison to that of single Higgs production) and reads [126]:

$$\sigma^{ggF}_{SM}(pp \to hh) = 36.69^{+6\%}_{-23\%} \text{ fb}. \tag{3.2}$$

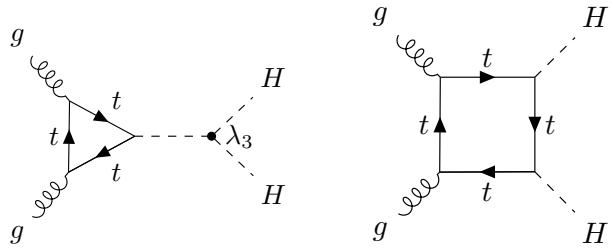

Figure 3.1: Diagrams contributing to the double Higgs production via gluon fusion in the SM. Internal fermion lines indicated by t correspond to the SM top quarks. The black dot indicates the trilinear Higgs coupling λ_3.

Another important, though sub-leading, contribution to the double Higgs production comes from the vector boson fusion (VBF) channel displayed in Figure 3.2. His channel has also been widely studied in the literature [28, 127–135], in the SM it has predicted cross-section of [136]:

$$\sigma^{VBF}_{SM}(pp \to hhjj) = 2.055^{+0.001}_{-0.001} \text{ fb}. \tag{3.3}$$

While the VBF channel is subdominant compared to the ggF in the SM, with a cross-section about an order of magnitude smaller:

$$\sigma^{VBF}_{SM}(pp \to hhjj) < 10\% \times \sigma^{ggF}_{SM}(pp \to hh), \tag{3.4}$$

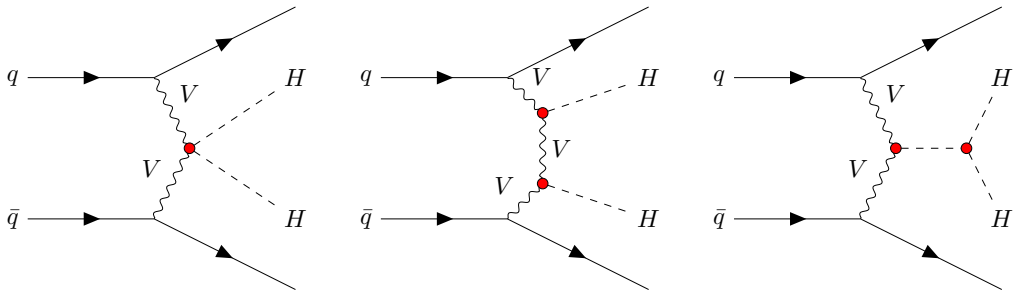

Figure 3.2: Diagrams contributing to the double Higgs production via vector boson fusion.

it may still be very interesting from the point of view of new physics searches. First, it offers the distinct advantage of a clean experimental signature compared to the ggF, characterized by two forward jets with a large rapidity gap, making it much easier to isolate the signal from the background. Moreover, double Higgs production via VBF may play a crucial role in the searches for new physics. Despite its small cross-section in the SM, even minor modifications of interactions between Higgs and gauge bosons may lead to a significant enhancement of the VBF double Higgs production cross-section, making it an important target for experimental investigations. For this reason, a model independent study of the VBF channel in the SMEFT is essential to determine the potential for enhancing this process in the current and future accelerator experiments. Whereas recent work [30] focused on the e^+e^- colliders, this chapter is dedicated to the hadronic colliders, with emphasis on the HL-LHC experiment. Our primary goal is to evaluate the maximal possible enhancement of the VBF double Higgs production process, including terms $\mathcal{O}(1/\Lambda^2)$ (LO in the EFT expansion) and $\mathcal{O}(1/\Lambda^4)$ (NLO in the EFT expansion, non-negligible higher order contributions $\mathcal{O}(1/\Lambda^6)$ would suggest problems with the EFT expansion). By taking into account current constraints on the SMEFT Wilson coefficients, as well as considerations such as EFT validity, we aim to provide a comprehensive description of the VBF double-Higgs production process, and more realistic perspective on the potential of BSM physics significantly impacting these channels.

This chapter is organized as follows. In Section 3.2 we list the dimension-6 and dimension-8 SMEFT operators that are relevant for this analysis, alongside all relevant assumptions and other preliminaries. Section 3.3 includes analytical formulas for $VV \to HH$ helicity amplitudes and corresponding cross-section plots, which enables us to identify the leading-order behavior. Then, Section 3.4 includes the results of numerical simulations and answers the question of the maximal possible enhancement of double Higgs production via VBF in SMEFT.

3.2 Preliminaries

3.2.1 Relevant operators

To affect the process of double Higgs production via VBF, the SMEFT operators can be inserted into three types of vertices: hhh, hVV, and $hhVV$ (red dots on diagrams in Figure 3.2, h indicates the Higgs and V indicates the gauge boson). For the hhh vertex, at least three powers of the scalar field φ are required, without any contributions from the gauge fields W or B. For the hVV vertex, at least one power of φ and at least two powers of the gauge fields W or B are needed, whereas for the $hhVV$ vertex, at least two powers of φ and at least two powers of the gauge fields W or B are necessary. The relevant classes of the SMEFT operators from Tables A.1, A.4 and A.2 that can impact this process

are summarized in Table 3.1.

	Operator class	
Vertex	Dimension-6	Dimension-8
hhh	φ^6, $\varphi^4 D^2$	φ^8, $\varphi^6 D^2$, $\varphi^4 D^4$
hVV, $hhVV$	$\varphi^4 D^2$, $X^2\varphi^2$	$\varphi^6 D^2$, $\varphi^4 D^4$, $X^2\varphi^4$, $X^2\varphi^2 D^2$, $X\varphi^4 D^2$

Table 3.1: Classes of SMEFT dimension-6 and dimension-8 operators affecting vertices relevant for double Higgs boson production via VBF. For the full list of operators see Tables A.1, A.4 and A.2.

Table 3.2 presents the specific operators that may affect one or both of the two VBF processes of interest: $WW \to hh$ and $ZZ \to hh$. For the dimension-6 operators, we take into account all possible contributions, whereas for dimension-8 operators, which are quite numerous, we have chosen a representative example from each class from Table 3.1.

Dimension-6		Dimension-8	
Q_φ	$(\varphi^\dagger\varphi)^3$	Q_{φ^8}	$(\varphi^\dagger\varphi)^4$
$Q_{\varphi\Box}$	$(\varphi^\dagger\varphi)\Box(\varphi^\dagger\varphi)$	$Q_{\varphi^6 D^2}$	$(\varphi^\dagger\varphi)(\varphi^\dagger D_\mu\varphi)^*(\varphi^\dagger D^\mu\varphi)$
$Q_{\varphi D}$	$\left(\varphi^\dagger D^\mu\varphi\right)^*\left(\varphi^\dagger D_\mu\varphi\right)$	$Q_{\varphi^6\Box}$	$(\varphi^\dagger\varphi)^2\Box(\varphi^\dagger\varphi)$
$Q_{\varphi W}$	$\varphi^\dagger\varphi\, W^I_{\mu\nu}W^{I\mu\nu}$	$Q^{(1)}_{\varphi^4 D^4}$	$(D_\mu\varphi^\dagger D_\nu\varphi)(D^\nu\varphi^\dagger D^\mu\varphi)$
$Q_{\varphi B}$	$\varphi^\dagger\varphi\, B_{\mu\nu}B^{\mu\nu}$	$Q^{(1)}_{W^2\varphi^4}$	$(\varphi^\dagger\varphi)^2 W^I_{\mu\nu}W^{I\mu\nu}$
$Q_{\varphi WB}$	$\varphi^\dagger\tau^I\varphi\, W^I_{\mu\nu}B^{\mu\nu}$	$Q^{(1)}_{W^2\varphi^2 D^2}$	$(D^\mu\varphi^\dagger D^\nu\varphi)W^I_{\mu\rho}W^{I\rho}_\nu$
		$Q^{(1)}_{W\varphi^4 D^2}$	$(\varphi^\dagger\varphi)(D^\mu\varphi^\dagger\tau^I D^\nu\varphi)W^I_{\mu\nu}$
		$Q^{(1)}_{B^2\varphi^4}$	$(\varphi^\dagger\varphi)^2 B_{\mu\nu}B^{\mu\nu}$
		$Q^{(1)}_{B^2\varphi^2 D^2}$	$(D^\mu\varphi^\dagger D^\nu\varphi)B_{\mu\rho}B^\rho_\nu$
		$Q^{(1)}_{B\varphi^4 D^2}$	$(\varphi^\dagger\varphi)(D^\mu\varphi^\dagger D^\nu\varphi)B_{\mu\nu}$

Table 3.2: Chosen bosonic SMEFT dimension-6 and dimension-8 operators affecting the $VV \to hh$ process and double Higgs boson production via VBF.

Important comments are in place here. As we are interested in the most general features of the VBF part of the process, we neglect the impact of the SMEFT operators on the fermionic external lines and on the decays of the Higgs pair to the final states (such operators can also be independently investigated using other processes). Additionally, we neglect all CP-violating (CPV) operators due to their high degree of suppression. Moreover, all calculations are performed under the assumption that only one of the WCs is non-zero at a time. Finally, we neglect the running effects on WCs. We leave all these issues for future extended analyses.

3.2.2 Bounds on Wilson coefficients

To estimate the possible impact of SMEFT operators on the double Higgs production via VBF, one must assign numerical values to the Wilson coefficients. For the dimension-6 WCs, in the first approximation we assume the maximal values of the WCs allowed by current fits to experimental data, as

detailed in [43, 44]. Based on this, we use the following ranges for the dimension-6 WCs:

$$|C_{\varphi\Box}| \lesssim \frac{\pi}{\text{TeV}^2}, \quad |C_{\varphi D}| \lesssim \frac{1}{\text{TeV}^2}, \quad |C_{\varphi W}| \lesssim \frac{0.5}{\text{TeV}^2}, \quad |C_{\varphi B}| \lesssim \frac{0.5}{\text{TeV}^2}, \quad |C_{\varphi WB}| \lesssim \frac{0.5}{\text{TeV}^2}, \tag{3.5}$$

with a limit on C^{φ} derived from experimental constraints on the trilinear Higgs coupling [29]:

$$-\frac{10}{\text{TeV}^2} \lesssim C^{\varphi} \lesssim \frac{2}{\text{TeV}^2}. \tag{3.6}$$

These values are slightly larger than the maximal allowed values cited in the references above. If such fits are not yet available, as it is the case for the remainder of the dimension-6 and all the dimension-8 WCs, we assume the approach of [137], based on the study of the validity of the EFT expansion, which leads to a particular power-counting of WCs, also known as Naive Dimensional Analysis (NDA):

$$\frac{C_i}{\Lambda^{D-4}} = \frac{g_*^{n_i-2} \times c_i}{\Lambda^{D-4}} \tag{3.7}$$

where D is the dimension of SMEFT operator, n is the number of fields involved, $g_* \leq 4\pi$ is the UV coupling to the SM, and c_i is an additional suppression factor related, e.g., to additional symmetries such as shift symmetry or custodial symmetry. As a result, we get:

$$\begin{gathered} C_{\varphi^8} = g_*^6\, c_{\varphi^8}\ , \quad C_{\varphi^6\Box} = g_*^4\, c_{\varphi^6\Box}\ , \quad C_{\varphi^6 D^2} = g_*^4\, c_{\varphi^6 D^2}\ , \quad C^{(i)}_{\varphi^4 D^4} = g_*^2\, c^{(i)}_{\varphi^4 D^4}\ . \\ C^{(i)}_{V^2\varphi^4} = g_*^4\, c^{(1)}_{V^2\varphi^4}\ , \qquad C^{(i)}_{V^2\varphi^2 D^2} = g_*^2\, c^{(1)}_{V^2\varphi^2 D^2}\ , \qquad C^{(i)}_{V\varphi^4 D^2} = g_*^3\, c^{(1)}_{V\varphi^4 D^2}\ . \end{gathered} \tag{3.8}$$

with $V = W$ or B. Initially, we assume the maximal possible value of $g_* = 4\pi$ with no additional suppression factors ($c_i = 1$). This corresponds to a rather unrealistic (and very strongly coupled) UV scenario. We use the above numbers as input for the initial helicity cross-section estimates to identify their leading order behavior, but in order to get more realistic estimates of the maximal possible enhancement, we utilize the EFT validity requirements as summarized in the following section. For all plots regarding the dimension-8 WCs, we use the cut-off scale of $\Lambda = 10$ TeV. Finally, although our choice of dimension-8 WCs seems arbitrary, we think that, since they represent at least one example of relevant classes from the Table 3.1, this choice is sufficient to present the main results and conclusions of this work, which are applicable to all operators in the corresponding classes.

3.2.3 EFT validity conditions

To ensure the validity of the EFT expansion and impose independent constraints on the Wilson coefficients, we apply the conditions on the convergence of the EFT series. First, let us assume that we investigate the dependence of the total cross-sections for the $VV \to HH$ (as before with $VV = WW$ or ZZ) process on a chosen **single** dimension-6 WC C_i. In such a case, the total cross-section can be expressed as a sum of the SM, dimension-6 and dimension-6^2 contributions:

$$\sigma(s, C_i, \Lambda)^{VV}_{SMEFT} = \sigma(s)^{VV}_{SM} + \frac{C_i}{\Lambda^2}\sigma(s)^{VV}_{D6} + \frac{C_i^2}{\Lambda^4}\sigma(s)^{VV}_{D6^2} + \mathcal{O}\left(\frac{1}{\Lambda^6}\right). \tag{3.9}$$

Here, the terms proportional to σ^{VV}_{SM}, σ^{VV}_{D6} and $\sigma^{VV}_{D6^2}$ represent contributions to the cross-section appearing in the SM, and at the dimension-6 $\mathcal{O}(1/\Lambda^2)$ and the dimension-6^2 $\mathcal{O}(1/\Lambda^4)$ orders of the EFT expansion, respectively. We can rewrite this expression in the following form:

$$\sigma(s, C_i, \Lambda)^{VV}_{SMEFT} = \sigma(s)^{VV}_{SM}\left(1 + \frac{C_i}{\Lambda^2}\frac{\sigma(s)^{VV}_{D6}}{\sigma(s)^{VV}_{SM}} + \frac{C_i^2}{\Lambda^4}\frac{\sigma(s)^{VV}_{D6^2}}{\sigma(s)^{VV}_{SM}}\right). \tag{3.10}$$

To ensure the validity of the EFT, we require that the expansion in powers of $1/\Lambda$ converges. While we lack the necessary tools to verify convergence to an arbitrary EFT order, we adopt a practical criterion by demanding that the SMEFT contributions to the cross-section have to be smaller than the SM prediction and have to decrease order-by-order. Here, we assume that satisfying such a criterion up to the $\mathcal{O}(1/\Lambda^4)$ order is sufficient to ensure overall convergence. This can be translated into the following conditions:

$$\frac{C_i}{\Lambda^2}\frac{\sigma(s)^{VV}_{D6}}{\sigma(s)^{VV}_{SM}} \leq \delta \qquad \& \qquad \frac{C_i}{\Lambda^2}\frac{\sigma(s)^{VV}_{D6^2}}{\sigma(s)^{VV}_{D6}} \leq \delta, \tag{3.11}$$

where δ is a parameter defining the speed of convergence that should be chosen as $\delta < 1$. The equation above is equivalent to:

$$\Delta^{VV}_{D6}(s, C_i, \Lambda) = \max\left[\left|\frac{C_i}{\Lambda^2}\frac{\sigma(s)^{VV}_{D6}}{\sigma(s)^{VV}_{SM}}\right|, \left|\frac{C_i}{\Lambda^2}\frac{\sigma(s)^{VV}_{D6^2}}{\sigma(s)^{VV}_{D6}}\right|\right] \leq \delta < 1. \tag{3.12}$$

The ratios in Equation(3.12) quantify the relative magnitude of the dimension-6 and the SM contributions, and of the dimension-6^2 and the dimension-6 contributions. Similarly, we can extend this procedure to the dimension-8 WCs, with the cross-section of form:

$$\sigma(s, C_i, \Lambda)^{VV}_{SMEFT} = \sigma(s)^{VV}_{SM}\left(1 + \frac{C_i}{\Lambda^4}\frac{\sigma(s)^{VV}_{D8}}{\sigma(s)^{VV}_{SM}}\right). \tag{3.13}$$

Based on this, we define:

$$\Delta^{VV}_{D8}(s, C_i, \Lambda) = \left|\frac{C_i}{\Lambda^4}\frac{\sigma(s)^{VV}_{D8}}{\sigma(s)^{VV}_{SM}}\right| \leq \delta < 1. \tag{3.14}$$

Here, σ^{VV}_{D8} corresponds to the total cross-section that is linear in a given dimension-8 WC, i.e. evaluated up to the order $\mathcal{O}(1/\Lambda^4)$ in the EFT expansion. Imposing these conditions allows us to derive realistic upper bounds on the WCs and estimate the maximal possible enhancement of the VBF double Higgs production process within the region of EFT validity.

A few remarks are in order here. First, for some processes contributions at a given EFT order (which may include the lowest order SM terms) can vanish or be strongly suppressed, accidentally or due to some model symmetry. In such cases, the definitions of Δ^{VV}_{D6} and Δ^{VV}_{D8} should be properly refined to avoid potential issues arising due to vanishing denominators. However, for the considered $VV \to HH$ processes, the SM result is proportional to the gauge and Higgs couplings and is not suppressed by any mechanism, nor does such suppression occur for higher-order terms. Thus, here, we may use the definitions (3.12) and (3.14) without modifications.

Second, for simplicity in estimating the maximal size of the WCs allowed by conditions (3.12) and (3.14) we assume only one non-vanishing C_i at a time. The situation may become more complex when analyzing the dependence on several WCs simultaneously. Interference or cancellations between them may occur and, the EFT expansion may remain valid even for higher values of individual WCs than for the "marginalised" case of one non-vanishing WC at a time, eventually allowing for larger cross-section enhancement. Therefore, the bounds we discuss in the next section should be treated as generic EFT estimates, without accounting for eventual fine-tuning between WCs. A more detailed analysis including fine-tuning effects would require assuming a specific pattern of WC values, usually known only when a concrete UV model is assumed to generate the WCs through a decoupling procedure.

Third, the WCs considered in this work alter a much wider group of processes than just VBS double Higgs production. For such processes, imposing constraints corresponding to those given in (3.12)

and (3.14) may lead to additional, potentially even stronger limits on a given WC. Ideally, we could extend this analysis to other processes sensitive to the considered set of WCs, however at this time we leave this task for future, focusing on the process of VBS double Higgs production only.

Our approach should be viewed as complementary to the perturbative unitarity constraints (see e.g [40, 138–141]). It provides an additional criterion to consider when studying processes within the SMEFT framework, rather than replacing such constraints. However, one should note that the existing analyses of unitarity constraints generally do not take consistently into account dimension-6^2 contributions.

Finally, we should stress that the bounds on $VV \to HH$ rates which we obtain assuming the EFT convergence criterion are not the absolute upper values, even barring the eventual fine-tuning between WCs mentioned above. In specific UV models stronger enhancement may be possible — however, in such cases calculations should instead be done directly within the given model, without using the EFT as an intermediate step.

3.3 Helicity amplitudes and cross-sections

Double Higgs boson production via VBF is a complicated multi-particle process in the SM, which becomes even more involved in SMEFT. For this reason, before performing numerical calculations of the cross-sections, it is instructive to study the anatomy of individual on-shell sub-amplitudes contributing to the full amplitude. More specifically, we study the on-shell scattering of opposite-sign $W^\pm$ bosons or a pair of neutral Z bosons into a pair of Higgs bosons H, namely:

$$V(p_1, \lambda_1) + V(p_2, \lambda_1) \to h(p_3) + h(p_4), \tag{3.15}$$

where $V = W^\pm$ or Z, p_i are the four-momenta of the initial and final states, and λ_i represent the polarizations of the initial heavy vector bosons. The scattering is assumed to occur in the xz-plane with the initial incoming particle of three-momentum $\vec{p}_1$ moving in the direction of the positive z-axis direction, and the outgoing particle of three-momentum $\vec{p}_3$ moving in the positive x- and z-axis direction. In the center-of-mass (CoM) frame, the kinematics is then described by:

$$\begin{aligned} &p_1 = (E_1, 0, 0, |\vec{p}_1|)\ , \quad p_2 = (E_1, 0, 0, -|\vec{p}_1|)\ , \\ &p_3 = (E_3, |\vec{p}_3|\sin\theta, 0, |\vec{p}_3|\cos\theta)\ , \quad p_4 = (E_3, -|\vec{p}_3|\sin\theta, 0, -|\vec{p}_3|\cos\theta)\ , \end{aligned} \tag{3.16}$$

where $\theta \in [0, \pi]$ is the CoM scattering angle between the incoming and outgoing particles. Moreover, we have:

$$s = (p_1 + p_2)^2 = (p_3 + p_4)^2 = (2E_1)^2 = (2E_3)^2, \quad |\vec{p}_1| = \sqrt{\frac{s}{4} - M_V^2}, \quad |\vec{p}_3| = \sqrt{\frac{s}{4} - M_H^2}. \tag{3.17}$$

The three polarization vectors (two transverse — $\pm$ and longitudinal - 0) of the initial heavy vector bosons moving along the z axis with momenta p_1 and p_2 are given by:

$$\begin{aligned} &\epsilon_\pm^\mu(p_1) = \frac{1}{\sqrt{2}}(0, 1, \pm i, 0), \quad \epsilon_0^\mu(p_1) = \frac{1}{M_V}\left(|\vec{p_1}|, 0, 0, E_1\right), \\ &\epsilon_\pm^\mu(p_2) = \frac{1}{\sqrt{2}}(0, 1, \mp i, 0), \quad \epsilon_0^\mu(p_2) = \frac{1}{M_V}\left(|\vec{p_1}|, 0, 0, -E_1\right). \end{aligned} \tag{3.18}$$

The helicity amplitude for the $VV \to hh$ process can be expressed as:

$$\mathcal{M}^{VV}_{\lambda_1\lambda_2} \equiv \mathcal{M}^{VVHH}_{\lambda_1\lambda_2}(\theta, s, G_F, M_W, M_Z, M_H, C_i). \tag{3.19}$$

Not all the 9 possible helicity configurations are independent. As we neglect CP-violating WCs, the following relations hold:

$$\mathcal{M}^{VV}_{++} = \mathcal{M}^{VV}_{--}, \quad \mathcal{M}^{VV}_{+-} = \mathcal{M}^{VV}_{-+}, \quad \mathcal{M}^{VV}_{0\pm} = \mathcal{M}^{VV}_{\pm 0}, \tag{3.20}$$

leaving a total of 4 independent helicity structures. The differential cross-section for a given helicity is given by:

$$\left(\frac{d\sigma^{VV}}{d\Omega}\right)_{\lambda_1\lambda_2} = \frac{1}{2!}\frac{1}{9}\frac{1}{64\pi^2 s}\left|\mathcal{M}^{VV}_{\lambda_1\lambda_2}(\theta, s, G_F, M_W, M_Z, M_H, C_i)\right|^2 , \tag{3.21}$$

and the helicity cross-section:

$$\sigma(s)^{VV}_{\lambda_1\lambda_2} = \int_0^{2\pi} d\varphi \int_{\theta_{cut}}^{\pi-\theta_{cut}} d\theta \sin\theta \left(\frac{d\sigma^{VV}}{d\Omega}\right)_{\lambda_1\lambda_2} . \tag{3.22}$$

Summing over relevant helicities, the total cross-section is:

$$\sigma(s)^{VV} = \sigma(s)^{VV}_{00} + 2\sigma(s)^{VV}_{++} + 2\sigma(s)^{VV}_{+-} + 4\sigma(s)^{VV}_{0+}. \tag{3.23}$$

Explicit formulae for the leading order helicity amplitudes are provided in Appendix F for the $WW \to HH$ process and in Appendix G for the $ZZ \to HH$ process. All amplitudes and corresponding numerical results in this section were generated using the following chain of programs:

`SmeftFR` $\to$ `FeynArts` $\to$ `FeynCalc`

For all plots and numerical results, we assume the sign of WCs is chosen so as to maximize the cross-sections and to ensure their positivity across all energies. Figures 3.3 and 3.4 ($WW \to HH$) and Figures 3.5 and 3.6 ($ZZ \to HH$) present the relative enhancement of the SM cross-sections, defined as:

$$R^{VV} = \frac{\sigma^{VV}_{SMEFT}}{\sigma^{VV}_{SM}} . \tag{3.24}$$

Based on the formulas for helicity amplitudes displayed in Appendices F and G in Eqs. (F.1)–(G.3) and from the plots in Figures 3.3–3.6, we can draw the following conclusions:

1. **Standard Model contributions**
   From Eqs. (F.1) and (G.1), the amplitude behaves as:

   $$\mathcal{M}^{VV}_{SM} \xrightarrow{s>>M_V^2} \text{const.}, \quad \sigma^{VV}_{SM} \propto \frac{1}{s} \xrightarrow{s>>M_V^2} 0, \tag{3.25}$$

   which is consistent with the literature.

2. **Dimension-6 SMEFT operators contributions**
   For the plots in Figures 3.3 and 3.5, we used numerical values of the WCs dictated by fits to experimental data, following Eqs. (3.6) and (3.5). A more precise determination and application of these values, based on the perturbativity condition formulated in Eq. (3.12), is discussed in Section 3.4. From Eqs. (F.2) and (G.2), and Figures 3.3 and 3.5, we observe the following effects of the considered WCs:

   - C_φ – small relative enhancement of the R^{VV} ratio, with minimal differences between the dimension-6 and dimension-6^2 contributions.

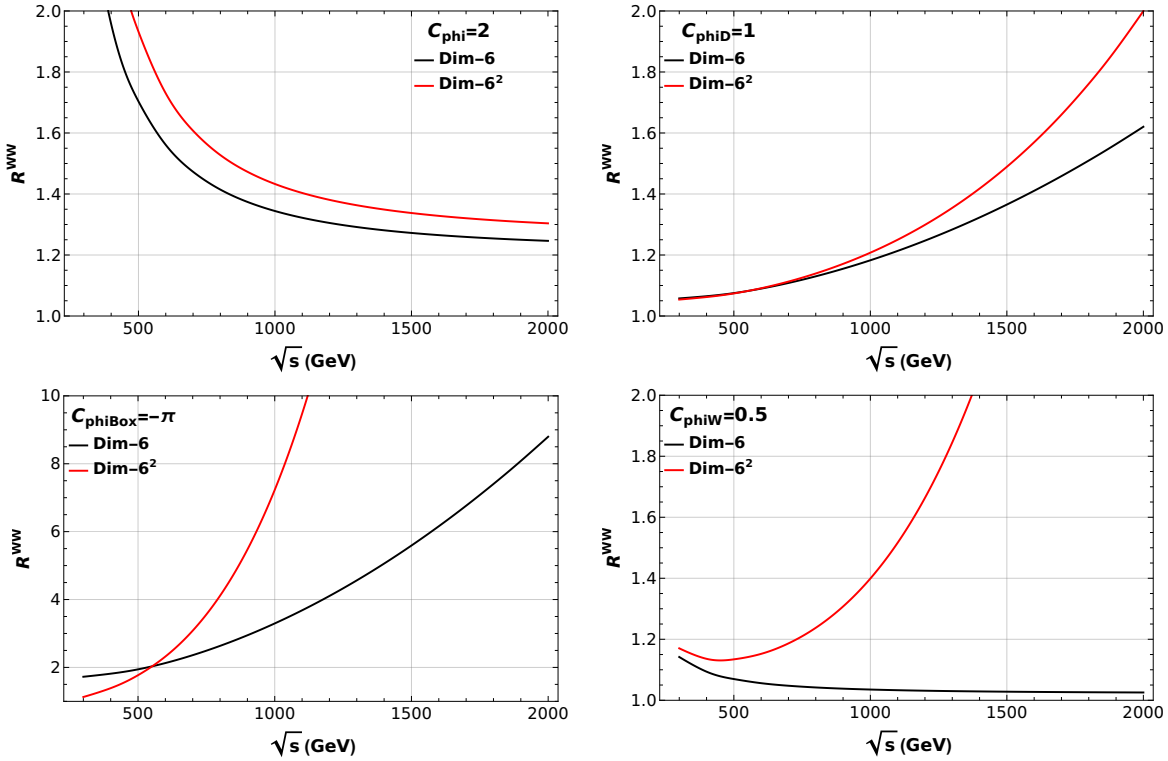

Figure 3.3: Ratios R^{WW} between angular-integrated cross-sections in the SMEFT and the SM for chosen values of C_φ, $C_{\varphi D}$, $C_{\varphi\Box}$ and $C_{\varphi W}$ Wilson coefficients, including dimension-6 (black lines) and dimension-6^2 (red lines) terms. $\Lambda = 1$ TeV and $\theta \in [-\pi/18, \pi/18]$ are assumed.

- $C_{\varphi D}$ – small enhancement of the R^{VV} ratio, with visible energy dependence:
  - $R^{VV} \propto s$ at the dimension-6 level,
  - $R^{VV} \propto s^2$ at the dimension-6^2 level.

  and numerical differences between the dimension-6 and dimension-6^2 contributions reaching at most 20% for high energies.
- $C_{\varphi\Box}$ – significant enhancement of the R^{VV} ratio, with visible energy dependence:
  - $R^{VV} \propto s$ at the dimension-6 level,
  - $R^{VV} \propto s^2$ at the dimension-6^2 level,

  with the dimension-6 contributions dominating for $\sqrt{s} \leq 500$ GeV, and the dimension-6^2 for $\sqrt{s} \geq 1000$ GeV.
- $C_{\varphi W}$ – significant enhancement of the R^{VV} ratio with visible energy dependence:
  - $R^{VV} \propto 1$ at the dimension-6 level,
  - $R^{VV} \propto s^2$ at the dimension-6^2 level,

  leading to a significant difference between the dimension-6 and dimension-6^2 contributions, quickly growing with s.
- $C_{\varphi B}$ and $C_{\varphi WB}$ – small enhancement of the R^{VV} ratio with visible energy dependence:

  - $R^{VV} \propto 1$ at the dimension-6 level,

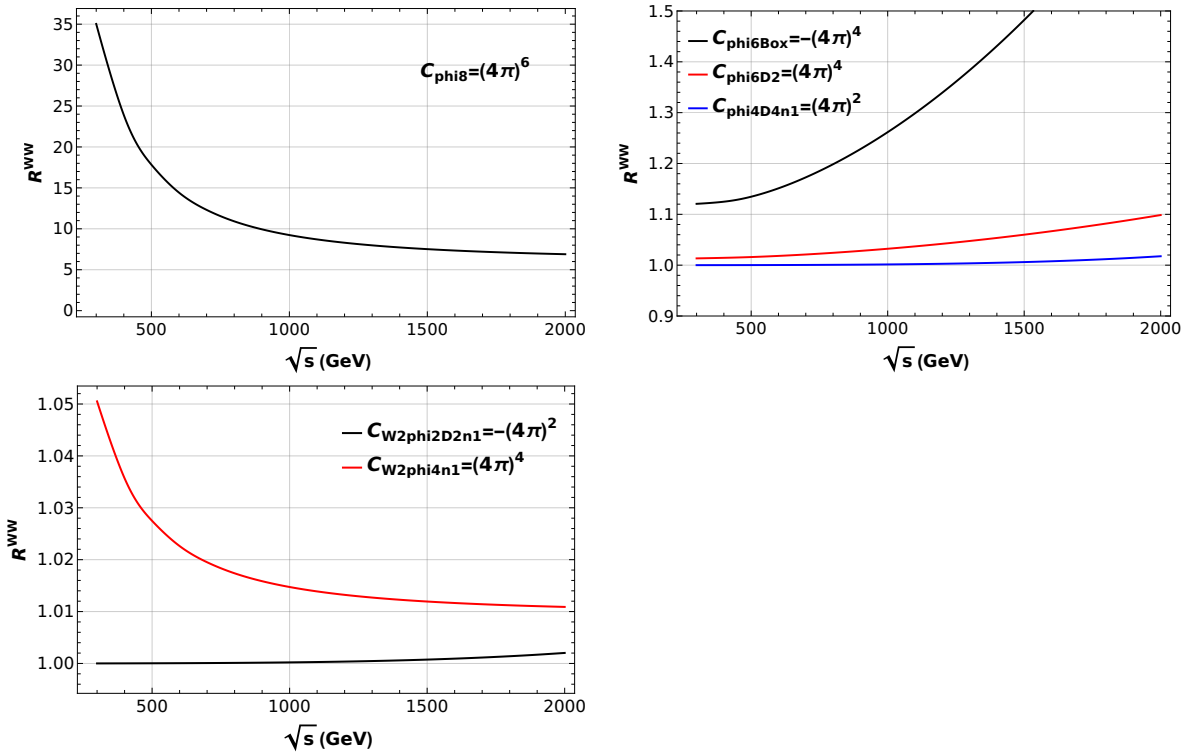

Figure 3.4: Ratios R^{WW} between angular-integrated cross-sections in the SMEFT and the SM for chosen values of C_{φ^8}, $C_{\varphi^6\Box}$, $C_{\varphi^6 D^2}$, $C^{(1)}_{\varphi^4 D^4}$, $C^{(1)}_{W^2\varphi^4}$, $C^{(1)}_{W^2\varphi^2 D^2}$ and $C^{(1)}_{W\varphi^4 D^2}$ dimension-8 Wilson coefficients. $\Lambda = 1$ TeV and $\theta \in [-\pi/18, \pi/18]$ are assumed.

– $R^{VV} \propto s^2$ at the dimension-6^2 level,

again leading to visible difference between the dimension-6 and dimension-6^2 contributions, quickly growing with s.

Concluding, the most promising dimension-6 Wilson coefficients for $VV \to HH$ cross-section enhancement are $C_{\varphi\Box}$ and $C_{\varphi W}$.

3. **Dimension-8 SMEFT operators contributions**
For the plots in Figures 3.4 and 3.6, we used numerical values of the WCs following the NDA, as described in Section 3.2.2 through Eqs (3.7) and (3.8), with $g_* = 4\pi$ and $\Lambda = 10$ TeV as benchmark values of the generic UV coupling magnitude and cut-off scale. A more precise determination of these values, based on the perturbativity condition given by Eq. (3.14), is discussed in Section 3.4. From Eqs. (F.3) and (G.3), and Figures 3.4 and 3.6 we can observe the following effects of the considered dimension-8 WCs:

- C_{φ^8} – very significant enhancement of the R^{VV} at low $\sqrt{s}$, that can be attributed to the large numerical value of this WC dictated by the NDA.
- $C_{\varphi^6\Box}$, $C_{\varphi^6 D}$ and $C^{(1)}_{\varphi^4 D^4}$ – moderate enhancement of the ratio $R^{VV} \propto s^2$, with the largest contribution coming from $C_{\varphi^6\Box}$. Effects of $C^{(1)}_{\varphi^4 D^4}$ are strongly suppressed due to its small numerical value dictated by the NDA.

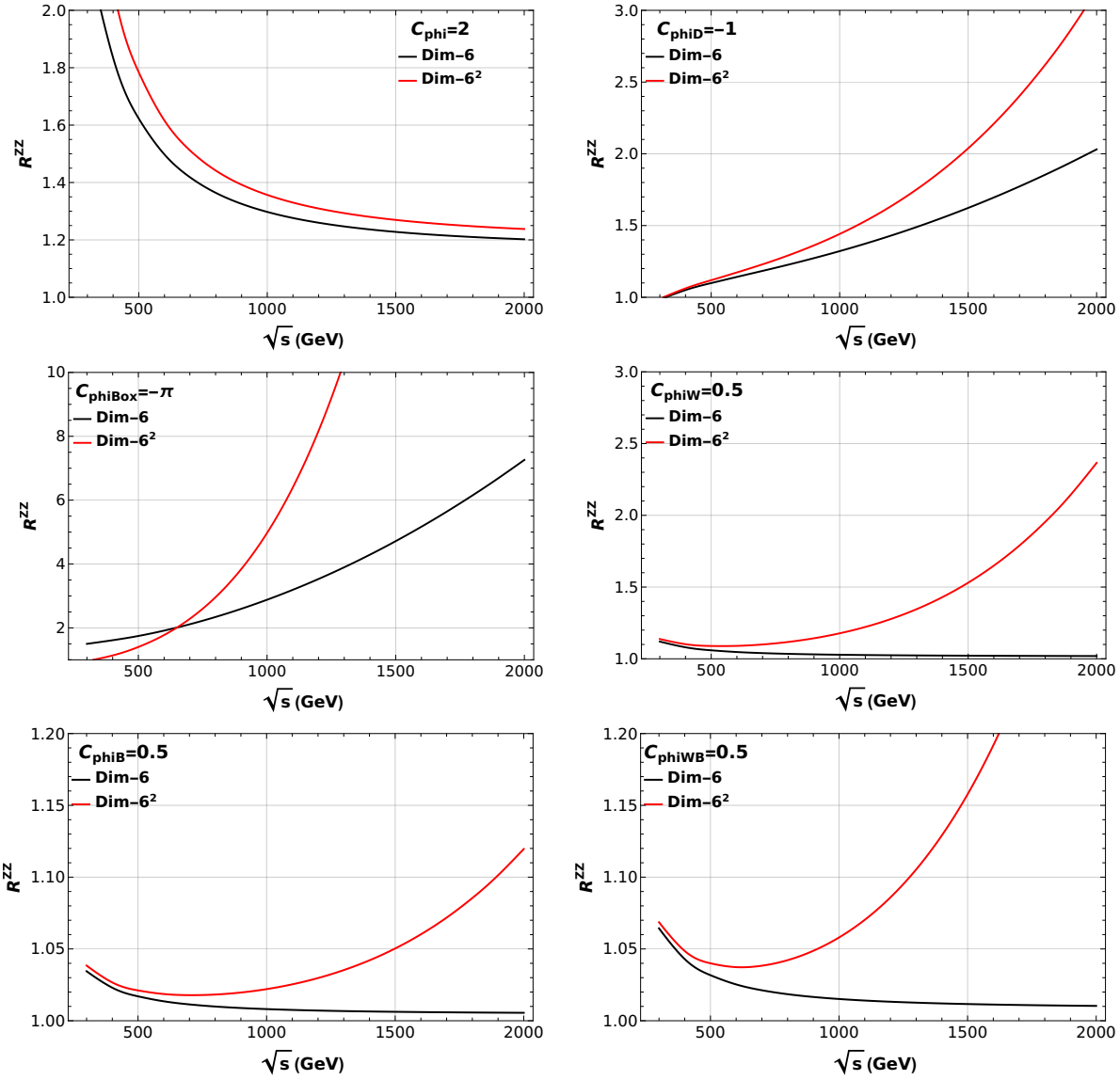

Figure 3.5: Ratios R^{ZZ} between angular-integrated cross-sections in the SMEFT and the SM for chosen values of C_φ, $C_{\varphi D}$, $C_{\varphi\Box}$, $C_{\varphi W}$, $C_{\varphi B}$ and $C_{\varphi WB}$ Wilson coefficients, including dimension-6 (black lines) and dimension-6^2 (red lines) terms. $\Lambda = 1$ TeV and $\theta \in [-\pi/18, \pi/18]$ are assumed.

- $C^{(1)}_{V^2\varphi^2D^2}$ – negligible enhancement of the $R^{VV} \propto s^2$ due to its small numerical values dictated by the NDA.
- $C^{(1)}_{V^2\varphi^4}$ – minimal enhancement of the $R^{VV} \propto s$.
- $C^{(1)}_{V\varphi^4D^2}$ – no contribution at dimension-8 order due to the vanishing of the SM interference terms. The first non-zero contributions appear at the dimension-8^2 level.

Summing up, the most promising dimension-8 Wilson coefficients that can lead to the strongest cross-section enhancement are: C_{φ^8}, $C_{\varphi^6\Box}$ and (to a lesser extent) $C^{(1)}_{V^2\varphi^4}$. Also, as one can see, the allowed maximal numerical values of the WCs are more important for cross-section enhancement than

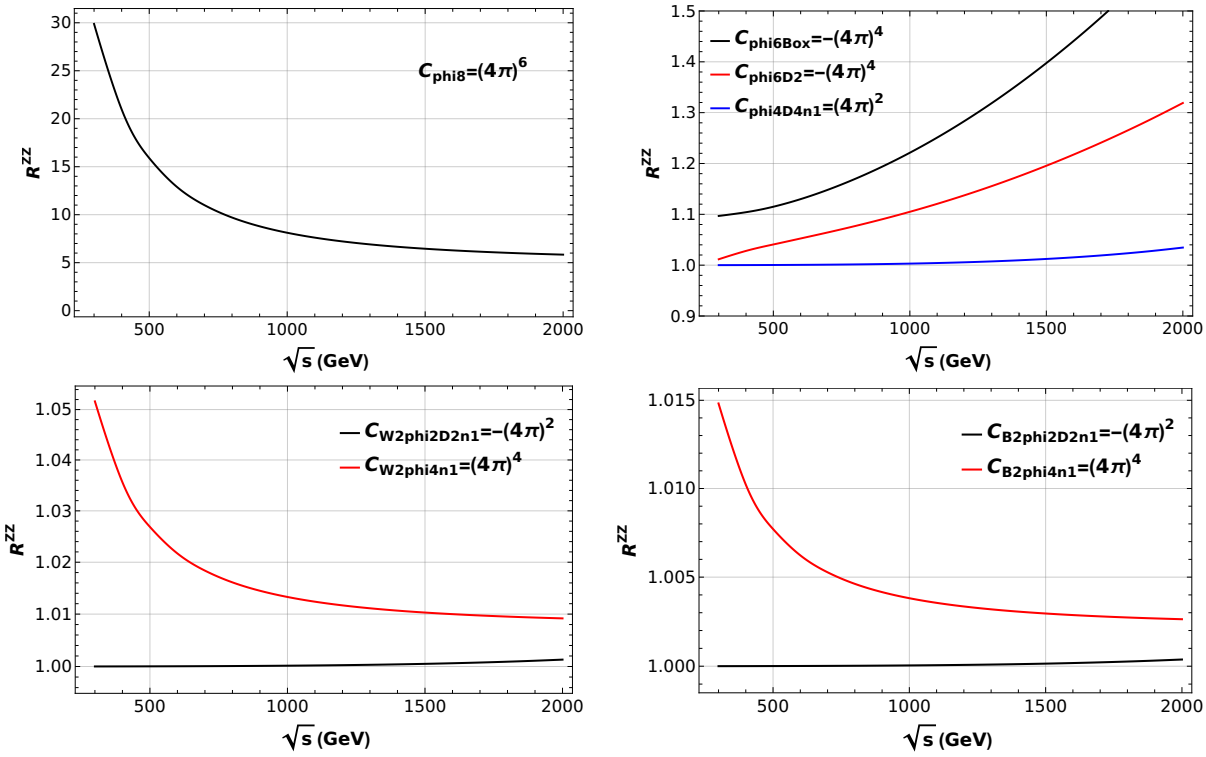

Figure 3.6: Ratios R^{ZZ} between angular-integrated cross-sections in the SMEFT and the SM for chosen values of C_{φ^8}, $C_{\varphi^6\Box}$, $C_{\varphi^6 D^2}$, $C^{(1)}_{\varphi^4 D^4}$, $C^{(1)}_{B^2\varphi^4}$, $C^{(1)}_{W^2\varphi^4}$, $C^{(1)}_{B^2\varphi^2 D^2}$ and $C^{(1)}_{W\varphi^4 D^2}$ dimension-8 Wilson coefficients. $\Lambda = 1$ TeV and $\theta \in [-\pi/18, \pi/18]$ are assumed.

the energy dependence.

Finally, we want to re-emphasize that our particular selection of a representative subset of dimension-8 operators should not affect the final conclusions. We selected at least one operator from each class in Table 3.1, with no indication that a different choice would lead to significantly different results.

3.4 Maximal enhancement of the double Higgs production via VBF in SMEFT

We can now turn our attention towards finally answering the central question at hand:

What is the maximal enhancement of the double Higgs boson production rate via vector boson fusion at the HL-LHC in SMEFT?

The answer requires an analysis of the full process $pp \to hh +$ jets, rather than just the $VV \to hh$ sub-process, which we discussed in the previous sections, in order to analytically understand the most important effects of the higher-dimensional SMEFT operators. To this end, we performed a numerical Monte Carlo analysis of this process for the HL-LHC experiment. The results were obtained using `MadGraph - v3_4_1` [142] event generator utilizing `UFO` [88] model files generated with `SmeftFR v3.02` [73]. The process of interest is:

```
p p > h h j j
```

where `p` represents the initial protons, `h` the Higgs bosons, and `j` the final-state jets. We utilized the VBF-specific cuts on kinematic variables that are based on the ATLAS recommendations (following [28, 40, 81]) on M_{jj} - invariant the mass of a pair of jets, $\Delta\eta_{jj}$ - the rapidity separation of jets, η_j - the rapidity of individual jets, Δp_{Tj} - the transverse momentum of jets, and M_{hh} - the invariant mass of the pair of Higgs bosons:

$$M_{jj} \geq 700 \text{ GeV}, \quad \Delta\eta_{jj} \geq 5, \quad |\eta_j| \leq 4.5, \quad p_{Tj} \geq 25 \text{ GeV}, \quad M_{hh} \geq 400 \text{ GeV}. \tag{3.26}$$

It should be noted that a more detailed study including Higgs decays to final states, may require more refined and final-state-specific cuts on kinematic variables.

Moreover, we assumed all fermion masses — apart from the top quark — to be equal to zero, and the flavor mixing matrices to be equal to identity. The numerical values of the input parameters are in line with the default `SmeftFR` v3 "G_F" default input scheme and read:

$$\begin{aligned} &G_F = 1.1638 \times 10^{-5} \text{ GeV}^{-2}, \quad M_Z = 91.1876 \text{ GeV}, \quad M_W = 80.379 \text{ GeV}, \\ &M_H = 125.35 \text{ GeV}, \quad M_t = 172.76 \text{ GeV}. \end{aligned} \tag{3.27}$$

We run the simulations for the HL-LHC experiment with the energy $\sqrt{s} = 14$ TeV and integrated luminosity of $\mathcal{L} = 3000$ fb^{-1}.

To ensure the EFT validity, we chose input numerical values of WCs in accordance with the validity conditions introduced in Equations (3.12) and (3.14). As one can note, the specific values of parameters $\Delta^{VV}_{6,8}(s, C_i, \Lambda)$ depend not only on the $\frac{C}{\Lambda^{2,4}}$ ratio, but also on the energy of the process s. This fact has important consequences. While these conditions can be satisfied at a specific energy scale s_1, they may be violated at a different scale $s_2 \neq s_1$. This is a direct consequence of the energy dependence of SMEFT amplitudes and cross-section. We identify two distinct scenarios based on the energy dependence of the amplitudes (and, consequently, cross-sections), and discuss them separately in the following subsections:

1. **Scenario** #1 - constant contribution dominates the amplitude at high energies:

$$\mathcal{M}^{VV}_{SMEFT} \xrightarrow{s>>M_V^2} \text{const.}, \quad \sigma^{VV}_{SMEFT} \propto \frac{1}{s} \xrightarrow{s>>M_V^2} 0, \tag{3.28}$$

2. **Scenario** #2 - energy dependence dominates the amplitude at high energies:

$$\mathcal{M}^{VV}_{SMEFT} \xrightarrow{s>>M_V^2} s^{1,2}, \quad \sigma^{VV}_{SMEFT} \propto s^{0,1}. \tag{3.29}$$

3.4.1 Scenario #1 - constant contribution dominates the amplitude at high energies

This is the case for the C_φ, C_{φ^8}, $C_{V^2\varphi^4}$ Wilson coefficients, as can be verified from the corresponding helicity amplitudes given in Equations (F.1)–(G.3) and from the plots in Figures 3.3–3.6. In this case, since the leading contribution to the amplitude remains constant, we have:

$$\mathcal{M}^{VV}_{SMEFT} \xrightarrow{s>>M_V^2} \text{const.}, \quad \sigma^{VV}_{SMEFT} \propto \frac{1}{s} \xrightarrow{s>>M_V^2} 0, \quad \Delta^{VV}_{6,8}(s, C_i, \Lambda) \xrightarrow{s>>M_V^2} \text{const.}. \tag{3.30}$$

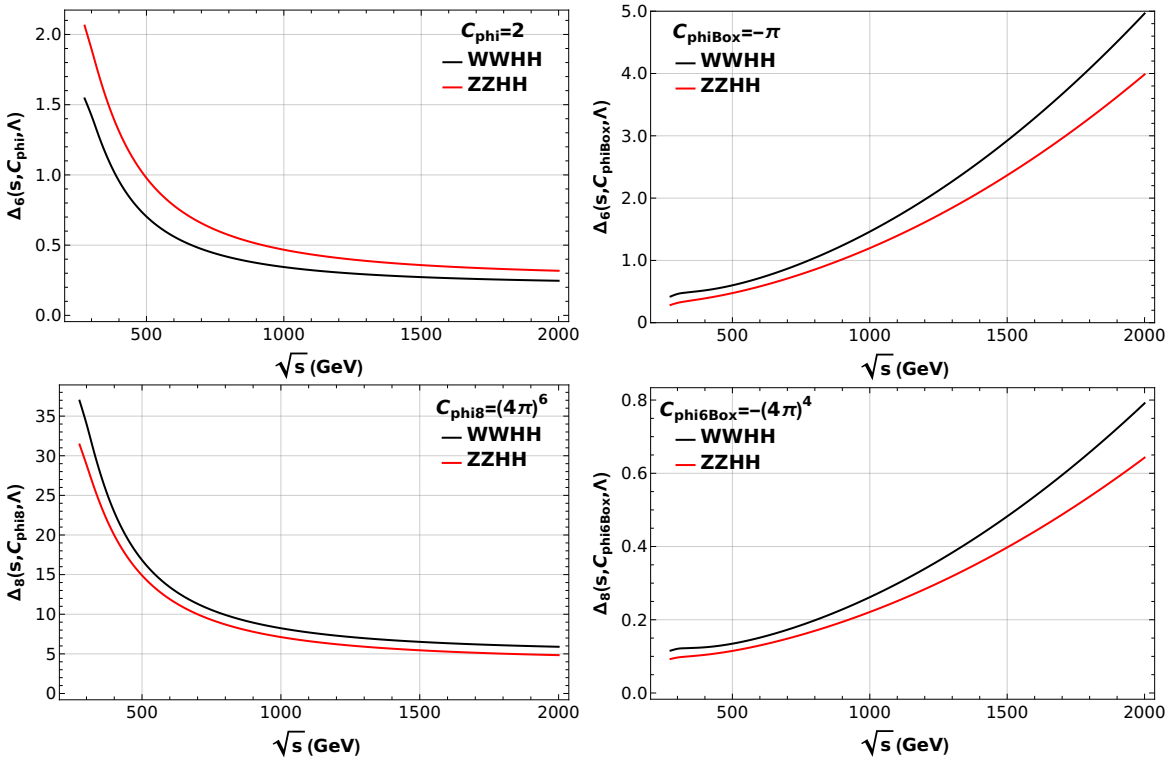

Figure 3.7: Dependence of $\Delta_{6,8}(s, C_i, \Lambda)$ on the energy scale s for two different scenarios. Left panel — leading contribution to the amplitude is constant at high energies. Right panel — leading contribution to the amplitude scales with s. Both $VV \to HH$ processes are taken into account. $\Lambda = 1$ TeV (dimension-6 WCs) or $\Lambda = 10$ TeV (dimension-8 WCs) and $\theta \in [-\pi/18, \pi/18]$ assumed.

Additionally, there are contributions to the amplitudes of the order $\mathcal{O}\left(\frac{1}{s}\right)$, negligible at higher energies, that may become relevant at low scales. This implies that $\Delta^{VV}_{6,8}(s, C_i, \Lambda)$ reaches maximum at the lowest available energy scale, near the Higgs pair production threshold $\sqrt{s} \approx 250$ GeV. Therefore, to ensure the validity of the SMEFT expansion, we impose the conditions (3.12) and (3.14) at this **lowest** available energy scale. This in turn determines the maximal possible value of $C/\Lambda^{2,4}$, ensuring the EFT expansion validity for all higher energy scales. This behavior of $\Delta^{VV}_{6,8}(s, C_i, \Lambda)$ is illustrated in the left panel of Figure 3.7.

Table 3.3 presents the maximal allowed values of $\frac{C^{VV}_{MAX}}{\Lambda^2}$ (dimension-6 WCs) or $\frac{C^{VV}_{MAX}}{\Lambda^4}$ (dimension-8 WCs) for two chosen values of $\Delta^{VV}_{6,8}(s, C_i, \Lambda) = 0.5, 1$, where $V = W, Z$. Since we obtain competing constraints from two VBF processes, bolded values correspond to the more stringent constraints imposed by the respective process. Empty cells indicate that the corresponding Wilson coefficient does not affect the process under consideration.

To observe how the maximum values vary with $\Delta^{VV}_{6,8}(s, C_i, \Lambda)$, we display results for two scenarios:

- $\Delta^{VV}_{6,8}(s, C_i, \Lambda) = 0.5$ - corresponding to a requirement of reasonably fast EFT expansion convergence,
- $\Delta^{VV}_{6,8}(s, C_i, \Lambda) = 1$ - corresponding to the "borderline" EFT expansion validity requirement.

In the last final four columns, $\Delta\sigma_{D6,8}$ and $\Delta N_{D6,8}$ represent the maximal cross-section and number

of event enhancements relative to the SM, including contributions from dimension-6 and dimension-8 operators, respectively. We define these quantities as:

$$\Delta\sigma_{D6,8} = (\sigma_{D6,8}^{SMEFT} - \sigma^{SM})/\sigma^{SM}, \quad \Delta N_{D6,8} = N_{D6,8}^{SMEFT} - N^{SM} \tag{3.31}$$

As we are interested in the most general features of the VBF part of the full process, we neglect the decays of Higgs pair into final states, leaving more detailed study for future work.

Table 3.3 indicates that relatively large values of WCs can lead to significant enhancement, especially for $C^{(1)}_{V^2\varphi^4}$ operators. While these values may not be entirely realistic, they may serve as an initial estimate of the magnitude of enhancement related to these dimension-8 Wilson coefficients.

WC	$\Delta^{VV}_{D6,D8}(\sqrt{s}=2m_h)$	$\frac{C^{WW}_{MAX}}{\Lambda^{2,4}}$	$\frac{C^{ZZ}_{MAX}}{\Lambda^{2,4}}$	$\Delta\sigma_{D6}$	ΔN_{D6}	$\Delta\sigma_{D8}$	ΔN_{D8}
C_φ	0.5	**0.63** [1/TeV^2]	0.72 [1/TeV^2]	32%	622	32%	622
	1	**1.27** [1/TeV^2]	1.45 [1/TeV^2]	74%	1440	74%	1440
C_{φ^8}	0.5	**5.22** [1/TeV^4]	5.99 [1/TeV^4]	-	-	31%	607
	1	**10.45** [1/TeV^4]	11.99 [1/TeV^4]	-	-	74%	1440
$C^{(1)}_{B^2\varphi^4}$	0.5	-	**71.90** [1/TeV^4]	-	-	5217%	102×10^3
	1	-	**143.80** [1/TeV^4]	-	-	20874%	407×10^3
$C^{(1)}_{W^2\varphi^4}$	0.5	21.46 [1/TeV^4]	**20.63** [1/TeV^4]	-	-	1339%	26×10^3
	1	42.93 [1/TeV^4]	**41.27** [1/TeV^4]	-	-	5456%	106×10^3

Table 3.3: Maximal enhancement of the double Higgs production process via VBF for Scenario #1 WCs. $\frac{C^{VV}_{MAX}}{\Lambda^{2,4}}$ represents the maximal allowed value of WC, constrained by the requirement of $\Delta^{VV}_{6,8}(\sqrt{s}=2m_h) \leq 0.5, 1$. $\Delta\sigma_{D6,8}$ and $\Delta N_{D6,8}$ correspond to the maximal cross-section and event number enhancements relative to the SM, including contributions from dimension-6 and dimension-8 operators, respectively.

3.4.2 Scenario #2 - energy dependence dominates the amplitude at high energies

This is the case for the $C_{\varphi\Box}$, $C_{\varphi D}$, $C_{\varphi W}$, $C_{\varphi WB}$, $C_{\varphi B}$, $C_{\varphi^6\Box}$, $C_{\varphi^6 D^2}$, $C_{V^2\varphi^2 D^2}$ and $C_{\varphi^4 D^4}$ Wilson coefficients. The energy-dependent corrections dominate the amplitude, leading to:

$$\mathcal{M}^{VV}_{SMEFT} \xrightarrow{s>>M_V^2} s^{1,2}, \quad \sigma^{VV}_{SMEFT} \propto s^{0,1}, \quad \Delta^{VV}_{6,8}(s, C_i, \Lambda) \propto s^{0,1}, \tag{3.32}$$

in other words, $\Delta^{VV}_{6,8}(s, C_i, \Lambda)$ increases with energy. This behavior is illustrated in the right panel of Figure 3.7. As a consequence, we need to ensure the validity of the EFT expansion at the **maximal** energy scale available in the process, by imposing validity conditions (3.12) and (3.14) at such scale.

We can identify the center-of-mass energy s of VBF double Higgs production process with the Higgs pair invariant mass $s \equiv m^2_{hh}$. This allows us to determine the maximal energy scale s_{MAX} by applying cut on $m^2_{hh} \leq s_{MAX}$ in the Monte Carlo simulation, ensuring that no more than 1% of the total number of events are excluded. This approach guarantees the validity of the EFT for the entire process.

Table 3.4 presents the maximal allowed values of $\frac{C^{VV}_{MAX}}{\Lambda^2}$ (dimension-6 WCs) or $\frac{C^{VV}_{MAX}}{\Lambda^4}$ (dimension-8 WCs) alongside the corresponding maximal energies of the process $\sqrt{s}_{MAX}$. We present the results for

two chosen values of $\Delta^{VV}_{6,8}(s, C_i, \Lambda) = 0.5, 1$, where $V = W, Z$. Bolded values again correspond to the more stringent constraints imposed by the respective process ($WW \to HH$ or $ZZ \to HH$). Empty cells indicate that the corresponding Wilson coefficient does not affect the process under consideration. $\Delta\sigma_{D6,8}$ and $\Delta N_{D6,8}$, given by Equations in 3.31, represent the maximal cross-section enhancement and the excess of the number of events relative to the SM, including contributions from dimension-6 and dimension-8 operators, respectively.

We conclude that for this class of WCs, the imposed validity conditions provide significantly stronger constraints on the allowed maximal values of WCs. As a consequence, these conditions strongly limit the potential enhancement of the double Higgs production via VBF process.

WC	$\sqrt{s}_{MAX}$	$\Delta^{VV}_{6,8}(\sqrt{s}_{MAX})$	$\frac{C^{WW}_{MAX}}{\Lambda^{2,4}}$	$\frac{C^{ZZ}_{MAX}}{\Lambda^{2,4}}$	$\Delta\sigma_{D6}$	ΔN_{D6}	$\Delta\sigma_{D8}$	ΔN_{D8}
$C_{\varphi\Box}$	2 TeV	0.5	**-0.20** [1/TeV^2]	-0.25 [1/TeV^2]	7.4%	144	6.9%	133
		1	**-0.40** [1/TeV^2]	-0.50 [1/TeV^2]	17%	330	14%	269
$C_{\varphi D}$	2 TeV	0.5	0.80 [1/TeV^2]	**0.46** [1/TeV^2]	1.1%	22	1.4%	26
		1	1.61 [1/TeV^2]	**0.93** [1/TeV^2]	2.9%	57	2.8%	54
$C_{\varphi W}$	2 TeV	0.5	**0.0018** [1/TeV^2]	0.0036 [1/TeV^2]	$< 1\%$	$\mathcal{O}(1)$	$< 1\%$	$\mathcal{O}(1)$
		1	**0.0036** [1/TeV^2]	0.0071 [1/TeV^2]	$< 1\%$	$\mathcal{O}(1)$	$< 1\%$	$\mathcal{O}(1)$
$C_{\varphi WB}$	2 TeV	0.5	-	**0.0067** [1/TeV^2]	$< 1\%$	$\mathcal{O}(1)$	$< 1\%$	$\mathcal{O}(1)$
		1	-	**0.0134** [1/TeV^2]	$< 1\%$	$\mathcal{O}(1)$	$< 1\%$	$\mathcal{O}(1)$
$C_{\varphi B}$	2 TeV	0.5	-	**0.012** [1/TeV^2]	$< 1\%$	$\mathcal{O}(1)$	$< 1\%$	$\mathcal{O}(1)$
		1	-	**0.024** [1/TeV^2]	$< 1\%$	$\mathcal{O}(1)$	$< 1\%$	$\mathcal{O}(1)$
$C_{\varphi^6\Box}$	2 TeV	0.5	**-1.57** [1/TeV^4]	-1.94 [1/TeV^4]	-	-	10%	193
		1	**-3.15** [1/TeV^4]	-3.89 [1/TeV^4]	-	-	23%	440
$C_{\varphi^6 D^2}$	2 TeV	0.5	-12.64 [1/TeV^4]	**-3.91** [1/TeV^4]	-	-	0.4%	7
		1	-25.29 [1/TeV^4]	**-7.81** [1/TeV^4]	-	-	2%	41
$C^{(1)}_{\varphi^4 D^4}$	2 TeV	0.5	0.45 [1/TeV^4]	**0.23** [1/TeV^4]	-	-	0.8%	17
		1	0.90 [1/TeV^4]	**0.46** [1/TeV^4]	-	-	2%	47
$C^{(1)}_{W^2\varphi^2 D^2}$	5 TeV	0.5	**-0.12** [1/TeV^4]	-0.20 [1/TeV^4]	-	-	0.6%	13
		1	**-0.24** [1/TeV^4]	-0.40 [1/TeV^4]	-	-	3%	56
$C^{(1)}_{B^2\varphi^2 D^2}$	5 TeV	0.5	-	**-0.69** [1/TeV^4]	-	-	4.4%	86
		1	-	**-1.38** [1/TeV^4]	-	-	21%	406

Table 3.4: Maximal enhancement of the double Higgs production process via VBF for Scenario #2 WCs. $\frac{C^{VV}_{MAX}}{\Lambda^{2,4}}$ represents the maximal allowed value of WC, constrained by the requirement of $\Delta^{VV}_{6,8}(\sqrt{s}_{MAX}) \leq 0.5, 1$. $\Delta\sigma_{D6,8}$ and $\Delta N_{D6,8}$ correspond to the maximal cross-section and event number enhancements relative to the SM, including contributions from dimension-6 and dimension-8 operators, respectively.

3.5 Summary and conclusions

In this chapter, we presented a study of the impact of the higher-dimensional operators in SMEFT — a widely used EFT tailored for new physics searches — on the process of the double Higgs boson production via vector boson fusion. Although VBF channel is highly suppressed in comparison to

gluon fusion, it is characterized by distinct experimental signature and strong sensitivity to BSM interactions, making it particularly interesting from the point of view of new physics searches.

We began by identifying the classes of the dimension-6 and dimension-8 SMEFT operators that could affect the process of interest, selecting a set that was further used in our analysis. In case of dimension-6 operators, we selected all 6 CP-conserving operators in the Warsaw basis, as CP-violating effects are highly suppressed and negligible in the context of this work. For dimension-8 operators, given the high number of independent structures, we selected a representative set of 10 CP-conserving operators. We believe that this choice is sufficient to capture general conclusions on the maximal enhancement of the double Higgs VBF production process in SMEFT.

In the next step, we discussed the choice of numerical values of Wilson coefficients corresponding to the selected SMEFT operators. For the dimension-6 WCs, we adopted values consistent with constraints from the global SMEFT fits to experimental data. With the lack of corresponding constraints for the dimension-8 WCs, we decided to follow so-called Naive Dimension Analysis, to put initial estimates on their values.

Next, we introduced the method that allowed us to impose more realistic constraints on the SMEFT WCs of interest, and as a result, on the VBF double Higgs production enhancement. This method is based on the study of EFT validity, understood as ensuring the convergence of the EFT expansion. We formalized this condition through by demanding that the SMEFT corrections to the $VV \to HH$ ($V = W, Z$) cross-section should decrease order-by-order with the EFT expansion.

Further, we analyzed the $VV \to HH$ cross-sections in the presence of the SMEFT dimension-6 and dimension-8 operators. We performed analytical calculations, presented relevant plots, and identified the most promising WCs in terms of cross-section enhancement.

Finally, we performed a numerical simulation of the full process of double Higgs production via VBF at the HL-LHC, incorporating EFT validity requirements. We divided the dimension-6 and dimension-8 WCs into categories, based on the energy dependence of their contributions to the $VV \to HH$ amplitude. As a result, we obtained estimates for the cross-section and number of event enhancements. The enhancements were generally small for energy-dependent WCs and only somewhat higher for energy- independent ones, especially for the dimension-8 WCs. However, the signal remained limited in most cases, suggesting restricted applicability of VBF double Higgs production for new physics searches within the region of SMEFT validity.

Chapter 4

Top-down approach: Vector-like fermions, real scalar and Higgs boson phenomenology

4.1 Introduction and motivation

Having described in detail the two studies based on the Standard Model Effective Field Theory and the bottom-up approach, this chapter presents a study in line with the top-down logic. We focus on specific models that extend the Standard Model by heavy fermion multiplets whose left-handed and right-handed components transform identically under the SM gauge group. Unlike the SM chiral fermions, these particles, known as vector-like fermions (VLF) (see e.g., [143–159]), can form gauge-invariant mass terms ($\overline{\Psi}_L \Psi_R$ + h.c.) that remain unbounded as they lack a connection to the gauge symmetry breaking mechanism. Vector-like quarks (VLQ) and leptons (VLL) have been studied extensively in various contexts, including:

- stability of the electroweak vacuum [160–164],
- double Higgs boson production enhancement [165, 166],
- electroweak phase transition (EWPT) and baryogenesis [167–176],
- $g-2$ muon magnetic moment anomaly [177–183],
- gauge coupling unification [184–190],
- flavor physics [191–194],
- electroweak precision observables (EWPO) [162, 195–197],
- dark matter [198–200].

The magnitude of the impact of a given VLF model scenario on these phenomena depends on its structure: specific field content and the allowed ranges of its masses and couplings. The allowed parameter space of a particular model scenario can depend on both experimental measurements and theoretical considerations (e.g., consistency conditions). For example, direct searches for VLF conducted by ATLAS [201–206] and CMS [207–211] experiments provide lower bounds on their masses. Then, addition of theoretical assumptions (VLF masses cannot be too large while, at the same time, the VLF Yukawa couplings remain small to have significant impact on phenomenology) and consistency conditions (such as vacuum stability and perturbativity), leads us to the prediction of optimal range of parameters of the model, which can be further used to assess its impact on phenomena of interest. This is the scope of the analysis presented in this chapter - to provide independent theoretical constraints on the parameter space of a chosen VLF model scenarios and examine their potential impact on phenomenology. The VLF model scenarios considered in this work are considered under several assumptions, such as uniform Dirac masses and VLF Yukawa couplings, applied in order to limit the number of free parameters and to simplify the calculations. Relaxing our assumptions may lead, apart from increased complexity of the models, to weakening the discussed constraints and for this reason our results cannot be "blindly" generalized to all possible VLF extensions. In the literature there are examples of theories with more complicated BSM sectors, containing in addition to VLF multiplets also (pseudo)scalar and/or vector particles (e.g., [166, 192, 198–200, 212]), or with more complicated structure of VLF parameters (e.g., flavor non-diagonal and interacting with the SM fermions [191–194]). These conditions should then be applied in a case by case manner to determine allowed parameter space for a given scenario. However, we believe that the results and conclusions of our analysis hold in general even for more complex models, and suggest that the scope of applicability of VLF models may be limited.

Since our analysis suggests that due to strong theoretical constraints on their parameter space, models containing VLF have very limited impact on phenomenology, we investigated the possibility of weakening those constraints by extending it by real scalar singlet. This simple SM extension has been extensively studied in various contexts, such as:

- EWPT and collider phenomenology [213–223],
- EWPT and gravitational waves [224, 225],
- dark matter [226–228].

Additionally, we applied the theoretical constraints worked out for the VLF models to the scalar singlet model itself, again finding its parameter space more limited than in the existing literature.

In order to illustrate the impact of theoretical constraints on the VLF and real scalar models, we analyze their influence on four examples of phenomena often studied in the literature: double Higgs production, electroweak precision observables (EWPO), electroweak phase transition (EWPT), and gauge couplings unification. We show that the maximal enhancement of double Higgs production (taking into account single Higgs production constraints) is at most 15% - far below current experimental limits [111,112]. Moreover, the VLF contributions to $\mathbb{S}$ and $\mathbb{T}$ oblique parameters are far below current experimental limits [11]. Finally, we show that 1- and 2- step EWPT can occur only for a limited range of scalar singlet parameters, with negligible impact of VLF. All in all, we conclude that due to the rigorous inclusion of theoretical constraints on the studied models, their phenomenological implications may be far more limited than previously thought. We also demonstrate how top-down and bottom-up approaches can intersect and complement each other. Taking as an example double Higgs production process, we present the matching procedure between VLQ extension and dimension-6 SMEFT in a simplified case. It illustrates the interplay between constraints on model parameters and on the SMEFT Wilson coefficients, highlighting the convergence of top-down and bottom-up approaches.

This chapter is organized as follows. First, we introduce the models and relevant notation in Section 4.2. Then, we introduce and describe the theoretical constraints used throughout this analysis in Section 4.3. Next, in Section 4.4 we utilize those constraints to determine the parameter space of specific model scenarios, extending the SM by: VLF only - Section 4.4.1, scalar singlet only - Section 4.4.2, and VLF with scalar singlet together - Section 4.4.3. Additionally, we study the impact of including additional VLF couplings (like e.g., VLF-SM Yukawa interactions) in Section 4.4.4 and discuss gauge couplings unification in Section 4.4.5. Section 4.5 is dedicated to the detailed study of consequences of considered models with obtained parameter space on phenomenology: double Higgs boson production via gluon fusion 4.5.1, electroweak precision observables 4.5.2 and electroweak phase transition 4.5.3. Finally, we describe the example of matching between VLQ and SMEFT in Section 4.5.4, and conclude in Section 4.6.

4.2 The model: vector-like fermions and real scalar

In this chapter, we consider a class of models with SM particle content extended by adding heavy vector-like fermion multiplets and/or real scalar field with $\mathbb{Z}_2$ symmetry. The resulting Lagrangian contains, apart from the SM fields, vector-like quarks or leptons in doublet and singlet representations of the $SU(2)$ weak isospin gauge group (as detailed in Table 4.1), and a new gauge singlet scalar field.

ψ	$SU(3)_c$	$SU(2)_L$	Y_W	T_3	Q_{EM}
$Q^d_{L,R} = \begin{pmatrix} U^d_{L,R} \\ D^d_{L,R} \end{pmatrix}$	3	2	$+1/6$	$+1/2$ $-1/2$	$+2/3$ $-1/3$
$U^s_{L,R}$	3	1	$+2/3$	0	$+2/3$
$D^s_{L,R}$	3	1	$-1/3$	0	$-1/3$
$L^d_{L,R} = \begin{pmatrix} N^d_{L,R} \\ E^d_{L,R} \end{pmatrix}$	1	2	$-1/2$	$+1/2$ $-1/2$	0 -1
$N^s_{L,R}$	1	1	0	0	0
$E^s_{L,R}$	1	1	-1	0	-1

Table 4.1: VLF multiplets extending the SM field content. The superscripts d and s denote $SU(2)$ doublets and singlets, respectively.

The vector-like fermions are assumed to interact with the SM particles only through Yukawa couplings between VLF and the SM Higgs. While mixed Yukawa couplings between SM and new VLF can also be considered, such terms would only further shrink the allowed parameter space of models studied in this work, so we decided to neglect them (for details see Section 4.4.3). The SM scalar potential and scalar doublet φ have the same form as in Eqs. ((1.12), (1.13)).

New terms in the Lagrangian containing the VLF Dirac masses and Yukawa interactions between VLF and the SM Higgs read:

$$\begin{aligned}\mathcal{L} \supset &- \sum_{i,j=1}^{n_Q} M^{ij}_{Q^d} \bar{Q}^d_i Q^d_j - \sum_{i,j=1}^{n_U} \left(M^{ij}_{U^s} \bar{U}^s_i U^s_j + (y^{ij}_U \bar{Q}^d_i \tilde{\varphi} U^s_j + \text{h.c.}) \right) - \sum_{i,j=1}^{n_D} \left(M^{ij}_{D^s} \bar{D}^s_i D^s_j + (y^{ij}_D \bar{Q}^d_i \varphi D^s_j + \text{h.c.}) \right) \\ &- \sum_{i,j=1}^{n_L} M^{ij}_{L^d} \bar{L}^d_i L^d_j - \sum_{i,j=1}^{n_N} \left(M^{ij}_{N^s} \bar{N}^s_i N^s_j + (y^{ij}_N \bar{L}^d_i \tilde{\varphi} N^s_j + \text{h.c.}) \right) - \sum_{i,j=1}^{n_E} \left(M^{ij}_{E^s} \bar{E}^s_i E^s_j + (y^{ij}_E \bar{L}^d_i \varphi E^s_j + \text{h.c.}) \right),\end{aligned} \tag{4.1}$$

Eq. (4.1) describes a broad class of models, with the upper summation indices indicating the number of VLF doublets and singlets added to the SM Lagrangian. For example, $n_Q = n_U = 1$, $n_D = 0$ corresponds to a model with one $SU(2)$ vector-like quark doublet, one "up-type" vector-like quark singlet and no "down-type" vector-like quark singlets. In each model scenario, we consider vector-like quarks OR leptons at a time, so in this case we have $n_L = n_N = n_E = 0$ (note that $\sum_1^0 = 0$).

In order to understand the most interesting and common features of the studied VLF models, we decided to limit the number of free parameters in the Lagrangian (4.1) by assuming mass and coupling matrices to be VLF-flavor diagonal, real, and identical for each generation. In the $F = (F^d, F^s)$ interaction basis (where $F^d \in \{U^d, D^d, N^d, E^d\}$ and $F^s \in \{U^s, D^s, N^s, E^s\}$), the mass matrices (after the spontaneous symmetry breaking) can be then written in the following form:

$$\bar{F}_L \circ \widetilde{\mathbf{M}}_F \circ F_R = (\bar{F}^d, \bar{F}^s)_L \circ \begin{pmatrix} M_{F^d} & \frac{1}{\sqrt{2}} v\, y_F \\ \frac{1}{\sqrt{2}} v\, y_F & M_{F^s} \end{pmatrix} \circ \begin{pmatrix} F^d \\ F^s \end{pmatrix}_R . \tag{4.2}$$

Diagonalization of $\widetilde{\mathbf{M}}_F$ the symmetric mass matrix requires a unitary rotation V_F that transforms the VLF states from the interaction (F^d, F^s) to the mass (F^1, F^2) basis. The rotation is the same for left-

and right-handed states and can be parametrized by a single angle γ_F:

$$\begin{pmatrix} F^d \\ F^s \end{pmatrix} = V_F \circ \begin{pmatrix} F_1 \\ F_2 \end{pmatrix} = \begin{pmatrix} \cos\gamma_F & -\sin\gamma_F \\ \sin\gamma_F & \cos\gamma_F \end{pmatrix} \circ \begin{pmatrix} F_1 \\ F_2 \end{pmatrix}, \quad \tan 2\gamma = \frac{\sqrt{2}\, y_F\, v}{M_{F^d} - M_{F^s}}. \tag{4.3}$$

Diagonalization procedure results in:

$$(\bar{F}^d, \bar{F}^s)_L \circ \begin{pmatrix} M_{F^d} & \frac{1}{\sqrt{2}}\, v\, y_F \\ \frac{1}{\sqrt{2}}\, v\, y_F & M_{F^s} \end{pmatrix} \circ \begin{pmatrix} F^d \\ F^s \end{pmatrix}_R = (\bar{F}_1, \bar{F}_2)_L \circ \begin{pmatrix} M_{F_1} & 0 \\ 0 & M_{F_2} \end{pmatrix} \circ \begin{pmatrix} F_1 \\ F_2 \end{pmatrix}_R, \tag{4.4}$$

with eigenvalues of mass matrix (i.e., physical masses) equal to:

$$\begin{aligned} M_{F_1} &= \frac{1}{2}\left(M_{F^d} + M_{F^s} + \sqrt{(M_{F^d} - M_{F^s})^2 + 2v^2 y_F^2} \right), \\ M_{F_2} &= \frac{1}{2}\left(M_{F^d} + M_{F^s} - \sqrt{(M_{F^d} - M_{F^s})^2 + 2v^2 y_F^2} \right). \end{aligned} \tag{4.5}$$

We can also write corresponding interaction terms in the mass basis:

$$(\bar{F}^d, \bar{F}^s)_L \circ \begin{pmatrix} 0 & \frac{1}{\sqrt{2}}\, h\, y_F \\ \frac{1}{\sqrt{2}}\, h\, y_F & 0 \end{pmatrix} \circ \begin{pmatrix} F^d \\ F^s \end{pmatrix}_R = (\bar{F}_1, \bar{F}_2)_L \circ \begin{pmatrix} Y'_F & Y_F \\ Y_F & -Y'_F \end{pmatrix} \circ \begin{pmatrix} F_1 \\ F_2 \end{pmatrix}_R, \tag{4.6}$$

with:

$$Y'_F = \frac{1}{\sqrt{2}}\, y_f\, \sin 2\gamma_F, \quad Y_F = \frac{1}{\sqrt{2}}\, y_f\, \cos 2\gamma_F. \tag{4.7}$$

In addition to the VLF, in part of this analysis we further extend the SM Lagrangian by a real scalar singlet S with an unbroken $\mathbb{Z}_2$ symmetry [1], under which $S \to -S$. The full scalar potential reads:

$$V(\varphi, S) = V_{SM}(\varphi) + \frac{1}{2}\mu_S^2\, S^2 + \frac{1}{2}\lambda_{HS}\, \varphi^\dagger\varphi\, S^2 + \frac{1}{4}\lambda_S\, S^4, \tag{4.8}$$

where φ is defined in Eq. 1.13. For the reasons of convenience, in this chapter we adopted a slightly modified form of the Standard Model potential compared to Eq. 1.12($\frac{\lambda}{2} \to \lambda$):

$$V_{SM}(\varphi) = -\mu^2 \varphi^\dagger\varphi + \lambda(\varphi^\dagger\varphi)^2. \tag{4.9}$$

This change in notation is properly accounted for where necessary. Assuming vanishing vacuum expectation value (vev) for S (without excluding the possibility of S acquiring vev at some point during the evolution of the universe), leads to the following tree level masses for the scalar particles:

$$M_H^2 = 2\lambda v^2 = 2\mu^2, \quad M_S^2 = \mu_S^2 + \frac{1}{2}\lambda_{HS} v^2\,. \tag{4.10}$$

In order to illustrate the effects of different types of BSM fields on phenomenology, we distinguish three specific classes of models:

- Class A - models with SM extended by vector-like fermions only,

[1] Such discrete symmetry is assumed to simplify some formulae, but it is not crucial for the present work since it forbids terms linear and cubic in S which do not alter β functions used to obtain the main results of our analysis

- Class B - models with SM extended by the real scalar only,
- Class C - models extended by both vector-like fermions and real scalar.

Additionally, we vary the number of VLF multiplets in Class A and B, following the notation of (4.1), and consider three representative benchmark "Scenarios":

- Scenario I - n VLF doublets, $2 \times n$ VLF singlets (n of "up-type" and n of "down-type"),
- Scenario II - n VLF doublets, n "up-type" VLF singlets, 0 "down-type" VLF singlets,
- Scenario III - n VLF doublets, 0 "up-type" VLF singlets, n "down-type" VLF singlets.

In what follows, n will refer to the number of VLF families (single family's composition is dependent on specific scenario). As already mentioned, we always consider vector-like quarks and leptons separately. More specifically, we have:

- Scenario I with VLQ and $n = 1$ corresponds to:

$$n_Q = n_U = n_D = 1, \quad n_L = n_E = n_N = 0, \tag{4.11}$$

- Scenario II with VLQ and $n = 2$ corresponds to:

$$n_Q = n_U = 2, \quad n_L = n_E = n_N = n_D = 0, \tag{4.12}$$

- Scenario III with VLL and $n = 2$ corresponds to:

$$n_L = n_E = 2, \quad n_Q = n_U = n_D = n_N = 0. \tag{4.13}$$

The SM input parameters used in this analysis are set following [229], with updated experimental input parameters taken as central values from [11]:

$$\begin{aligned} &M_t = 172.83 \text{ GeV}, \quad g_1(M_\text{t}) = \sqrt{5/3} \times g' = \sqrt{5/3} \times 0.358144, \\ &g_2(M_\text{t}) = 0.64772, \quad g_3(M_\text{t}) = 1.1646, \quad y_\text{t}(M_\text{t}) = 0.93436, \quad \lambda(M_\text{t}) = 0.12637. \end{aligned} \tag{4.14}$$

Finally, we verified that the theoretical and experimental uncertainties associated with the input parameters do not significantly alter our results and conclusions.

4.3 Theoretical constraints

4.3.1 Short introduction to the renormalization group equations

Theoretical constraints considered in this work are based on the energy-scale dependence of model parameters, governed by the renormalization group equations (RGE). RGE are a direct consequence of the renormalization procedure, which replaces *bare* quantities (fields ϕ^0, coupling constants κ^0, ...) in favor of *renormalized* ones (ϕ, κ, ...) to make the theory finite and predictive. This procedure introduces an arbitrary energy scale μ, called **renormalization** scale, and leads to the dependence of **renormalized** parameters on μ (although physical observables and initial *bare* quantities are μ -

independent). This dependence is described by the RGEs, which encode the μ - evolution through the β functions. For a given coupling $\kappa(\mu)$, the RGE take the form:

$$\frac{d\kappa(\mu)}{d\ln\mu} = \beta_\kappa. \tag{4.15}$$

Corrections to β_κ functions can be calculated systematically order-by-order in perturbation theory.

As a simple example, consider the running of the fine structure constant α_{em} in QED. The QED Lagrangian is given by:

$$\mathcal{L}_{\text{QED}} = \bar{\psi^0}(i\not{D} - m^0)\psi^0 - \frac{1}{4}\left(F^0_{\mu\nu}\right)^2, \quad \not{D} = i\not{\partial} - ie^0\not{A}^0, \tag{4.16}$$

where e^0 and m^0 are the *bare* electric charge and fermion mass, A^0_μ and ψ^0 are the *bare* photon and fermion fields, and $F^0_{\mu\nu} = \partial_\mu A^0_\nu - \partial_\nu A^0_\mu$ is the *bare* field strength tensor. At leading order (1-loop), the beta function for the *renormalized* fine-structure constant $\alpha_{em} = \frac{e^2}{4\pi}$ is given by:

$$\beta(\alpha_{em}) = \frac{2\alpha^2_{em}}{3\pi^2}. \tag{4.17}$$

The solution to this equation dictates the running of $\alpha_{em}(\mu)$:

$$\alpha_{em}(\mu) = \frac{\alpha_{em}\left(\mu_0\right)}{1 - \frac{1}{3\pi}\alpha_{em}\left(\mu_0\right)\ln\frac{\mu}{\mu_0}}. \tag{4.18}$$

where $\alpha\left(\mu_0\right)$ is the fine-structure constant at some reference scale μ_0. One can easily notice, that this expression "blows-up" at the scale Λ_L^{QED}:

$$\alpha_{em}(\mu) = \frac{\alpha\left(\mu_0\right)}{1 - \frac{1}{3\pi}\alpha\left(\mu_0\right)\ln\frac{\mu}{\mu_0}} \xrightarrow{\mu\to\Lambda_L^{QED}} \infty, \quad \Lambda_L^{QED} = \mu_0 \exp\left(\frac{3\pi}{\alpha_{em}(\mu_0)}\right), \tag{4.19}$$

where Λ_L^{QED} is the so-called **Landau pole** - the energy scale at which the coupling constant α_{em} becomes infinite, signaling the breakdown of perturbation theory.

Using the initial value $\alpha(\mu_0 = m_e = 0.511\text{ MeV}) = \frac{1}{137}$, we find that:

$$\Lambda_L^{QED} \gg M_{PL} \approx 10^{19}\text{ GeV}. \tag{4.20}$$

The Λ_L^{QED} lies at an energy scale far beyond the reach of our experiments and beyond the expected QED validity range, but it illustrates an important point, that even a well established theory like QED may cease to be perturbative at sufficiently high energy scale.

For a more formal derivation of RGE see e.g., [1–3]. The 1-loop β-functions for the SM and BSM model scenarios considered in this chapter are presented in Appendix H.

4.3.2 Three validity conditions

We treat the model scenarios introduced in the previous section as effective theories valid up to a given cut-off energy scale Λ, up to which relevant constraints have to be satisfied. Below, we present three conditions, on which we based this analysis.

1. **Stability of the electroweak vacuum**
   We require that the scalar potential is bounded from below. In models of Class A, this corresponds to the condition that the Higgs self-coupling λ is positive up to the cut-off scale Λ [2]

$$\lambda(\mu) > 0 \quad \text{for} \quad \mu \leq \Lambda \,. \tag{4.21}$$

2. **Perturbativity of the model couplings up to the cut-off scale Λ**

$$\kappa_i(\mu) \leq 4\pi \quad \text{for} \quad \mu \leq \Lambda \,, \tag{4.22}$$

   where $\kappa_i = (\lambda, y_t^2, g_1^2, g_2^2, g_3^2, y_F^2, \lambda_{HS}, \lambda_S)$. This condition is related to the breakdown of the perturbative expansion discussed in the previous Section 4.3.1, with 4π being the maximal value of the coupling constant for which higher-order loop corrections may remain convergent.

3. **Stability of the perturbative expansion up to the cut-off scale Λ**

$$\min_{[\mu, \mu\times 10^{\delta}]} \left| \frac{\beta_{\kappa_i}^{(2)}(\mu)}{\beta_{\kappa_i}^{(1)}(\mu)} \right| \leq \Delta \quad \text{for} \quad \mu \leq \Lambda \,. \tag{4.23}$$

   where (1) and (2) superscripts indicate, respectively, 1-loop and 2-loop contribution to a β-function for a given coupling. We consider the ratio of 2- and 1-loop contributions minimized over some range of μ scale, in order to avoid its artificial large values around points where a given 1-loop term vanishes. Δ is a maximal allowed value of such regularized ratio. For our numerical analysis, we choose $\delta = 1$ and $\Delta = 0.4$. We checked that the constraints on the model parameters following from the condition (4.23) depend weakly on the precise values of δ and Δ (more specifically, using higher value of $\Delta = 0.6$ leads to increase of maximal allowed values of couplings by $\mathcal{O}(20\%)$). This condition is analogous to those discussed in the previous Chapter, where the validity of the EFT expansion was controlled through Equations (3.12) and (3.14). In this case, we rely on RGE to ensure the perturbative expansion validity.

In addition to those theoretical constraints given by the Eqs. (4.21), (4.22), (4.23), we take into account additional conditions relevant for the discussion. This includes: experimental limits on the triple Higgs coupling, single and double Higgs production, existing bounds on masses of VLF and real scalar, electroweak precision observables and gauge couplings unification. The combination of all of those factors leads to the final bounds on the parameter space of considered VLF and real scalar models.

For the numerical calculations, we use the 2-loop RGE obtained with SARAH [230] and cross-checked with RGBeta [231] codes. In Appendix H we collect 1-loop contributions (2-loop contributions are too lengthy to be displayed in a user-friendly and readable manner), that serve us as a basis of the explanation of various observed effects. Finally, we include vector-like fermions and scalar contributions to the β-functions only for (renormalization) energy scales μ above their respective masses - $\mu \geq M_F$ for vector-like fermions and $\mu \geq M_S$ for scalar singlet.

[2] In models with the singlet scalar (classes B and C) stability of the scalar potential (4.8) requires also: $\lambda_{HS}(\mu) > -2\sqrt{\lambda(\mu)\lambda_S(\mu)}$ and $\lambda_S(\mu) > 0$ for $\mu \leq \Lambda$. Both are always fulfilled for models considered in this work. Both couplings, λ_S and λ_{HS}, are positive at all relevant scales if they are positive at low scale $\mu = M_t$ because the leading contributions (H.5) to their β functions are positive.

4.4 Allowed parameter space of VLF models

In this section, we examine the impact of conditions (4.21), (4.22), (4.23) on the VLF sector defined in Section 4.2 (see Eq. (4.1) and Table 4.1) on the number of VLF multiplets, their masses and couplings. As a result, we obtain maximal allowed values of VLF Yukawa couplings for a given cut-off Λ for which our conditions are satisfied. As we show, these values are too small for VLF to have any significant impact on phenomenology. In order to somehow alleviate these stringent constraints, the additional real scalar field S is introduced in Sections 4.4.2 and 4.4.3.

As mentioned before, in order to limit the number of free parameters in the VLF model, we assume uniform values of Dirac masses of VLF doublets and singlets, and a single universal value of all VLF Yukawa couplings. This simplifies formulas for physical masses and mixing matrix of VLF - Eqs. (4.5), (4.3):

$$\begin{gathered} M_{F^d} = M_{F^s} = M_F, \quad y_F = y, \quad \gamma_F = \gamma = \frac{\pi}{4}, \\ M_{F_{1/2}} = M_F \pm \frac{\sqrt{2}}{2} v y_F, \quad V_F = \begin{pmatrix} \cos\frac{\pi}{4} & -\sin\frac{\pi}{4} \\ \sin\frac{\pi}{4} & \cos\frac{\pi}{4} \end{pmatrix}. \end{gathered} \tag{4.24}$$

We assume the lower limit of VLF masses $M_F \gtrsim 1$ TeV, which is based on the results of recent direct searches from ATLAS [201–206] and CMS [207–211] experiments. As for the upper limit, too large M_F values would lead to their effective decoupling and negligible impact on the phenomenology and modifications of the SM couplings. For this reason, we consider masses of VLF and scalar between $\mathcal{O}(1 \div 10)$ TeV. Also, the cut-off scale Λ needs to be larger than the heaviest particle in the model, but its too large value leads to significant shrinking of the parameter space. Therefore, we chose the range $\Lambda = 100 \div 1000$ TeV.

4.4.1 SM extended with vector-like fermions only – Case A

We begin by studying the impact of VLF on the running of SM couplings. Plots in Figure 4.1 show how varying VLF Yukawa couplings influences the running of λ, the gauge couplings g_1 and g_2 and the top Yukawa coupling y_t. For simplicity, we assume $n = 1$ (behavior of models with larger numbers of VLF families is qualitatively very similar, see Figure 4.4 and discussion in Section 4.4.5). Plots in Figure 4.1 reveal, that in the case of VLF only, the main source of constraints comes from VLF impact on the Higgs quartic coupling λ and vacuum stability condition given by Eq. (4.21), as already relatively small values of VLF Yukawa couplings y have a visible "negative" impact on running of λ. Looking closer, the left panel of Figure 4.1 leads to the two regimes that can be distinguished depending on the magnitude of y: 1) VLF with small (or vanishing) Yukawa couplings, and 2) VLF with larger Yukawa couplings.

1. **VLF with small (or vanishing) Yukawa couplings**
   In this scenario, VLF have a positive impact on the stability of the EW vacuum compared to the SM, potentially leading to stability up to the Planck scale. This behavior by looking at 1-loop RGEs. For $y = 0$, VLF contributions directly influence the running of g_1 and g_2 gauge couplings (see Eq. (H.4)), which in turn increases the values of β_λ (see Eq. (H.3)). Inclusion of VLQ multiplets leads to a more significant effect compared with VLL, as the number of degrees of freedom affect RGE running through the color factor N_c' in Eq. (H.4). In the case of g_1, this effect is more model-dependent due to the differences in hypercharges between quarks and leptons.

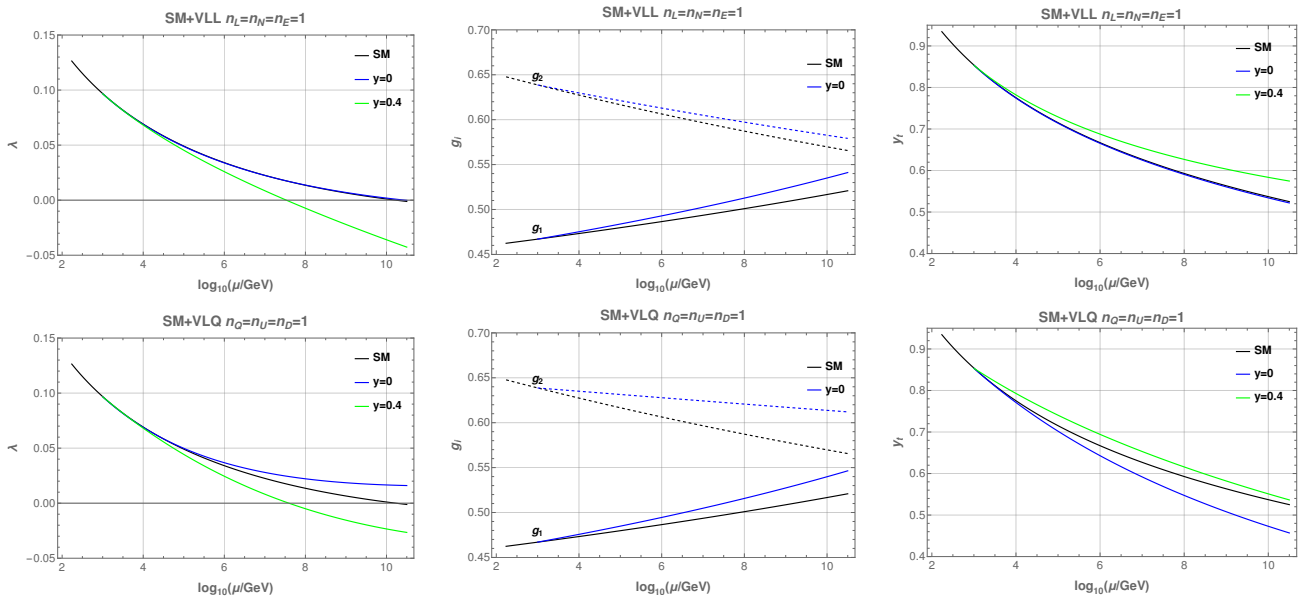

Figure 4.1: Running of λ (left column), g_1 and g_2 (continuous and dashed lines respectively, middle column) and y_t (right column) at 2-loop in the SM extended by VLF assuming $M_F = 1$ TeV and varying VLF Yukawa coupling y.

2. **VLF with larger Yukawa couplings**
   Increase in the VLF Yukawa couplings typically has a negative impact on the stability of the EW vacuum. For values larger than a certain critical value, the EW vacuum becomes unstable. This can be again understood through the 1-loop RGEs: the leading VLF contribution to the running of λ is proportional to the factor $(2\lambda - y_F^2)y_F^2$ (first equation in (H.4)). For small values of y_F^2, this term remains positive, but turns negative for $y_F^2 > 2\lambda$. As y_F^2 grows, so is the overall negative contribution, and soon overcomes the indirect positive contribution mentioned before. This effect is even stronger with the positive effect of VLF on β_{y_t}, which indirectly amplifies the negative term in β_λ that is proportional to y_t^4 (first equation in (H.3)).

The maximal Yukawa coupling value that satisfies the stability condition (4.21) depends not only on the cut-off scale Λ but also on the masses of VLF M_F. The effects from VLF are stronger for smaller masses, as lighter particles modify the RGE from lower energy scales. This applies to both scenarios - those which improve and those which worsen stability of the EW vacuum. Figure 4.2 illustrates this relation for two values of y in Scenario I with VLQ.

As discussed above, VLF with Yukawa couplings larger than some critical values have negative impact on the EW vacuum stability. The larger are these couplings, the lower is the energy scale at which λ turns negative. Thus, requiring λ to remain positive until a chosen cut-off scale Λ imposes an upper limit on the Yukawa coupling, y_{MAX}, in a given model[3] (we remind the reader that couplings without explicit scale-dependence denote these couplings renormalized at the scale of the top quark mass, $\mu = M_t$).

Negative contributions to β_λ from VLF increase with their corresponding Yukawa couplings. Thus, the maximal allowed value of the Yukawa coupling in a given model, y_{MAX}, is a decreasing function

[3]Here, we assumed that all VLF's Yukawa couplings are equal. In more general models, this upper bound applies to a combination of different Yukawa couplings.

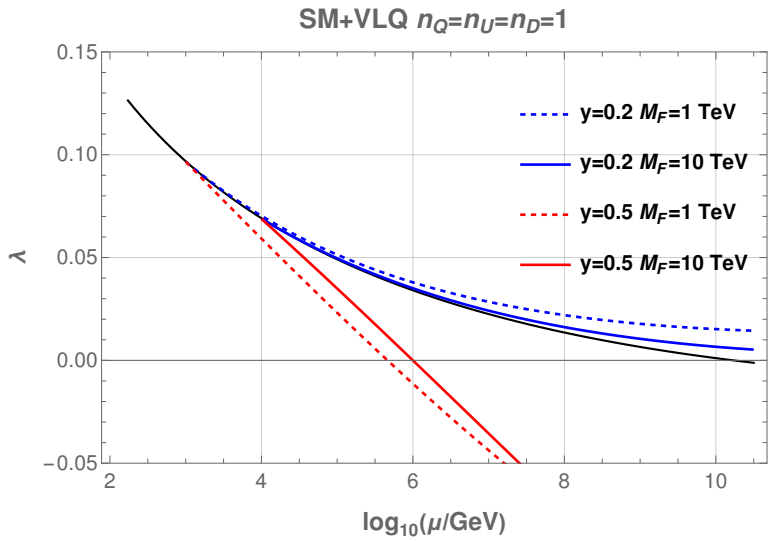

Figure 4.2: Running of λ coupling for chosen values of M_F and y. The black line indicates λ of the SM.

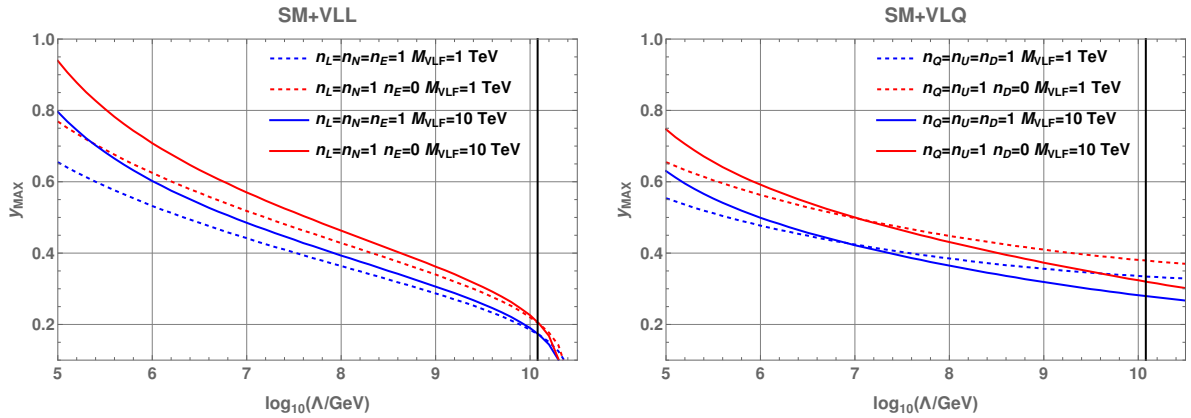

Figure 4.3: The maximal values of the VLF Yukawa coupling that satisfy the stability condition up to a given scale μ. $M_F = 1, 10$ TeV. The vertical lines represent the energy scale at which the SM stability breaks down.

of the cut-off scale Λ. Such dependence for scales above the $10^{9\div10}$ GeV (i.e., the scale at which λ becomes negative in the SM) differs significantly for VLL and VLQ models. In VLL models, y_{MAX} rapidly drops to zero, while in VLQ models, y_{MAX} decreases much more gradually. This difference follows from the impact of VLF with small Yukawa couplings on the RGE evolution of λ, illustrated in the upper row of plots in Figure 4.1. Namely, VLL can only slightly improve the EW vacuum stability, and only for very small values of Yukawa couplings. On the other hand, the addition of VLQ with moderate Yukawa couplings may stabilize the EW vacuum even up to the Planck scale.

Several examples of $y_{MAX}(\Lambda)$ evolution for VLL and VLQ models are presented in Figure 4.3. The largest possible values of y_{MAX}, corresponding to the lowest cut-off scale considered in this study, $\Lambda = 100$ TeV, for Scenarios I and II in VLL and VLQ models, and for two different values of M_F, are collected in Table 4.2.

	Scenario	y_{MAX}	
		$M_F = 1$ TeV	$M_F = 10$ TeV
VLQ	$n_Q = n_U = n_D = 1$	0.55	0.63
	$n_Q = n_U = 1$ $n_D = 0$	0.66	0.75
VLL	$n_L = n_E = n_N = 1$	0.66	0.80
	$n_L = n_N = 1$ $n_N = 0$	0.77	0.94

Table 4.2: The maximal values of VLF Yukawa couplings allowed by the conditions (4.21)–(4.23) up to the cut-off scale $\Lambda = 100$ TeV for two different values of M_F.

Impact of number of VLF multiplets

Finally, one can also discuss the impact of increasing the number of VLF multiplets on the running of the SM couplings. Once again, we can distinguish two different regimes:

1. **VLF with small (or vanishing) Yukawa couplings** - left panel on Figure 4.4
   As one can notice, increasing number of VLF multiplets while keeping $Y = 0$, leads to the "improvement" in vacuum stability (eventually leading to the breakdown of perturbative expansion). However, as this case is less interesting from the point of view of applications and phenomenology considered in this work, we won't discuss it further.

2. **VLF with larger Yukawa couplings** - right panel on Figure 4.4
   For values of Yukawa coupling Y, for which we have "negative" impact on vacuum stability with $n = 1$, increasing number of VLF multiplets can only strengthen this problem. It can be explained by the VLF contributions to the λ coupling - Eq. (H.4). In the first approximation, the "negative" impact on λ is caused by term $\propto -n_F y^4$. Moreover, this implies that in the regime of our interest cases in which this factor is the same are identical (e.g., $n = 1$ & $y = 0.4$ and $n = 2$ & $y = 0.34$), which further justifies our choice of focusing on the case with number of VLF multiplets $n = 1$.

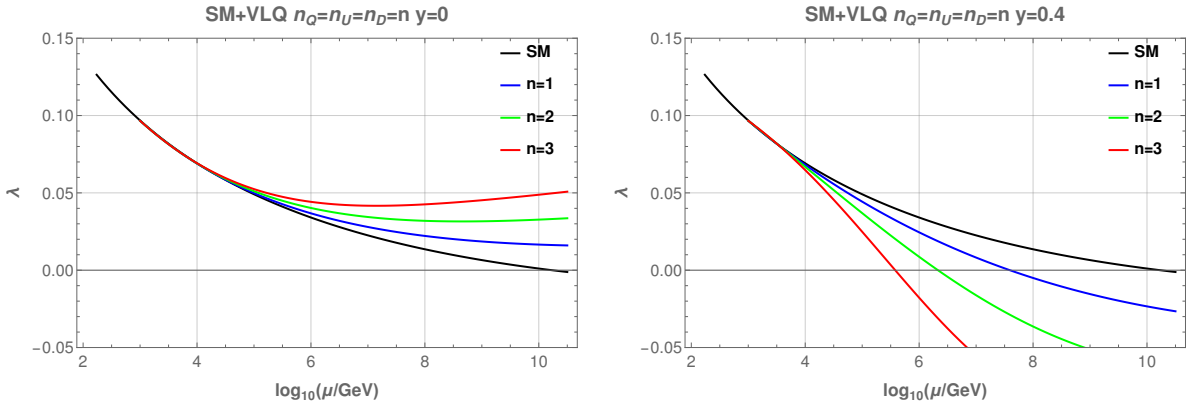

Figure 4.4: Impact of varying number of VLQ multiplets on the running of λ for small (vanishing) Yukawa coupling - left panel, and larger Yukawa coupling - right panel.

The results presented in this section indicate that, in all considered scenarios, the maximal values

of VLF Yukawa couplings allowed by the EW stability condition are relatively small, with $y_{MAX} < 1$. As we will see later, this suggests a limited phenomenological consequences of such SM extensions that could be experimentally tested in the near future. Many previous studies that explore the phenomenology of VLF models (e.g., [167,168,170–176]) often require large Yukawa couplings to generate observable effects. The present analysis suggests, however, that achieving such large couplings may not be possible in perturbative models with a stable EW vacuum.

The impact of VLF on the EW vacuum stability presented here, aligns with the results of a similar study [161], and we successfully reproduce their results. However, our work examines a broader class of VLF model scenarios, emphasizing their potential observable effects on phenomenology (discussed in detail in Section 4.5).

While our analysis obviously does not exhaust all possible VLF scenarios, it suggests that the simple EW vacuum stability requirement strongly constraints the allowed parameter space of these models. Testing VLF models with a more complex pattern of different couplings would require a case by case study, which lies beyond the scope of this work.

4.4.2 SM extended with real scalar singlet – Case B

To study the full freedom in constructing VLF models and extend their allowed parameter space, we first consider an extension of the SM with the real scalar singlet, S, with a tree-level potential defined in Eq. (4.8). We begin our analysis by exploring the theoretical constraints on the SM extended by the real scalar singlet alone.

The primary effect of S arises from its coupling to the SM Higgs scalar, λ_{HS}, which contributes positively to β_λ (see the first equation in Eq. (H.5)). Additionally, the singlet self-coupling, λ_S, indirectly enhances λ through its positive contribution to $\beta_{\lambda_{HS}}$ (second equation in Eq. (H.5)). As a consequence, increasing the scalar couplings λ_{HS} and λ_S, and/or reducing M_S leads to higher values of λ, positively affecting the stability of the EW vacuum. For instance, one gets absolute stability up to the Planck scale for $M_S = 1$ TeV, $\lambda_S = 0$ and $\lambda_{HS} \gtrsim 0.3$. This behavior is illustrated in the left panel in Figure 4.5.

However, too high increase in the values of λ_S and λ_{HS} can result in a loss of perturbativity, i.e., violation of the condition(s) in Eqs.(4.22) and/or (4.23) below the chosen cut-off scale Λ. Figure 4.5 illustrates the regions in the λ_S-λ_{HS} plane that are consistent with these conditions for chosen values of scale Λ and the singlet mass M_S. Table 4.3 provides the maximal values of the coupling λ_{HS}^{max} for different values of λ_S, Λ and singlet mass M_S. As expected, increasing the value of M_S relaxes the upper bound on λ_{HS}, while increasing λ_S or Λ leads to a stricter limit on this coupling.

λ_{HS}^{max}				
λ_S	$M_S = 1$ TeV	$M_S = 5$ TeV	$M_S = 1$ TeV	$M_S = 5$ TeV
	$\Lambda = 100$ TeV		$\Lambda = 1000$ TeV	
0	3.18	4.34	2.33	2.90
1	1.60	3.16	-	1.03

Table 4.3: Maximal allowed values of λ_{HS} in the SM extended by the real singlet satisfying the perturbativity conditions for selected values of λ_S, Λ and M_S. An empty cell indicates violation of conditions, even for $\lambda_{HS} = 0$.

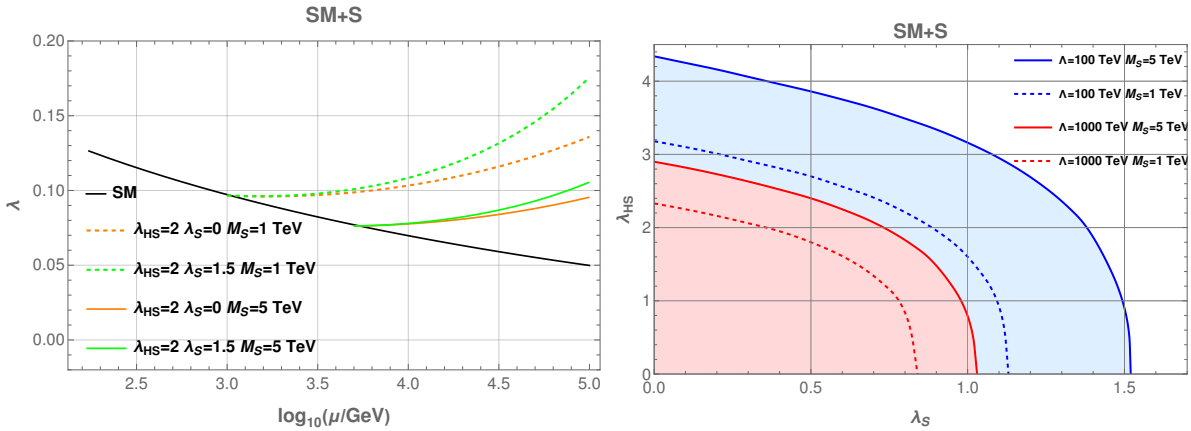

Figure 4.5: Left panel - the impact of the scalar couplings λ_{HS}, λ_S and the mass M_S on running of λ. Right panel - the parameter space of the SM extended by the real singlet allowed by the perturbativity constraints up to $\Lambda = 100, 1000$ TeV with varying $M_S = 1, 5$ TeV.

Our approach offers a new and independent way for studying the parameter values in the real scalar model and can be seen as complementary to the previous works (e.g., [213–215]) by further constraining the parameter space of this model. It highlights the importance of moving beyond the naive study of perturbativity as given by the condition (4.22) alone, by taking into account the differences between 1- and 2-loop contributions to the RGE.

4.4.3 SM extended with vector-like fermions and real scalar singlet – Case C

Since the addition of the real singlet to the model improves the stability of the EW vacuum through its positive effect on the running of λ, it should also relax constraints on the VLF Yukawa couplings summarized in Table 4.2. However, studying the constraints on y_{MAX} in the presence of extra singlet scalar field, we must also take into account potential violation of the perturbativity conditions in Eqs. (4.22) and (4.23) as we increase the values of new scalar couplings.

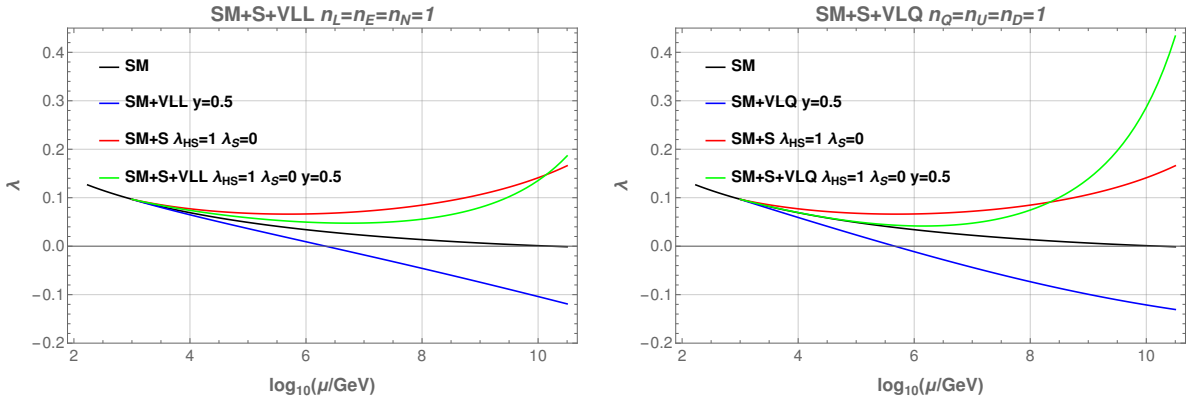

Figure 4.6: Running of λ in the combined SM+S+VLF model, with $M_S = 1$ TeV and $M_F = 1$ TeV.

As demonstrated earlier, in the model with the SM extended only by the singlet scalar, all conditions in Eqs. (4.21)–(4.23) are satisfied as long as the values λ_S and λ_{HS} small enough to avoid

problems with perturbativity. It turns out, that the inclusion of VLF with Yukawa couplings large enough to have meaningful phenomenological effects further strengthens the constraints imposed by conditions in Eqs. (4.21)–(4.23). This occurs due to the fact, that VLF not only negatively affect the vacuum stability (see Section 4.4.1) but also strengthen problems with perturbativity. The reason of the latter effect is evident from Eq. (H.6), where additional fermions contribute positively to $\beta_{\lambda_{HS}}$ proportionally to the sum of squares of their Yukawa coupling.

The impact of VLF on the RGE running λ is illustrated with examples in Figure 4.6. The Higgs self-coupling λ in models with S and VLF (green curves) is lower at low scales but higher at high scales compared to the model without VLF (red curves). These effects result in stronger constraints on the singlet scalar couplings λ_S and especially λ_{HS}. The stability condition in Eq. (4.21) leads to a lower bound on λ_{HS} as a function of λ_S, while the perturbativity conditions in Eqs. (4.22) and (4.23) lead to a corresponding upper bound. The impact of VLF on the λ_{HS}–λ_S parameter space, dependent on the value of their Yukawa couplings, is presented in Figure 4.7 (for comparison, see the corresponding plot without VLF shown in Figure 4.5) and in Table 4.4

The allowed region in the λ_S–λ_{HS} plane decreases as the VLF Yukawa couplings increase, eventually shrinking to the point that defines their maximal allowed value y_{MAX}. The addition of the singlet S to the model increases the maximal Yukawa couplings by up to about 50% compared to pure VLF models, as evident from a comparison between Tables 4.2 and 4.4.[4]

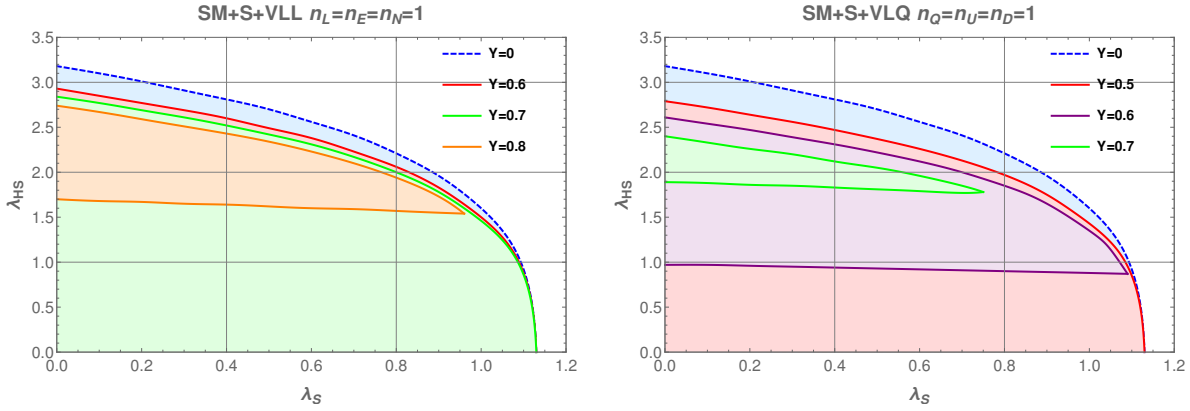

Figure 4.7: Allowed regions of the singlet scalar couplings in the SM extended by the real singlet and the VLF for the cut-off scale $\Lambda = 100$ TeV with $M_F = M_S = 1$ TeV, and for different values of the VLF Yukawa coupling Y. The dashed blue contour is the same as in Figure 4.5.

4.4.4 Models with additional VLF couplings

So far, we have assumed that there are no tree-level interactions between the VLF and the singlet scalar S or the SM fermions. The discussion below examines these additional interactions, demonstrating that the introduction of such couplings generally leads to a further shrinking of the allowed parameter space.

[4]We accept points in the parameter space which do not satisfy condition (4.23) for β_λ with $\delta = 1$ when it is clear that this is due to $\beta_\lambda^{(1)}(\mu) \approx 0$ and all other conditions remain satisfied.

Scenario	SM+VLF		SM+S+VLF			
	y_{MAX}		$\lambda_{HS}^{y_{MAX}}$	y_{MAX}	$\lambda_{HS}^{y_{MAX}}$	y_{MAX}
	$M_F = 1$ TeV	$M_F = 10$ TeV	$M_F = 1$ TeV		$M_F = 10$ TeV	
$n_Q = n_U = n_D = 1$	0.55	0.63	2.30	0.74	2.46	0.87
$n_Q = n_U = 1$ $n_D = 0$	0.65	0.74	2.55	0.91	2.66	1.07
$n_L = n_E = n_N = 1$	0.65	0.79	2.59	0.93	2.71	1.16
$n_L = n_N = 1$ $n_N = 0$	0.76	0.92	2.77	1.11	2.85	1.40

Table 4.4: Comparison between the maximal values of VLF Yukawa couplings y_{MAX} allowed by the conditions in Eqs.(4.21)–(4.23), up to the cut-off scale $\Lambda = 100$ TeV with $\Delta = 0.4$, between the SM+VLF scenario (second column – the same as Table 4.2) and the SM+S+VLF scenario (third column). For the SM+S+VLF model, we also include the corresponding values of $\lambda_{HS}^{y_{MAX}}$ at which y_{MAX} can be achieved. $M_S = 1$ TeV, $\lambda_S = 0$ and $M_F = 1, 10$ TeV assumed.

VLF and real scalar couplings

The simplest way of including the VLF-S interaction is by adding the following terms to the Lagrangian:

$$\begin{aligned} &-\sum_{i=1}^{n_Q} y_{QS} S \bar{Q}_i^d Q_i^d - \sum_{j=1}^{n_U} y_{US} S \bar{U}_j^s U_j^s - \sum_{k=1}^{n_D} y_{DS} S \bar{D}_k^s D_k^s \\ &-\sum_{i=1}^{n_L} y_{LS} S \bar{L}_i^d L_i^d - \sum_{j=1}^{n_N} y_{NS} S \bar{N}_j^s N_j^s - \sum_{k=1}^{n_E} y_{ES} S \bar{E}_k^s E_k^s \,. \end{aligned} \tag{4.25}$$

The presence of non-vanishing VLF-S Yukawa couplings imposes even stronger bounds from the perturbativity conditions in Eqs. (4.22) and (4.23). This arises from the positive contribution to $\beta_{\lambda_{HS}}$ from the new Yukawa couplings, proportional to y_{XS}, $X = Q, U, D, L, N, E$, increasing λ_{HS} during evolution. This has an indirect effect on β_λ through a term proportional to λ_{HS}^2 (see Eq. (H.5)). The impact of this is illustrated in the left panel of Figure 4.8, where, for simplicity, we assumed that all new Yukawa couplings are equal: $y_{XS} \equiv y_S$. Figure 4.8 demonstrates how non-vanishing y_S pushes λ to larger values, resulting in more serious problems with perturbativity than in the case of $y_S = 0$. In consequence, this leads to smaller allowed maximal values of VLF-Higgs Yukawa coupling.

VLF and SM fermion couplings

Similarly, we can include additional interactions between the VLF and SM fermions. For simplicity, we assume that the only non-vanishing couplings are between the third generation of SM quarks (q_L, t_R and b_R) and the VLQ in the $n_Q = n_U = n_D = 1$ scenario. As a result, we get the following extra terms in the Lagrangian:

$$\begin{aligned} &- y_{Qt} \left(\bar{Q}_L^d \tilde{\varphi} t_R + \text{h.c.} \right) - y_{Uq} \left(\bar{q}_L \tilde{\varphi} U_R^s + \text{h.c.} \right) \\ &- y_{Qb} \left(\bar{Q}_L^d \varphi b_R + \text{h.c.} \right) - y_{Dq} \left(\bar{q}_L \varphi D_R^s + \text{h.c.} \right) \,. \end{aligned} \tag{4.26}$$

Non-vanishing VLQ-SM quark Yukawa couplings have a similar effect on the allowed parameter space as the VLF-Higgs Yukawa couplings discussed earlier in this section. They introduce additional negative contributions to β_λ, strengthening the problems with vacuum stability, and making it more severe than in the SM alone or in the case of VLF-Higgs interaction only. An example of the impact of non-vanishing VLQ-SM quark Yukawa couplings for a simple case where $y_{Qt} = y_{Uq} = y_{Qb} = y_{Dq} = y_{Qq}$, is illustrated in the right panel of Figure 4.8. In conclusion, even relatively small values of VLF-SM fermion couplings can destabilize the EW vacuum.

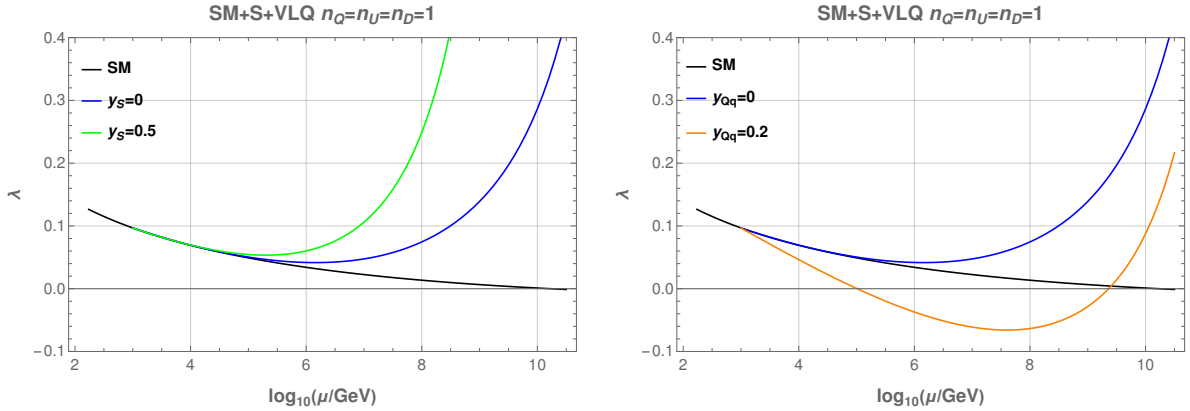

Figure 4.8: Running of λ in the combined SM+S+VLF model for $M_S = 1$ TeV and $M_F = 1$ TeV with $y_F = 0.5$, $\lambda_{HS} = 1$ and $\lambda_S = 0$, including VLF-S Yukawa (left panel) and VLF-SM fermion (right panel) couplings.

4.4.5 Gauge couplings unification in models with VLF and number of VLF multiplets

Satisfying the vacuum stability and perturbativity conditions in Eqs. (4.21)–(4.23) is essential for the theoretical consistency of any BSM model. However, one may think of a number of additional considerations, that while not obligatory, can provide insights into the model and its predictive power. One such condition is gauge couplings unification (for more detailed discussion of unification, see, e.g., [232–235]).

We start by defining the scales μ_{ij} at which pairs of gauge couplings, g_i and g_j, have equal values, i.e., when $\Delta g_{ij} \equiv g_i(\mu_{ij}) - g_j(\mu_{ij}) = 0$. In the SM, these scales are quite different with $\mu_{23} > 3 \times \mu_{12}$, with no single point at which all gauge couplings unify.

Grand unification theories favor models in which all three scales μ_{ij} are close to one other. Moreover, high unification scales of order 10^{15} GeV, are preferred to prevent proton decay occurring too quickly. VLF models (as we exclude scalar singlet since it does not affect running of gauge couplings), have been studied in this context [184–190]. We find it worthwhile to investigate whether unification of the gauge couplings can be realized within the model scenarios considered in this work.

In Figure 4.9 we illustrate the impact of the number of the VLF multiplets on the scale of gauge coupling unification for a given VLF mass of $M_F = 3$ TeV. It is important to note that the VLF Yukawa coupling y does not impact the running of gauge couplings at the 1-loop level. A closer look at the plots in these figures reveals the following trends (see Section 4.2 for model classification):

- **SM + VLL models** (crosses in Figure 4.9):

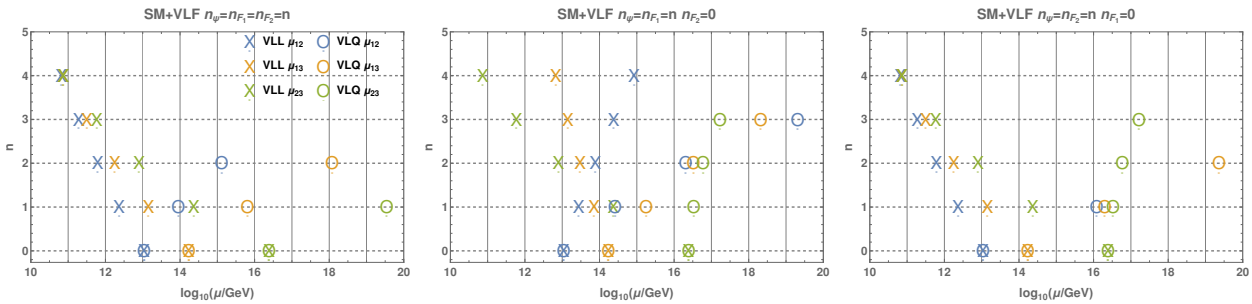

Figure 4.9: Energy scales μ_{ij} at which pairs of running gauge couplings become equal in models with n families of VLL (crosses) or VLQ (circles) with $M_F = 3$ TeV. The 2-loop RGE were used. $n_\psi \in \{n_Q, n_L\}$, $n_{F_1} \in \{n_U, n_N\}$ and $n_{F_2} \in \{n_D, n_E\}$.

  - **Scenario I** (left panel) and **Scenario III** (right panel)
    As n increases, the gauge coupling convergence points become closer to each other, but the intersection points shift to lower energy scales.
  - **Scenario II** (middle panel)
    For $n = 1, 2$, the gauge couplings converge closer to each other, but already for $n = 3$ they begin to diverge.

- **SM + VLQ models** (circles in Figure 4.9):
  - **Scenario I** (left panel)
    The $\Delta g_{23} = 0$ point lies above the Planck scale, even for $n = 1$.
  - **Scenario II** (middle panel)
    For $n = 1, 2$, the gauge couplings converge closer to each other, but for $n = 3$ they start diverging, with all intersection points shifting to higher energy scales.
  - **Scenario III** (right panel)
    For $n = 1$, the gauge couplings converge closer to each other, but already for $n = 2$ the $\Delta g_{12} = 0$ point lies above the Planck scale.

As we verified, varying the VLF mass M_F between 1 TeV and 10 TeV does not significantly alter this picture, with the conclusions remaining essentially unchanged.

Based on the discussion above, it is clear that the VLQ Scenario II with $n = 2$ (to a lesser extent also $n = 1, 3$) and Scenario III with $n = 1$ are the most promising configurations for the realization of grand unification of gauge couplings in the considered VLF models. All other cases are disfavored for various reasons. All VLL scenarios with moderate n have a positive impact on unification of gauge couplings compared to the SM. However, the corresponding unification scales are too low. The VLQ Scenario I has a negative impact on unification, as already for $n = 2$, g_2 and g_3 couplings converge above the Planck scale. The situation is similar for the VLQ Scenario III when $n \geq 2$.

Models with large cut-off scales and a significant number of the VLF multiplets are disfavored, not only from the point of view of the potential unification of gauge couplings. As shown in Section 4.4.1, in Figure 4.4, increasing the number of the VLF multiplets may affect the EW vacuum stability and perturbativity conditions in Eqs. (4.21)–(4.23). Focusing solely on the perturbativity conditions, and requiring their validity up to the Planck scale with the vanishing VLF Yukawa couplings $y = 0$, provides an upper bounds on the number of the VLF multiplets presented in Table 4.5.

	SM+VLL	SM+VLQ
Scenario I	$n_L^{max} = 4$	$n_Q^{max} = 2$
Scenario II	$n_L^{max} = 12$	$n_Q^{max} = 3$
Scenario III	$n_L^{max} = 4$	$n_Q^{max} = 3$

Table 4.5: The Maximal number of allowed VLF multiplet families, determined by the perturbativity conditions.

A final remark regarding models with the VLL is in order here. As discussed in Section 4.4.1, in these models, the EW vacuum becomes unstable around $10^{9\div10}$ GeV, even for the vanishing VLF Yukawa couplings. It is therefore reasonable to consider higher cut-off scales only when the singlet scalar S is also added to the model to improve its stability. Since the singlet does not affect the RGE for gauge couplings, the results presented in this section remain valid for SM+S+VLL models.

4.5 Impact on phenomenology

As discussed in Section 4.4, the interplay between the stability condition (4.21), and perturbativity conditions (4.22), (4.23) results in a surprisingly small parameter space for the VLF models. While the inclusion of the real scalar slightly relaxes the upper limit on the VLF Yukawa couplings, we shall demonstrate that these couplings are still insufficient to generate rich phenomenology. The experimental signatures that could be tested in the near future are quite limited. In this section, we explore three examples of phenomena that can be associated with considered models: double Higgs boson production via gluon fusion, electroweak precision observables and the electroweak phase transition.

4.5.1 Double Higgs boson production

The process of double Higgs boson production is one of the most promising remaining areas where BSM physics has the potential so significantly alter SM predictions, with the current experimental limits far above the level of the present experimental precision:

$$\begin{aligned} \sigma(pp \to HH) &< 2.4 \times \sigma^{SM}(pp \to HH), \text{ ATLAS [111]}, \\ \sigma(pp \to HH) &< 3.4 \times \sigma^{SM}(pp \to HH), \text{ CMS [112]}. \end{aligned} \tag{4.27}$$

The dominant production channel for a Higgs pair is via gluon fusion, with the leading-order contributions presented in the diagrams in Figure 4.10 (in the SM, Q refers to the top quark) [5]. Enhancement of the double Higgs production cross-section in the considered models can occur through modifications of the same diagrams in one of the following ways:

1. **Modification of the triple Higgs coupling**
   This can be realized through insertions of either a heavy scalar S or VLQ, see Figure 4.12.

2. **VLQ loop contributions**
   This can be realized by replacing Q in the box and triangle diagrams in Figure 4.10 with VLQ.

[5] Results in this section were obtained using `FeynRules` [80] and `MadGraph5_aMC@NLO` [142] packages. All diagrams in this thesis are produced using [236].

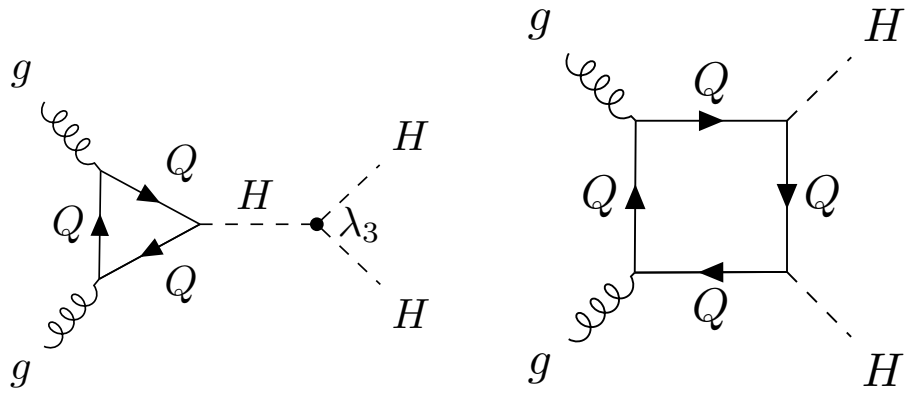

Figure 4.10: Diagrams contributing to the double Higgs production via gluon fusion. Internal fermion lines, denoted by Q, can represent either SM quarks or VLQ multiplets. The black dot indicates the triple Higgs coupling λ_3.

We define the differences between the cross-sections for the gluon fusion processes of single and double Higgs boson production in the SM and its extensions as:

$$K^X_{\text{final}} = \frac{\sigma^{SM+X}_{\text{ggF}}(pp \to \text{final}) - \sigma^{SM}_{\text{ggF}}(pp \to \text{final})}{\sigma^{SM}_{\text{ggF}}(pp \to \text{final})}\,, \tag{4.28}$$

where X represents either S or VLF, and the "final" state refers to H for single Higg production and HH for double Higgs production. From an experimental perspective, we are particularly interested in scenarios that predict a significant enhancement of K^X_{HH} while ensuring that K^X_H remains within the current experimental bounds.

We discuss both of these contributions separately in the following pages.

Modification of the triple Higgs coupling

Interactions of the Higgs boson with new particles can modify the triple Higgs coupling λ_3 which, if sizable, may directly impact the process of double Higgs boson production. This coupling can be defined as:

$$\lambda_3 = \left.\frac{d^3\left(V_0(H,0) + V_0^{CW}(H,0)\right)}{dH^3}\right|_{H=v} = \lambda_3^{SM} + \Delta\lambda_3^{BSM} = \lambda_{3,\text{tree}}^{SM} + \Delta\lambda_3^{SM} + \Delta\lambda_3^{BSM}\,, \tag{4.29}$$

with the tree-level potential given by Eq. (4.8) and its Coleman-Weinberg part by Eq. (J.1).

The current allowed 95% confidence level intervals for the trilinear Higgs coupling modifier, defined as $\kappa_{\lambda_3} = \lambda_3/\lambda_3^{SM}$, read:

$$\begin{aligned} \kappa_{\lambda_3} &\in [-0.4, 6.3],\ \text{ATLAS [111]}, \\ \kappa_{\lambda_3} &\in [-1.24, 6.49],\ \text{CMS [112]}. \end{aligned} \tag{4.30}$$

still leaving a lot of space for the BSM physics.

The leading tree-level contribution to the trilinear Higgs coupling in the SM reads:

$$\lambda_{3,\text{tree}}^{SM} = 3M_H^2/v, \tag{4.31}$$

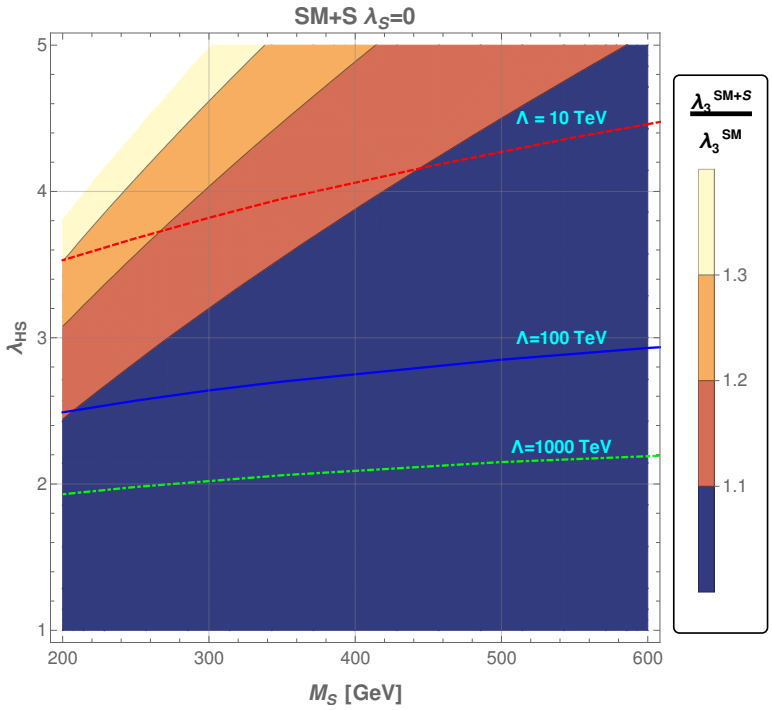

Figure 4.11: Contours of relative triple Higgs coupling enhancement in the SM extended by scalar singlet. The red-dashed, blue-solid and green-dot-dashed lines indicate the maximal value of λ_{HS} allowed by the perturbativity constraints up to, respectively, $\Lambda = 10, 100, 1000$ TeV with $\Delta = 0.4$ (compare Eq. (4.23)).

below, we classify the leading one-loop contributions to λ_3.

- One-loop top-quark induced contribution:

$$\Delta\lambda_3^{SM} \approx -\frac{3M_t^4}{v^3\pi^2}. \tag{4.32}$$

- One-loop real scalar singlet induced contribution:

$$\Delta\lambda_3^{S} \approx \frac{\lambda_{HS}^3 v^3}{32\pi^2 M_S^2}. \tag{4.33}$$

- One-loop VLF induced contribution:

$$\Delta\lambda_3^{VLF} \approx n_{F_1}\frac{N_c' v^3 y_{F_1}^6}{8\pi^2 M_{F_1}^2} + n_{F_2}\frac{N_c' v^3 y_{F_2}^6}{8\pi^2 M_{F_2}^2}, \tag{4.34}$$

  where N_c' represents the number of colors of the VLF multiplets , and the summation over $n_{F_1} \in \{n_U, n_N\}$, $n_{F_2} \in \{n_D, n_E\}$ and $y_{F_1} \in \{y_U, y_N\}$, $y_{F_2} \in \{y_D, y_E\}$ is assumed.

Another, more involved method of calculating the higher-order corrections to the triple Higgs coupling is to directly calculate loop diagrams contributing to the hhh vertex (see e.g., [237–239]). In other words, we have to explicitly calculate the diagrams displayed in Figure 4.12 in the low-energy

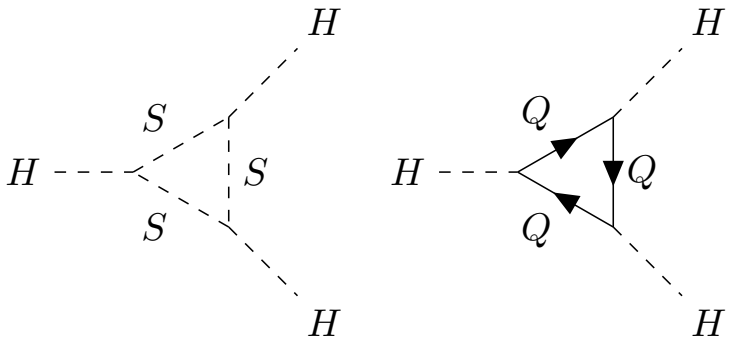

Figure 4.12: One-loop diagrams contributing to the triple Higgs coupling: real scalar S — panel, and fermion contributions - right panel, where Q can be either SM quarks or VLQ multiplets.

limit, where $M_{VLF}, M_S \gg p$. These calculations allowed us to cross-check and confirm formulas presented in Eqs. (4.33), (4.34).

The Effects of the scalar singlet are shown in Figure 4.11, which illustrates the corresponding relative enhancement of the triple Higgs coupling, $\kappa_{\lambda_3}^{SM+S} = \lambda_3^{SM+S}/\lambda_3^{SM}$. The contours of maximal allowed values of λ_{HS} for chosen cut-off scales Λ are obtained utilizing perturbativity conditions (4.21)–(4.23).

For the cut-off scale of $\Lambda \leq 100$ TeV, the enhancement of λ_3 from scalar singlet contributions is at most $\sim 10\%$ for $M_S \geq 200$ GeV, resulting in a moderate, at most $K_{HH}^S \approx -8\%$, decrease in the double Higgs production cross-section. This decrease is due to the destructive interference between the box and triangle diagrams presented in Figure 4.10).

The addition of VLF also has some impact on λ_3, though this effect i minimal. We estimate its maximal possible value by using the values from Table 4.4 and inserting them into the Eq. (4.34). As a result, we find negligible contributions with $|\Delta\lambda_3^{VLF}/\lambda_3^{SM}| \ll 1\%$ for all considered cases, leaving no potential for a significant modification of the triple Higgs coupling modification by VLF fields alone.

VLQ loop contributions

As we have seen, heavy VLQ do not significantly alter the triple Higgs coupling λ_3. However, their impact may become much more important when considering their influence through the box and triangle loop gluon fusion diagrams presented in Figure 4.10. When considering such corrections, one must account for the fact that loop contributions to the double and single Higgs boson production are closely related. The Feynman diagrams for the latter can be derived from Figure 4.10 by replacing one of the external Higgs fields with a vev insertion. Consequently, all relevant amplitudes are proportional to the same combination of VLQ parameters:

$$\mathcal{M}_{gghh}^{VLQ\triangle} \propto \mathcal{M}_{gghh}^{VLQ\square} \propto \mathcal{M}_{ggh}^{VLQ} \propto n_U \frac{y_U^2}{M_U^2} + n_D \frac{y_D^2}{M_D^2}, \tag{4.35}$$

which in agreement with the leading-order terms in the low-energy expansion of the corresponding one-loop diagrams. For this reason, apart from the theoretical constraints considered already in this work, another important source of limits on VLQ model parameters comes from the the current limits on the single Higgs production. The available experimental data [112] places strong constraints - around 10% at 68% CL and approximately 18% at 95% CL - on the deviations of the single Higgs

SM+VLQ	y_{MAX}^{RGE}	y_{MAX}^{H}	K_{HH}^{VLQ}	y_{MAX}^{RGE}	y_{MAX}^{H}	K_{HH}^{VLQ}
	68% CL			95% CL		
$n_Q = n_U = n_D = 1$	0.74	**0.65**	+8.4%	**0.74**	0.89	+11.3%
$n_Q = n_U = n_D = 2$	0.60	**0.46**	+8.2%	**0.60**	0.63	+15.0%
$n_Q = n_U = n_D = 3$	0.50	**0.37**	+8.3%	**0.50**	0.51	+15.5%
$n_Q = n_U = 1\ n_D = 0$	**0.91**	0.92	+8.2%	**0.91**	1.26	+8.2%
$n_Q = n_U = 2\ n_D = 0$	0.74	**0.65**	+8.4%	**0.74**	0.89	+11.3%
$n_Q = n_U = 3\ n_D = 0$	0.65	**0.53**	+8.2%	**0.66**	0.73	+13.5%

Table 4.6: The maximal enhancement of the double Higgs production cross-section from VLQ loop gluon fusion diagrams for $M_F = 1$ TeV. y_{MAX}^{RGE} and y_{MAX}^{H} indicate the maximal values allowed by perturbativity and by single Higgs production constraints, respectively (the latter at CL=68% or 95% [112]). In each case, bold font highlights the stronger constraint that is taken into account.

boson production rate via gluon fusion from its SM value. This condition may, depending on the choice of Δ in (4.23), impose stronger constraints on the maximal values of VLF Yukawa couplings than those listed in Table 4.4. This is illustrated in Table 4.6.

Table 4.6 indicates that the enhancement of the double Higgs production rate resulting from the VLQ loop contributions, K_{HH}^{VLQ}, reaches at most $\sim 15\%$. Even this modest enhancement should be viewed as an optimistic scenario. As discussed earlier, in models including a scalar singlet, this positive contribution can be further minimized by the negative scalar contribution to the triple Higgs coupling. Moreover, increasing VLQ mass M_Q can also only further suppress the impact of VLQ on the process. Additionally, the effects of increasing the number of VLQ multiplets can be deduced from the form of the amplitudes in Eq. (4.35). For instance, assuming identical masses for all multiplets, a scenario with $n = 1$ and a given value of Y is equivalent to $n = N$ with $Y \to Y/\sqrt{N}$. As a consequence, the corresponding bounds on K_{HH}^{VLQ} are only marginally affected by varying n (as illustrated in the 4th column of Table 4.6).

A comparison between the results presented in Table 4.6 and the relatively weak experimental constraints on the Higgs boson pair production at 95% CL, as given in Eq. 4.27, reveals that it is unlikely for VLQ multiplets to significantly affect the process of double Higgs production in any observable way in the foreseeable future.

4.5.2 Electroweak precision observables: corrections to $\mathbb{S}$, $\mathbb{T}$ and $\mathbb{U}$ oblique parameters

Short introduction to the $\mathbb{STU}$ oblique parameters

Additional constraints on the parameter space of the models considered in this work may arise from measurements of so-called electroweak precision observables (EWPO). In our analysis, we focus on the Peskin-Takeuchi $\mathbb{S}$, $\mathbb{T}$ and $\mathbb{U}$ oblique parameters which parametrize one-loop contributions to the electroweak gauge bosons self-energies (i.e., vacuum polarization or oblique corrections) [240–242]. These parameters are defined under three main assumptions regarding the structure of the new physics particle content and interactions:

1. Preservation of the SM electroweak gauge group $SU(2)_L \times U(1)_Y$.

2. Suppression of new physics couplings to light fermions.

3. The mass scale of new physics is much larger than the electroweak scale.

Under these assumptions, we can express the three observable oblique parameters $\mathbb{STU}$ in terms of new physics contributions to the transverse parts of the vacuum polarization functions of the electroweak gauge bosons $\Pi^{\text{new}}_{XY}(q^2)$. These self-energy functions contribute to the oblique parameters in the following way:

$$\begin{aligned}
&\alpha_{em}(M_Z)T \equiv \frac{\Pi^{\text{new}}_{WW}(0)}{M_W^2} - \frac{\Pi^{\text{new}}_{ZZ}(0)}{M_Z^2}, \\
&\frac{\alpha_{em}(M_Z)}{4s^2c^2}S \equiv \frac{\Pi^{\text{new}}_{ZZ}\left(M_Z^2\right) - \Pi^{\text{new}}_{ZZ}(0)}{M_Z^2} - \frac{c^2-s^2}{cs}\frac{\Pi^{\text{new}}_{Z\gamma}\left(M_Z^2\right)}{M_Z^2} - \frac{\Pi^{\text{new}}_{\gamma\gamma}\left(M_Z^2\right)}{M_Z^2}, \\
&\frac{\alpha_{em}(M_Z)}{4s^2}(S+U) \equiv \frac{\Pi^{\text{new}}_{WW}\left(M_W^2\right) - \Pi^{\text{new}}_{WW}(0)}{M_W^2} - \frac{c}{s}\frac{\Pi^{\text{new}}_{Z\gamma}\left(M_Z^2\right)}{M_Z^2} - \frac{\Pi^{\text{new}}_{\gamma\gamma}\left(M_Z^2\right)}{M_Z^2}.
\end{aligned} \tag{4.36}$$

where $c = \cos\theta_W$, $s = \sin\theta_W$, and θ_W is the weak mixing angle.

By construction, these parameters vanish in the SM $\mathbb{S} = \mathbb{T} = \mathbb{U} = 0$, and any experimental deviation from these values would indicate the presence of new physics. On the other hand, for a specific new physics model that affects these parameters, one may impose constraints on the model's parameter space by comparing theoretical predictions with the latest experimental measurements of $\mathbb{STU}$ [11]:

$$\mathbb{S} = -0.02 \pm 0.10, \quad \mathbb{T} = 0.03 \pm 0.12, \quad \mathbb{U} = 0.01 \pm 0.11. \tag{4.37}$$

In general, $\mathbb{S}$ and $\mathbb{T}$ provide stronger constraints on new physics models than $\mathbb{U}$. $\mathbb{T}$ measures custodial symmetry violation and is particularly sensitive to the mass splitting between new particles within multiplets, whereas $\mathbb{S}$ is sensitive to the impact of new physics on neutral current processes and can be affected, e.g., by composite Higgs models.

The requirement of consistency with the experimental values of the $\mathbb{STU}$ parameters is a highly efficient method to ensure compliance with the electroweak precision data, and allows one to test the viability of new physics scenarios.

$\mathbb{STU}$ oblique parameters in the presence of VLF

In the context of VLF, as the singlet scalar does not contribute to $\mathbb{S}$, $\mathbb{T}$ and $\mathbb{U}$ parameters due to the $\mathbb{Z}_2$ symmetry of its potential, there have been a number of extensive studies addressing this issue (see e.g., [162, 195–197]). Current experimental constraints, obtained with $\mathbb{U}$ fixed to zero (again, $\mathbb{U}$ is suppressed by additional factor of M_i^2/M_Z^2 compared with $\mathbb{S}$, and $\mathbb{T}$, see [243]), are as follows [11]:

$$\begin{aligned}
&\mathbb{T} = 0.04 \pm 0.6, \\
&\mathbb{S} = -0.01 \pm 0.07.
\end{aligned} \tag{4.38}$$

The formulas for the corrections to the $\mathbb{S}$ and $\mathbb{T}$ parameters in the presence of VLF have been worked out in [195] and are collected in Appendix I. These parameters, by definition, come only from the BSM sector, so that in the absence of mixing between VLF and the SM fermions one has:

$$\begin{aligned}
&\mathbb{T} \equiv \mathbb{T}_{VLF}, \\
&\mathbb{S} \equiv \mathbb{S}_{VLF}.
\end{aligned} \tag{4.39}$$

A comparison between the constraints on VLF models based on considerations of model consistency (EW vacuum stability plus perturbativity) and single Higgs production, with those based on the precision $\mathbb{S}$ and $\mathbb{T}$ electroweak observables is presented in Table 4.7 and Figure 4.13.

Several comments are relevant here. In the model scenarios considered in this work, we assume the same number of left- and right-handed VLF multiplets. This significantly simplifies the formulae from [195] (again, see Appendix I). Moreover, we assume identical VLF masses M_{VLF} and Yukawa couplings y_{VLF}, which limits the effect of VLF on the $\mathbb{S}$ and $\mathbb{T}$ parameters. More specifically, for "Scenario I", where we have the same number of VLF doublets and "up-type" and "down-type" singlets, one has $\mathbb{T} = 0$, as such setup preserves custodial symmetry. For other scenarios, the contribution to $\mathbb{T}$ is significantly larger than to $\mathbb{S}$, but remains well below the experimental constraints. Finally, VLL scenarios have far smaller impact than VLQ due to the absence of the N_c color factor (see formulas in Appendix I). Since increasing M_{VLF} only leads to a further decrease in the values of $\mathbb{S}$ and $\mathbb{T}$ parameters - even after taking into account the increase in the maximum allowed values of the VLF Yukawas - we conclude that for the model scenarios studied in this work, the theoretical consistency conditions provide a much stronger constraints than those arising from the experimental bounds on the oblique parameters $\mathbb{S}$ and $\mathbb{T}$.

SM+VLQ	y_{MAX}^{RGE}	$\mathbb{T}_{VLF}$	$\mathbb{S}_{VLF}$
$n_Q = n_U = n_D = 1$	0.74	0	0.006
$n_Q = n_U = n_D = 2$	0.60	0	0.007
$n_Q = n_U = n_D = 3$	0.50	0	0.008
$n_Q = n_U = 1\ n_D = 0$	0.91	0.041	0.012
$n_Q = n_U = 2\ n_D = 0$	0.74	0.035	0.015
$n_Q = n_U = 3\ n_D = 0$	0.65	0.031	0.018

Table 4.7: Maximal contributions to $\mathbb{T}$ and $\mathbb{S}$ oblique parameters for the maximal allowed values of VLQ Yukawa couplings for $M_{VLF} = 1$ TeV, two different model scenarios and varying number of VLF multiplets.

4.5.3 Electroweak phase transition

Finally, we turn our attention to the last phenomenon studied in this thesis in relation to the VLF and real scalar models: the electroweak phase transition (for a more detailed review, see e.g., [244]). This hypothetical process is of particular interest due to its potential role in explanation of baryogenesis and the observed matter-antimatter asymmetry in the universe. Moreover, it may leave detectable traces in gravitational wave (GW) signals, making it a target for near-future GW experiments such as LISA, which seeks to capture signals from cosmological phase transitions [245].

Introducing the electroweak phase transition

One of the most promising solutions of the observed matter-antimatter asymmetry in the universe is electroweak baryogenesis (EWBG). It offers a mechanism that may satisfy three Sakharov conditions necessary for creation of matter-antimatter (or baryon) asymmetry [246]: a) Baryon number B violation, b) C- and CP-violation, c) Departure from thermal equilibrium. In such scenario, EWBG occurs

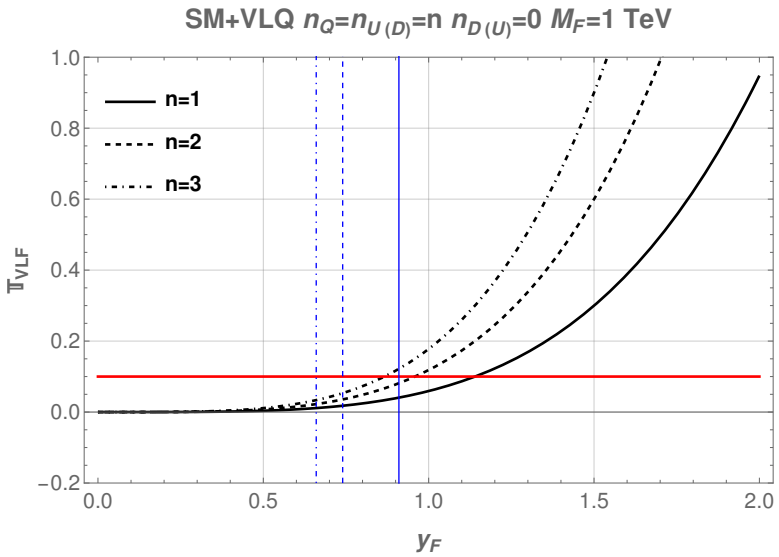

Figure 4.13: Value of $\mathbb{T}$ parameter as function of VLF Yukawa coupling y_F (black lines) for two model scenarios and different number of VLF families. Also shown are: theoretical upper bounds on y_F (blue lines) and the experimental upper bound on $\mathbb{T}$ (red line)

.

in the early universe during the process of the electroweak phase transition (EWPT). This process occurs when the hot, radiation-dominated early universe cools down and the Higgs boson field settles to its true vacuum, spontaneously breaking the electroweak $SU(2)_L \times U(1)_Y$ symmetry. EWBG can successfully generate the observed baryon asymmetry if EWPT satisfy above conditions in the following way:

1. **Departure from thermal equilibrium**
   EWPT has to be of **first order** to ensure a departure from thermal equilibrium. A first order transition occurs when a potential barrier separates the two minima of the Higgs potential: the symmetric phase $\langle h \rangle = 0$ and the broken $\langle h \rangle \neq 0$ phase. It leads to the non-zero probability of Higgs field tunneling through the barrier and thereby creating expanding bubbles of broken phase. Bubbles grow and collide, driving the system out of equilibrium. This process is illustrated in Fig. 4.14. In contrast, **second order** or **cross over** phase transitions (as it is the case for the SM with the observed Higgs mass) lead to smooth evolution and fail to fulfill the condition of the departure from thermal equilibrium. .

2. **C- and CP-violation**
   Sources of sufficiently strong C- and CP-violation are necessary to generate an asymmetry between particles and antiparticles during EWPT. As the bubbles of the broken phase expand, particles in plasma scatter of the bubble walls, generating this asymmetry through C- and CP-violating interactions. This in turn can bias B-violating **sphaleron** processes to produce more baryons than anti-baryons. In case of the SM, CP-violating phases in the CKM and PMNS matrices are not sufficient to generate required ratios.

3. **Baryon number B violation**
   Baryon number B violation is provided by non-perturbative sphaleron process in the electroweak theory. However, in order to prevent wash out of generated baryon asymmetry, the EWPT has

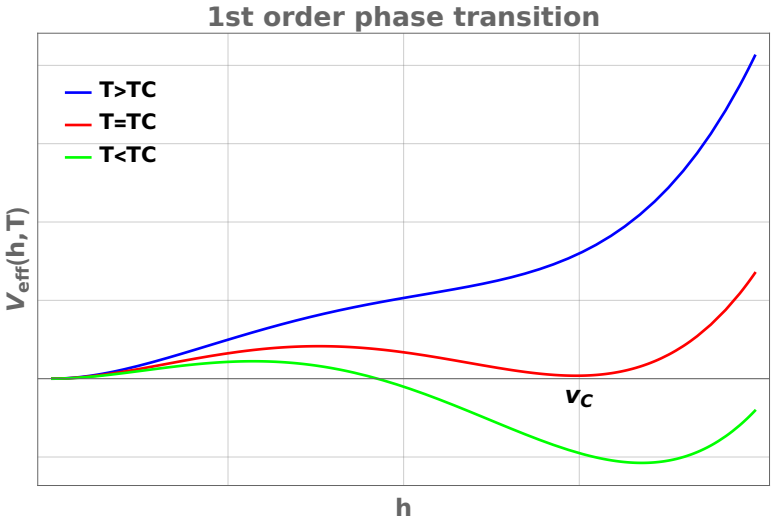

Figure 4.14: Thermal evolution of the potential corresponding to the first order phase transition. Potential barrier separates the symmetric $\langle h \rangle = 0$ and the broken $\langle h \rangle \neq 0$ phases.

to be **strongly first order**. This ensures suppression of sphaleron processes inside the bubbles of broken phase, preventing the washout of the asymmetry. The phase transition is considered strong if the following condition is satisfied:

$$\xi = \frac{v_C(T_C)}{T_C} \gtrsim (0.6 \div 1.0), \tag{4.40}$$

where v_C is the VEV of the Higgs field broken phase at the critical temperature, $T = T_C$ - see Fig. 4.14.

In terms of theoretical description, the EWPT can be studied using the temperature dependent effective potential. In the case of one-loop effective potential in the SM with additional singlet scalar field (for review see e.g. [247, 248]) reads:

$$V_{\text{eff}}(H, S, T) = V_0(H, S) + V_{CW}(H, S) + V_T(H, S, T)\,. \tag{4.41}$$

with V_0 being a tree-level potential (4.8), V_{CW} denotes the one-loop correction known also as the Coleman-Weinberg potential [249] and V_T is the finite-temperature contribution (for further details, see Appendix J).

EWPT with real scalar singlet

The real scalar model with the tree-level potential given by Eq. (4.8), depending on the specific values of couplings and masses, can generate either 1- or 2-step EWPT.

- **1-step EWPT**
  In this case, the system begins in the high-temperature minimum with $\langle H \rangle = \langle S \rangle = 0$, and later transitions to the EW vacuum with $\langle H \rangle \neq 0$, $\langle S \rangle = 0$. This occurs for $\mu_S^2 > 0$, which ensures $\langle S \rangle = 0$. In this region of parameter, the value of λ_S is irrelevant, allowing us to choose $\lambda_S = 0$ to maximize the allowed value of the λ_{HS} coupling. The parameter space corresponding

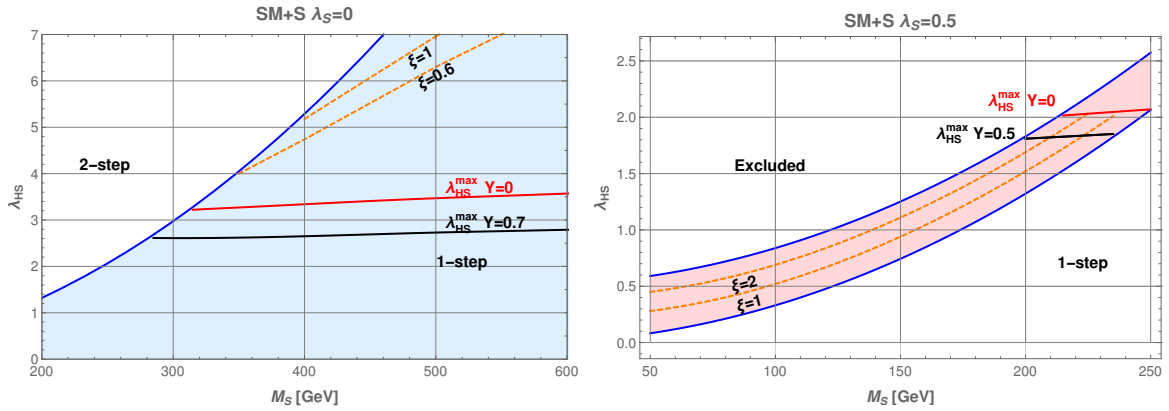

Figure 4.15: The shaded regions represent parts of the parameter space that allow for the 1-step (left panel) and 2-step (right panel) EWPT in the SM extended by a scalar singlet. The orange dashed lines correspond to the strength of the EWPT $\xi = 0.6$ or $\xi = 1$ (1-step) and $\xi = 1$ or $\xi = 2$ (2-step). The red and black lines indicate the maximal values of λ_{HS} allowed by the perturbativity constraints up to $\Lambda = 100$ TeV for two different values of the VLF Yukawa couplings. The values of λ_S were chosen as 0 and 0.5 for the 1- and 2-step transitions, respectively.

to the 1-step EWPT is presented in the left panel in Figure 4.15. The blue line marks the boundary between the 1- and 2-step regions. The red and black lines represent the maximal allowed values of $\lambda_{HS}(M_S)$ obtained under the constraints in Eqs. (4.22) and (4.23), assuming $\Lambda = 100$ TeV for two values of the VLF Yukawa couplings. The orange dashed lines indicate values of $\lambda_{HS}(M_S)$ corresponding to the strength of the EWPT, $\xi = 0.6, 1.0$. The region of the parameter space where $\xi \geq 0.6$ in the singlet scalar extension is almost entirely excluded, in contrast to the corresponding area presented in [213]. This results follow from our careful treatment of perturbativity conditions.

- **2-step EWPT**
  This is the case when, for some range of temperatures, the minimum of the effective potential is located at $\langle H \rangle = 0$, $\langle S \rangle \neq 0$. This can be realized for $\mu_S^2 < 0$, with a further condition ensuring that at zero temperature the EW vacuum corresponds to the global minimum of the potential:

$$V_0(v, 0) < V_0(0, w)\,, \tag{4.42}$$

  which can be translated into bounds on λ_{HS}. A 2-step EWPT is possible if:

$$2\frac{M_S^2}{v^2} \leq \lambda_{HS} \leq 2\frac{M_S^2}{v^2} + \sqrt{2}\frac{M_H\sqrt{\lambda_S}}{v}\,. \tag{4.43}$$

  The allowed 2-step region is indicated by the red area in the right plot in Figure 4.15. The lower and upper limits from Eq. (4.43) for $\lambda_S = 0.5$ are indicated by the blue lines. The specific choice of λ_S allows for reasonably large value of λ_{HS} while still leaving sufficient space for the 2-step EWPT to occur. The red line, as in the case of the 1-step EWPS, indicates the maximal possible values of λ_{HS}.

EWPT with vector-like fermions

VLF can also affect the mechanism of the EWPT through thermal and loop corrections to the effective potential (see Appendix J). In the high-temperature $M/T \ll 1$ expansion of thermal effects, fermions

do not significantly contribute to the formation of a potential barrier for the Higgs field, unlike bosons, which in general lead to cubic terms in the potential. However, in scenarios where the critical temperature is much lower than the fermion masses - which aligns well with the scope of this work, where VLF are relatively heavy - the small-temperature expansion $M/T \gg 1$ is more appropriate. In this regime, the leading contribution to the thermal potential are similar for both fermions and bosons. This could result in a non-trivial impact of VLF on the EWPT and the thermal history of the universe (see e.g., [167, 247]).

Nevertheless, due to the strong constraints on the values of the VLF Yukawa couplings obtained in this work, the impact of these particles on the EWPT is very limited. For the maximal allowed values of the VLF Yukawas y_F in SM+VLF models, as presented in Table 4.4, we obtained ξ_{SM+VLF} to be very close to ξ_{SM}. The inclusion of the scalar singlet allows for a slightly larger maximal values of y_F, see Table 4.4, which are still not sufficient to have any significant impact on the EWPT, indicating $\xi_{SM+S+VLF} \approx \xi_{SM+S}$. We verified that changes in ξ due to the presence of VLF are at most of the order $\mathcal{O}(10\%)$.

4.5.4 Constraints from matching to SMEFT

Other limitations in the parameter space of the model scenarios considered in this work may arise from constraints on the Standard Model Effective Field Theory Wilson coefficients (SMEFT is properly introduced in Chapter 2). These constraints are typically obtained by fitting SMEFT to available experimental data under certain assumptions. Recent examples of such procedures can be found in [43, 44].

The process of relating SMEFT coefficients to heavy BSM extensions is known as *matching*. In this process, the heavy BSM particles (or degrees of freedom) are integrated out to match the remaining expressions with the SMEFT coefficients. Depending on the BSM model, the matching procedure can be complex and tedious; hence, several publicly available tools have been developed to automate it. For examples of these tools and further details on the procedure, see [56, 57, 250, 251].

In this section, we provide a simple example illustrating how this method highlights the critical role of combining bottom-up and top-down approaches in searches for physics beyond the Standard Model. Specifically, we examine the process of double Higgs boson production via gluon fusion (previously discussed in this work) in the presence of VLQ.

VLQ loop contributions

Let us begin with box and triangle diagrams from Figure 4.10. After integrating out heavy VLQ, one obtains two contact interaction vertices (we neglect modifications to the triple Higgs coupling considering it is negligible, see discussion in the previous Section): ggH and $ggHH$ - indicated by red dots in Figure 4.16. SMEFT dimension-6 operator in the Warsaw basis that can generate this effective interaction reads [13, 74]:

$$\mathcal{L}_{SMEFT} \supset C_{\varphi G} \varphi^\dagger \varphi G^A_{\mu\nu} G^{A\mu\nu}. \tag{4.44}$$

It corresponds to the Feynman rules relevant for the double Higgs production process, which are presented in Table 4.9. One can immediately notice that both contributions have the same structure and origin; it is sufficient to consider only a single Higgs amplitude ggH for matching.

Direct calculations lead to the SMEFT amplitude of form (p_i are incoming gluon momenta):

$$i\mathcal{M}^{gg\to H}_{SMEFT} = 2vC^{\varphi G}\delta^{g_1 g_2} \times \left(m_H^2 \left(\bar{\varepsilon}^*(p_1) \cdot \bar{\varepsilon}^*(p_2)\right) - 2\left(\overline{p_1} \cdot \bar{\varepsilon}^*(p_2)\right)\left(\overline{p_2} \cdot \bar{\varepsilon}^*(p_1)\right)\right), \tag{4.45}$$

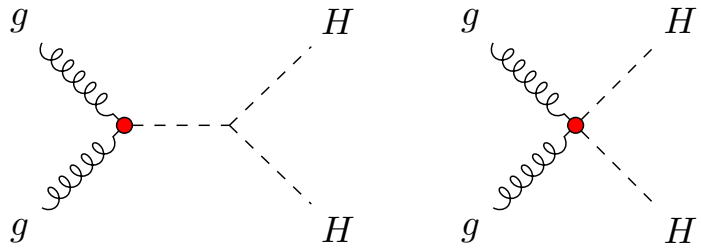

Figure 4.16: Diagrams contributing to the double Higgs production via gluon fusion, with effective contact interactions remaining after integrating out heavy VLQ.

vertex	Feynman rule
ggH	$4iv\delta_{a_1a_2}C^{\varphi G}\left(p_1^{\mu_2}p_2^{\mu_1} - p_1\cdot p_2\eta_{\mu_1\mu_2}\right)$
$ggHH$	$4i\delta_{a_1a_2}C^{\varphi G}\left(p_1^{\mu_2}p_2^{\mu_1} - p_1\cdot p_2\eta_{\mu_1\mu_2}\right)$

Table 4.8: Feynman rules for the Higgs-gluon vertices in SMEFT.

which we can compare with the corresponding amplitude in the VLQ model in the limit of heavy VLQ mass ($M_{VLF} >> v$):

$$\mathcal{M}_{VLQ}^{ggH} = -\left(n_U\frac{Y_U^2}{M_{U1}M_{U2}} + n_D\frac{Y_D^2}{M_{D1}M_{D2}}\right)\frac{vg_s^2\delta^{g_1g_2}}{24\pi^2}\times \\ \left(m_H^2\left(\bar{\varepsilon}^*(p_1)\cdot\bar{\varepsilon}^*(p_2)\right) - 2\left(\overline{p_1}\cdot\bar{\varepsilon}^*(p_2)\right)\left(\overline{p_2}\cdot\bar{\varepsilon}^*(p_1)\right)\right). \tag{4.46}$$

Comparison between the two expressions reveals matching condition:

$$C^{\varphi G} = -\left(n_U\frac{Y_U^2}{M_U^2} + n_D\frac{Y_D^2}{M_D^2}\right)\frac{g_s^2}{48\pi^2}. \tag{4.47}$$

We can now compare it with the existing constraints on the $C_{\varphi G}$ Wilson coefficient to derive conclusions about the parameter space of the studied model. Following [44], one finds the following 95% confidence level exclusion bounds:

	Individual ($1/\text{TeV}^2$)	Marginalized ($1/\text{TeV}^2$)
$C_{\varphi G}$	[-0.002,0.005]	[-0.019,0.003]

Table 4.9: Current limits on $C_{\varphi G}$ Wilson coefficient from [44].

The two types of constraints should be interpreted in the following way:

- **Individual**: This limit is obtained by fitting experimental data assuming only the $C_{\varphi G}$ Wilson coefficient is non-zero. This leads to:

$$n_U\frac{Y_U^2}{M_U^2} + n_D\frac{Y_D^2}{M_D^2} \leq \frac{0.002}{\text{TeV}^2}\times\frac{48\pi^2}{g_s^2}, \tag{4.48}$$

- **Marginalized**: This limit considers correlations between $C_{\varphi G}$ and other Wilson coefficients, leading to:

$$n_U\frac{Y_U^2}{M_U^2} + n_D\frac{Y_D^2}{M_D^2} \leq \frac{0.019}{\text{TeV}^2}\times\frac{48\pi^2}{g_s^2}, \tag{4.49}$$

Assuming uniform values of Yukawa couplings and VLQ masses, we present the constraints on VLQ Yukawa couplings for various model scenarios in Table 4.9.

SM+VLQ	y_{MAX}^{SMEFT}	
	Individual	Marginalized
$n_Q = n_U = n_D = 1$	0.56	1.74
$n_Q = n_U = n_D = 2$	0.40	1.23
$n_Q = n_U = n_D = 3$	0.33	1.00
$n_Q = n_U = 1\ n_D = 0$	0.80	2.46
$n_Q = n_U = 2\ n_D = 0$	0.56	1.74
$n_Q = n_U = 3\ n_D = 0$	0.46	1.42

Table 4.10: Maximal allowed values of VLQ Yukawa coupling for $M_F = 1$ TeV and various model scenarios, for two different fitting assumptions.

Comparison between Table 4.9 with Table 4.6 reveals that the constraints for the "Individual" case are more stringent than the theoretical constraints considered so far in this work. However, this scenario assumes that only a single SMEFT WC, $C_{\varphi G}$, is present, which is unlikely in realistic VLQ (and more generally BSM) scenarios where multiple operators are generated simultaneously. Thus, the "Marginalized" scenario provides a more realistic, however less stringent, bound. To achieve even tighter constraints, further precision data and dedicated fits for the VLQ models would be necessary. While this goes beyond the current scope of this work, it highlights the importance of combining top-down and bottom-up approaches in the future studies.

4.6 Summary and conclusions

In this chapter, we studied the impact of the Standard Model extensions involving vector-like fermions (VLF) and/or the real scalar singlet S on the stability of the electroweak vacuum, the perturbativity of the model couplings, and the possible unification of the gauge couplings. We divided our analysis into three broader model classes, each characterized by a different set of extra fields: only VLF; only a singlet scalar; both VLF and a scalar. The VLF models were further classified based on the fermion types (quarks/leptons) and numbers of extra multiplets, differing by transformation properties with respect to the SM gauge group. In order to study the most general features of the discussed models, we assumed equal masses and couplings for the VLF multiplets, excluding effects related to flavor-like structure of their parameters.

Following the introduction of the models, we defined a set of theoretical conditions, summarized in Eqs. (4.21)–(4.23), which play a central role in deriving the final results of this chapter. These conditions impose stability and perturbativity requirements, are based on 1- and 2-loop renormalization group equations (RGEs), and allow us to derive constraints on the parameter space of the considered models. Additionally, we incorporated various experimental bounds, including bounds on the masses of VLF and the real scalar field, as well as constraints arising from the trilinear Higgs coupling single and double Higgs production.

In models containing only vector-like fermions, electroweak stability considerations impose strong upper bounds on the magnitude of the VLF Yukawa couplings. The specific limits on such couplings,

denoted as y_{MAX}, depend on the details of models and the assumed cut-off scale Λ, up to which the theoretical constraints should be satisfied. For all studied scenarios, we find $y_{MAX} < 1$ for $\Lambda \geq 100$ TeV. On the other hand, scalar singlet extension of the SM offers better prospects for EW vacuum, improving with the increase of singlet scalar couplings, λ_{HS} and λ_S. However, this model encounters problems with perturbativity when the scalar couplings become too large. Finally, models with both VLF families and real scalar have fewer issues with EW vacuum stability compared to the case of only VLF, but the interplay between the VLF and the scalar singlet results in more serious problems with perturbativity than those encountered when only the scalar or only VLF are considered. Our analysis shows that the upper bounds on VLF Yukawa couplings can be somewhat relaxed due to the presence of the singlet scalar. Nevertheless, such enhancement of y_{MAX} is never larger than about 50%.

Results of this analysis should not be blindly generalized to all model that consider VLF as a viable SM extension. In models with more complicated pattern of VLF masses and couplings, the criteria of electroweak vacuum stability and perturbativity should be applied on model-by-model basis and the results will vary accordingly. However, our analysis suggests that pure VLF models, eventually extended with one real scalar singlet, have serious limitations concerning their allowed parameter ranges and in general may not be sufficient to explain phenomenological effects for which they were often used. Addition of new fields and/or more complicated pattern of VLF parameters will modify RGE evolution and may affect the stability of the scalar potential and the position of Landau poles for various couplings. Nevertheless, our analysis suggests that the constraints from the stability and perturbativity requirements can be important in such extended models and should always be checked as a part of realistic phenomenological analyses of a given SM extension, as we illustrated in this chapter for the set of simplified VLF scenarios.

Next, we analyzed the implications of the obtained parameter space on the phenomenology of the double Higgs boson production, electroweak precision observables, and the electroweak phase transition. Addition of scalar singlet to the SM can enhance the triple Higgs coupling λ_3 while simultaneously suppressing the double Higgs production rate. In contrast, the addition of VLF fields has a negligible effect on λ_3 but may affect the rate of Higgs boson pair production via gluon fusion through contributions to the triangle and box loops in the amplitude. Still, within the allowed parameter space, the VLF loops may enhance the double Higgs production rate by at most 15%, partly due to the related constraints on the single Higgs production. Consequently, the impact of VLF is very limited and impossible to detect with current or near-future experimental accuracy.

We also examined the impact of the studied VLF model scenarios on the electroweak precision observables: $\mathbb{S}$, $\mathbb{T}$ and $\mathbb{U}$ oblique parameters, which provide an important source of constraints on new physics affecting the self-energies of electroweak gauge bosons. We found that constraints on the model's parameter space resulting from experimental bounds on these parameters are weaker than those arising from theoretical EW stability and perturbativity conditions, and from single Higgs production measurements.

Furthermore, we demonstrated that the parameter space of the SM+S model is heavily constrained, leaving very little room for a strong first order EWPT, one of the necessary conditions for successful electroweak baryogenesis. We also showed that addition of VLF, with Yukawa couplings within the allowed parameter space, has minimal impact on the EWPT, leading to the conclusion that the strong first order phase transition in the SM with VLF only cannot be realized.

Finally, we presented the procedure of matching between VLQ model and SMEFT in a simplified scenario, considering only double Higgs boson production via gluon fusion with single SMEFT Wilson coefficient C_φ, highlighting it as a possible source of additional constraints on the model parameter

space. Moreover, it served as an example of the interplay between top-down and bottom-up approaches to new physics searches.

The results presented in this chapter provide an independent set of constraints for models that extend the Standard Model with vector-like fermions and the real scalar field. We believe that these constraints are an important addition to the existing literature in the context of the considered model scenarios. Although we examine only a small subset of all possible BSM models, even those containing vector-like fermions and scalar particles, our methodology can be readily applied to study other theoretical frameworks. It serves as a comprehensive example of the top-down approach crucial for future developments in high-energy physics.

Chapter 5

Summary

Particle physics has been a mature and well-established field of science long before the completion of this thesis. Its crowning achievement — the Standard Model of fundamental interactions — was gradually developed throughout the XXth century, and finally completed in 2012 with the discovery of the Higgs boson. Although the Standard Model has been enormously successful in describing and explaining a wide range of phenomena on the shortest scales in terms of fundamental quantum fields, it falls short in addressing a number of key observations, such as the lack of proper explanation of matter-antimatter asymmetry, the origin, and composition of dark matter and dark energy, or lack of consistent inclusion of gravity, strongly indicating the existence of physics beyond the Standard Model. Unfortunately, despite decades of enormous effort by the particle physics community to uncover the nature of beyond the Standard Model physics, no Standard Model extension has been experimentally confirmed to date.

Various strategies can be employed in the search for physics beyond the Standard Model. For the purpose of this thesis, these strategies are distinguished into two broad categories: bottom-up and top-down approaches.

The bottom-up approach is closely related to experimental searches and focuses on identifying the discrepancies between observed data and Standard Model predictions to gain insights into the nature of beyond the Standard Model physics. This approach has been widely and successfully applied in endeavors such as the prediction of W and Z bosons properties or the precise predictions of the Higgs and top quark masses from LEP data. For the purpose of beyond the Standard Model physics searches, this approach was formalized through the use of the Effective Field Theory, which provide a model-independent framework to analyze deviations from the SM predictions, relying on the observation that low-energy phenomena can be accurately described without the detailed knowledge of the underlying theory. Examples of EFTs include Fermi theory of weak interactions, as well as Higgs Effective Field Theory (HEFT) and Standard Model Effective Field Theory (SMEFT), which are all commonly used in the context of beyond the Standard Model searches.

The top-down approach is a more model-dependent strategy, in which one starts with fundamental principles and symmetries to propose theories extending the Standard Model by introducing specific new fields to address particular issues. The historical record of successes for this approach is broad and includes, for example, the discoveries of Higgs, Z and W bosons, postulated earlier by the unified theory of electroweak interactions. Examples of the Standard Model extensions designed to address specific issues include supersymmetry, various extensions involving more scalar fields, axions and axion-like particles, or models with additional gauge bosons. However, none of these extensions have been

experimentally confirmed.

Although distinct, both of these approaches should be seen as complementary to one another. With the LHC reaching its energy limit, the primary means of discovering beyond the Standard Model physics may lie in indirect measurements, tracking its effects on various precision observables in the form of deviations from the Standard Model predictions. The bottom-up approach provides an efficient framework for parametrizing such discrepancies through Effective Field Theory, offering invaluable hints on the form of fundamental theory. On the other hand, the top-down approach offers means to interpret these results, identifying the most promising Standard Model extension. This thesis follows this logic, demonstrating the examples of research studies that utilize both bottom-up and top-down approaches.

After introducing all key concepts relevant for this work in the Introduction, we presented three research projects: two belonging to the bottom-up, and one to the top-down category of approaches.

The first project, "`SmeftFR` v3 – Feynman rules generator for the Standard Model Effective Field Theory", provided a detailed description of a numerical tool designed to automate highly complex and complicated calculations within the SMEFT framework. Thoroughly validated, this tool represents a significant contribution to the literature and is in line with efforts of the high-energy physics community.

The second project, "Double Higgs production via vector boson fusion at next-to-leading order in SMEFT", presents a model-independent study of a specific process: double Higgs boson production via vector-boson fusion within the SMEFT framework. Utilizing the `SmeftFR` v3 code and basing on the requirements of the validity of the EFT expansion, it provides an estimate of the maximal impact of beyond the Standard Model physics on this process for HL-LHC collider experiment. The results indicate rather limited impact of new physics on this process.

Finally, the third project "Vector-like fermions, real scalar, and Higgs boson phenomenology", is an example of the top-down approach. In this work, we introduced two popular beyond the Standard Model extensions: with vector-like fermions and with additional real scalar singlet. By formulating and imposing constraints based on the requirements of perturbativity and vacuum stability of the theory, we determined the allowed parameter space of these classes of models. These results were then used to estimate the potential impact of considered new particles on the phenomenology of single and double Higgs boson production, electroweak precision observables and the electroweak phase transition. Our results indicated that such impact is very limited. Additionally, we provided an example of a matching procedure between the SMEFT operators and VLF and real scalar singlet, providing an explicit a bridge between bottom-up and top-down approaches to new physics searches.

All in all, the specific choice of research projects making up this thesis, the obtained results, and the methodologies employed present a comprehensive picture of the modern approach to searches for physics beyond the Standard Model. The combination of bottom-up and top-down approaches highlights the importance of both strategies and their complementary nature. Although the results indicate potential challenges in detecting significant deviations from the Standard Model predictions - at least with this particular choice of processes and models — they also laid a solid groundwork for the author's future contributions to the field of high-energy particle physics.

Appendix for Chapter 2

A SMEFT operator basis in SmeftFR v3

All dimension-6 operators in the "Warsaw" basis are presented in Table A.1 (copied here for completeness from [13]). The naming of SmeftFR variables corresponding to the WCs of these operators is straightforward: each variable name consists of subscripts that identify a given operator, with direct transcriptions of "tilde" symbol and Greek letters to the Latin alphabet. Operator names are represented by strings to avoid the accidental use of other similarly named variables. For example, one may consider the following WCs in OpList6:

$$Q_{\varphi} \to \text{“phi”}$$
$$Q_{\varphi D} \to \text{“phiD”}$$
$$Q_{\varphi\Box} \to \text{“phiBox”}$$
$$Q_{\varphi\widetilde{W}} \to \text{“phiWtilde”}$$
$$Q^{(3)}_{lq} \to \text{“lq3”}$$
$$Q^{(8)}_{quqd} \to \text{“quqd8”}$$

The full list of all dimension-5 and -6 operators available in SmeftFR v3 contains the following:

OpList6 = { "G", "Gtilde", "W", "Wtilde", "phi", "phiBox", "phiD", "phiW", "phiB", "phiWB", "phiWtilde", "phiBtilde", "phiWtildeB", "phiGtilde", "phiG", "ephi", "dphi", "uphi", "eW", "eB", "uG", "uW", "uB", "dG", "dW", "dB", "phil1", "phil3", "phie", "phiq1", "phiq3", "phiu", "phid", "phiud", "ll", "qq1", "qq3", "lq1", "lq3", "ee", "uu", "dd", "eu", "ed", "ud1", "ud8", "le", "lu", "ld", "qe", "qu1", "qu8", "qd1", "qd8", "ledq", "quqd1", "quqd8", "lequ1", "lequ3", "vv", "duq", "qqu", "qqq", "duu" }

Similarly, SmeftFR v3 takes as input the bosonic dimension-8 operators from Tables A.2, A.3, A.4 (copied here for completeness from [76]). The naming convention is identical to that used for dimension-6 operators. For example:

$$Q^{(1)}_{\varphi^4 D^4} \to \text{“phi4D4n1”}$$
$$Q_{\varphi^6\Box} \to \text{“phi6Box”}$$
$$Q^{(4)}_{G^2B^2} \to \text{“G2B2n4”}$$
$$Q^{(2)}_{W^2B\varphi^2} \to \text{“W2Bphi2n2”}$$
$$Q^{(1)}_{W^2\varphi^2D^2} \to \text{“W2phi2D2n1”}$$

Table A.2 collects operators constructed solely from the Higgs doublet, φ, and covariant derivatives. In this Table, we modified the basis of the $\varphi^6 D^2$ class of operators to establish a direct connection to

the Warsaw basis. The original operators were defined in [76] as:

$$Q_{\varphi^6}^{(1)} = (\varphi^\dagger\varphi)^2(D_\mu\varphi^\dagger D^\mu\varphi)\,, \quad Q_{\varphi^6}^{(2)} = (\varphi^\dagger\varphi)(\varphi^\dagger\tau^I\varphi)(D_\mu\varphi^\dagger\tau^I D^\mu\varphi)\,, \tag{A.1}$$

and instead, we use:

$$Q_{\varphi^6\Box} = (\varphi^\dagger\varphi)^2\Box(\varphi^\dagger\varphi)\,, \quad Q_{\varphi^6 D^2} = (\varphi^\dagger\varphi)(\varphi^\dagger D_\mu\varphi)^*(\varphi^\dagger D^\mu\varphi)\,, \tag{A.2}$$

which naturally extends the definition of the dimension-6 operators $Q_{\varphi\Box}$ and $Q_{\varphi D}$ from Table A.1. Additionally, we added the number of covariant derivatives in the naming of the operators from the $\varphi^4 D^4$ class to avoid confusion with the SM quartic Higgs operator, φ^4.

Table A.3 collects the operators that are constructed solely from gauge field strength tensors. Each operator in this Table contains exactly four field strength tensors, and the operators are further divided into the following categories:

- X^4, operators where only one of the field strength tensors from the B, W or G gauge fields appears,
- X^3X', operators where the G field strength tensor appears thrice, along with a B field strength tensor,
- $X^2X'^2$, operators consisting of two pairs of different field strength tensors.

The notation in this Table follows exactly that of [76]. Finally, Table A.4 lists the operators that are a combination of Higgs doublets, φ, and gauge field strength tensors.

The full list of names of bosonic dimension-8 operators in the basis of [76] (including basis modifications described above) that can be included in `SmeftFR` v3 calculations reads:

```
OpList8 = { "phi8", "phi6Box", "phi6D2", "G2phi4n1", "G2phi4n2", "W2phi4n1", "W2phi4n2", "W2phi4n3",
"W2phi4n4", "WBphi4n1", "WBphi4n2", "B2phi4n1", "B2phi4n2", "G4n1", "G4n2", "G4n3", "G4n4", "G4n5",
"G4n6", "G4n7", "G4n8", "G4n9", "W4n1", "W4n2", "W4n3", "W4n4", "W4n5", "W4n6", "B4n1", "B4n2", "B4n3",
"G3Bn1", "G3Bn2", "G3Bn3", "G3Bn4", "G2W2n1", "G2W2n2", "G2W2n3", "G2W2n4", "G2W2n5", "G2W2n6", "G2W2n7",
"G2B2n1", "G2B2n2", "G2B2n3", "G2B2n4", "G2B2n5", "G2B2n6", "G2B2n7", "W2B2n1", "W2B2n2", "W2B2n3",
"W2B2n4", "W2B2n5", "W2B2n6", "W2B2n7", "phi4D4n1", "phi4D4n2", "phi4D4n3", "G3phi2n1", "G3phi2n2",
"W3phi2n1", "W3phi2n2", "W2Bphi2n1", "W2Bphi2n2", "G2phi2D2n1", "G2phi2D2n2", "G2phi2D2n3",
"W2phi2D2n1", "W2phi2D2n2", "W2phi2D2n3", "W2phi2D2n4", "W2phi2D2n5", "W2phi2D2n6", "WBphi2D2n1",
"WBphi2D2n2", "WBphi2D2n3", "WBphi2D2n4", "WBphi2D2n5", "WBphi2D2n6", "B2phi2D2n1", "B2phi2D2n2",
"B2phi2D2n3", "Wphi4D2n1", "Wphi4D2n2", "Wphi4D2n3", "Wphi4D2n4", "Bphi4D2n1", "Bphi4D2n2" }
```

A.1 Dimension-5 and -6 operators

$$Q_{\nu\nu} = \varepsilon_{jk}\varepsilon_{mn}\varphi^j\varphi^m\left(l_p^k\right)^T C l_r^n \equiv \left(\widetilde{\varphi}^\dagger l_p\right)^T C\left(\widetilde{\varphi}^\dagger l_r\right). \tag{A.3}$$

X^3		φ^6 and $\varphi^4 D^2$		$\psi^2\varphi^3$	
Q_G	$f^{ABC}G_\mu^{A\nu}G_\nu^{B\rho}G_\rho^{C\mu}$	Q_φ	$(\varphi^\dagger\varphi)^3$	$Q_{e\varphi}$	$(\varphi^\dagger\varphi)(\bar{l}_p e_r \varphi)$
$Q_{\widetilde{G}}$	$f^{ABC}\widetilde{G}_\mu^{A\nu}G_\nu^{B\rho}G_\rho^{C\mu}$	$Q_{\varphi\Box}$	$(\varphi^\dagger\varphi)\Box(\varphi^\dagger\varphi)$	$Q_{u\varphi}$	$(\varphi^\dagger\varphi)(\bar{q}_p u_r \widetilde{\varphi})$
Q_W	$\epsilon^{IJK}W_\mu^{I\nu}W_\nu^{J\rho}W_\rho^{K\mu}$	$Q_{\varphi D}$	$\left(\varphi^\dagger D^\mu\varphi\right)^*\left(\varphi^\dagger D_\mu\varphi\right)$	$Q_{d\varphi}$	$(\varphi^\dagger\varphi)(\bar{q}_p d_r \varphi)$
$Q_{\widetilde{W}}$	$\epsilon^{IJK}\widetilde{W}_\mu^{I\nu}W_\nu^{J\rho}W_\rho^{K\mu}$				

$X^2\varphi^2$		$\psi^2 X\varphi$		$\psi^2\varphi^2 D$	
$Q_{\varphi G}$	$\varphi^\dagger\varphi\, G_{\mu\nu}^A G^{A\mu\nu}$	Q_{eW}	$(\bar{l}_p\sigma^{\mu\nu}e_r)\tau^I\varphi W_{\mu\nu}^I$	$Q_{\varphi l}^{(1)}$	$i(\varphi^\dagger \overset{\leftrightarrow}{D}_\mu \varphi)(\bar{l}_p\gamma^\mu l_r)$
$Q_{\varphi\widetilde{G}}$	$\varphi^\dagger\varphi\, \widetilde{G}_{\mu\nu}^A G^{A\mu\nu}$	Q_{eB}	$(\bar{l}_p\sigma^{\mu\nu}e_r)\varphi B_{\mu\nu}$	$Q_{\varphi l}^{(3)}$	$i(\varphi^\dagger \overset{\leftrightarrow}{D}_\mu^I \varphi)(\bar{l}_p\tau^I\gamma^\mu l_r)$
$Q_{\varphi W}$	$\varphi^\dagger\varphi\, W_{\mu\nu}^I W^{I\mu\nu}$	Q_{uG}	$(\bar{q}_p\sigma^{\mu\nu}T^A u_r)\widetilde{\varphi}\, G_{\mu\nu}^A$	$Q_{\varphi e}$	$i(\varphi^\dagger \overset{\leftrightarrow}{D}_\mu \varphi)(\bar{e}_p\gamma^\mu e_r)$
$Q_{\varphi\widetilde{W}}$	$\varphi^\dagger\varphi\, \widetilde{W}_{\mu\nu}^I W^{I\mu\nu}$	Q_{uW}	$(\bar{q}_p\sigma^{\mu\nu}u_r)\tau^I\widetilde{\varphi}\, W_{\mu\nu}^I$	$Q_{\varphi q}^{(1)}$	$i(\varphi^\dagger \overset{\leftrightarrow}{D}_\mu \varphi)(\bar{q}_p\gamma^\mu q_r)$
$Q_{\varphi B}$	$\varphi^\dagger\varphi\, B_{\mu\nu}B^{\mu\nu}$	Q_{uB}	$(\bar{q}_p\sigma^{\mu\nu}u_r)\widetilde{\varphi}\, B_{\mu\nu}$	$Q_{\varphi q}^{(3)}$	$i(\varphi^\dagger \overset{\leftrightarrow}{D}_\mu^I \varphi)(\bar{q}_p\tau^I\gamma^\mu q_r)$
$Q_{\varphi\widetilde{B}}$	$\varphi^\dagger\varphi\, \widetilde{B}_{\mu\nu}B^{\mu\nu}$	Q_{dG}	$(\bar{q}_p\sigma^{\mu\nu}T^A d_r)\varphi\, G_{\mu\nu}^A$	$Q_{\varphi u}$	$i(\varphi^\dagger \overset{\leftrightarrow}{D}_\mu \varphi)(\bar{u}_p\gamma^\mu u_r)$
$Q_{\varphi WB}$	$\varphi^\dagger\tau^I\varphi\, W_{\mu\nu}^I B^{\mu\nu}$	Q_{dW}	$(\bar{q}_p\sigma^{\mu\nu}d_r)\tau^I\varphi\, W_{\mu\nu}^I$	$Q_{\varphi d}$	$i(\varphi^\dagger \overset{\leftrightarrow}{D}_\mu \varphi)(\bar{d}_p\gamma^\mu d_r)$
$Q_{\varphi\widetilde{W}B}$	$\varphi^\dagger\tau^I\varphi\, \widetilde{W}_{\mu\nu}^I B^{\mu\nu}$	Q_{dB}	$(\bar{q}_p\sigma^{\mu\nu}d_r)\varphi\, B_{\mu\nu}$	$Q_{\varphi ud}$	$i(\widetilde{\varphi}^\dagger D_\mu \varphi)(\bar{u}_p\gamma^\mu d_r)$

$(\bar{L}L)(\bar{L}L)$		$(\bar{R}R)(\bar{R}R)$		$(\bar{L}L)(\bar{R}R)$	
Q_{ll}	$(\bar{l}_p\gamma_\mu l_r)(\bar{l}_s\gamma^\mu l_t)$	Q_{ee}	$(\bar{e}_p\gamma_\mu e_r)(\bar{e}_s\gamma^\mu e_t)$	Q_{le}	$(\bar{l}_p\gamma_\mu l_r)(\bar{e}_s\gamma^\mu e_t)$
$Q_{qq}^{(1)}$	$(\bar{q}_p\gamma_\mu q_r)(\bar{q}_s\gamma^\mu q_t)$	Q_{uu}	$(\bar{u}_p\gamma_\mu u_r)(\bar{u}_s\gamma^\mu u_t)$	Q_{lu}	$(\bar{l}_p\gamma_\mu l_r)(\bar{u}_s\gamma^\mu u_t)$
$Q_{qq}^{(3)}$	$(\bar{q}_p\gamma_\mu\tau^I q_r)(\bar{q}_s\gamma^\mu\tau^I q_t)$	Q_{dd}	$(\bar{d}_p\gamma_\mu d_r)(\bar{d}_s\gamma^\mu d_t)$	Q_{ld}	$(\bar{l}_p\gamma_\mu l_r)(\bar{d}_s\gamma^\mu d_t)$
$Q_{lq}^{(1)}$	$(\bar{l}_p\gamma_\mu l_r)(\bar{q}_s\gamma^\mu q_t)$	Q_{eu}	$(\bar{e}_p\gamma_\mu e_r)(\bar{u}_s\gamma^\mu u_t)$	Q_{qe}	$(\bar{q}_p\gamma_\mu q_r)(\bar{e}_s\gamma^\mu e_t)$
$Q_{lq}^{(3)}$	$(\bar{l}_p\gamma_\mu\tau^I l_r)(\bar{q}_s\gamma^\mu\tau^I q_t)$	Q_{ed}	$(\bar{e}_p\gamma_\mu e_r)(\bar{d}_s\gamma^\mu d_t)$	$Q_{qu}^{(1)}$	$(\bar{q}_p\gamma_\mu q_r)(\bar{u}_s\gamma^\mu u_t)$
		$Q_{ud}^{(1)}$	$(\bar{u}_p\gamma_\mu u_r)(\bar{d}_s\gamma^\mu d_t)$	$Q_{qu}^{(8)}$	$(\bar{q}_p\gamma_\mu T^A q_r)(\bar{u}_s\gamma^\mu T^A u_t)$
		$Q_{ud}^{(8)}$	$(\bar{u}_p\gamma_\mu T^A u_r)(\bar{d}_s\gamma^\mu T^A d_t)$	$Q_{qd}^{(1)}$	$(\bar{q}_p\gamma_\mu q_r)(\bar{d}_s\gamma^\mu d_t)$
				$Q_{qd}^{(8)}$	$(\bar{q}_p\gamma_\mu T^A q_r)(\bar{d}_s\gamma^\mu T^A d_t)$

$(\bar{L}R)(\bar{R}L)$ and $(\bar{L}R)(\bar{L}R)$		B-violating	
Q_{ledq}	$(\bar{l}_p^j e_r)(\bar{d}_s q_t^j)$	Q_{duq}	$\epsilon^{\alpha\beta\gamma}\epsilon_{jk}\left[(d_p^\alpha)^T C u_r^\beta\right]\left[(q_s^{\gamma j})^T C l_t^k\right]$
$Q_{quqd}^{(1)}$	$(\bar{q}_p^j u_r)\epsilon_{jk}(\bar{q}_s^k d_t)$	Q_{qqu}	$\epsilon^{\alpha\beta\gamma}\epsilon_{jk}\left[(q_p^{\alpha j})^T C q_r^{\beta k}\right]\left[(u_s^\gamma)^T C e_t\right]$
$Q_{quqd}^{(8)}$	$(\bar{q}_p^j T^A u_r)\epsilon_{jk}(\bar{q}_s^k T^A d_t)$	Q_{qqq}	$\epsilon^{\alpha\beta\gamma}\epsilon_{jn}\epsilon_{km}\left[(q_p^{\alpha j})^T C q_r^{\beta k}\right]\left[(q_s^{\gamma m})^T C l_t^n\right]$
$Q_{lequ}^{(1)}$	$(\bar{l}_p^j e_r)\epsilon_{jk}(\bar{q}_s^k u_t)$	Q_{duu}	$\epsilon^{\alpha\beta\gamma}\left[(d_p^\alpha)^T C u_r^\beta\right]\left[(u_s^\gamma)^T C e_t\right]$
$Q_{lequ}^{(3)}$	$(\bar{l}_p^j\sigma_{\mu\nu}e_r)\epsilon_{jk}(\bar{q}_s^k\sigma^{\mu\nu}u_t)$		

Table A.1: The full set of dimension-6 operators in the Warsaw basis [13]. The sub-tables in the two upper rows collect all operators except for the four-fermion ones, which are collected separately in the sub-tables of the two bottom rows.

A.2 Dimension-8 bosonic operators

φ^8		$\varphi^6 D^2$		$\varphi^4 D^4$	
Q_{φ^8}	$(\varphi^\dagger\varphi)^4$	$Q_{\varphi^6\Box}$	$(\varphi^\dagger\varphi)^2\Box(\varphi^\dagger\varphi)$	$Q^{(1)}_{\varphi^4 D^4}$	$(D_\mu\varphi^\dagger D_\nu\varphi)(D^\nu\varphi^\dagger D^\mu\varphi)$
		$Q_{\varphi^6 D^2}$	$(\varphi^\dagger\varphi)(\varphi^\dagger D_\mu\varphi)^*(\varphi^\dagger D^\mu\varphi)$	$Q^{(2)}_{\varphi^4 D^4}$	$(D_\mu\varphi^\dagger D_\nu\varphi)(D^\mu\varphi^\dagger D^\nu\varphi)$
				$Q^{(3)}_{\varphi^4 D^4}$	$(D_\mu\varphi^\dagger D^\mu\varphi)(D_\nu\varphi^\dagger D^\nu\varphi)$

Table A.2: Dimension-8 operators containing only the Higgs field. Table taken from ref. [76] except for the two operators in $\varphi^6 D^2$ class that have been modified as discussed in this Appendix.

$X^4,\ X^3X'$		$X^2X'^2$	
$Q^{(1)}_{G^4}$	$(G^A_{\mu\nu}G^{A\mu\nu})(G^B_{\rho\sigma}G^{B\rho\sigma})$	$Q^{(1)}_{G^2W^2}$	$(W^I_{\mu\nu}W^{I\mu\nu})(G^A_{\rho\sigma}G^{A\rho\sigma})$
$Q^{(2)}_{G^4}$	$(G^A_{\mu\nu}\widetilde{G}^{A\mu\nu})(G^B_{\rho\sigma}\widetilde{G}^{B\rho\sigma})$	$Q^{(2)}_{G^2W^2}$	$(W^I_{\mu\nu}\widetilde{W}^{I\mu\nu})(G^A_{\rho\sigma}\widetilde{G}^{A\rho\sigma})$
$Q^{(3)}_{G^4}$	$(G^A_{\mu\nu}G^{B\mu\nu})(G^A_{\rho\sigma}G^{B\rho\sigma})$	$Q^{(3)}_{G^2W^2}$	$(W^I_{\mu\nu}G^{A\mu\nu})(W^I_{\rho\sigma}G^{A\rho\sigma})$
$Q^{(4)}_{G^4}$	$(G^A_{\mu\nu}\widetilde{G}^{B\mu\nu})(G^A_{\rho\sigma}\widetilde{G}^{B\rho\sigma})$	$Q^{(4)}_{G^2W^2}$	$(W^I_{\mu\nu}\widetilde{G}^{A\mu\nu})(W^I_{\rho\sigma}\widetilde{G}^{A\rho\sigma})$
$Q^{(5)}_{G^4}$	$(G^A_{\mu\nu}G^{A\mu\nu})(G^B_{\rho\sigma}\widetilde{G}^{B\rho\sigma})$	$Q^{(5)}_{G^2W^2}$	$(W^I_{\mu\nu}\widetilde{W}^{I\mu\nu})(G^A_{\rho\sigma}G^{A\rho\sigma})$
$Q^{(6)}_{G^4}$	$(G^A_{\mu\nu}G^{B\mu\nu})(G^A_{\rho\sigma}\widetilde{G}^{B\rho\sigma})$	$Q^{(6)}_{G^2W^2}$	$(W^I_{\mu\nu}W^{I\mu\nu})(G^A_{\rho\sigma}\widetilde{G}^{A\rho\sigma})$
$Q^{(7)}_{G^4}$	$d^{ABE}d^{CDE}(G^A_{\mu\nu}G^{B\mu\nu})(G^C_{\rho\sigma}G^{D\rho\sigma})$	$Q^{(7)}_{G^2W^2}$	$(W^I_{\mu\nu}G^{A\mu\nu})(W^I_{\rho\sigma}\widetilde{G}^{A\rho\sigma})$
$Q^{(8)}_{G^4}$	$d^{ABE}d^{CDE}(G^A_{\mu\nu}\widetilde{G}^{B\mu\nu})(G^C_{\rho\sigma}\widetilde{G}^{D\rho\sigma})$	$Q^{(1)}_{G^2B^2}$	$(B_{\mu\nu}B^{\mu\nu})(G^A_{\rho\sigma}G^{A\rho\sigma})$
$Q^{(9)}_{G^4}$	$d^{ABE}d^{CDE}(G^A_{\mu\nu}G^{B\mu\nu})(G^C_{\rho\sigma}\widetilde{G}^{D\rho\sigma})$	$Q^{(2)}_{G^2B^2}$	$(B_{\mu\nu}\widetilde{B}^{\mu\nu})(G^A_{\rho\sigma}\widetilde{G}^{A\rho\sigma})$
$Q^{(1)}_{W^4}$	$(W^I_{\mu\nu}W^{I\mu\nu})(W^J_{\rho\sigma}W^{J\rho\sigma})$	$Q^{(3)}_{G^2B^2}$	$(B_{\mu\nu}G^{A\mu\nu})(B_{\rho\sigma}G^{A\rho\sigma})$
$Q^{(2)}_{W^4}$	$(W^I_{\mu\nu}\widetilde{W}^{I\mu\nu})(W^J_{\rho\sigma}\widetilde{W}^{J\rho\sigma})$	$Q^{(4)}_{G^2B^2}$	$(B_{\mu\nu}\widetilde{G}^{A\mu\nu})(B_{\rho\sigma}\widetilde{G}^{A\rho\sigma})$
$Q^{(3)}_{W^4}$	$(W^I_{\mu\nu}W^{J\mu\nu})(W^I_{\rho\sigma}W^{J\rho\sigma})$	$Q^{(5)}_{G^2B^2}$	$(B_{\mu\nu}\widetilde{B}^{\mu\nu})(G^A_{\rho\sigma}G^{A\rho\sigma})$
$Q^{(4)}_{W^4}$	$(W^I_{\mu\nu}\widetilde{W}^{J\mu\nu})(W^I_{\rho\sigma}\widetilde{W}^{J\rho\sigma})$	$Q^{(6)}_{G^2B^2}$	$(B_{\mu\nu}B^{\mu\nu})(G^A_{\rho\sigma}\widetilde{G}^{A\rho\sigma})$
$Q^{(5)}_{W^4}$	$(W^I_{\mu\nu}W^{I\mu\nu})(W^J_{\rho\sigma}\widetilde{W}^{J\rho\sigma})$	$Q^{(7)}_{G^2B^2}$	$(B_{\mu\nu}G^{A\mu\nu})(B_{\rho\sigma}\widetilde{G}^{A\rho\sigma})$
$Q^{(6)}_{W^4}$	$(W^I_{\mu\nu}W^{J\mu\nu})(W^I_{\rho\sigma}\widetilde{W}^{J\rho\sigma})$	$Q^{(1)}_{W^2B^2}$	$(B_{\mu\nu}B^{\mu\nu})(W^I_{\rho\sigma}W^{I\rho\sigma})$
$Q^{(1)}_{B^4}$	$(B_{\mu\nu}B^{\mu\nu})(B_{\rho\sigma}B^{\rho\sigma})$	$Q^{(2)}_{W^2B^2}$	$(B_{\mu\nu}\widetilde{B}^{\mu\nu})(W^I_{\rho\sigma}\widetilde{W}^{I\rho\sigma})$
$Q^{(2)}_{B^4}$	$(B_{\mu\nu}\widetilde{B}^{\mu\nu})(B_{\rho\sigma}\widetilde{B}^{\rho\sigma})$	$Q^{(3)}_{W^2B^2}$	$(B_{\mu\nu}W^{I\mu\nu})(B_{\rho\sigma}W^{I\rho\sigma})$
$Q^{(3)}_{B^4}$	$(B_{\mu\nu}B^{\mu\nu})(B_{\rho\sigma}\widetilde{B}^{\rho\sigma})$	$Q^{(4)}_{W^2B^2}$	$(B_{\mu\nu}\widetilde{W}^{I\mu\nu})(B_{\rho\sigma}\widetilde{W}^{I\rho\sigma})$
$Q^{(1)}_{G^3B}$	$d^{ABC}(B_{\mu\nu}G^{A\mu\nu})(G^B_{\rho\sigma}G^{C\rho\sigma})$	$Q^{(5)}_{W^2B^2}$	$(B_{\mu\nu}\widetilde{B}^{\mu\nu})(W^I_{\rho\sigma}W^{I\rho\sigma})$
$Q^{(2)}_{G^3B}$	$d^{ABC}(B_{\mu\nu}\widetilde{G}^{A\mu\nu})(G^B_{\rho\sigma}\widetilde{G}^{C\rho\sigma})$	$Q^{(6)}_{W^2B^2}$	$(B_{\mu\nu}B^{\mu\nu})(W^I_{\rho\sigma}\widetilde{W}^{I\rho\sigma})$
$Q^{(3)}_{G^3B}$	$d^{ABC}(B_{\mu\nu}\widetilde{G}^{A\mu\nu})(G^B_{\rho\sigma}G^{C\rho\sigma})$	$Q^{(7)}_{W^2B^2}$	$(B_{\mu\nu}W^{I\mu\nu})(B_{\rho\sigma}\widetilde{W}^{I\rho\sigma})$
$Q^{(4)}_{G^3B}$	$d^{ABC}(B_{\mu\nu}G^{A\mu\nu})(G^B_{\rho\sigma}\widetilde{G}^{C\rho\sigma})$		

Table A.3: Dimension-8 operators containing only the gauge field strength tensors. Table taken from ref. [76].

$X^3\varphi^2$		$X^2\varphi^4$	
$Q^{(1)}_{G^3\varphi^2}$	$f^{ABC}(\varphi^\dagger\varphi)G^{A\nu}_\mu G^{B\rho}_\nu G^{C\mu}_\rho$	$Q^{(1)}_{G^2\varphi^4}$	$(\varphi^\dagger\varphi)^2 G^A_{\mu\nu}G^{A\mu\nu}$
$Q^{(2)}_{G^3\varphi^2}$	$f^{ABC}(\varphi^\dagger\varphi)G^{A\nu}_\mu G^{B\rho}_\nu \widetilde{G}^{C\mu}_\rho$	$Q^{(2)}_{G^2\varphi^4}$	$(\varphi^\dagger\varphi)^2 \widetilde{G}^A_{\mu\nu}G^{A\mu\nu}$
$Q^{(1)}_{W^3\varphi^2}$	$\epsilon^{IJK}(\varphi^\dagger\varphi)W^{I\nu}_\mu W^{J\rho}_\nu W^{K\mu}_\rho$	$Q^{(1)}_{W^2\varphi^4}$	$(\varphi^\dagger\varphi)^2 W^I_{\mu\nu}W^{I\mu\nu}$
$Q^{(2)}_{W^3\varphi^2}$	$\epsilon^{IJK}(\varphi^\dagger\varphi)W^{I\nu}_\mu W^{J\rho}_\nu \widetilde{W}^{K\mu}_\rho$	$Q^{(2)}_{W^2\varphi^4}$	$(\varphi^\dagger\varphi)^2 \widetilde{W}^I_{\mu\nu}W^{I\mu\nu}$
$Q^{(1)}_{W^2B\varphi^2}$	$\epsilon^{IJK}(\varphi^\dagger\tau^I\varphi)B^\nu_\mu W^{J\rho}_\nu W^{K\mu}_\rho$	$Q^{(3)}_{W^2\varphi^4}$	$(\varphi^\dagger\tau^I\varphi)(\varphi^\dagger\tau^J\varphi)W^I_{\mu\nu}W^{J\mu\nu}$
$Q^{(2)}_{W^2B\varphi^2}$	$\epsilon^{IJK}(\varphi^\dagger\tau^I\varphi)(\widetilde{B}^{\mu\nu}W^J_{\nu\rho}W^{K\rho}_\mu + B^{\mu\nu}W^J_{\nu\rho}\widetilde{W}^{K\rho}_\mu)$	$Q^{(4)}_{W^2\varphi^4}$	$(\varphi^\dagger\tau^I\varphi)(\varphi^\dagger\tau^J\varphi)\widetilde{W}^I_{\mu\nu}W^{J\mu\nu}$
		$Q^{(1)}_{WB\varphi^4}$	$(\varphi^\dagger\varphi)(\varphi^\dagger\tau^I\varphi)W^I_{\mu\nu}B^{\mu\nu}$
		$Q^{(2)}_{WB\varphi^4}$	$(\varphi^\dagger\varphi)(\varphi^\dagger\tau^I\varphi)\widetilde{W}^I_{\mu\nu}B^{\mu\nu}$
		$Q^{(1)}_{B^2\varphi^4}$	$(\varphi^\dagger\varphi)^2 B_{\mu\nu}B^{\mu\nu}$
		$Q^{(2)}_{B^2\varphi^4}$	$(\varphi^\dagger\varphi)^2 \widetilde{B}_{\mu\nu}B^{\mu\nu}$

$X^2\varphi^2D^2$		$X\varphi^4D^2$	
$Q^{(1)}_{G^2\varphi^2D^2}$	$(D^\mu\varphi^\dagger D^\nu\varphi)G^A_{\mu\rho}G^{A\rho}_\nu$	$Q^{(1)}_{W\varphi^4D^2}$	$(\varphi^\dagger\varphi)(D^\mu\varphi^\dagger\tau^I D^\nu\varphi)W^I_{\mu\nu}$
$Q^{(2)}_{G^2\varphi^2D^2}$	$(D^\mu\varphi^\dagger D_\mu\varphi)G^A_{\nu\rho}G^{A\nu\rho}$	$Q^{(2)}_{W\varphi^4D^2}$	$(\varphi^\dagger\varphi)(D^\mu\varphi^\dagger\tau^I D^\nu\varphi)\widetilde{W}^I_{\mu\nu}$
$Q^{(3)}_{G^2\varphi^2D^2}$	$(D^\mu\varphi^\dagger D_\mu\varphi)G^A_{\nu\rho}\widetilde{G}^{A\nu\rho}$	$Q^{(3)}_{W\varphi^4D^2}$	$\epsilon^{IJK}(\varphi^\dagger\tau^I\varphi)(D^\mu\varphi^\dagger\tau^J D^\nu\varphi)W^K_{\mu\nu}$
$Q^{(1)}_{W^2\varphi^2D^2}$	$(D^\mu\varphi^\dagger D^\nu\varphi)W^I_{\mu\rho}W^{I\rho}_\nu$	$Q^{(4)}_{W\varphi^4D^2}$	$\epsilon^{IJK}(\varphi^\dagger\tau^I\varphi)(D^\mu\varphi^\dagger\tau^J D^\nu\varphi)\widetilde{W}^K_{\mu\nu}$
$Q^{(2)}_{W^2\varphi^2D^2}$	$(D^\mu\varphi^\dagger D_\mu\varphi)W^I_{\nu\rho}W^{I\nu\rho}$	$Q^{(1)}_{B\varphi^4D^2}$	$(\varphi^\dagger\varphi)(D^\mu\varphi^\dagger D^\nu\varphi)B_{\mu\nu}$
$Q^{(3)}_{W^2\varphi^2D^2}$	$(D^\mu\varphi^\dagger D_\mu\varphi)W^I_{\nu\rho}\widetilde{W}^{I\nu\rho}$	$Q^{(2)}_{B\varphi^4D^2}$	$(\varphi^\dagger\varphi)(D^\mu\varphi^\dagger D^\nu\varphi)\widetilde{B}_{\mu\nu}$
$Q^{(4)}_{W^2\varphi^2D^2}$	$i\epsilon^{IJK}(D^\mu\varphi^\dagger\tau^I D^\nu\varphi)W^J_{\mu\rho}W^{K\rho}_\nu$		
$Q^{(5)}_{W^2\varphi^2D^2}$	$\epsilon^{IJK}(D^\mu\varphi^\dagger\tau^I D^\nu\varphi)(W^J_{\mu\rho}\widetilde{W}^{K\rho}_\nu - \widetilde{W}^J_{\mu\rho}W^{K\rho}_\nu)$		
$Q^{(6)}_{W^2\varphi^2D^2}$	$i\epsilon^{IJK}(D^\mu\varphi^\dagger\tau^I D^\nu\varphi)(W^J_{\mu\rho}\widetilde{W}^{K\rho}_\nu + \widetilde{W}^J_{\mu\rho}W^{K\rho}_\nu)$		
$Q^{(1)}_{WB\varphi^2D^2}$	$(D^\mu\varphi^\dagger\tau^I D_\mu\varphi)B_{\nu\rho}W^{I\nu\rho}$		
$Q^{(2)}_{WB\varphi^2D^2}$	$(D^\mu\varphi^\dagger\tau^I D_\mu\varphi)B_{\nu\rho}\widetilde{W}^{I\nu\rho}$		
$Q^{(3)}_{WB\varphi^2D^2}$	$i(D^\mu\varphi^\dagger\tau^I D^\nu\varphi)(B_{\mu\rho}W^{I\rho}_\nu - B_{\nu\rho}W^{I\rho}_\mu)$		
$Q^{(4)}_{WB\varphi^2D^2}$	$(D^\mu\varphi^\dagger\tau^I D^\nu\varphi)(B_{\mu\rho}W^{I\rho}_\nu + B_{\nu\rho}W^{I\rho}_\mu)$		
$Q^{(5)}_{WB\varphi^2D^2}$	$i(D^\mu\varphi^\dagger\tau^I D^\nu\varphi)(B_{\mu\rho}\widetilde{W}^{I\rho}_\nu - B_{\nu\rho}\widetilde{W}^{I\rho}_\mu)$		
$Q^{(6)}_{WB\varphi^2D^2}$	$(D^\mu\varphi^\dagger\tau^I D^\nu\varphi)(B_{\mu\rho}\widetilde{W}^{I\rho}_\nu + B_{\nu\rho}\widetilde{W}^{I\rho}_\mu)$		
$Q^{(1)}_{B^2\varphi^2D^2}$	$(D^\mu\varphi^\dagger D^\nu\varphi)B_{\mu\rho}B_\nu{}^\rho$		
$Q^{(2)}_{B^2\varphi^2D^2}$	$(D^\mu\varphi^\dagger D_\mu\varphi)B_{\nu\rho}B^{\nu\rho}$		
$Q^{(3)}_{B^2\varphi^2D^2}$	$(D^\mu\varphi^\dagger D_\mu\varphi)B_{\nu\rho}\widetilde{B}^{\nu\rho}$		

Table A.4: Dimension-8 operators containing both the gauge field strength tensors and the Higgs field. Table taken (and modified according to our notation) from ref. [76].

B Predefined input schemes formulas for the electroweak sector

The electroweak parameters, $\bar{g}$, $\bar{g}'$, v and λ, after expansion in powers of $1/\Lambda$, can be written in the following form:

$$\begin{aligned}
\bar{g} &= \bar{g}_{SM} + \frac{1}{\Lambda^2}\bar{g}_{D6} + \frac{1}{\Lambda^4}\bar{g}_{D8} \,, \\
\bar{g}' &= \bar{g}'_{SM} + \frac{1}{\Lambda^2}\bar{g}'_{D6} + \frac{1}{\Lambda^4}\bar{g}'_{D8} \,, \\
v &= v_{SM} + \frac{1}{\Lambda^2}v_{D6} + \frac{1}{\Lambda^4}v_{D8} \,, \\
\lambda &= \lambda_{SM} + \frac{1}{\Lambda^2}\lambda_{D6} + \frac{1}{\Lambda^4}\lambda_{D8} \,,
\end{aligned} \tag{B.1}$$

with the exact form of "SM", "D6" and "D8" depending on the particular choice of the input scheme. Below, we present the relevant expressions for the two input schemes included as predefined routines in the `SmeftFR` v3 distribution.

"GF" input scheme

In this scheme, the Fermi constant G_F (extracted from the muon lifetime measurement) and the masses of the gauge and Higgs bosons M_Z, M_W, M_H are used as the input parameters. To relate them to the quantities defined in Eq. (B.1), we define the following abbreviations:

$$\begin{aligned}
\Delta M &= \sqrt{M_Z^2 - M_W^2} \,, \\
\mathcal{B}_6(C_{ll}, C_{\varphi l3}) &= -2(C_{ll}^{2112} - C_{\varphi l3}^{11} - C_{\varphi l3}^{22}) \,, \\
\mathcal{B}_8(C_{ll}, C_{\varphi l3}, C_{\varphi l1}) &= (C_{ll}^{2112})^2 + \frac{1}{4}(C_{le}^{2112})^2 - 2C_{ll}^{2112}C_{\varphi l3}^{11} - 2C_{ll}^{2112}C_{\varphi l3}^{22} \\
&+ (C_{\varphi l3}^{11})^2 + (C_{\varphi l3}^{22})^2 + 4C_{\varphi l3}^{11}C_{\varphi l3}^{22} \\
&+ C_{\varphi l1}^{21}C_{\varphi l3}^{12} - C_{\varphi l1}^{12}C_{\varphi l3}^{21} + C_{\varphi l1}^{12}C_{\varphi l1}^{21} - C_{\varphi l3}^{12}C_{\varphi l3}^{21} \,.
\end{aligned} \tag{B.2}$$

Then one can express quantities in Eq. (B.1) as:

$$\begin{aligned}
v_{SM} &= \frac{1}{2^{1/4}\sqrt{G_F}} \,, \\
v_{D6} &= \frac{v_{SM}}{4\sqrt{2}G_F}\mathcal{B}_6 \,, \\
v_{D8} &= \frac{v_{SM}}{64G_F^2}(\mathcal{B}_6^2 + 8\mathcal{B}_8) \,,
\end{aligned} \tag{B.3}$$

$$\begin{aligned}
\bar{g}_{SM} &= 2^{5/4}\sqrt{G_F}M_W \,, \\
\bar{g}_{D6} &= -\frac{\bar{g}_{SM}}{4\sqrt{2}G_F}\mathcal{B}_6 \,, \\
\bar{g}_{D8} &= \frac{\bar{g}_{SM}}{64G_F^2}(\mathcal{B}_6^2 - 8\mathcal{B}_8) \,,
\end{aligned} \tag{B.4}$$

$$\bar{g}'_{SM} = 2^{5/4}\sqrt{G_F}\Delta M^2 \,,$$

$$
\begin{aligned}
\bar{g}'_{D6} &= \frac{\bar{g}'_{SM}}{4\sqrt{2}G_F\Delta M}\left(-M_Z^2 C_{\varphi D} - 4M_W\Delta M C_{\varphi WB} - \Delta M^2\mathcal{B}_6\right) , \\
\bar{g}'_{D8} &= \frac{\bar{g}'_{SM}}{16G_F^2\Delta M^2}\Big[-2M_Z^2(2C_{\varphi^6 D^2} + \mathcal{B}_6 C_{\varphi D}) + \Delta M^2(\mathcal{B}_6^2 - 8\mathcal{B}_8 - 16C_{\varphi WB}^2) \\
&- 8M_W\Big(2M_W C^{(3)}_{W^2\varphi^4} + 2\Delta M C^{(1)}_{WB\varphi^4} + \Delta M(\mathcal{B}_6 + 4C_{\varphi B} + 4C_{\varphi W})C_{\varphi WB}\Big)\Big] ,
\end{aligned} \tag{B.5}
$$

$$
\begin{aligned}
\lambda_{SM} &= \sqrt{2}G_F M_H^2 , \\
\lambda_{D6} &= \frac{\lambda_{SM}}{4G_F}\left[\frac{6}{G_F M_H^2}C_\varphi - \sqrt{2}\Big(\mathcal{B}_6 + 4C_{\varphi\Box} - C_{\varphi D}\Big)\right] , \\
\lambda_{D8} &= \frac{\lambda_{SM}}{16G_F^2}\left[\Big(\mathcal{B}_6^2 - 4\mathcal{B}_8 - 8C_{\varphi^6\Box} + 2C_{\varphi^2 D^2}\Big) + \frac{6\sqrt{2}}{G_F M_H^2}\Big(\mathcal{B}_6 C_\varphi + 2C_{\varphi 8}\Big)\right] .
\end{aligned} \tag{B.6}
$$

"AEM" input scheme

In this input scheme, the input parameters for the electroweak sector are chosen to be the electromagnetic coupling α_{em}, and the masses of gauge and Higgs bosons M_Z, M_W, and M_H. Using the abbreviation $\Delta M = \sqrt{M_Z^2 - M_W^2}$, the quantities defined in Eq. (B.1) are given by:

$$
\begin{aligned}
v_{SM} &= \frac{M_W\Delta M}{M_Z\sqrt{\pi\alpha_{em}}} , \\
v_{D6} &= -\frac{\bar{g}_{SM}M_W^3}{4\pi\alpha_{em}M_Z^2}\left(M_W C_{\varphi D} + 4\Delta M C_{\varphi WB}\right) , \\
v_{D8} &= \frac{v_{SM}M_W^5}{32\pi^2\alpha_{em}^2 M_Z^4}\Big[3M_W^3 C_{\varphi D}^2 - 4M_W\Delta M^2 C_{\varphi^6 D^2} - 8(M_Z^2 - 5M_W^2)\Delta M C_{\varphi D}C_{\varphi WB} \\
&+ 16\Delta M^2\Big(4M_W C_{\varphi WB}^2 - \Delta M C^{(1)}_{WB\varphi^4} + \frac{M_Z^2 - 2M_W^2}{M_W}C^{(3)}_{WB\varphi^4}\Big) \\
&- 32\Delta M^3(C_{\varphi B} + C_{\varphi W})C_{\varphi WB}\Big] ,
\end{aligned} \tag{B.7}
$$

$$
\begin{aligned}
\bar{g}_{SM} &= \frac{2M_Z\sqrt{\pi\alpha_{em}}}{\Delta M} , \\
\bar{g}_{D6} &= -v_{D6} , \\
\bar{g}_{D8} &= \frac{\bar{g}_{SM}M_W^5}{32\pi^2\alpha_{em}^2 M_Z^4}\Big[-M_W^3 C_{\varphi D}^2 + 4M_W\Delta M^2 C_{\varphi^6 D^2} + 8(M_Z^2 - 3M_W^2)\Delta M C_{\varphi D}C_{\varphi WB} \\
&- 16\Delta M^2\Big(2M_W C_{\varphi WB}^2 - \Delta M C^{(1)}_{WB\varphi^4} + \frac{M_Z^2 - 2M_W^2}{M_W}C^{(3)}_{WB\varphi^4}\Big) \\
&+ 32\Delta M^3(C_{\varphi B} + C_{\varphi W})C_{\varphi WB}\Big] ,
\end{aligned} \tag{B.8}
$$

$$
\begin{aligned}
\bar{g}'_{SM} &= \frac{2M_Z\sqrt{\pi\alpha_{em}}}{M_W} , \\
\bar{g}'_{D6} &= -\frac{\bar{g}'_{SM}\Delta M^2 M_W^2}{4\pi\alpha_{em}M_Z^2}C_{\varphi D} ,
\end{aligned}
$$

$$
\begin{aligned}
\bar{g}'_{D8} &= \frac{\bar{g}'_{SM} M_W^4 \Delta M^2}{32\pi^2 \alpha_{em}^2 M_Z^4} \Big[(M_W^2 + 3M_Z^2) C_{\varphi D}^2 - 16\Delta M^2 C_{\varphi WB}^2 + 16 M_W \Delta M C_{\varphi D} C_{\varphi WB} \\
&- 4\Delta M^2 \Big(C_{\varphi^6 D^2} + 4 C^{(3)}_{W^2\varphi^4} \Big) \Big] \,, \qquad \text{(B.9)}
\end{aligned}
$$

$$
\begin{aligned}
\lambda_{SM} &= \frac{\pi \alpha_{em} M_H^2 M_Z^2}{\Delta M^2} \,, \\
\lambda_{D6} &= \frac{3\Delta M^2 M_W^2}{\pi \alpha_{em} M_Z^2} C_\varphi - 2M_H^2 C_{\varphi\Box} + \frac{M_H^2 M_Z^2}{2\Delta M^2} C_{\varphi D} + 2 M_W \Delta M C_{\varphi WB} \,, \\
\lambda_{D8} &= \frac{M_W^2}{4\pi^2 \alpha_{em}^2 M_Z^4} \Big[12 M_W^2 \Delta M^4 2 C_{\varphi 8} - 6 M_W^3 \Delta M^2 C_\varphi (M_W C_{\varphi D} + 4\Delta M C_{\varphi WB}) \\
&+ \pi \alpha_{em} M_Z^2 M_H^2 \Big(-4\Delta M^2 C_{\varphi^6 \Box} + M_Z^2 C_{\varphi^2 D^2} + 8 M_W \Delta M (C_{\varphi B} + C_{\varphi W}) C_{\varphi WB} \\
&+ \frac{2 M_W (M_Z^2 - 2M_W^2)}{\Delta M} C_{\varphi D} C_{\varphi WB} - 4 M_W^2 C_{\varphi WB}^2 \\
&+ 4 M_W \Delta M C^{(1)}_{WB\varphi^4} - 4 (M_Z^2 - 2M_W^2) C^{(3)}_{WB\varphi^4} \Big) \Big] \,. \qquad \text{(B.10)}
\end{aligned}
$$

C File structure of SmeftFR v3 and arguments of the user available routines

Below we display all relevant Tables taken from [73], with:

- a list of all files and directories included in the SmeftFR v3 distribution - Table C.1,
- a description of available options for SmeftFR v3 routines - Tables C.2, C.3, C.4, C.5, C.6,
- the names of variables containing Feynman rules expressions - Table C.7.

SmeftFR-init.nb smeft_fr_init.m	Notebook and equivalent text script generating SMEFT Lagrangian in mass basis and Feynman rules in *Mathematica* format.
SmeftFR-interfaces.nb smeft_fr_interfaces.m	Notebook and text script with routines for exporting Feynman rules in various formats: WCxf, Latex, UFO and FeynArts.
SmeftFR_v3.pdf	package manual in pdf format.
code	sub-directory with package code and utilities.
lagrangian	sub-directory with expressions for the SM Lagrangian and dimension-5, 6 and 8 operators coded in FeynRules format.
definitions	sub-directory with templates of SMEFT "model files" and example of numerical input for Wilson coefficients in WCxf format.
output	sub-directory with dynamically generated model "parameter files" and output for Feynman rules in various formats, by default *Mathematica*, Latex, UFO and FeynArts are generated.

Table C.1: Files and directories included in SmeftFR v3 package.

Option	Allowed values	Description
Operators	list of operators	Subset of SMEFT operators included in calculations. Default: all $d = 5$ and $d = 6$ operators.
Gauge	**Unitary**, Rxi	Choice of gauge fixing conditions.
ExpansionOrder	0, **1** or 2	SMEFT interactions are expanded to $1/\Lambda^{2\,\text{ExpansionOrder}}$ (default: $1/\Lambda^2$).
WCXFInitFile	**""**	Name of file with numerical values of Wilson coefficients in the WCxf format. If this option is not set, all WCs are initialised to 0.
RealParameters	**False**, True	Some codes like MadGraph 5 accept only real values of parameters. If this option is set to True, imaginary part of complex parameters are truncated in `FeynRules` model files.
InputScheme	**"GF"**, "AEM", ...	Selection of input parameters scheme, see discussion in Sections 2.2.2, 2.3.1, 2.3.2.
CKMInput	"no", **"yes"**, "force"	Decides if corrections to CKM matrix are included (use "force" to add them even their relative size exceeds the threshold defined in variable `SMEFT$CKMTreshold` (default: 0.2).
MaxParticles	**6**	Only Feynman rules with less then MaxParticles external legs are calculated. Does not affect UFO and FeynArts output.
MajoranaNeutrino	**False**, True	Neutrinos are treated as Majorana spinors if $Q_{\nu\nu}$ is included in the operator list or this option is set to True, massless Weyl spinors otherwise.
Correct4Fermion	False, **True**	Corrects relative sign of some 4-fermion interactions, fixing results of `FeynRules` .
WBFirstLetter	**"c"**	Customisable first letter of Wilson coefficient names in Warsaw basis (default $c_G, \ldots$).
MBFirstLetter	**"C"**	Customisable first letter of Wilson coefficient names in mass basis (default $C_G, \ldots$).

Table C.2: The allowed options of `SMEFTInitializeModel` routine. If an option is not specified, the default value (marked above in boldface) is assumed.

Option	Allowed values	Description
Expansion	"none",**"smeft"**, "user"	Decides which parametrization is used to describe interaction vertices - with Z_X normalisation constants in an unexpanded form ("none"), using "default" SMEFT parameters ("smeft") or user-defined set of parameters ("user") (see Section 2.4.4 and examples in Figs. 2.2, 2.3, 2.4).
InteractionFile	*filename*	Name of the file with mass basis Lagrangian and vertices generated by `SMEFTOutput` routine. Default: `output/smeft_feynman_rules.m`
ModelFile	*filename*	Name of the model file containing SMEFT parameters in mass basis generated by `SMEFTOutput` routine. Default: `output/smeft_par_MB.fr`
Include4Fermion	False, **True**	4-fermion vertices are not fully supported by `FeynRules` - for extra safety calculations of them can be switched off by setting this option to False.
IncludeBL4Fermion	**False**, True	Baryon and lepton number violating 4-fermion vertices can be in principle evaluated by `FeynRules`, but including them may lead to compatibility problems with other codes - e.g. MadGraph 5 reports errors if such vertices are present in UFO file. Thus in `SmeftFR` evaluation of such vertices is by default switched off. Set this option to True to include them.

Table C.3: Options of `SMEFTInitializeMB` routine, with default values marked in boldface.

Option	Allowed values	Description
Operators	default: all operators	List with subset of Wilson coefficients to be included in the SMEFT parameter file (`ReadWCXFInput` only)
RealParameters	False, True	Decides if only real values of Wilson coefficients given in WCxf file are included in SMEFT parameter file. The default value of this option is the same as set in the routine SMEFTInitializeModel, see Table C.2.
OverwriteTarget	**False**, True	If set to True, target file is overwritten without warning

Table C.4: Options of `ReadWCXFInput` and `WCXFToSMEFT` routines. Default values are marked in boldface. Options RealParameters and OverwriteTarget affect only `WCXFToSMEFT`.

Option name	Allowed values	Description
Expansion	**"none"**, "smeft"	Decides which parametrization is used to describe interaction vertices - with Z_X normalisation constants in an unexpanded form ("none") or using default SMEFT parameters ("smeft") (see discussion in Section 2.4.4 and examples in Figs. 2.2, 2.3,2.4).
FullDocument	False, **True**	By default a complete document is generated, with all headers necessary for compilation. If set to False, headers are stripped off and the output file can be, without modifications, included into other Latex documents.
ScreenOutput	**False**, True	For debugging purposes, if set to True the Latex output is printed also to the screen.

Table C.5: Options of `SMEFTToLatex` routine, with default values marked in boldface.

Option name	Allowed values	Description
Output	**"output/UFO"**	default UFO output sub-directory, can be modified to other user-defined location.
CorrectIO	False, **True**	By default only "NP" interaction order parameter is left in vertices containing WCs of higher order operators. By setting this option to "False", preserves all IOs generated by native `FeynRules` UFO interface
AddDecays	**False**, True	UFO format can contain expressions for 2-body decays, switched off by default.

Table C.6: Options of `SMEFTToUFO` routine, with default values marked in boldface.

`LeptonGaugeVertices`	`QuarkGaugeVertices`
`LeptonHiggsGaugeVertices`	`QuarkHiggsGaugeVertices`
`QuarkGluonVertices`	
`GaugeSelfVertices`	`GaugeHiggsVertices`
`GluonSelfVertices`	`GluonHiggsVertices`
`GhostVertices`	
`FourLeptonVertices`	`FourQuarkVertices`
`TwoQuarkTwoLeptonVertices`	
`DeltaLTwoVertices`	`BLViolatingVertices`

Table C.7: Names of variables defined in the file `output/smeft_feynman_rules.m` containing expressions for Feynman rules. Parts of mass basis Lagrangian are stored in equivalent set of variables, with "`Vertices`" replaced by "`Lagrangian`" in part of their names (i.e. `LeptonGaugeVertices` → `LeptonGaugeLagrangian`, *etc.*).

D Adding fermionic dimension-8 operators to SmeftFR v3

Dimension-8 bosonic operators listed above do not exhaust all possible SMEFT operators that one may want to take into account. It is therefore important to know how to include in SmeftFR v3 operators containing fermionic fields. As the procedure is currently still rather complex, we decided not to make it a standard feature of the published code, but rather to provide detailed instructions for a chosen example of a fermionic operator.

The instructions below refer to specific line numbers in SmeftFR v3.02. The corresponding locations should be easily identifiable, even if they are changed, in newer versions. We're working in the basis of [76], but operators in any basis (bosonic and fermionic) can be added in this or a similar way. Below we list the steps to follow in order to add exemplary two-fermion dimension-8 operators.

D.1 Adding first operator

Operator that we are going to add reads (Table 7 in [76]):

$$Q^{(4)}_{e^2BH^2D} = (\bar{e}_p \gamma^\nu e_r) \left(H^\dagger \overleftrightarrow{D}^\mu H \right) \widetilde{B}_{\mu\nu} \tag{D.1}$$

As mentioned, we assume that the starting version of the code is identical to the one available on the SmeftFR webpage as v3.02. The following modifications need to be done:

1. Go to /lagrangian directory and create new file 29_TwoFermionDim8.fr containing the definition of the operator:

```
LQe2Bphi2Dn4 := Module[ {sp1,sp2,ii,jj,ff1,ff2,mu,nu,al,be,aux},

aux = (Phi8bar[jj] DC[Phi8[jj],mu] - DC[Phi8bar[jj],mu] Phi8[jj])
lRbar[sp1,ff1].lR[sp2,ff2] Ga[nu,sp1,sp2] Eps[mu,nu,al,be]/2 HC[FS[B,al,be]];

aux = ExpandIndices[ ToExpression[SMEFT$WB <> "e2Bphi2Dn4"][ff1,ff2]aux,
FlavorExpand->{SU2W,SU2D} ];

aux /.SMEFTGaugeRules];
```

2. Open file /code/smeft_variables.m and make the following changes:
   (a) Line 85: change SMEFT$Dim8Operators by adding "e2Bphi2Dn4".
   (b) Line 126: add TwoFermionOperators8 = {"e2Bphi2Dn4"};.
   (c) Line 163: change Tensor2WC by adding {"e2Bphi2Dn4", VLR,VLR,True,False}.
   (d) Line 234: change Tensor2Class by adding "e2Bphi2Dn4" -> 2.
   (e) Line 299: change Tensor2Ind by adding
   "e2Bphi2Dn4" -> {{1, 1, True}, {1, 2, False}, {1, 3, False},
   {2, 2, True}, {2, 3, False}, {3, 3, True}}.
3. Open file /code/smeft_io.m and:

(a) Line 204: change `SMEFTLoadLagrangian` function by adding
`Get[FileNameJoin[{SMEFT$Path,"lagrangian","29_TwoFermionDim8.fr"}]];`.

4. Open file `/code/smeft_functions.m` and:

   (a) Line 125: change `GenerateOperatorLists` function by adding
   `SMEFT$Dim8FermionOperators = ToExpression[1 <> #]`
   `& /@ Intersection[Join[ TwoFermionOperators8 ], SMEFT$OperatorList ];`.

   (b) Line 131: change `SMEFT$Dim8NullList` in `GenerateOperatorLists` function in the following way
   `SMEFT$Dim8NullList = Join[ (# -> 0 & /@ SMEFT$Dim8BosonOperators), (#[__] -> 0 & /@ SMEFT$Dim8FermionOperators) ];`.

5. Open file `/code/smeft_initialization.m` and:

   (a) Line 268: change `SMEFTLoadModel` function by adding
   `SMEFT$LGferm6 = 0;`.

   (b) Line 285: change `SMEFTLoadModel` function by adding
   `If[ SMEFT$ExpansionOrder > 1,`
   `If[ MemberQ[ SMEFT$OperatorList, # ], SMEFT$LGferm6 = SMEFT$LGferm6 + Lam^2 ToExpression["LQ"<>#] ] & /@ TwoFermionOperators8;];`.

6. Open file `/code/smeft_gaugeint.m` and:

   (a) Line 19: modify `tmp` variable by adding `SMEFT$LGferm6`
   `tmp = SMEFT$LGferm + SMEFT$LGferm6/.G[___]->0 /.uq[___]->0/.dq[___]->0;`.

7. Go to `smeft_fr_init.m` and `SmeftFR-init.nb` and add `"e2Bphi2Dn4"` to the `OpList8` which lists all available dimension-8 operators.

D.2 Adding subsequent operators

Once the first operator has been added, including the next one is much simpler and requires changes in only two files in `/code` directory. We will present this on the another example (again, Table 7 in [76]):

$$Q^{(4)}_{e^2WH^2D} = (\bar{e}_p\gamma^\nu e_r)\left(H^\dagger \overleftrightarrow{D}^{I\mu} H\right)\widetilde{W}^I_{\mu\nu} \tag{D.2}$$

1. Open file `/lagrangian/29_TwoFermionDim8.fr` and add next operator.

```
LQe2Wphi2Dn4 := Module[{sp1,sp2,m,ii,jj,ff1,ff2,mu,nu,al,be,aux},

aux = 2 Ta[m,ii,jj] (Phi8bar[ii] DC[Phi8[jj],mu] - DC[Phi8bar[ii],mu] Phi8[jj])
lRbar[sp1,ff1].lR[sp2,ff2] Ga[nu,sp1,sp2] Eps[mu,nu,al,be]/2 HC[FS[Wi,al,be,m]];

aux = ExpandIndices[ ToExpression[SMEFT$WB <> "e2Wphi2Dn4"][ff1,ff2] aux,
FlavorExpand->{SU2W,SU2D} ];

aux /.  SMEFTGaugeRules ];
```

2. Open file `/code/smeft_variables.m` and follow the instructions below:

   (a) Line 85: change `SMEFT$Dim8Operators` by adding `"e2Wphi2Dn4"`.

   (b) Line 126: change `TwoFermionOperators8` by adding `"e2Wphi2Dn4"`.

   (c) Line 164: change `Tensor2WC` by adding `{"e2Wphi2Dn4", VLR,VLR,True,False}`.

   (d) Line 235: change `Tensor2Class` by adding `"e2Wphi2Dn4" -> 2`.

   (e) Line 302: change `Tensor2Ind` by adding
   `"e2Wphi2Dn4" -> {{1, 1, True}, {1, 2, False}, {1, 3, False}, {2, 2, True}, {2, 3, False}, {3, 3, True}}`.

3. Go to `smeft_fr_init.m` and `SmeftFR-init.nb` and add `"e2Wphi2Dn4"` to the `OpList8` which lists all available dimension-8 operators.

E SmeftFR v3 numerical validation

All comparisons were generated using SmeftFR v3.02.

E.1 Dimension-6 $\mathcal{O}(1/\Lambda^2)$ validation

Cross-sections comparison

For the cross-sections comparison, all particle widths, fermion masses, and Yukawa couplings, except for the top quark, were assumed to be zero. Each cross-section was calculated assuming that all but one Wilson coefficient was set to zero and the non-vanishing one (displayed in the left column of Table E.1) had the value of $\left|\frac{C_i}{\Lambda^2}\right| = 10^{-6}$ GeV^{-2}, while its sign was always chosen to increase $\mathcal{O}(1/\Lambda^2)$ cross- section with respect to SM. The results are summarized in the second and third columns of Table E.1. As one can note, differences between both codes at the $\mathcal{O}(1/\Lambda^2)$ level never exceed 1%.

Matrix elements comparison

We have used a similar procedure for the matrix element comparison. Once again each matrix elements $\mathcal{A}$ were calculated assuming that all but one Wilson coefficient was set to zero, and the non-vanishing one had the value of $\left|\frac{C_i}{\Lambda^2}\right| = 10^{-6}$ GeV^{-2}. We obtained almost identical results from SMEFTsim and SmeftFR for all of the studied processes, see Tables E.2 and E.3, with the relative differences defined as:

$$\Delta = \left|\mathcal{A}_{\texttt{SmeftFR}} - \mathcal{A}_{\texttt{SMEFTsim}}\right| / \mathcal{A}_{\texttt{SMEFTsim}}, \tag{E.1}$$

never exceeding 0.1%.

Differences in notation between SmeftFR and SMEFTsim

SmeftFR and SMEFTsim use the same Warsaw basis [13]. However, there are some differences after the rotation to the mass basis for four-fermion couplings. SmeftFR notation is given in detail in [74] while SMEFTsim uses a notation equivalent to [252]. The relations between four-fermion WCs in SMEFTsim ($\tilde{C}$) and SmeftFR (C) bases relevant for comparisons between the codes are given by (V is the CKM matrix):

$$\begin{aligned}
\tilde{C}^{(1)ijkl}_{quqd} &= V^{im} C^{(1)mjkl}_{quqd} \\
\tilde{C}^{(8)ijkl}_{quqd} &= V^{im} C^{(8)mjkl}_{quqd} \\
\tilde{C}^{(1)ijkl}_{lequ} &= V^{km} C^{(1)ijml}_{lequ} \\
\tilde{C}^{(3)ijkl}_{lequ} &= V^{km} C^{(3)ijml}_{lequ}
\end{aligned} \tag{E.2}$$

Finally, one has to take into account the symmetrization properties of four-fermion operators. These are automatically taken into account by SmeftFR if numerical values of WCs are initialized with WCXFInput command and, when running SmeftFR v3 interfaces, by the SMEFTInitializeMB routine. If the user decides to set their values "by hand" in the MadGraph5 run, then they has to keep track of these dependencies on their own.

	SMEFT@NLO $\mathcal{O}(1/\Lambda^2)$	SmeftFR $\mathcal{O}(1/\Lambda^2)$	SmeftFR $\mathcal{O}(1/\Lambda^4)$
$\mu^+\mu^- \to t\bar{t}$			
SM	0.16606 ± 0.00026	0.16608 ± 0.00024	-
C_{uW}^{33}	0.41862 ± 0.00048	0.41816 ± 0.00047	-
$C_{\varphi u}^{33}$	0.16725 ± 0.00027	0.16730 ± 0.00025	-
C_{lu}^{2233}	6.488 ± 0.016	6.491 ± 0.014	-
$C_{\varphi WB}$	0.21923 ± 0.00032	0.21940 ± 0.00030	0.22419 ± 0.00030
$C_{\varphi D}$	0.18759 ± 0.00030	0.18759 ± 0.00027	0.18829 ± 0.00027
$\gamma\gamma \to t\bar{t}$			
SM	0.0037498 ± 0.0000050	0.0037498 ± 0.0000050	-
C_{uW}^{33}	0.008229 ± 0.000012	0.008235 ± 0.000012	-
$C_{\varphi WB}$	0.0053056 ± 0.0000086	0.0053056 ± 0.0000086	0.0055809 ± 0.0000090
$C_{\varphi D}$	0.0045856 ± 0.0000061	0.0045895 ± 0.0000064	0.0045882 ± 0.0000069
$c\bar{c} \to t\bar{t}$			
SM	0.9553 ± 0.0017	0.9511 ± 0.0023	-
C_{uG}^{33}	1.1867 ± 0.0023	1.1854 ± 0.0021	-
C_{uW}^{33}	0.9641 ± 0.0018	0.9599 ± 0.0024	-
$C_{\varphi u}^{33}$	0.9555 ± 0.0017	0.9513 ± 0.0023	-
$C_{\varphi q3}^{33}$	0.9558 ± 0.0017	0.9515 ± 0.0023	-
C_{qu1}^{2233}	1.0111 ± 0.0018	1.0059 ± 0.0015	-
$C_{\varphi WB}$	0.9568 ± 0.0018	0.9520 ± 0.0018	0.9522 ± 0.0018
$C_{\varphi D}$	0.9558 ± 0.0017	0.9511 ± 0.0018	0.9511 ± 0.0018
$pp \to t\bar{t}$			
SM	510.35 ± 0.72	510.46 ± 0.68	-
C_{uG}^{33}	664.33 ± 1.16	666.34 ± 0.90	671.08 ± 0.97
C_{uW}^{33}	510.63 ± 0.70	510.70 ± 0.80	-
$C_{\varphi u}^{33}$	510.37 ± 0.72	510.47 ± 0.68	-
$C_{\varphi q3}^{33}$	510.39 ± 0.72	510.65 ± 0.80	-
$\sum_{i=1,2} C_{qu1}^{ii33}$	516.31 ± 0.58	516.14 ± 0.64	-
$C_{\varphi WB}$	510.49 ± 0.68	510.52 ± 0.71	508.94 ± 0.79
$C_{\varphi D}$	510.38 ± 0.72	510.47 ± 0.68	508.89 ± 0.79

Table E.1: Cross-sections (in pb) obtained using MadGraph5 with UFO models provided by SMEFTatNLO at the $\mathcal{O}(1/\Lambda^2)$ order of the EFT expansion and SmeftFR at the $\mathcal{O}(1/\Lambda^2)$ and $\mathcal{O}(1/\Lambda^4)$ orders of the EFT expansion for a chosen set of processes and SMEFT operators. An empty cell indicates that no $\mathcal{O}(1/\Lambda^4)$ terms appear in the amplitude.

	SmeftFR	SMEFTsim	Δ
g g > g g			
SM	54.806	54.791	0.03%
C_G	149.35	149.35	0.00%
$C_{\tilde{G}}$	149.35	149.33	0.01%
z z > w+ w-			
SM	3.2688	3.2688	0.00%
C_W	20.602	20.602	0.00%
$C_{\tilde{W}}$	20.661	20.661	0.00%
$C_{\varphi WB}$	3.7462	3.7462	0.00%
$C_{\varphi\Box}$	3.4727	3.4727	0.00%
$C_{\varphi D}$	3.5563	3.5563	0.00%
a a > w+ w-			
SM	0.5168	0.5168	0.00%
C_W	3.4688	3.4726	0.11%
$C_{\tilde{W}}$	3.4793	3.4802	0.03%
$C_{\varphi WB}$	0.7838	0.7838	0.00%
w+ w- > w+ w-			
SM	0.4593	0.4593	0.00%
C_W	3.6653	3.6653	0.00%
$C_{\tilde{W}}$	3.6774	3.6774	0.00%
$C_{\varphi\Box}$	0.5375	0.5375	0.00%
$C_{\varphi D}$	0.4818	0.4818	0.00%
h h > h h			
SM	0.2024	0.2024	0.00%
C_φ	1.1980	1.1980	0.00%
$C_{\varphi\Box}$	0.9399	0.9399	0.00%
$C_{\varphi D}$	0.1024	0.1024	0.00%
w+ w- > h h			
SM	0.0218	0.0218	0.00%
$C_{\varphi W}$	0.4662	0.4662	0.00%
$C_{\varphi\Box}$	0.1221	0.1221	0.00%
$C_{\varphi D}$	0.0663	0.0663	0.00%
z z > h h			
SM	0.0416	0.0416	0.00%
$C_{\varphi W}$	0.3088	0.3088	0.00%
$C_{\varphi\tilde{W}}$	0.2968	0.2968	0.00%
$C_{\varphi B}$	0.0658	0.0658	0.00%
$C_{\varphi\tilde{B}}$	0.0626	0.0626	0.00%
$C_{\varphi WB}$	0.1210	0.1210	0.00%
$C_{\varphi\tilde{W}B}$	0.1148	0.1148	0.00%
g g > h h			
SM	0.0000	0.0000	0.00%
$C_{\varphi G}$	0.1373	0.1373	0.00%
$C_{\varphi\tilde{G}}$	0.1373	0.1373	0.00%
e+ e- > z h			
SM	0.0021	0.0021	0.00%
C_{eW}^{11}	0.3336	0.3336	0.00%
C_{eB}^{11}	0.0972	0.0972	0.00%
$C_{\varphi l1}^{11}$	0.2559	0.2559	0.00%
$C_{\varphi l3}^{11}$	0.2536	0.2536	0.00%
$C_{\varphi e}^{11}$	0.1956	0.1956	0.00%

	SmeftFR	SMEFTsim	Δ
e+ e- > h h			
SM	0.0000	0.0000	0.00%
$C_{e\varphi}^{11}$	0.0706	0.0706	0.00%
e+ e- > w+ w-			
SM	0.0169	0.0169	0.00%
C_{eW}^{11}	1.6746	1.6745	0.00%
$C_{\varphi l1}^{11}$	0.1830	0.1830	0.00%
$C_{\varphi l3}^{11}$	0.3096	0.3096	0.00%
$C_{\varphi e}^{11}$	0.2175	0.2175	0.00%
ū d > w- z			
SM	0.0034	0.0034	0.00%
C_{uW}^{11}	0.2495	0.2495	0.00%
C_{dW}^{11}	0.2490	0.2490	0.00%
$C_{\varphi q3}^{11}$	0.1955	0.1955	0.00%
$C_{\varphi ud}^{11}$	0.0418	0.0418	0.00%
ū u > h h			
SM	0.0000	0.0000	0.00%
$C_{u\varphi}^{11}$	0.0235	0.0235	0.00%
d̄ d > h h			
SM	0.0000	0.0000	0.00%
$C_{d\varphi}^{11}$	0.0235	0.0235	0.00%
ū u > z h			
SM	0.0008	0.0008	0.00%
C_{uW}^{11}	0.1113	0.1113	0.00%
C_{uB}^{11}	0.0325	0.0325	0.00%
$C_{\varphi q1}^{11}$	0.0601	0.0601	0.00%
$C_{\varphi q3}^{11}$	0.0884	0.0884	0.00%
$C_{\varphi u}^{11}$	0.0802	0.0802	0.00%
d̄ d > z h			
SM	0.0010	0.0010	0.00%
C_{dW}^{11}	0.1115	0.1115	0.00%
C_{dB}^{11}	0.0327	0.0327	0.00%
$C_{\varphi q1}^{11}$	0.0916	0.0916	0.00%
$C_{\varphi q3}^{11}$	0.0916	0.0916	0.00%
$C_{\varphi d}^{11}$	0.0715	0.0715	0.00%
ū d > w- h			
SM	0.0016	0.0016	0.00%
C_{uW}^{11}	0.1424	0.1424	0.00%
C_{dW}^{11}	0.1424	0.1424	0.00%
$C_{\varphi q3}^{11}$	0.0377	0.0377	0.00%
$C_{\varphi ud}^{11}$	0.1767	0.1767	0.00%
g g > ū u			
SM	0.5291	0.5291	0.00%
C_{uG}^{11}	0.6130	0.6130	0.00%
g g > d̄ d			
SM	0.5291	0.5291	0.00%
C_{dG}^{11}	0.6130	0.6130	0.00%

Table E.2: Matrix elements and their relative differences for a given processes obtained using `MadGraph5` with UFO models provided by `SmeftFR` and `SMEFTsim` at the $\mathcal{O}(1/\Lambda^2)$ order of the EFT expansion. Bosonic and 2-fermion dimension-6 WCs included.

	SmeftFR	SMEFTsim	Δ
e+ e- > e+ e-			
SM	0.0196	0.0196	0.00%
C_{ll}^{1111}	1.4222	1.4222	0.00%
C_{le}^{1111}	2.7660	2.7660	0.00%
C_{ee}^{1111}	1.4265	1.4265	0.00%
e+ e- > mu+ mu-			
SM	0.0067	0.0067	0.00%
C_{ll}^{1122}	0.4173	0.4173	0.00%
C_{le}^{1122}	0.5555	0.5555	0.00%
C_{ee}^{1122}	1.5393	1.5393	0.00%
c c̄ > t t̄			
SM	0.6131	0.6131	0.00%
C_{qq1}^{2233}	1.0491	1.0491	0.00%
C_{qq3}^{2233}	1.0491	1.0491	0.00%
C_{qu1}^{2233}	1.1046	1.1046	0.00%
C_{qu8}^{2233}	1.0479	1.0479	0.00%
C_{uu}^{2233}	1.0272	1.0272	0.00%
s s̄ > b b̄			
SM	0.5638	0.5638	0.00%
C_{qq1}^{2233}	0.9648	0.9648	0.00%
C_{qq3}^{2233}	0.9648	0.9648	0.00%
C_{qu1}^{2233}	1.0464	1.0464	0.00%
C_{qu8}^{2233}	0.9940	0.9940	0.00%
C_{dd}^{2233}	0.9298	0.9298	0.00%
b b̄ > t t̄			
SM	0.3540	0.3540	0.00%
C_{qq1}^{3333}	0.6352	0.6352	0.00%
C_{qq3}^{3333}	2.1164	2.1164	0.00%
C_{qu1}^{3333}	0.8183	0.8183	0.00%
C_{qu8}^{3333}	0.7886	0.7886	0.00%
C_{qd1}^{3333}	0.5939	0.5939	0.00%
C_{qd8}^{3333}	0.4697	0.4697	0.00%
C_{ud1}^{3333}	0.4461	0.4461	0.00%
C_{ud8}^{3333}	0.4596	0.4596	0.00%
C_{quqd1}^{3333}	1.2776	1.2776	0.00%
C_{quqd8}^{3333}	0.4656	0.4656	0.00%

	SmeftFR	SMEFTsim	Δ
mu+ mu- > t t̄			
SM	0.0305	0.0305	0.00%
C_{lq1}^{2233}	1.1088	1.1088	0.00%
C_{lq3}^{2233}	1.7862	1.7862	0.00%
C_{eu}^{2233}	1.2129	1.2129	0.00%
C_{lu}^{2233}	1.2129	1.2129	0.00%
C_{qe}^{2233}	0.0305	0.0305	0.00%
C_{lequ1}^{2233}	1.4427	1.4427	0.00%
C_{lequ1}^{2233}	4.8271	4.8271	0.00%
e+ e- > b b̄			
SM	0.0164	0.0164	0.00%
C_{lq1}^{1133}	1.7684	1.7684	0.00%
C_{lq3}^{1133}	1.7684	1.7684	0.00%
C_{ed}^{1133}	1.6042	1.6042	0.00%
C_{ld}^{1133}	0.2982	0.2982	0.00%
C_{qe}^{1133}	0.0164	0.0164	0.00%
C_{ledq}^{1133}	1.5163	1.5163	0.00%
e+ mu- > s b̄			
SM	0.0000	0.0000	0.00%
C_{lq1}^{1223}	1.4681	1.4681	0.00%
C_{lq3}^{1223}	1.4681	1.4681	0.00%
C_{ed}^{1223}	1.4681	1.4681	0.00%
C_{ld}^{1223}	0.2708	0.2708	0.00%
C_{ledq}^{1223}	0.7500	0.7500	0.00%
e+ e- > d d̄			
SM	0.0164	0.0164	0.00%
C_{qe}^{1111}	0.2759	0.2759	0.00%

Table E.3: Matrix elements and their relative differences for a given processes obtained using MadGraph5 with UFO models provided by SmeftFR and SMEFTsim at the $\mathcal{O}(1/\Lambda^2)$ order of the EFT expansion. 4-fermion dimension-6 WCs included.

E.2 Dimension-8 $\mathcal{O}(1/\Lambda^4)$ validation

We have utilized a similar procedure for matrix elements comparison for dimension-8 operators, at the $\mathcal{O}(1/\Lambda^4)$ order of the EFT expansion. Each matrix element was calculated assuming that all but one Wilson coefficient was set to zero and the non-vanishing one had the value of $\left|\frac{C_i}{\Lambda^2}\right| = 10^{-11}$ GeV^{-4} (`SmeftFR` v3 uses the basis of [76] while `AnomalousGaugeCoupling` uses the basis of [109] for Dimension-8 operators and the translations between the operators in both bases can be found in the first and second rows of Table E.5). Despite the difference in input scheme between the codes, which had to be taken into account by tuning the input parameters of `AnomalousGaugeCoupling` (`AGC`) accordingly, we obtained almost identical results from `AGC` and `SmeftFR` v3 codes for all of the studied processes.

Basis of [76]	Basis of [109]	`SmeftFR`	`AGC`	Δ
`w+ w- > h h`				
SM		0.0218	0.0218	0.00%
$C^{(2)}_{\varphi D^4}$	$C^{(0)}_S$	0.2191	0.2191	0.00%
$C^{(3)}_{\varphi D^4}$	$C^{(1)}_S$	1.5868	1.5868	0.00%
$C^{(1)}_{\varphi D^4}$	$C^{(2)}_S$	0.2191	0.2191	0.00%
$\frac{1}{2}C^{(2)}_{W^2\varphi^2 D^2}$	$C^{(0)}_M$	2.5622	2.5622	0.00%
$-\frac{1}{2}C^{(1)}_{W^2\varphi^2 D^2}$	$C^{(1)}_M$	0.2307	0.2307	0.00%
$\frac{1}{4}\left(C^{(1)}_{W^2\varphi^2 D^2} - C^{(4)}_{W^2\varphi^2 D^2}\right)$	$C^{(7)}_M$	0.0576	0.0576	0.00%
`z z > h h`				
SM		0.0416	0.0416	0.00%
$C^{(2)}_{\varphi D^4}$	$C^{(0)}_S$	0.0916	0.0916	0.00%
$C^{(3)}_{\varphi D^4}$	$C^{(1)}_S$	1.7156	1.7156	0.00%
$C^{(1)}_{\varphi D^4}$	$C^{(2)}_S$	1.7156	1.7156	0.00%
$\frac{1}{2}C^{(2)}_{W^2\varphi^2 D^2}$	$C^{(0)}_M$	1.5589	1.5589	0.00%
$-\frac{1}{2}C^{(1)}_{W^2\varphi^2 D^2}$	$C^{(1)}_M$	0.1773	0.1773	0.00%
$C^{(1)}_{B^2\varphi^2 D^2}$	$C^{(2)}_M$	0.5406	0.5406	0.00%
$-C^{(4)}_{B^2\varphi^2 D^2}$	$C^{(3)}_M$	0.0920	0.0920	0.00%
$\frac{1}{2}C^{(1)}_{WB\varphi^2 D^2}$	$C^{(4)}_M$	0.4761	0.4761	0.00%
$\frac{1}{2}C^{(4)}_{WB\varphi^2 D^2}$	$C^{(5)}_M$	0.1456	0.1456	0.00%
$\frac{1}{4}\left(C^{(1)}_{W^2\varphi^2 D^2} - C^{(4)}_{W^2\varphi^2 D^2}\right)$	$C^{(7)}_M$	0.0580	0.0580	0.00%

Table E.4: Matrix elements and their relative differences for a given processes obtained using `MadGraph5` with UFO models provided by `SmeftFR` and `AGC` at the $\mathcal{O}(1/\Lambda^4)$ order of the EFT expansion.

Basis of [76]	Basis of [109]	SmeftFR	AGC	Δ
w+ w+ > w+ w+				
SM		2.9395	2.9395	0.00%
$C^{(2)}_{\varphi D^4}$	$C^{(0)}_S$	6.5868	6.5868	0.00%
$C^{(3)}_{\varphi D^4}$	$C^{(1)}_S$	2.9307	2.9307	0.00%
$C^{(1)}_{\varphi D^4}$	$C^{(2)}_S$	2.9307	2.9307	0.00%
$\frac{1}{2}C^{(2)}_{W^2\varphi^2D^2}$	$C^{(0)}_M$	4.2146	4.2146	0.00%
$-\frac{1}{2}C^{(1)}_{W^2\varphi^2D^2}$	$C^{(1)}_M$	2.6295	2.6295	0.00%
$\frac{1}{4}\left(C^{(1)}_{W^2\varphi^2D^2} - C^{(4)}_{W^2\varphi^2D^2}\right)$	$C^{(7)}_M$	3.9113	3.9113	0.00%
$\frac{1}{4}C^{(1)}_{W^4}$	$C^{(0)}_T$	23.541	23.541	0.00%
$\frac{1}{4}C^{(3)}_{W^4}$	$C^{(1)}_T$	98.636	98.636	0.00%
$\frac{1}{16}\left(C^{(1)}_{W^4} + C^{(3)}_{W^4} + C^{(4)}_{W^4}\right)$	$C^{(2)}_T$	6.2602	6.2602	0.00%
z z > z z				
SM		0.0820	0.0820	0.00%
$C^{(2)}_{\varphi D^4}$	$C^{(0)}_S$	2.6660	2.6660	0.00%
$C^{(3)}_{\varphi D^4}$	$C^{(1)}_S$	2.6660	2.6660	0.00%
$C^{(1)}_{\varphi D^4}$	$C^{(2)}_S$	2.6660	2.6660	0.00%
$\frac{1}{2}C^{(2)}_{W^2\varphi^2D^2}$	$C^{(0)}_M$	3.9388	3.9388	0.00%
$-\frac{1}{2}C^{(1)}_{W^2\varphi^2D^2}$	$C^{(1)}_M$	0.6317	0.6317	0.00%
$C^{(1)}_{B^2\varphi^2D^2}$	$C^{(2)}_M$	1.3635	1.3635	0.00%
$-C^{(4)}_{B^2\varphi^2D^2}$	$C^{(3)}_M$	0.2214	0.2214	0.00%
$\frac{1}{2}C^{(1)}_{WB\varphi^2D^2}$	$C^{(4)}_M$	1.1997	1.1997	0.00%
$-\frac{1}{2}C^{(4)}_{WB\varphi^2D^2}$	$C^{(5)}_M$	1.0921	1.0921	0.00%
$\frac{1}{4}\left(C^{(1)}_{W^2\varphi^2D^2} - C^{(4)}_{W^2\varphi^2D^2}\right)$	$C^{(7)}_M$	0.3474	0.3474	0.00%
$\frac{1}{4}C^{(1)}_{W^4}$	$C^{(0)}_T$	57.045	57.045	0.00%
$\frac{1}{4}C^{(3)}_{W^4}$	$C^{(1)}_T$	57.045	57.045	0.00%
$\frac{1}{16}\left(C^{(1)}_{W^4} + C^{(3)}_{W^4} + C^{(4)}_{W^4}\right)$	$C^{(2)}_T$	13.2092	13.2092	0.00%
$\frac{1}{2}C^{(1)}_{W^2B^2}$	$C^{(5)}_T$	18.870	18.870	0.00%
$\frac{1}{2}C^{(3)}_{W^2B^2}$	$C^{(6)}_T$	18.870	18.870	0.00%
$\frac{1}{16}\left(C^{(1)}_{W^2B^2} + C^{(3)}_{W^2B^2} + C^{(4)}_{W^2B^2}\right)$	$C^{(7)}_T$	4.4206	4.4206	0.00%
$C^{(1)}_{B^4}$	$C^{(8)}_T$	6.2832	6.2832	0.00%
$\frac{1}{4}\left(2C^{(1)}_{B^4} + C^{(2)}_{B^4}\right)$	$C^{(9)}_T$	1.5190	1.5190	0.00%

Table E.5: Matrix elements and their relative differences for a given processes obtained using MadGraph5 with UFO models provided by SmeftFR and AGC at the $\mathcal{O}(1/\Lambda^4)$ order of the EFT expansion.

Appendix for Chapter 3

In the following two sections, we present the helicity amplitudes for $WW \to HH$ and $ZZ \to HH$ processes, including SMEFT contributions from the dimension-6 and dimension-8 operators collected in Table 3.2. For each amplitude, we display only the leading order terms in the high energy limit ($M_V^2/s \to 0$), neglecting interference terms between different Wilson coefficients. We start with the $WW \to HH$ process in section F and present the Standard Model contribution in Eq. (F.1), the dimension-6 and dimension-6^2 contributions in Eq. (F.2), and the dimension-8 contributions in Eq. (F.3). Similarly, for the $ZZ \to HH$ process, we present the SM contribution in Eq. (G.1), the dimension-6 and dimension-6^2 contributions in Eq. (G.2), and the dimension-8 and contributions in Eq. (G.3).

F $W^+W^- \to HH$ helicity amplitude

F.1 SM

$$\begin{aligned}
\mathcal{M}_{00}^{WW,\,SM} &= \sqrt{2} G_F M_H^2 \left[1 + 2\left(1 - \frac{4}{\sin^2\theta}\right)\frac{M_W^2}{M_H^2}\right], \\
\mathcal{M}_{\pm\pm}^{WW,\,SM} &= \mathcal{O}\left(\frac{1}{s}\right), \\
\mathcal{M}_{\pm\mp}^{WW,\,SM} &= 2\sqrt{2} G_F M_W^2, \\
\mathcal{M}_{0\pm}^{WW,\,SM} &= \mathcal{M}_{\pm 0}^{WW,\,SM} = \mathcal{O}\left(\frac{1}{\sqrt{s}}\right).
\end{aligned} \tag{F.1}$$

F.2 Dimension-6 SMEFT

$$\begin{aligned}
\mathcal{M}_{00}^{WW,\,D6} =& -3\sqrt{2} C_\varphi \left(\frac{1}{G_F \Lambda^2}\right) - 20 C_{\varphi W}\left(\frac{M_W^2}{\Lambda^2}\right) + \frac{1}{2}(4C_{\varphi\Box} - C_{\varphi D})\left(\frac{s}{\Lambda^2}\right) && \textbf{dim-6} \\
& - 28\sqrt{2} C_{\varphi W}^2 \left(\frac{M_W^2}{\Lambda^2}\right)\left(\frac{1}{G_F\Lambda^2}\right) + \sqrt{2}(4C_{\varphi\Box}^2 + \frac{1}{4}C_{\varphi D}^2)\left(\frac{1}{G_F\Lambda^2}\right)\left(\frac{s}{\Lambda^2}\right), && \textbf{(dim-6)}^2 \\
\mathcal{M}_{\pm\pm}^{WW,\,D6} =& -(4C_{\varphi\Box} - C_{\varphi D})\left(\frac{M_W^2}{\Lambda^2}\right) + 2C_{\varphi W}\left(\frac{s}{\Lambda^2}\right) \\
& - 2\sqrt{2}(4C_{\varphi\Box}^2 + \frac{1}{4}C_{\varphi D}^2)\left(\frac{M_W^2}{\Lambda^2}\right)\left(\frac{1}{G_F\Lambda^2}\right) + 6\sqrt{2} C_{\varphi W}^2 \left(\frac{1}{G_F\Lambda^2}\right)\left(\frac{s}{\Lambda^2}\right),
\end{aligned} \tag{F.2}$$

$$
\begin{aligned}
\mathcal{M}_{\pm\mp}^{WW,\,D6} =&(4C_{\varphi\Box}-C_{\varphi D})\left(\frac{M_W^2}{\Lambda^2}\right)\\
&+\sqrt{2}(4C_{\varphi\Box}^2+\frac{1}{4}C_{\varphi D}^2)\left(\frac{M_W^2}{\Lambda^2}\right)\left(\frac{1}{G_F\Lambda^2}\right)+2\sqrt{2}C_{\varphi W}^2\left(\frac{1}{G_F\Lambda^2}\right)\left(\frac{s}{\Lambda^2}\right),\\
\mathcal{M}_{0\pm}^{WW,\,D6} =&-4\sqrt{2}\cot\theta C_{\varphi W}\left(\frac{\sqrt{s}M_W}{\Lambda^2}\right)-8C_{\varphi W}^2\cot\theta\left(\frac{1}{G_F\Lambda^2}\right)\left(\frac{\sqrt{s}M_W}{\Lambda^2}\right).
\end{aligned}
$$

F.3 Dimension-8 SMEFT

$$
\begin{aligned}
\mathcal{M}_{00}^{WW,\,D8} =&-6C_{\varphi^8}\left(\frac{1}{G_F^2\Lambda^4}\right)+\frac{\sqrt{2}}{4}\left(8C_{\varphi^6\Box}-C_{\varphi^6D^2}\right)\frac{s}{\Lambda^2}\frac{1}{G_F\Lambda^2}-\frac{1}{8}C_{\varphi^4D^4}^{(1)}\left(\cos^2\theta+1\right)\left(\frac{s^2}{\Lambda^4}\right)\\
&-14\sqrt{2}C_{W^2\varphi^4}^{(1)}\left(\frac{M_W^2}{\Lambda^2}\right)\left(\frac{1}{G_F\Lambda^2}\right)+\frac{1}{2}C_{W^2\varphi^2D^2}^{(1)}(\sin^2\theta+1)\left(\frac{M_W^2}{\Lambda^2}\right)\left(\frac{s}{\Lambda^2}\right)\\
&+\frac{5i}{2^{5/4}}C_{W\varphi^4D^2}^{(1)}\left(\frac{M_W}{\sqrt{G_F}\Lambda^2}\right)\left(\frac{s}{\Lambda^2}\right),\\
\mathcal{M}_{\pm\pm}^{WW,\,D8} =&-\frac{\sqrt{2}}{2}\left(8C_{\varphi^6\Box}-C_{\varphi^6D^2}\right)\frac{M_W^2}{\Lambda^2}\frac{1}{G_F\Lambda^2}+\frac{1}{4}C_{\varphi^4D^4}^{(1)}\sin^2\theta\left(\frac{M_W^2}{\Lambda^2}\right)\left(\frac{s}{\Lambda^2}\right)\\
&-\frac{1}{4}C_{W^2\varphi^2D^2}^{(1)}\left(\frac{s^2}{\Lambda^4}\right)+3\sqrt{2}C_{W^2\varphi^4}^{(1)}\left(\frac{1}{G_F\Lambda^2}\right)\left(\frac{s}{\Lambda^2}\right)-\frac{3i}{2^{5/4}}C_{W\varphi^4D^2}^{(1)}\left(\frac{M_W}{\sqrt{G_F}\Lambda^2}\right)\left(\frac{s}{\Lambda^2}\right),\\
\mathcal{M}_{\pm\mp}^{WW,\,D8} =&\frac{\sqrt{2}}{4}\left(8C_{\varphi^6\Box}-C_{\varphi^6D^2}\right)\frac{M_Z^2}{\Lambda^2}\frac{1}{G_F\Lambda^2}+\frac{1}{4}C_{\varphi^4D^4}^{(1)}\sin^2\theta\left(\frac{M_W^2}{\Lambda^2}\right)\left(\frac{s}{\Lambda^2}\right)\\
&-\frac{1}{8}\sin^2\theta C_{W^2\varphi^2D^2}^{(1)}\left(\frac{s^2}{\Lambda^4}\right)+2^{3/4}C_{W\varphi^4D^2}^{(1)}\left(\frac{M_W}{\sqrt{G_F}\Lambda^2}\right)\left(\frac{M_W^2}{\Lambda^2}\right),\\
\mathcal{M}_{0\pm}^{WW,\,D8} =&\frac{1}{8\sqrt{2}}C_{\varphi^4D^4}^{(1)}\sin2\theta\left(\frac{s^{3/2}M_W}{\Lambda^4}\right)\\
&-4C_{W^2\varphi^4}^{(1)}\cot\theta\left(\frac{s^{1/2}M_W}{\Lambda^2}\right)\left(\frac{1}{G_F\Lambda^2}\right)-\frac{1}{8\sqrt{2}}C_{W^2\varphi^2D^2}^{(1)}\sin2\theta\left(\frac{s^{3/2}M_W}{\Lambda^4}\right)\\
&+2^{1/4}iC_{W\varphi^4D^2}^{(1)}\cot\theta\left(\frac{M_W}{\sqrt{G_F}\Lambda^2}\right)\left(\frac{M_W\sqrt{s}}{\Lambda^2}\right).
\end{aligned}
\tag{F.3}
$$

G $ZZ\to HH$ helicity amplitude

G.1 SM

$$
\begin{aligned}
\mathcal{M}_{00}^{ZZ,\,SM} &= \sqrt{2}G_FM_H^2\left[1+2\left(1-\frac{4}{\sin^2\theta}\right)\frac{M_Z^2}{M_H^2}\right],\\
\mathcal{M}_{\pm\pm}^{ZZ,\,SM} &= \mathcal{O}\left(\frac{1}{s}\right),\\
\mathcal{M}_{\pm\mp}^{ZZ,\,SM} &= 2\sqrt{2}G_FM_Z^2,\\
\mathcal{M}_{0\pm}^{ZZ,\,SM} &= \mathcal{M}_{\pm0}^{ZZ,\,SM}=\mathcal{O}\left(\frac{1}{\sqrt{s}}\right).
\end{aligned}
\tag{G.1}
$$

G.2 Dimension-6 SMEFT

$$
\begin{aligned}
\mathcal{M}_{00}^{ZZ,\,D6} =& -3\sqrt{2}C_{\varphi}\left(\frac{1}{G_F\Lambda^2}\right)+(2C_{\varphi\Box}+C_{\varphi D})\left(\frac{s}{\Lambda^2}\right) && \textbf{dim-6}\\
&-20C_{\varphi W}\left(\frac{M_W^2}{\Lambda^2}\right)+20C_{\varphi B}\left(\frac{M_W^2-M_Z^2}{\Lambda^2}\right)-20C_{\varphi WB}\left(\frac{M_W\sqrt{M_Z^2-M_W^2}}{\Lambda^2}\right)\\
&+\sqrt{2}(4C_{\varphi\Box}^2-\frac{3}{4}C_{\varphi D}^2)\left(\frac{1}{G_F\Lambda^2}\right)\left(\frac{s}{\Lambda^2}\right) && \textbf{(dim-6)}^2\\
&+28\sqrt{2}C_{\varphi B}^2\left(\frac{M_W^2-M_Z^2}{\Lambda^2}\right)\left(\frac{1}{G_F\Lambda^2}\right)+12\sqrt{2}C_{\varphi WB}^2\left(1-\frac{5}{6}\frac{M_W^2}{\sqrt{2}M_Z^2}\right)\left(\frac{1}{G_F\Lambda^2}\right)\left(\frac{M_Z^2}{\Lambda^2}\right),\\
\mathcal{M}_{\pm\pm}^{ZZ,\,D6} =& -2(2C_{\varphi\Box}+C_{\varphi D})\left(\frac{M_Z^2}{\Lambda^2}\right)\\
&+2C_{\varphi W}\left(\frac{M_W^2}{M_Z^2}\right)\left(\frac{s}{\Lambda^2}\right)+2C_{\varphi B}\left(1-\frac{M_W^2}{M_Z^2}\right)\left(\frac{s}{\Lambda^2}\right)+2C_{\varphi WB}\frac{M_W}{M_Z}\sqrt{1-\frac{M_W^2}{M_Z^2}}\left(\frac{s}{\Lambda^2}\right)\\
&-2\sqrt{2}(4C_{\varphi\Box}^2-\frac{3}{4}C_{\varphi D}^2)\left(\frac{M_Z^2}{\Lambda^2}\right)\left(\frac{1}{G_F\Lambda^2}\right)+6\sqrt{2}C_{\varphi W}^2\left(\frac{M_W^2}{M_Z^2}\right)\left(\frac{1}{G_F\Lambda^2}\right)\left(\frac{s}{\Lambda^2}\right) && \text{(G.2)}\\
&+6\sqrt{2}C_{\varphi B}^2\left(1-\frac{M_W^2}{M_Z^2}\right)\left(\frac{1}{G_F\Lambda^2}\right)\left(\frac{s}{\Lambda^2}\right)+2\sqrt{2}C_{\varphi WB}^2\left(1-\frac{M_W^2}{\sqrt{2}M_Z^2}\right)\left(\frac{1}{G_F\Lambda^2}\right)\left(\frac{s}{\Lambda^2}\right),\\
\mathcal{M}_{\pm\mp}^{ZZ,\,D6} =& (4C_{\varphi\Box}+C_{\varphi D})\left(\frac{M_Z^2}{\Lambda^2}\right)\\
&+\sqrt{2}(4C_{\varphi\Box}^2-\frac{1}{2}C_{\varphi D}^2)\left(\frac{M_Z^2}{\Lambda^2}\right)\left(\frac{1}{G_F\Lambda^2}\right)+2\sqrt{2}C_{\varphi W}^2\left(\frac{M_W^2}{M_Z^2}\right)\left(\frac{1}{G_F\Lambda^2}\right)\left(\frac{s}{\Lambda^2}\right)\\
&+2\sqrt{2}C_{\varphi B}^2\left(1-\frac{M_W^2}{M_Z^2}\right)\left(\frac{1}{G_F\Lambda^2}\right)\left(\frac{s}{\Lambda^2}\right)+\frac{1}{\sqrt{2}}C_{\varphi WB}^2\left(\frac{1}{G_F\Lambda^2}\right)\left(\frac{s}{\Lambda^2}\right),\\
\mathcal{M}_{0\pm}^{ZZ,\,D6} =& -4\sqrt{2}\cot\theta C_{\varphi W}\left(\frac{M_W^2}{M_Z^2}\right)\left(\frac{\sqrt{s}M_Z}{\Lambda^2}\right)\\
&-4\sqrt{2}\cot\theta C_{\varphi B}\left(1-\frac{M_W^2}{M_Z^2}\right)\left(\frac{\sqrt{s}M_Z}{\Lambda^2}\right)-4\sqrt{2}\cot\theta C_{\varphi WB}\sqrt{1-\frac{M_W^2}{M_Z^2}}\left(\frac{\sqrt{s}M_W}{\Lambda^2}\right)\\
&-8\cot\theta C_{\varphi W}^2\left(\frac{M_W^2}{M_Z^2}\right)\left(\frac{1}{G_F\Lambda^2}\right)\left(\frac{\sqrt{s}M_Z}{\Lambda^2}\right)\\
&-8\cot\theta C_{\varphi B}^2\left(1-\frac{M_W^2}{M_Z^2}\right)\left(\frac{1}{G_F\Lambda^2}\right)\left(\frac{\sqrt{s}M_Z}{\Lambda^2}\right)-4\cot\theta C_{\varphi WB}^2\left(1-\frac{M_W^2}{M_Z^2}\right)\left(\frac{1}{G_F\Lambda^2}\right)\left(\frac{\sqrt{s}M_Z}{\Lambda^2}\right).
\end{aligned}
$$

G.3 Dimension-8 SMEFT

$$
\begin{aligned}
\mathcal{M}_{00}^{ZZ,\,D8} =& -6C_{\varphi^8}\left(\frac{1}{G_F^2\Lambda^4}\right)+\sqrt{2}\left(2C_{\varphi^6\Box}+C_{\varphi^6D^2}\right)\frac{s}{\Lambda^2}\frac{1}{G_F\Lambda^2}-\frac{1}{2}C_{\varphi^4D^4}^{(1)}\left(\frac{s^2}{\Lambda^4}\right)\\
&+14\sqrt{2}C_{B^2\varphi^4}^{(1)}\left(\frac{M_W^2-M_Z^2}{\Lambda^2}\right)\left(\frac{1}{G_F\Lambda^2}\right)+\frac{1}{2}C_{B^2\varphi^2D^2}^{(1)}\left(1-\frac{M_W^2}{M_Z^2}\right)(\sin^2\theta+1)\left(\frac{M_Z^2}{\Lambda^2}\right)\left(\frac{s}{\Lambda^2}\right)
\end{aligned}
$$

$$
\begin{aligned}
&- \frac{5i}{2^{5/4}} C^{(1)}_{B\varphi^4 D^2} \left(\frac{\sqrt{M_Z^2 - M_W^2}}{\sqrt{G_F}\Lambda^2} \right) \left(\frac{s}{\Lambda^2} \right), \\
\mathcal{M}^{ZZ,\,D8}_{\pm\pm} =& -2\sqrt{2} \left(2C_{\varphi^6\Box} + C_{\varphi^6 D^2} \right) \frac{M_Z^2}{\Lambda^2} \frac{1}{G_F \Lambda^2} + C^{(1)}_{\varphi^4 D^4} \left(\frac{M_Z^2}{\Lambda^2} \right) \left(\frac{s}{\Lambda^2} \right) \\
&- \frac{1}{4} C^{(1)}_{B^2\varphi^2 D^2} \left(1 - \frac{M_W^2}{M_Z^2} \right) \left(\frac{s^2}{\Lambda^4} \right) - \frac{3i}{2^{5/4}} C^{(1)}_{B\varphi^4 D^2} \left(\frac{\sqrt{M_Z^2 - M_W^2}}{\sqrt{G_F}\Lambda^2} \right) \left(\frac{s}{\Lambda^2} \right), \qquad \text{(G.3)} \\
\mathcal{M}^{ZZ,\,D8}_{\pm\mp} =& \sqrt{2} \left(2C_{\varphi^6\Box} + \frac{3}{4} C_{\varphi^6 D^2} \right) \frac{M_W^2}{\Lambda^2} \frac{1}{G_F \Lambda^2} \\
&- \frac{1}{8} C^{(1)}_{B^2\varphi^2 D^2} \left(1 - \frac{M_W^2}{M_Z^2} \right) \sin^2\theta \left(\frac{s^2}{\Lambda^4} \right) + 2^{3/4} i C^{(1)}_{B\varphi^4 D^2} \left(\frac{\sqrt{M_Z^2 - M_W^2}}{\sqrt{G_F}\Lambda^2} \right) \left(\frac{M_Z^2}{\Lambda^2} \right), \\
\mathcal{M}^{ZZ,\,D8}_{0\pm} =& 4C^{(1)}_{B^2\varphi^4} \left(1 - \frac{M_W^2}{M_Z^2} \right) \cot\theta \left(\frac{s^{1/2} M_Z}{\Lambda^2} \right) \left(\frac{1}{G_F \Lambda^2} \right) \\
&- \frac{1}{8\sqrt{2}} C^{(1)}_{B^2\varphi^2 D^2} \left(1 - \frac{M_W^2}{M_Z^2} \right) \sin 2\theta \left(\frac{s^{3/2} M_Z}{\Lambda^4} \right) + 2^{1/4} i C^{(1)}_{B\varphi^4 D^2} \cot\theta \left(\frac{\sqrt{M_Z^2 - M_W^2}}{\sqrt{G_F}\Lambda^2} \right) \left(\frac{M_Z \sqrt{s}}{\Lambda^2} \right).
\end{aligned}
$$

Appendix for Chapter 4

H RGE for models with extended scalar and vector-like sectors

Below, we present the 1-loop RGE for all relevant couplings in the model scenarios discussed in this work, $\kappa_i = (\lambda, y_t^2, g_1^2, g_2^2, g_3^2, y_F^2, \lambda_{HS}, \lambda_S)$, divided into contributions from various sectors of the theory which The 1- and 2-loop contributions (latter too lengthy to be displayed), were derived using SARAH package [230] and validated with RGBeta [231].

$$\beta_{\kappa_i}^{(1)} = \beta_{\kappa_i}^{SM(1)} + \beta_{\kappa_i}^{VLF(1)} + \beta_{\kappa_i}^{S(1)} + \beta_{\kappa_i}^{VLF(1)\times S(1)} \tag{H.1}$$

with:

$$\frac{d\kappa_i(\mu)}{d\ln\mu} = \beta_{\kappa_i}\left(\kappa_j(\mu)\right) \equiv \beta_{\kappa_i} \tag{H.2}$$

H.1 SM sector

$$\begin{aligned}
\beta_{\lambda}^{SM(1)} &= \frac{1}{16\pi^2}\left[\frac{9}{8}\left(\frac{3}{25}g_1^4 + g_2^4 + \frac{2}{5}g_1^2 g_2^2\right) - 6y_t^4 + 24\lambda^2 + 12y_t^2\lambda - \frac{9}{5}g_1^2\lambda - 9g_2^2\lambda\right] \\
\beta_{y_t^2}^{SM(1)} &= \frac{y_t^2}{16\pi^2}\left[9y_t^2 - \frac{17}{10}g_1^2 - \frac{9}{2}g_2^2 - 16g_3^2\right] \\
\beta_{g_1^2}^{SM(1)} &= \frac{1}{16\pi^2}\left[\frac{41}{5}g_1^4\right], \\
\beta_{g_2^2}^{SM(1)} &= \frac{1}{16\pi^2}\left[-\frac{19}{3}g_2^4\right], \\
\beta_{g_3^2}^{SM(1)} &= \frac{1}{16\pi^2}\left[-14g_3^4\right].
\end{aligned} \tag{H.3}$$

H.2 Vector-like fermion sector

$$
\begin{aligned}
\beta_{\lambda}^{VLF(1)} &= \frac{1}{16\pi^2}\left[2n_{F_1}N_c'\left(4y_{F_1}^2\lambda - 2y_{F_1}^4\right) + 2n_{F_2}N_c'\left(4y_{F_2}^2\lambda - 2y_{F_2}^4\right)\right], \\
\beta_{y_t^2}^{VLF(1)} &= \frac{y_t^2}{16\pi^2}\left[4N_c'\left(n_{F_1}y_{F_1}^2 + n_{F_2}y_{F_2}^2\right)\right], \\
\beta_{g_1^2}^{VLF(1)} &= \frac{g_1^4}{16\pi^2}\left[\frac{8}{5}N_c'\left(2n_{\psi}Y_{W_{\psi}}^2 + n_{F_1}Y_{W_{F1}}^2 + n_{F_2}Y_{W_{F2}}^2\right)\right], \\
\beta_{g_2^2}^{VLF(1)} &= \frac{1}{16\pi^2}\left[\frac{4}{3}N_c'n_{\psi}g_2^4\right], \\
\beta_{g_3^2}^{VLF(1)} &= \frac{1}{16\pi^2}\left[\frac{4}{3}n_3g_3^4\right],
\end{aligned}
$$

$$
\begin{aligned}
\beta_{y_{F_1}^2}^{VLF(1)} &= \frac{y_{F_1}^2}{16\pi^2}\Bigg[3y_{F_1}^2 + 4n_{F_1}N_c'y_{F_1}^2 + 6y_t^2 - 16\hat{n}_F^{VLQ}g_3^2 - \frac{9}{2}g_2^2 - \frac{18}{5}g_1^2\left(Y_{W_H}^2 + 2Y_{W_{F1}}Y_{W_{\psi}}\right) \\
&\qquad + \Delta_{n_{F_1},n_{F_2}}\left(5 + 4n_{F_1}N_c'\right)y_{F_2}^2\Bigg], \\
\beta_{y_{F_2}^2}^{VLF(1)} &= \frac{y_{F_2}^2}{16\pi^2}\Bigg[3y_{F_2}^2 + 4n_{F_2}N_c'y_{F_2}^2 + 6y_t^2 - 16\hat{n}_F^{VLQ}g_3^2 - \frac{9}{2}g_2^2 - \frac{18}{5}g_1^2\left(Y_{W_H}^2 + 2Y_{W_{F2}}Y_{W_{\psi}}\right) \\
&\qquad + \Delta_{n_{F_1},n_{F_2}}\left(5 + 4n_{F_2}N_c'\right)y_{F_1}^2\Bigg],
\end{aligned}
\tag{H.4}
$$

where N_c' is a number of colours of VLF, $n_{F_1} \in \{n_U, n_N\}$, $n_{F_2} \in \{n_D, n_E\}$, $n_{\psi} \in \{n_Q, n_L\}$, $n_3 = 2n_Q + n_U + n_D$, $y_{F_1} \in \{y_U, y_N\}$, $y_{F_2} \in \{y_D, y_E\}$, $Y_{W_H} = 1/2$, $Y_{W_{\psi}} \in \{Y_{W_Q}, Y_{W_L}\}$, $Y_{W_{F1}} \in \{Y_{W_U}, Y_{W_N}\}$, $Y_{W_{F2}} \in \{Y_{W_D}, Y_{W_E}\}$.

H.3 Real scalar sector

$$
\begin{aligned}
\beta_{\lambda}^{S(1)} &= \frac{1}{16\pi^2}\left[\frac{1}{2}\lambda_{HS}^2\right] \\
\beta_{\lambda_{HS}}^{S(1)} &= \frac{\lambda_{HS}}{16\pi^2}\left[12\lambda + 6\lambda_S + 4\lambda_{HS} + 6y_t^2 - \frac{3}{2}g_1^2 - \frac{9}{2}g_2^2\right] \\
\beta_{\lambda_S}^{S(1)} &= \frac{1}{16\pi^2}\left[2\lambda_{HS}^2 + 18\lambda_S^2\right].
\end{aligned}
\tag{H.5}
$$

H.4 Vector-like fermion $\times$ real scalar sector

$$
\beta_{\lambda_{HS}}^{VLF(1)\times S(1)} = \frac{\lambda_{HS}}{16\pi^2}\left[4N_c'(n_{F_1}y_{F_1}^2 + n_{F_2}y_{F_2}^2)\right]. \tag{H.6}
$$

I $\mathbb{S}$ and $\mathbb{T}$ oblique parameters in the presence of VLF

The General formulas for the $\mathbb{S}$ and $\mathbb{T}$ oblique parameters in the presence of VLF can be found in [195]. In the simplified scenarios analyzed in this work, they reduce to:

$$\begin{aligned}\mathbb{T}_{VLF} =&\frac{N_c}{8\pi \sin^2\theta_W \cos^2\theta_W} \times \left[\sum_{\alpha,i}\left[\left|\mathcal{V}_{\alpha i}\right|^2\left(\theta_+\left(x_\alpha,x_i\right)+\theta_-\left(x_\alpha,x_i\right)\right)\right]\right.\\ &\left.-\sum_{\beta<\alpha}\left[\left|\mathcal{U}_{\alpha\beta}\right|^2\left(\theta_+\left(x_\alpha,x_\beta\right)+\theta_-\left(x_\alpha,x_\beta\right)\right)\right]-\sum_{j<i}\left[\left|\mathcal{D}_{ij}\right|^2\left(\theta_+\left(x_i,x_j\right)+\theta_-\left(x_i,x_j\right)\right)\right]\right],\end{aligned} \tag{I.7}$$

$$\begin{aligned}\mathbb{S}_{VLF} =&\frac{N_c}{\pi} \times \left[\sum_{\alpha,i}\left[\left|\mathcal{V}_{\alpha i}\right|^2\left(\psi_+\left(x_\alpha,x_i\right)+\psi_-\left(x_\alpha,x_i\right)\right)\right]\right.\\ &\left.-\sum_{\beta<\alpha}\left[\left|\mathcal{U}_{\alpha\beta}\right|^2\left(\chi_+\left(x_\alpha,x_\beta\right)+\chi_-\left(x_\alpha,x_\beta\right)\right)\right]-\sum_{j<i}\left[\left|\mathcal{D}_{ij}\right|^2\left(\chi_+\left(x_i,x_j\right)+\chi_-\left(x_i,x_j\right)\right)\right]\right],\end{aligned} \tag{I.8}$$

where:

$$\begin{aligned}&x_{i(\alpha)} \equiv M_{i(\alpha)}^2/M_Z^2,\\ &\theta_+\left(x_1,x_2\right) \equiv x_1+x_2-\frac{2x_1x_2}{x_1-x_2}\ln\frac{x_1}{x_2},\\ &\theta_-\left(x_1,x_2\right) \equiv 2\sqrt{x_1x_2}\left(\frac{x_1+x_2}{x_1-x_2}\ln\frac{x_1}{x_2}-2\right),\end{aligned} \tag{I.9}$$

$$\begin{aligned}f\left(x_1,x_2\right) \equiv &\begin{cases}-2\sqrt{\Delta}\left(\arctan\frac{x_1-x_2+1}{\sqrt{\Delta}}-\arctan\frac{x_1-x_2-1}{\sqrt{\Delta}}\right) & \Delta>0\\ 0 & \Delta=0\\ \sqrt{-\Delta}\ln\frac{x_1+x_2-1+\sqrt{-\Delta}}{x_1+x_2-1-\sqrt{-\Delta}} & \Delta<0\end{cases},\\ &\Delta=-1-x_1^2-x_2^2+2x_1+2x_2+2x_1x_2.\end{aligned} \tag{I.10}$$

$$\begin{aligned}\chi_+\left(x_1,x_2\right) \equiv&\frac{x_1+x_2}{2}-\frac{\left(x_1-x_2\right)^2}{3}+\left[\frac{\left(x_1-x_2\right)^3}{6}-\frac{1}{2}\frac{x_1^2+x_2^2}{x_1-x_2}\right]\ln\frac{x_1}{x_2}+\frac{x_1-1}{6}f\left(x_1,x_1\right)\\ &+\frac{x_2-1}{6}f\left(x_2,x_2\right)+\left[\frac{1}{3}-\frac{x_1+x_2}{6}-\frac{\left(x_1-x_2\right)^2}{6}\right]f\left(x_1,x_2\right),\\ \chi_-\left(x_1,x_2\right) \equiv&-\sqrt{x_1x_2}\left[2+\left(x_1-x_2-\frac{x_1+x_2}{x_1-x_2}\right)\ln\frac{x_1}{x_2}+\frac{f\left(x_1,x_1\right)+f\left(x_2,x_2\right)}{2}-f\left(x_1,x_2\right)\right],\end{aligned} \tag{I.11}$$

$$\begin{aligned}\psi_+\left(x_\alpha,x_i\right) \equiv&\frac{22x_\alpha+14x_i}{9}-\frac{1}{9}\ln\frac{x_\alpha}{x_i}+\frac{11x_\alpha+1}{18}f\left(x_\alpha,x_\alpha\right)+\frac{7x_i-1}{18}f\left(x_i,x_i\right),\\ \psi_-\left(x_\alpha,x_i\right) \equiv&-\sqrt{x_\alpha x_i}\left[4+\frac{f\left(x_\alpha,x_\alpha\right)+f\left(x_i,x_i\right)}{2}\right].\end{aligned} \tag{I.12}$$

Greek indices denote summation over "up-type" states, while Latin indices over "down-type" fields. The matrices $\mathcal{V}, \mathcal{U}$ and $\mathcal{D}$, defined for the scenarios in this work, along with the simplified expressions for the $\mathbb{S}_{VLF}$ and $\mathbb{T}_{VLF}$ parameters read:

- Scenario I:

$$\begin{aligned}
\mathcal{V} =&\mathcal{U} = \mathcal{D} = \begin{pmatrix} \cos\gamma_F^2 & \cos\gamma_F \sin\gamma_F \\ \cos\gamma_F \sin\gamma_F & \sin\gamma_F^2 \end{pmatrix}, \quad \mathbb{T}_{VLF} = 0, \\
\mathbb{S}_{VLF} =&\frac{N_c}{\pi} \times |\mathcal{V}_{21}|^2 \left[\psi_+(x_-, x_+) + \psi_-(x_-, x_+) + \right. \\
&\left. \psi_+(x_+, x_-) + \psi_-(x_+, x_-) - 2\chi_+(x_-, x_+) - 2\chi_-(x_-, x_+)\right], \\
x_\pm =&M_\pm^2/M_Z^2, \quad M_\pm = M_{U\pm} = M_{D\pm} = M_F \pm \frac{\sqrt{2}}{2} v y_F.
\end{aligned} \tag{I.13}$$

- Scenario II:

$$\begin{aligned}
\mathcal{V} =& \begin{pmatrix} \cos\gamma_F \\ \sin\gamma_F \end{pmatrix}, \quad \mathcal{U} = \begin{pmatrix} \cos\gamma_F^2 & \cos\gamma_F \sin\gamma_F \\ \cos\gamma_F \sin\gamma_F & \sin\gamma_F^2 \end{pmatrix}, \quad \mathcal{D} = \mathbb{I}, \\
\mathbb{T}_{VLF} =&\frac{N_c}{8\pi \sin^2\theta_W \cos^2\theta_W} \times \Big[|\mathcal{V}_{11}|^2 \left(\theta_+(x_{U+}, x_D) + \theta_-(x_{U+}, x_D)\right) \\
&+ |\mathcal{V}_{21}|^2 \left(\theta_+(x_{U-}, x_D) + \theta_-(x_{U-}, x_D)\right) - |\mathcal{U}_{21}|^2 \left(\theta_+(x_{U-}, x_{U+}) + \theta_-(x_{U-}, x_{U+})\right)\Big], \\
\mathbb{S}_{VLF} =&\frac{N_c}{\pi} \times \Big[|\mathcal{V}_{11}|^2 \left(\psi_+(x_{U+}, x_D) + \psi_-(x_{U-}, x_D)\right) \\
&+ |\mathcal{V}_{21}|^2 \left(\psi_+(x_{U-}, x_D) + \psi_-(x_{U-}, x_D)\right)) - |\mathcal{U}_{21}|^2 \left(\chi_+(x_{U-}, x_{U+}) + \chi_-(x_{U-}, x_{U+})\right)\Big], \\
&x_{U\pm} = M_{U\pm}^2/M_Z^2, \quad M_{U\pm} = M_U \pm \frac{\sqrt{2}}{2} v y_U, \quad x_D = M_D^2/M_Z^2.
\end{aligned} \tag{I.14}$$

- Scenario III:

$$\begin{aligned}
\mathcal{V} =& \left(\cos\gamma_F, \sin\gamma_F\right), \quad \mathcal{U} = \mathbb{I}, \quad \mathcal{D} = \begin{pmatrix} \cos\gamma_F^2 & \cos\gamma_F \sin\gamma_F \\ \cos\gamma_F \sin\gamma_F & \sin\gamma_F^2 \end{pmatrix}, \\
\mathbb{T}_{VLF} =&\frac{N_c}{8\pi \sin^2\theta_W \cos^2\theta_W} \times \Big[|\mathcal{V}_{11}|^2 \left(\theta_+(x_{D1}, x_U) + \theta_-(x_{D1}, x_U)\right) \\
&+ |\mathcal{V}_{12}|^2 \left(\theta_+(x_{D-}, x_U) + \theta_-(x_{D-}, x_U)\right) - |\mathcal{D}_{21}|^2 \left(\theta_+(x_{D-}, x_{D+}) + \theta_-(x_{D-}, x_{D+})\right)\Big], \\
\mathbb{S}_{VLF} =&\frac{N_c}{\pi} \times \Big[|\mathcal{V}_{11}|^2 \left(\psi_+(x_U, x_{D+}) + \psi_-(x_U, x_{D+})\right) \\
&+ |\mathcal{V}_{12}|^2 \left(\psi_+(x_U, x_{D-}) + \psi_-(x_U, x_{D-})\right) - |\mathcal{D}_{21}|^2 \left(\chi_+(x_{D-}, x_{D+}) - \chi_-(x_{D-}, x_{D+})\right)\Big], \\
&x_{D\pm} = M_{D\pm}^2/M_Z^2, \quad M_{D\pm} = M_D \pm \frac{\sqrt{2}}{2} v y_F, \quad x_U = M_U^2/M_Z^2.
\end{aligned} \tag{I.15}$$

Uniform Dirac masses $M_{F^d} = M_{F^s} = M_F$ and VLF Yukawa couplings $y_F = y$ lead to the value of mixing angle $\gamma_F = \frac{\pi}{4}$.

J Effective potential

The general formula for the one-loop effective potential is given in Eq. 4.41. The Coleman-Weinberg part in the on-shell renormalization scheme with cut-off regularization reads:

$$\begin{aligned} V_{CW}(H) = &\sum_k \frac{r_k N_k}{64\pi^2}\left(2M_k^2(H)M_k^2(v) + M_k^4(H)\left(\log\frac{M_k^2(H)}{M_k^2(v)} - \frac{3}{2}\right)\right) \\ &- \frac{N_F}{64\pi^2}\sum_{i=1,2} n_{F_i}\left(M_{F_i}(H)^4\left(\log\frac{M_{F_i}(H)^2}{\mu_R^2} - \frac{3}{2}\right) + C_1\varphi^2 + C_2\varphi^4\right), \end{aligned} \tag{J.1}$$

where we use the following notation:

$$\begin{aligned} &k = (t, W, Z, h, S), \quad N_k = (12, 6, 3, 1, 1), \\ &M_k(H)^2 = M_{0,k}^2 + a_k h^2, \quad M_{0,k}^2 = \left(0, 0, 0, -\mu^2,\ \mu_S^2\right), \\ &a_k = \left(\frac{\lambda_t^2}{2}, \frac{g^2}{4}, \frac{g^2+g'^2}{4}, 3\lambda, \frac{1}{2}\lambda_{HS}\right), \\ &F = (VLQ, VLL), \quad N_F = (12, 4), \\ &n_{F_1} \in \{n_U, n_N\}, \quad n_{F_2} \in \{n_D, n_E\}, \\ &M_{F_{1(2)}} = M_F \pm \frac{\sqrt{2}}{2} y_F v, \end{aligned} \tag{J.2}$$

and particle statistics related sign equals to $r_k = +(-)$ for bosons (fermions).

The assumed renormalization conditions ensure that the Higgs mass and vev remain unchanged compared to the tree-level, and eliminate explicit dependence on the renormalization scale μ_R in the effective potential (apart from a field independent term which can be canceled by shifting the potential by a constant, such that $V(\varphi = 0) = 0$). These conditions read:

$$\frac{\partial}{\partial\varphi}V_{CW}\bigg|_{\varphi=v} = 0, \qquad \frac{\partial^2}{\partial\varphi^2}V_{CW}\bigg|_{\varphi=v} = 0. \tag{J.3}$$

The first line of Eq. (J.1) automatically satisfies the conditions in Eq. (J.3), whereas C_1 and C_2 in the second line are selected to ensure the same result. The temperature corrections to the effective potential are expressed as:

$$V_T(H, S, T) = \sum_k \frac{N_k T^4}{2\pi^2} J_{r_k}\left(M_k(H,S)/T\right) + N_F \sum_{i=1,2} \frac{n_{F_i} T^4}{2\pi^2} J_-\left(M_{F_i}(H,S)/T\right), \tag{J.4}$$

where the thermal functions $J_\pm(y)$ with $y = M/T$ given by:

$$J_\pm(y) = \pm\int_0^\infty \mathrm{d}x x^2 \log\left[1 \mp e^{-\sqrt{x^2+y^2}}\right]. \tag{J.5}$$

At $T \neq 0$, the field dependent scalar and longitudinal gauge boson masses are modified by thermal loop effects. These modifications are included as Π in the field dependent masses [253, 254]:

$$\Pi_H(0) \;=\; \left(\frac{3g^2}{16} + \frac{g'^2}{16} + \frac{\lambda}{2} + \frac{y_t^2}{4} + \frac{1}{2}\sum_F y_F^2 + \frac{\lambda_{HS}}{24}\right) T^2,$$

$$\begin{aligned}\Pi_s(0) &= \left(\frac{1}{6}\lambda_{HS} + \frac{1}{4}\lambda_S\right) T^2, \\ \Pi^L_{GB}(0) &= \frac{11}{6} T^2 \,\mathrm{diag}\left(g^2, g^2, g^2, g'^2\right). \end{aligned} \tag{J.6}$$

Bibliography

[1] S. Pokorski, GAUGE FIELD THEORIES, Cambridge University Press, 2005.

[2] M. E. Peskin, D. V. Schroeder, An Introduction to quantum field theory, Addison-Wesley, Reading, USA, 1995. doi:10.1201/9780429503559.

[3] M. D. Schwartz, Quantum Field Theory and the Standard Model, Cambridge University Press, 2014.

[4] G. Aad, et al., Observation of a new particle in the search for the Standard Model Higgs boson with the ATLAS detector at the LHC, Phys. Lett. B 716 (2012) 1–29. arXiv:1207.7214, doi:10.1016/j.physletb.2012.08.020.

[5] S. Chatrchyan, et al., Observation of a New Boson at a Mass of 125 GeV with the CMS Experiment at the LHC, Phys. Lett. B 716 (2012) 30–61. arXiv:1207.7235, doi:10.1016/j.physletb.2012.08.021.

[6] S. L. Glashow, J. Iliopoulos, L. Maiani, Weak Interactions with Lepton-Hadron Symmetry, Phys. Rev. D 2 (1970) 1285–1292. doi:10.1103/PhysRevD.2.1285.

[7] A. Boccaletti, et al., High precision calculation of the hadronic vacuum polarisation contribution to the muon anomalyarXiv:2407.10913.

[8] R. Aaij, et al., Measurement of lepton universality parameters in $B^+ \to K^+\ell^+\ell^-$ and $B^0 \to K^{*0}\ell^+\ell^-$ decays, Phys. Rev. D 108 (3) (2023) 032002. arXiv:2212.09153, doi:10.1103/PhysRevD.108.032002.

[9] A. V. Manohar, Introduction to Effective Field TheoriesarXiv:1804.05863, doi:10.1093/oso/9780198855743.003.0002.

[10] T. Appelquist, J. Carazzone, Infrared Singularities and Massive Fields, Phys. Rev. D 11 (1975) 2856. doi:10.1103/PhysRevD.11.2856.

[11] R. L. Workman, et al., Review of Particle Physics, PTEP 2022 (2022) 083C01. doi:10.1093/ptep/ptac097.

[12] W. Buchmuller, D. Wyler, Effective Lagrangian Analysis of New Interactions and Flavor Conservation, Nucl. Phys. B 268 (1986) 621–653. doi:10.1016/0550-3213(86)90262-2.

[13] B. Grzadkowski, M. Iskrzynski, M. Misiak, J. Rosiek, Dimension-Six Terms in the Standard Model Lagrangian, JHEP 10 (2010) 085. arXiv:1008.4884, doi:10.1007/JHEP10(2010)085.

[14] I. Brivio, J. Gonzalez-Fraile, M. C. Gonzalez-Garcia, L. Merlo, The complete HEFT Lagrangian after the LHC Run I, Eur. Phys. J. C 76 (7) (2016) 416. arXiv:1604.06801, doi:10.1140/epjc/s10052-016-4211-9.

[15] E. E. Jenkins, A. V. Manohar, P. Stoffer, Low-Energy Effective Field Theory below the Electroweak Scale: Operators and Matching, JHEP 03 (2018) 016, [Erratum: JHEP 12, 043 (2023)]. arXiv:1709.04486, doi:10.1007/JHEP03(2018)016.

[16] H. Georgi, An Effective Field Theory for Heavy Quarks at Low-energies, Phys. Lett. B 240 (1990) 447–450. doi:10.1016/0370-2693(90)91128-X.

[17] E. Eichten, B. R. Hill, An Effective Field Theory for the Calculation of Matrix Elements Involving Heavy Quarks, Phys. Lett. B 234 (1990) 511–516. doi:10.1016/0370-2693(90)92049-O.

[18] A. Dedes, K. Suxho, L. Trifyllis, The decay $h \to Z\gamma$ in the Standard-Model Effective Field Theory, JHEP 06 (2019) 115. arXiv:1903.12046, doi:10.1007/JHEP06(2019)115.

[19] A. Dedes, M. Paraskevas, J. Rosiek, K. Suxho, L. Trifyllis, The decay $h \to \gamma\gamma$ in the Standard-Model Effective Field Theory, JHEP 08 (2018) 103. arXiv:1805.00302, doi:10.1007/JHEP08(2018)103.

[20] S. Dawson, P. P. Giardino, Higgs decays to ZZ and $Z\gamma$ in the standard model effective field theory: An NLO analysis, Phys. Rev. D 97 (9) (2018) 093003. arXiv:1801.01136, doi:10.1103/PhysRevD.97.093003.

[21] J. M. Cullen, B. D. Pecjak, Higgs decay to fermion pairs at NLO in SMEFT, JHEP 11 (2020) 079. arXiv:2007.15238, doi:10.1007/JHEP11(2020)079.

[22] R. Gauld, B. D. Pecjak, D. J. Scott, One-loop corrections to $h \to b\bar{b}$ and $h \to \tau\bar{\tau}$ decays in the Standard Model Dimension-6 EFT: four-fermion operators and the large-m_t limit, JHEP 05 (2016) 080. arXiv:1512.02508, doi:10.1007/JHEP05(2016)080.

[23] R. Gauld, B. D. Pecjak, D. J. Scott, QCD radiative corrections for $h \to b\bar{b}$ in the Standard Model Dimension-6 EFT, Phys. Rev. D 94 (7) (2016) 074045. arXiv:1607.06354, doi:10.1103/PhysRevD.94.074045.

[24] C. Hartmann, M. Trott, Higgs Decay to Two Photons at One Loop in the Standard Model Effective Field Theory, Phys. Rev. Lett. 115 (19) (2015) 191801. arXiv:1507.03568, doi:10.1103/PhysRevLett.115.191801.

[25] C. Hartmann, M. Trott, On one-loop corrections in the standard model effective field theory; the $\Gamma(h \to \gamma\,\gamma)$ case, JHEP 07 (2015) 151. arXiv:1505.02646, doi:10.1007/JHEP07(2015)151.

[26] E. Vryonidou, C. Zhang, Dimension-six electroweak top-loop effects in Higgs production and decay, JHEP 08 (2018) 036. arXiv:1804.09766, doi:10.1007/JHEP08(2018)036.

[27] S. Dawson, P. P. Giardino, Electroweak corrections to Higgs boson decays to $\gamma\gamma$ and W^+W^- in standard model EFT, Phys. Rev. D 98 (9) (2018) 095005. arXiv:1807.11504, doi:10.1103/PhysRevD.98.095005.

[28] F. Bishara, R. Contino, J. Rojo, Higgs pair production in vector-boson fusion at the LHC and beyond, Eur. Phys. J. C 77 (7) (2017) 481. arXiv:1611.03860, doi:10.1140/epjc/s10052-017-5037-9.

[29] L. Alasfar, et al., Effective Field Theory descriptions of Higgs boson pair productionarXiv:2304.01968.

[30] D. Domenech, M. J. Herrero, R. A. Morales, M. Ramos, Double Higgs boson production at TeV e+e- colliders with effective field theories: Sensitivity to BSM Higgs couplings, Phys. Rev. D 106 (11) (2022) 115027. arXiv:2208.05452, doi:10.1103/PhysRevD.106.115027.

[31] R. L. Delgado, R. Gómez-Ambrosio, J. Martínez-Martín, A. Salas-Bernárdez, J. J. Sanz-Cillero, Production of two, three, and four Higgs bosons: where SMEFT and HEFT depart, JHEP 03 (2024) 037. arXiv:2311.04280, doi:10.1007/JHEP03(2024)037.

[32] S. Bhattacharya, S. Biswas, K. Pal, J. Wudka, Associated production of Higgs and single top at the LHC in presence of the SMEFT operators, JHEP 08 (2023) 015. arXiv:2211.05450, doi:10.1007/JHEP08(2023)015.

[33] F. Goertz, A. Papaefstathiou, L. L. Yang, J. Zurita, Higgs boson pair production in the D=6 extension of the SM, JHEP 04 (2015) 167. arXiv:1410.3471, doi:10.1007/JHEP04(2015)167.

[34] G. Heinrich, J. Lang, L. Scyboz, SMEFT predictions for gg → hh at full NLO QCD and truncation uncertainties, JHEP 08 (2022) 079, [Erratum: JHEP 10, 086 (2023)]. arXiv:2204.13045, doi:10.1007/JHEP08(2022)079.

[35] F. Maltoni, E. Vryonidou, C. Zhang, Higgs production in association with a top-antitop pair in the Standard Model Effective Field Theory at NLO in QCD, JHEP 10 (2016) 123. arXiv:1607.05330, doi:10.1007/JHEP10(2016)123.

[36] N. Deutschmann, C. Duhr, F. Maltoni, E. Vryonidou, Gluon-fusion Higgs production in the Standard Model Effective Field Theory, JHEP 12 (2017) 063, [Erratum: JHEP 02, 159 (2018)]. arXiv:1708.00460, doi:10.1007/JHEP12(2017)063.

[37] R. Grober, M. Muhlleitner, M. Spira, J. Streicher, NLO QCD Corrections to Higgs Pair Production including Dimension-6 Operators, JHEP 09 (2015) 092. arXiv:1504.06577, doi:10.1007/JHEP09(2015)092.

[38] G. Buchalla, M. Capozi, A. Celis, G. Heinrich, L. Scyboz, Higgs boson pair production in non-linear Effective Field Theory with full m_t-dependence at NLO QCD, JHEP 09 (2018) 057. arXiv:1806.05162, doi:10.1007/JHEP09(2018)057.

[39] J. J. Ethier, R. Gomez-Ambrosio, G. Magni, J. Rojo, SMEFT analysis of vector boson scattering and diboson data from the LHC Run II, Eur. Phys. J. C 81 (6) (2021) 560. arXiv:2101.03180, doi:10.1140/epjc/s10052-021-09347-7.

[40] A. Dedes, P. Kozów, M. Szleper, Standard model EFT effects in vector-boson scattering at the LHC, Phys. Rev. D 104 (1) (2021) 013003. arXiv:2011.07367, doi:10.1103/PhysRevD.104.013003.

[41] R. Bellan, et al., A sensitivity study of VBS and diboson WW to dimension-6 EFT operators at the LHC, JHEP 05 (2022) 039. arXiv:2108.03199, doi:10.1007/JHEP05(2022)039.

[42] R. Gomez-Ambrosio, Studies of Dimension-Six EFT effects in Vector Boson Scattering, Eur. Phys. J. C 79 (5) (2019) 389. arXiv:1809.04189, doi:10.1140/epjc/s10052-019-6893-2.

[43] J. Ellis, M. Madigan, K. Mimasu, V. Sanz, T. You, Top, Higgs, Diboson and Electroweak Fit to the Standard Model Effective Field Theory, JHEP 04 (2021) 279. arXiv:2012.02779, doi:10.1007/JHEP04(2021)279.

[44] J. J. Ethier, G. Magni, F. Maltoni, L. Mantani, E. R. Nocera, J. Rojo, E. Slade, E. Vryonidou, C. Zhang, Combined SMEFT interpretation of Higgs, diboson, and top quark data from the LHC, JHEP 11 (2021) 089. arXiv:2105.00006, doi:10.1007/JHEP11(2021)089.

[45] S. P. Martin, A Supersymmetry primer, Adv. Ser. Direct. High Energy Phys. 18 (1998) 1–98. arXiv:hep-ph/9709356, doi:10.1142/9789812839657_0001.

[46] M. Maniatis, The Next-to-Minimal Supersymmetric extension of the Standard Model reviewed, Int. J. Mod. Phys. A 25 (2010) 3505–3602. arXiv:0906.0777, doi:10.1142/S0217751X10049827.

[47] D. O'Connell, M. J. Ramsey-Musolf, M. B. Wise, Minimal Extension of the Standard Model Scalar Sector, Phys. Rev. D 75 (2007) 037701. arXiv:hep-ph/0611014, doi:10.1103/PhysRevD.75.037701.

[48] G. C. Branco, P. M. Ferreira, L. Lavoura, M. N. Rebelo, M. Sher, J. P. Silva, Theory and phenomenology of two-Higgs-doublet models, Phys. Rept. 516 (2012) 1–102. arXiv:1106.0034, doi:10.1016/j.physrep.2012.02.002.

[49] R. D. Peccei, H. R. Quinn, Constraints Imposed by CP Conservation in the Presence of Instantons, Phys. Rev. D 16 (1977) 1791–1797. doi:10.1103/PhysRevD.16.1791.

[50] M. Dine, W. Fischler, M. Srednicki, A Simple Solution to the Strong CP Problem with a Harmless Axion, Phys. Lett. B 104 (1981) 199–202. doi:10.1016/0370-2693(81)90590-6.

[51] P. Langacker, The Physics of Heavy Z' Gauge Bosons, Rev. Mod. Phys. 81 (2009) 1199–1228. arXiv:0801.1345, doi:10.1103/RevModPhys.81.1199.

[52] A. Adhikary, M. Olechowski, J. Rosiek, M. Ryczkowski, Theoretical constraints on models with vectorlike fermions, Phys. Rev. D 110 (7) (2024) 075029. arXiv:2406.16050, doi:10.1103/PhysRevD.110.075029.

[53] B. Henning, X. Lu, T. Melia, H. Murayama, 2, 84, 30, 993, 560, 15456, 11962, 261485, ...: Higher dimension operators in the SM EFT, JHEP 08 (2017) 016, [Erratum: JHEP 09, 019 (2019)]. arXiv:1512.03433, doi:10.1007/JHEP08(2017)016.

[54] J. Aebischer, M. Fael, A. Lenz, M. Spannowsky, J. Virto (Eds.), Computing Tools for the SMEFT, 2019. arXiv:1910.11003.

[55] L. Allwicher, et al., Computing tools for effective field theories: SMEFT-Tools 2022 Workshop Report, 14–16th September 2022, Zürich, Eur. Phys. J. C 84 (2) (2024) 170. arXiv:2307.08745, doi:10.1140/epjc/s10052-023-12323-y.

[56] J. Fuentes-Martín, M. König, J. Pagès, A. E. Thomsen, F. Wilsch, A proof of concept for matchete: an automated tool for matching effective theories, Eur. Phys. J. C 83 (7) (2023) 662. arXiv:2212.04510, doi:10.1140/epjc/s10052-023-11726-1.

[57] A. Carmona, A. Lazopoulos, P. Olgoso, J. Santiago, Matchmakereft: automated tree-level and one-loop matching, SciPost Phys. 12 (6) (2022) 198. arXiv:2112.10787, doi:10.21468/SciPostPhys.12.6.198.

[58] J. C. Criado, MatchingTools: a Python library for symbolic effective field theory calculations, Comput. Phys. Commun. 227 (2018) 42–50. arXiv:1710.06445, doi:10.1016/j.cpc.2018.02.016.

[59] S. Das Bakshi, J. Chakrabortty, S. K. Patra, CoDEx: Wilson coefficient calculator connecting SMEFT to UV theory, Eur. Phys. J. C 79 (1) (2019) 21. arXiv:1808.04403, doi:10.1140/epjc/s10052-018-6444-2.

[60] J. Fuentes-Martin, P. Ruiz-Femenia, A. Vicente, J. Virto, DsixTools 2.0: The Effective Field Theory Toolkit, Eur. Phys. J. C 81 (2) (2021) 167. arXiv:2010.16341, doi:10.1140/epjc/s10052-020-08778-y.

[61] J. Aebischer, J. Kumar, D. M. Straub, Wilson: a Python package for the running and matching of Wilson coefficients above and below the electroweak scale, Eur. Phys. J. C 78 (12) (2018) 1026. arXiv:1804.05033, doi:10.1140/epjc/s10052-018-6492-7.

[62] G. Guedes, P. Olgoso, J. Santiago, Towards the one loop IR/UV dictionary in the SMEFT: One loop generated operators from new scalars and fermions, SciPost Phys. 15 (4) (2023) 143. arXiv:2303.16965, doi:10.21468/SciPostPhys.15.4.143.

[63] S. Di Noi, L. Silvestrini, RGESolver: a C++ library to perform renormalization group evolution in the Standard Model Effective Theory, Eur. Phys. J. C 83 (3) (2023) 200. arXiv:2210.06838, doi:10.1140/epjc/s10052-023-11189-4.

[64] T. Giani, G. Magni, J. Rojo, SMEFiT: a flexible toolbox for global interpretations of particle physics data with effective field theories, Eur. Phys. J. C 83 (5) (2023) 393. arXiv:2302.06660, doi:10.1140/epjc/s10052-023-11534-7.

[65] P. Stangl, smelli – the SMEFT Likelihood, PoS TOOLS2020 (2021) 035. arXiv:2012.12211, doi:10.22323/1.392.0035.

[66] J. De Blas, et al., HEPfit: a code for the combination of indirect and direct constraints on high energy physics models, Eur. Phys. J. C 80 (5) (2020) 456. arXiv:1910.14012, doi:10.1140/epjc/s10052-020-7904-z.

[67] J. ter Hoeve, G. Magni, J. Rojo, A. N. Rossia, E. Vryonidou, The automation of SMEFT-assisted constraints on UV-complete models, JHEP 01 (2024) 179. arXiv:2309.04523, doi:10.1007/JHEP01(2024)179.

[68] I. Brivio, Y. Jiang, M. Trott, The SMEFTsim package, theory and tools, JHEP 12 (2017) 070. arXiv:1709.06492, doi:10.1007/JHEP12(2017)070.

[69] I. Brivio, SMEFTsim 3.0 — a practical guide, JHEP 04 (2021) 073. arXiv:2012.11343, doi:10.1007/JHEP04(2021)073.

[70] D. Barducci, et al., Interpreting top-quark LHC measurements in the standard-model effective field theoryarXiv:1802.07237.

[71] C. Degrande, G. Durieux, F. Maltoni, K. Mimasu, E. Vryonidou, C. Zhang, Automated one-loop computations in the standard model effective field theory, Phys. Rev. D 103 (9) (2021) 096024. arXiv:2008.11743, doi:10.1103/PhysRevD.103.096024.

[72] A. Dedes, M. Paraskevas, J. Rosiek, K. Suxho, L. Trifyllis, SmeftFR – Feynman rules generator for the Standard Model Effective Field Theory, Comput. Phys. Commun. 247 (2020) 106931. arXiv:1904.03204, doi:10.1016/j.cpc.2019.106931.

[73] A. Dedes, J. Rosiek, M. Ryczkowski, K. Suxho, L. Trifyllis, SmeftFR v3 – Feynman rules generator for the Standard Model Effective Field Theory, Comput. Phys. Commun. 294 (2024) 108943. arXiv:2302.01353, doi:10.1016/j.cpc.2023.108943.

[74] A. Dedes, W. Materkowska, M. Paraskevas, J. Rosiek, K. Suxho, Feynman rules for the Standard Model Effective Field Theory in R_ξ -gauges, JHEP 06 (2017) 143. arXiv:1704.03888, doi:10.1007/JHEP06(2017)143.

[75] L. Trifyllis, Theoretical and phenomenological aspects of the standard model effective field theory, Ph.D. thesis (2022). doi:10.12681/eadd/52779.

[76] C. W. Murphy, Dimension-8 operators in the Standard Model Effective Field Theory, JHEP 10 (2020) 174. arXiv:2005.00059, doi:10.1007/JHEP10(2020)174.

[77] H.-L. Li, Z. Ren, J. Shu, M.-L. Xiao, J.-H. Yu, Y.-H. Zheng, Complete set of dimension-eight operators in the standard model effective field theory, Phys. Rev. D 104 (1) (2021) 015026. arXiv:2005.00008, doi:10.1103/PhysRevD.104.015026.

[78] M. Misiak, M. Paraskevas, J. Rosiek, K. Suxho, B. Zglinicki, Effective Field Theories in R_ξ gauges, JHEP 02 (2019) 051. arXiv:1812.11513, doi:10.1007/JHEP02(2019)051.

[79] N. D. Christensen, C. Duhr, FeynRules - Feynman rules made easy, Comput. Phys. Commun. 180 (2009) 1614–1641. arXiv:0806.4194, doi:10.1016/j.cpc.2009.02.018.

[80] A. Alloul, N. D. Christensen, C. Degrande, C. Duhr, B. Fuks, FeynRules 2.0 - A complete toolbox for tree-level phenomenology, Comput. Phys. Commun. 185 (2014) 2250–2300. arXiv:1310.1921, doi:10.1016/j.cpc.2014.04.012.

[81] J. Kalinowski, P. Kozów, S. Pokorski, J. Rosiek, M. Szleper, S. Tkaczyk, Same-sign WW scattering at the LHC: can we discover BSM effects before discovering new states?, Eur. Phys. J. C 78 (5) (2018) 403. arXiv:1802.02366, doi:10.1140/epjc/s10052-018-5885-y.

[82] K. Doroba, J. Kalinowski, J. Kuczmarski, S. Pokorski, J. Rosiek, M. Szleper, S. Tkaczyk, The $W_L W_L$ Scattering at the LHC: Improving the Selection Criteria, Phys. Rev. D 86 (2012) 036011. arXiv:1201.2768, doi:10.1103/PhysRevD.86.036011.

[83] D. Buarque Franzosi, et al., Vector boson scattering processes: Status and prospects, Rev. Phys. 8 (2022) 100071. arXiv:2106.01393, doi:10.1016/j.revip.2022.100071.

[84] R. Covarelli, M. Pellen, M. Zaro, Vector-Boson scattering at the LHC: Unraveling the electroweak sector, Int. J. Mod. Phys. A 36 (16) (2021) 2130009. arXiv:2102.10991, doi:10.1142/S0217751X2130009X.

[85] C. S. Kim, M. V. N. Murthy, D. Sahoo, Inferring the nature of active neutrinos: Dirac or Majorana?, Phys. Rev. D 105 (11) (2022) 113006. arXiv:2106.11785, doi:10.1103/PhysRevD.105.113006.

[86] C. S. Kim, J. Rosiek, D. Sahoo, Probing the non-standard neutrino interactions using quantum statistics, Eur. Phys. J. C 83 (3) (2023) 221. arXiv:2209.10110, doi:10.1140/epjc/s10052-023-11355-8.

[87] S. Descotes-Genon, A. Falkowski, M. Fedele, M. González-Alonso, J. Virto, The CKM parameters in the SMEFT, JHEP 05 (2019) 172. arXiv:1812.08163, doi:10.1007/JHEP05(2019)172.

[88] C. Degrande, C. Duhr, B. Fuks, D. Grellscheid, O. Mattelaer, T. Reiter, UFO - The Universal FeynRules Output, Comput. Phys. Commun. 183 (2012) 1201–1214. arXiv:1108.2040, doi:10.1016/j.cpc.2012.01.022.

[89] J. Alwall, R. Frederix, S. Frixione, V. Hirschi, F. Maltoni, O. Mattelaer, H. S. Shao, T. Stelzer, P. Torrielli, M. Zaro, The automated computation of tree-level and next-to-leading order differential cross sections, and their matching to parton shower simulations, JHEP 07 (2014) 079. arXiv:1405.0301, doi:10.1007/JHEP07(2014)079.

[90] T. Gleisberg, S. Hoeche, F. Krauss, M. Schonherr, S. Schumann, F. Siegert, J. Winter, Event generation with SHERPA 1.1, JHEP 02 (2009) 007. arXiv:0811.4622, doi:10.1088/1126-6708/2009/02/007.

[91] A. Belyaev, N. D. Christensen, A. Pukhov, CalcHEP 3.4 for collider physics within and beyond the Standard Model, Comput. Phys. Commun. 184 (2013) 1729–1769. arXiv:1207.6082, doi:10.1016/j.cpc.2013.01.014.

[92] W. Kilian, T. Ohl, J. Reuter, WHIZARD: Simulating Multi-Particle Processes at LHC and ILC, Eur. Phys. J. C71 (2011) 1742. arXiv:0708.4233, doi:10.1140/epjc/s10052-011-1742-y.

[93] N. D. Christensen, C. Duhr, B. Fuks, J. Reuter, C. Speckner, Introducing an interface between WHIZARD and FeynRules, Eur. Phys. J. C72 (2012) 1990. arXiv:1010.3251, doi:10.1140/epjc/s10052-012-1990-5.

[94] T. Hahn, Generating Feynman diagrams and amplitudes with FeynArts 3, Comput. Phys. Commun. 140 (2001) 418–431. arXiv:hep-ph/0012260, doi:10.1016/S0010-4655(01)00290-9.

[95] T. Hahn, S. Paßehr, C. Schappacher, FormCalc 9 and Extensions, PoS LL2016 (2016) 068. arXiv:1604.04611, doi:10.1088/1742-6596/762/1/012065.

[96] V. Shtabovenko, R. Mertig, F. Orellana, New Developments in FeynCalc 9.0, Comput. Phys. Commun. 207 (2016) 432–444. arXiv:1601.01167, doi:10.1016/j.cpc.2016.06.008.

[97] J. Aebischer, et al., WCxf: an exchange format for Wilson coefficients beyond the Standard Model, Comput. Phys. Commun. 232 (2018) 71–83. arXiv:1712.05298, doi:10.1016/j.cpc.2018.05.022.

[98] E. E. Jenkins, A. V. Manohar, M. Trott, Renormalization Group Evolution of the Standard Model Dimension Six Operators I: Formalism and lambda Dependence, JHEP 10 (2013) 087. arXiv:1308.2627, doi:10.1007/JHEP10(2013)087.

[99] E. E. Jenkins, A. V. Manohar, M. Trott, Renormalization Group Evolution of the Standard Model Dimension Six Operators II: Yukawa Dependence, JHEP 01 (2014) 035. arXiv:1310.4838, doi:10.1007/JHEP01(2014)035.

[100] R. Alonso, E. E. Jenkins, A. V. Manohar, M. Trott, Renormalization Group Evolution of the Standard Model Dimension Six Operators III: Gauge Coupling Dependence and Phenomenology, JHEP 04 (2014) 159. arXiv:1312.2014, doi:10.1007/JHEP04(2014)159.

[101] J. A. M. Vermaseren, Axodraw, Comput. Phys. Commun. 83 (1994) 45–58. doi:10.1016/0010-4655(94)90034-5.

[102] J. M. Cornwall, D. N. Levin, G. Tiktopoulos, Derivation of Gauge Invariance from High-Energy Unitarity Bounds on the s Matrix, Phys. Rev. D10 (1974) 1145, [Erratum: Phys. Rev.D11,972(1975)]. doi:10.1103/PhysRevD.10.1145,10.1103/PhysRevD.11.972.

[103] C. E. Vayonakis, Born Helicity Amplitudes and Cross-Sections in Nonabelian Gauge Theories, Lett. Nuovo Cim. 17 (1976) 383. doi:10.1007/BF02746538.

[104] B. W. Lee, C. Quigg, H. B. Thacker, Weak Interactions at Very High-Energies: The Role of the Higgs Boson Mass, Phys. Rev. D16 (1977) 1519. doi:10.1103/PhysRevD.16.1519.

[105] M. S. Chanowitz, M. K. Gaillard, The TeV Physics of Strongly Interacting W's and Z's, Nucl. Phys. B261 (1985) 379–431. doi:10.1016/0550-3213(85)90580-2.

[106] G. N. Remmen, N. L. Rodd, Consistency of the Standard Model Effective Field Theory, JHEP 12 (2019) 032. arXiv:1908.09845, doi:10.1007/JHEP12(2019)032.

[107] K. Yamashita, C. Zhang, S.-Y. Zhou, Elastic positivity vs extremal positivity bounds in SMEFT: a case study in transversal electroweak gauge-boson scatterings, JHEP 01 (2021) 095. arXiv:2009.04490, doi:10.1007/JHEP01(2021)095.

[108] F. Maltoni, et al., Proposal for the validation of Monte Carlo implementations of the standard model effective field theoryarXiv:1906.12310.

[109] O. J. P. Éboli, M. C. Gonzalez-Garcia, Classifying the bosonic quartic couplings, Phys. Rev. D 93 (9) (2016) 093013. arXiv:1604.03555, doi:10.1103/PhysRevD.93.093013.

[110] P. A. Zyla, et al., Review of Particle Physics, PTEP 2020 (8) (2020) 083C01. doi:10.1093/ptep/ptaa104.

[111] G. Aad, et al., Constraints on the Higgs boson self-coupling from single- and double-Higgs production with the ATLAS detector using pp collisions at s=13 TeV, Phys. Lett. B 843 (2023) 137745. arXiv:2211.01216, doi:10.1016/j.physletb.2023.137745.

[112] A. Tumasyan, et al., A portrait of the Higgs boson by the CMS experiment ten years after the discovery., Nature 607 (7917) (2022) 60–68. arXiv:2207.00043, doi:10.1038/s41586-022-04892-x.

[113] S. Borowka, N. Greiner, G. Heinrich, S. P. Jones, M. Kerner, J. Schlenk, U. Schubert, T. Zirke, Higgs Boson Pair Production in Gluon Fusion at Next-to-Leading Order with Full Top-Quark Mass Dependence, Phys. Rev. Lett. 117 (1) (2016) 012001, [Erratum: Phys.Rev.Lett. 117, 079901 (2016)]. arXiv:1604.06447, doi:10.1103/PhysRevLett.117.079901.

[114] J. Baglio, F. Campanario, S. Glaus, M. Mühlleitner, M. Spira, J. Streicher, Gluon fusion into Higgs pairs at NLO QCD and the top mass scheme, Eur. Phys. J. C 79 (6) (2019) 459. arXiv:1811.05692, doi:10.1140/epjc/s10052-019-6973-3.

[115] D. de Florian, J. Mazzitelli, Higgs Boson Pair Production at Next-to-Next-to-Leading Order in QCD, Phys. Rev. Lett. 111 (2013) 201801. arXiv:1309.6594, doi:10.1103/PhysRevLett.111.201801.

[116] D. de Florian, J. Mazzitelli, Higgs pair production at next-to-next-to-leading logarithmic accuracy at the LHC, JHEP 09 (2015) 053. arXiv:1505.07122, doi:10.1007/JHEP09(2015)053.

[117] J. Grigo, J. Hoff, M. Steinhauser, Higgs boson pair production: top quark mass effects at NLO and NNLO, Nucl. Phys. B 900 (2015) 412–430. arXiv:1508.00909, doi:10.1016/j.nuclphysb.2015.09.012.

[118] M. Grazzini, G. Heinrich, S. Jones, S. Kallweit, M. Kerner, J. M. Lindert, J. Mazzitelli, Higgs boson pair production at NNLO with top quark mass effects, JHEP 05 (2018) 059. arXiv:1803.02463, doi:10.1007/JHEP05(2018)059.

[119] L.-B. Chen, H. T. Li, H.-S. Shao, J. Wang, Higgs boson pair production via gluon fusion at N^{3}LO in QCD, Phys. Lett. B 803 (2020) 135292. arXiv:1909.06808, doi:10.1016/j.physletb.2020.135292.

[120] L.-B. Chen, H. T. Li, H.-S. Shao, J. Wang, The gluon-fusion production of Higgs boson pair: N^{3}LO QCD corrections and top-quark mass effects, JHEP 03 (2020) 072. arXiv:1912.13001, doi:10.1007/JHEP03(2020)072.

[121] A. A H, H.-S. Shao, N^{3}LO+N^{3}LL QCD improved Higgs pair cross sections, JHEP 02 (2023) 067. arXiv:2209.03914, doi:10.1007/JHEP02(2023)067.

[122] J. Davies, G. Heinrich, S. P. Jones, M. Kerner, G. Mishima, M. Steinhauser, D. Wellmann, Double Higgs boson production at NLO: combining the exact numerical result and high-energy expansion, JHEP 11 (2019) 024. arXiv:1907.06408, doi:10.1007/JHEP11(2019)024.

[123] J. Davies, K. Schönwald, M. Steinhauser, H. Zhang, Next-to-leading order electroweak corrections to $gg \to HH$ and $gg \to gH$ in the large-m_t limit, JHEP 10 (2023) 033. arXiv:2308.01355, doi:10.1007/JHEP10(2023)033.

[124] R. Bonciani, G. Degrassi, P. P. Giardino, R. Gröber, Analytical Method for Next-to-Leading-Order QCD Corrections to Double-Higgs Production, Phys. Rev. Lett. 121 (16) (2018) 162003. arXiv:1806.11564, doi:10.1103/PhysRevLett.121.162003.

[125] L. Bellafronte, G. Degrassi, P. P. Giardino, R. Gröber, M. Vitti, Gluon fusion production at NLO: merging the transverse momentum and the high-energy expansions, JHEP 07 (2022) 069. arXiv:2202.12157, doi:10.1007/JHEP07(2022)069.

[126] J. Baglio, F. Campanario, S. Glaus, M. Mühlleitner, J. Ronca, M. Spira, $gg \to HH$: Combined uncertainties, Phys. Rev. D 103 (5) (2021) 056002. arXiv:2008.11626, doi:10.1103/PhysRevD.103.056002.

[127] F. A. Dreyer, A. Karlberg, J.-N. Lang, M. Pellen, Precise predictions for double-Higgs production via vector-boson fusion, Eur. Phys. J. C 80 (11) (2020) 1037. arXiv:2005.13341, doi:10.1140/epjc/s10052-020-08610-7.

[128] F. A. Dreyer, A. Karlberg, L. Tancredi, On the impact of non-factorisable corrections in VBF single and double Higgs production, JHEP 10 (2020) 131, [Erratum: JHEP 04, 009 (2022)]. arXiv:2005.11334, doi:10.1007/JHEP10(2020)131.

[129] F. A. Dreyer, A. Karlberg, Fully differential Vector-Boson Fusion Higgs Pair Production at Next-to-Next-to-Leading Order, Phys. Rev. D 99 (7) (2019) 074028. arXiv:1811.07918, doi:10.1103/PhysRevD.99.074028.

[130] T. Figy, Next-to-leading order QCD corrections to light Higgs Pair production via vector boson fusion, Mod. Phys. Lett. A 23 (2008) 1961–1973. arXiv:0806.2200, doi:10.1142/S0217732308028181.

[131] P. Bolzoni, F. Maltoni, S.-O. Moch, M. Zaro, Higgs production via vector-boson fusion at NNLO in QCD, Phys. Rev. Lett. 105 (2010) 011801. arXiv:1003.4451, doi:10.1103/PhysRevLett.105.011801.

[132] M. Cacciari, F. A. Dreyer, A. Karlberg, G. P. Salam, G. Zanderighi, Fully Differential Vector-Boson-Fusion Higgs Production at Next-to-Next-to-Leading Order, Phys. Rev. Lett. 115 (8) (2015) 082002, [Erratum: Phys.Rev.Lett. 120, 139901 (2018)]. arXiv:1506.02660, doi:10.1103/PhysRevLett.115.082002.

[133] F. A. Dreyer, A. Karlberg, Vector-Boson Fusion Higgs Production at Three Loops in QCD, Phys. Rev. Lett. 117 (7) (2016) 072001. arXiv:1606.00840, doi:10.1103/PhysRevLett.117.072001.

[134] J. Cruz-Martinez, T. Gehrmann, E. W. N. Glover, A. Huss, Second-order QCD effects in Higgs boson production through vector boson fusion, Phys. Lett. B 781 (2018) 672–677. arXiv:1802.02445, doi:10.1016/j.physletb.2018.04.046.

[135] M. Ciccolini, A. Denner, S. Dittmaier, Electroweak and QCD corrections to Higgs production via vector-boson fusion at the LHC, Phys. Rev. D 77 (2008) 013002. arXiv:0710.4749, doi:10.1103/PhysRevD.77.013002.

[136] F. A. Dreyer, A. Karlberg, Vector-Boson Fusion Higgs Pair Production at N^3LO, Phys. Rev. D 98 (11) (2018) 114016. arXiv:1811.07906, doi:10.1103/PhysRevD.98.114016.

[137] R. Contino, A. Falkowski, F. Goertz, C. Grojean, F. Riva, On the Validity of the Effective Field Theory Approach to SM Precision Tests, JHEP 07 (2016) 144. arXiv:1604.06444, doi:10.1007/JHEP07(2016)144.

[138] T. Corbett, O. J. P. Éboli, M. C. Gonzalez-Garcia, Unitarity Constraints on Dimension-Six Operators, Phys. Rev. D 91 (3) (2015) 035014. arXiv:1411.5026, doi:10.1103/PhysRevD.91.035014.

[139] W. Kilian, S. Sun, Q.-S. Yan, X. Zhao, Z. Zhao, Multi-Higgs boson production and unitarity in vector-boson fusion at future hadron colliders, Phys. Rev. D 101 (7) (2020) 076012. arXiv:1808.05534, doi:10.1103/PhysRevD.101.076012.

[140] E. d. S. Almeida, O. J. P. Éboli, M. C. Gonzalez–Garcia, Unitarity constraints on anomalous quartic couplings, Phys. Rev. D 101 (11) (2020) 113003. arXiv:2004.05174, doi:10.1103/PhysRevD.101.113003.

[141] H. E. Logan, Lectures on perturbative unitarity and decoupling in Higgs physicsarXiv:2207.01064.

[142] J. Alwall, M. Herquet, F. Maltoni, O. Mattelaer, T. Stelzer, MadGraph 5 : Going Beyond, JHEP 06 (2011) 128. arXiv:1106.0522, doi:10.1007/JHEP06(2011)128.

[143] H.-C. Cheng, B. A. Dobrescu, C. T. Hill, Electroweak symmetry breaking and extra dimensions, Nucl. Phys. B 589 (2000) 249–268. arXiv:hep-ph/9912343, doi:10.1016/S0550-3213(00)00401-6.

[144] N. Arkani-Hamed, A. G. Cohen, E. Katz, A. E. Nelson, The Littlest Higgs, JHEP 07 (2002) 034. arXiv:hep-ph/0206021, doi:10.1088/1126-6708/2002/07/034.

[145] T. Han, H. E. Logan, B. McElrath, L.-T. Wang, Loop induced decays of the little Higgs: H —> gg, gamma gamma, Phys. Lett. B 563 (2003) 191–202, [Erratum: Phys.Lett.B 603, 257–259 (2004)]. arXiv:hep-ph/0302188, doi:10.1016/j.physletb.2004.10.021.

[146] H.-C. Cheng, I. Low, L.-T. Wang, Top partners in little Higgs theories with T-parity, Phys. Rev. D 74 (2006) 055001. arXiv:hep-ph/0510225, doi:10.1103/PhysRevD.74.055001.

[147] J. Kang, P. Langacker, B. D. Nelson, Theory and Phenomenology of Exotic Isosinglet Quarks and Squarks, Phys. Rev. D 77 (2008) 035003. arXiv:0708.2701, doi:10.1103/PhysRevD.77.035003.

[148] G. Cacciapaglia, A. Carvalho, A. Deandrea, T. Flacke, B. Fuks, D. Majumder, L. Panizzi, H.-S. Shao, Next-to-leading-order predictions for single vector-like quark production at the LHC, Phys. Lett. B 793 (2019) 206–211. arXiv:1811.05055, doi:10.1016/j.physletb.2019.04.056.

[149] G. Cacciapaglia, A. Deandrea, L. Panizzi, N. Gaur, D. Harada, Y. Okada, Heavy Vector-like Top Partners at the LHC and flavour constraints, JHEP 03 (2012) 070. arXiv:1108.6329, doi:10.1007/JHEP03(2012)070.

[150] J. A. Aguilar-Saavedra, R. Benbrik, S. Heinemeyer, M. Pérez-Victoria, Handbook of vectorlike quarks: Mixing and single production, Phys. Rev. D 88 (9) (2013) 094010. arXiv:1306.0572, doi:10.1103/PhysRevD.88.094010.

[151] S. A. R. Ellis, R. M. Godbole, S. Gopalakrishna, J. D. Wells, Survey of vector-like fermion extensions of the Standard Model and their phenomenological implications, JHEP 09 (2014) 130. arXiv:1404.4398, doi:10.1007/JHEP09(2014)130.

[152] A. Angelescu, A. Djouadi, G. Moreau, Scenarii for interpretations of the LHC diphoton excess: two Higgs doublets and vector-like quarks and leptons, Phys. Lett. B 756 (2016) 126–132. arXiv:1512.04921, doi:10.1016/j.physletb.2016.02.064.

[153] A. Arhrib, R. Benbrik, S. J. D. King, B. Manaut, S. Moretti, C. S. Un, Phenomenology of 2HDM with vectorlike quarks, Phys. Rev. D 97 (2018) 095015. arXiv:1607.08517, doi:10.1103/PhysRevD.97.095015.

[154] D. Barducci, L. Panizzi, Vector-like quarks coupling discrimination at the LHC and future hadron colliders, JHEP 12 (2017) 057. arXiv:1710.02325, doi:10.1007/JHEP12(2017)057.

[155] A. Arhrib, R. Benbrik, J. El Falaki, M. Sampaio, R. Santos, Pseudoscalar decays to gauge bosons at the LHC and at a future 100 TeV collider, Phys. Rev. D 99 (3) (2019) 035043. arXiv:1809.04805, doi:10.1103/PhysRevD.99.035043.

[156] J. Song, Y. W. Yoon, $W\gamma$ decay of the elusive charged Higgs boson in the two-Higgs-doublet model with vectorlike fermions, Phys. Rev. D 100 (5) (2019) 055006. arXiv:1904.06521, doi:10.1103/PhysRevD.100.055006.

[157] F. del Aguila, L. Ametller, G. L. Kane, J. Vidal, Vector Like Fermion and Standard Higgs Production at Hadron Colliders, Nucl. Phys. B 334 (1990) 1–23. doi:10.1016/0550-3213(90)90655-W.

[158] S. Bhattacharya, S. Jahedi, J. Wudka, Probing heavy charged fermions at e^+e^- collider using the optimal observable technique, JHEP 05 (2022) 009. arXiv:2106.02846, doi:10.1007/JHEP05(2022)009.

[159] A. E. Cárcamo Hernández, K. Kowalska, H. Lee, D. Rizzo, Global analysis and LHC study of a vector-like extension of the Standard Model with extra scalars (9 2023). arXiv:2309.13968.

[160] K. Blum, R. T. D'Agnolo, J. Fan, Vacuum stability bounds on Higgs coupling deviations in the absence of new bosons, JHEP 03 (2015) 166. arXiv:1502.01045, doi:10.1007/JHEP03(2015)166.

[161] S. Gopalakrishna, A. Velusamy, Higgs vacuum stability with vectorlike fermions, Phys. Rev. D 99 (11) (2019) 115020. arXiv:1812.11303, doi:10.1103/PhysRevD.99.115020.

[162] A. Arsenault, K. Y. Cingiloglu, M. Frank, Vacuum stability in the Standard Model with vector-like fermions, Phys. Rev. D 107 (3) (2023) 036018. arXiv:2207.10332, doi:10.1103/PhysRevD.107.036018.

[163] G. Hiller, T. Höhne, D. F. Litim, T. Steudtner, Portals into Higgs vacuum stability, Phys. Rev. D 106 (11) (2022) 115004. arXiv:2207.07737, doi:10.1103/PhysRevD.106.115004.

[164] G. Hiller, T. Höhne, D. F. Litim, T. Steudtner, Vacuum Stability as a Guide for Model Bulding, 57th Rencontres de Moriond on Electroweak Interactions and Unified Theories, 2023. arXiv:2305.18520.

[165] G. Cacciapaglia, H. Cai, A. Carvalho, A. Deandrea, T. Flacke, B. Fuks, D. Majumder, H.-S. Shao, Probing vector-like quark models with Higgs-boson pair production, JHEP 07 (2017) 005. arXiv:1703.10614, doi:10.1007/JHEP07(2017)005.

[166] K. Cheung, A. Jueid, C.-T. Lu, J. Song, Y. W. Yoon, Disentangling new physics effects on nonresonant Higgs boson pair production from gluon fusion, Phys. Rev. D 103 (1) (2021) 015019. arXiv:2003.11043, doi:10.1103/PhysRevD.103.015019.

[167] D. Egana-Ugrinovic, The minimal fermionic model of electroweak baryogenesis, JHEP 12 (2017) 064. arXiv:1707.02306, doi:10.1007/JHEP12(2017)064.

[168] N. F. Bell, M. J. Dolan, L. S. Friedrich, M. J. Ramsey-Musolf, R. R. Volkas, Electroweak Baryogenesis with Vector-like Leptons and Scalar Singlets, JHEP 09 (2019) 012. arXiv:1903.11255, doi:10.1007/JHEP09(2019)012.

[169] H. Davoudiasl, I. Lewis, E. Ponton, Electroweak Phase Transition, Higgs Diphoton Rate, and New Heavy Fermions, Phys. Rev. D 87 (9) (2013) 093001. arXiv:1211.3449, doi:10.1103/PhysRevD.87.093001.

[170] M. Fairbairn, P. Grothaus, Baryogenesis and Dark Matter with Vector-like Fermions, JHEP 10 (2013) 176. arXiv:1307.8011, doi:10.1007/JHEP10(2013)176.

[171] A. Angelescu, P. Huang, Multistep Strongly First Order Phase Transitions from New Fermions at the TeV Scale, Phys. Rev. D 99 (5) (2019) 055023. arXiv:1812.08293, doi:10.1103/PhysRevD.99.055023.

[172] W. Chao, M. J. Ramsey-Musolf, Electroweak Baryogenesis, Electric Dipole Moments, and Higgs Diphoton Decays, JHEP 10 (2014) 180. arXiv:1406.0517, doi:10.1007/JHEP10(2014)180.

[173] Q.-H. Cao, K. Hashino, X.-X. Li, Z. Ren, J.-H. Yu, Electroweak phase transition triggered by fermion sector, JHEP 01 (2022) 001. arXiv:2103.05688, doi:10.1007/JHEP01(2022)001.

[174] O. Matsedonskyi, G. Servant, High-Temperature Electroweak Symmetry Non-Restoration from New Fermions and Implications for Baryogenesis, JHEP 09 (2020) 012. arXiv:2002.05174, doi:10.1007/JHEP09(2020)012.

[175] I. Baldes, T. Konstandin, G. Servant, A first-order electroweak phase transition from varying Yukawas, Phys. Lett. B 786 (2018) 373–377. arXiv:1604.04526, doi:10.1016/j.physletb.2018.10.015.

[176] M. Carena, A. Megevand, M. Quiros, C. E. M. Wagner, Electroweak baryogenesis and new TeV fermions, Nucl. Phys. B 716 (2005) 319–351. arXiv:hep-ph/0410352, doi:10.1016/j.nuclphysb.2005.03.025.

[177] Z. Poh, S. Raby, Vectorlike leptons: Muon g-2 anomaly, lepton flavor violation, Higgs boson decays, and lepton nonuniversality, Phys. Rev. D 96 (1) (2017) 015032. arXiv:1705.07007, doi:10.1103/PhysRevD.96.015032.

[178] A. Crivellin, M. Hoferichter, P. Schmidt-Wellenburg, Combined explanations of $(g-2)_{\mu,e}$ and implications for a large muon EDM, Phys. Rev. D 98 (11) (2018) 113002. arXiv:1807.11484, doi:10.1103/PhysRevD.98.113002.

[179] P. Athron, C. Balázs, D. H. Jacob, W. Kotlarski, D. Stöckinger, H. Stöckinger-Kim, New physics explanations of a_μ in light of the FNAL muon $g-2$ measurement, JHEP 09 (2021) 080. arXiv:2104.03691, doi:10.1007/JHEP09(2021)080.

[180] B. Abi, et al., Measurement of the Positive Muon Anomalous Magnetic Moment to 0.46 ppm, Phys. Rev. Lett. 126 (14) (2021) 141801. arXiv:2104.03281, doi:10.1103/PhysRevLett.126.141801.

[181] G. Hiller, C. Hormigos-Feliu, D. F. Litim, T. Steudtner, Anomalous magnetic moments from asymptotic safety, Phys. Rev. D 102 (7) (2020) 071901. arXiv:1910.14062, doi:10.1103/PhysRevD.102.071901.

[182] G. Hiller, C. Hormigos-Feliu, D. F. Litim, T. Steudtner, Model Building from Asymptotic Safety with Higgs and Flavor Portals, Phys. Rev. D 102 (9) (2020) 095023. arXiv:2008.08606, doi:10.1103/PhysRevD.102.095023.

[183] G. Hiller, C. Hormigos-Feliu, D. F. Litim, T. Steudtner, Asymptotically safe extensions of the Standard Model with flavour phenomenology, 54th Rencontres de Moriond on Electroweak Interactions and Unified Theories, 2019, pp. 415–418. arXiv:1905.11020.

[184] R. Dermisek, Unification of gauge couplings in the standard model with extra vectorlike families, Phys. Rev. D 87 (5) (2013) 055008. arXiv:1212.3035, doi:10.1103/PhysRevD.87.055008.

[185] B. Bhattacherjee, P. Byakti, A. Kushwaha, S. K. Vempati, Unification with Vector-like fermions and signals at LHC, JHEP 05 (2018) 090. arXiv:1702.06417, doi:10.1007/JHEP05(2018)090.

[186] D. Emmanuel-Costa, R. Gonzalez Felipe, Minimal string-scale unification of gauge couplings, Phys. Lett. B 623 (2005) 111–118. arXiv:hep-ph/0505257, doi:10.1016/j.physletb.2005.07.038.

[187] V. Barger, J. Jiang, P. Langacker, T. Li, String scale gauge coupling unification with vector-like exotics and non-canonical U(1)(Y) normalization, Int. J. Mod. Phys. A 22 (2007) 6203–6218. arXiv:hep-ph/0612206, doi:10.1142/S0217751X07038128.

[188] I. Dorsner, S. Fajfer, I. Mustac, Light vector-like fermions in a minimal SU(5) setup, Phys. Rev. D 89 (11) (2014) 115004. arXiv:1401.6870, doi:10.1103/PhysRevD.89.115004.

[189] K. Kowalska, D. Kumar, Road map through the desert: unification with vector-like fermions, JHEP 12 (2019) 094. arXiv:1910.00847, doi:10.1007/JHEP12(2019)094.

[190] U. C. Olivas, K. Kowalska, D. Kumar, Road map through the desert with scalars, JHEP 03 (2022) 132. arXiv:2112.11742, doi:10.1007/JHEP03(2022)132.

[191] F. del Aguila, M. Perez-Victoria, J. Santiago, Observable contributions of new exotic quarks to quark mixing, JHEP 09 (2000) 011. arXiv:hep-ph/0007316, doi:10.1088/1126-6708/2000/09/011.

[192] C. Bobeth, A. J. Buras, A. Celis, M. Jung, Patterns of Flavour Violation in Models with Vector-Like Quarks, JHEP 04 (2017) 079. arXiv:1609.04783, doi:10.1007/JHEP04(2017)079.

[193] A. Crivellin, M. Hoferichter, M. Kirk, C. A. Manzari, L. Schnell, First-generation new physics in simplified models: from low-energy parity violation to the LHC, JHEP 10 (2021) 221. arXiv:2107.13569, doi:10.1007/JHEP10(2021)221.

[194] J. a. M. Alves, G. C. Branco, A. L. Cherchiglia, C. C. Nishi, J. T. Penedo, P. M. F. Pereira, M. N. Rebelo, J. I. Silva-Marcos, Vector-like singlet quarks: A roadmap, Phys. Rept. 1057 (2024) 1–69. arXiv:2304.10561, doi:10.1016/j.physrep.2023.12.004.

[195] L. Lavoura, J. P. Silva, The Oblique corrections from vector - like singlet and doublet quarks, Phys. Rev. D 47 (1993) 2046–2057. doi:10.1103/PhysRevD.47.2046.

[196] J. Kearney, A. Pierce, N. Weiner, Vectorlike Fermions and Higgs Couplings, Phys. Rev. D 86 (2012) 113005. arXiv:1207.7062, doi:10.1103/PhysRevD.86.113005.

[197] H. Abouabid, A. Arhrib, R. Benbrik, M. Boukidi, J. E. Falaki, The oblique parameters in the 2HDM with vector-like quarks: confronting M $_W$ CDF-II anomaly, J. Phys. G 51 (7) (2024) 075001. arXiv:2302.07149, doi:10.1088/1361-6471/ad3f34.

[198] J. Fan, S. M. Koushiappas, G. Landsberg, Pseudoscalar Portal Dark Matter and New Signatures of Vector-like Fermions, JHEP 01 (2016) 111. arXiv:1507.06993, doi:10.1007/JHEP01(2016)111.

[199] A. Belyaev, A. Deandrea, S. Moretti, L. Panizzi, D. A. Ross, N. Thongyoi, Fermionic portal to vector dark matter from a new gauge sector, Phys. Rev. D 108 (9) (2023) 095001. arXiv:2204.03510, doi:10.1103/PhysRevD.108.095001.

[200] B. Barman, S. Bhattacharya, P. Ghosh, S. Kadam, N. Sahu, Fermion Dark Matter with Scalar Triplet at Direct and Collider Searches, Phys. Rev. D 100 (1) (2019) 015027. arXiv:1902.01217, doi:10.1103/PhysRevD.100.015027.

[201] G. Aad, et al., Search for single production of a vectorlike T quark decaying into a Higgs boson and top quark with fully hadronic final states using the ATLAS detector, Phys. Rev. D 105 (9) (2022) 092012. arXiv:2201.07045, doi:10.1103/PhysRevD.105.092012.

[202] G. Aad, et al., Search for pair-production of vector-like quarks in pp collision events at s=13 TeV with at least one leptonically decaying Z boson and a third-generation quark with the ATLAS detector, Phys. Lett. B 843 (2023) 138019. arXiv:2210.15413, doi:10.1016/j.physletb.2023.138019.

[203] G. Aad, et al., Search for pair-produced vector-like top and bottom partners in events with large missing transverse momentum in pp collisions with the ATLAS detector, Eur. Phys. J. C 83 (8) (2023) 719. arXiv:2212.05263, doi:10.1140/epjc/s10052-023-11790-7.

[204] G. Aad, et al., Search for third-generation vector-like leptons in pp collisions at $\sqrt{s} = 13$ TeV with the ATLAS detector, JHEP 07 (2023) 118. arXiv:2303.05441, doi:10.1007/JHEP07(2023)118.

[205] G. Aad, et al., Search for single production of vector-like T quarks decaying into Ht or Zt in pp collisions at $\sqrt{s} = 13$ TeV with the ATLAS detector, JHEP 08 (2023) 153. arXiv:2305.03401, doi:10.1007/JHEP08(2023)153.

[206] G. Aad, et al., Search for singly produced vector-like top partners in multilepton final states with 139 fb^{-1} of pp collision data at $\sqrt{s} = 13$ TeV with the ATLAS detector (7 2023). arXiv:2307.07584.

[207] A. Tumasyan, et al., Search for single production of a vector-like T quark decaying to a top quark and a Z boson in the final state with jets and missing transverse momentum at $\sqrt{s} = 13$ TeV, JHEP 05 (2022) 093. arXiv:2201.02227, doi:10.1007/JHEP05(2022)093.

[208] A. Tumasyan, et al., Search for a W' boson decaying to a vector-like quark and a top or bottom quark in the all-jets final state at $\sqrt{s} = 13$ TeV, JHEP 09 (2022) 088. arXiv:2202.12988, doi:10.1007/JHEP09(2022)088.

[209] A. Tumasyan, et al., Search for pair-produced vector-like leptons in final states with third-generation leptons and at least three b quark jets in proton-proton collisions at s=13TeV, Phys. Lett. B 846 (2023) 137713. arXiv:2208.09700, doi:10.1016/j.physletb.2023.137713.

[210] A. Tumasyan, et al., Search for pair production of vector-like quarks in leptonic final states in proton-proton collisions at $\sqrt{s} = 13$ TeV, JHEP 07 (2023) 020. arXiv:2209.07327, doi:10.1007/JHEP07(2023)020.

[211] A. Tumasyan, et al., Search for a vector-like quark T′→ tH via the diphoton decay mode of the Higgs boson in proton-proton collisions at $\sqrt{s}$ = 13 TeV, JHEP 09 (2023) 057. arXiv:2302.12802, doi:10.1007/JHEP09(2023)057.

[212] T. M. Hieu, Q. S. Sang, T. Q. Trang, On a standard model extension with vector-like fermions and Abelian symmetry, Commun. in Phys. 30 (3) (2020) 231–244. doi:10.15625/0868-3166/30/3/15071.

[213] D. Curtin, P. Meade, C.-T. Yu, Testing Electroweak Baryogenesis with Future Colliders, JHEP 11 (2014) 127. arXiv:1409.0005, doi:10.1007/JHEP11(2014)127.

[214] S. Profumo, M. J. Ramsey-Musolf, G. Shaughnessy, Singlet Higgs phenomenology and the electroweak phase transition, JHEP 08 (2007) 010. arXiv:0705.2425, doi:10.1088/1126-6708/2007/08/010.

[215] A. Noble, M. Perelstein, Higgs self-coupling as a probe of electroweak phase transition, Phys. Rev. D 78 (2008) 063518. arXiv:0711.3018, doi:10.1103/PhysRevD.78.063518.

[216] J. R. Espinosa, T. Konstandin, F. Riva, Strong Electroweak Phase Transitions in the Standard Model with a Singlet, Nucl. Phys. B 854 (2012) 592–630. arXiv:1107.5441, doi:10.1016/j.nuclphysb.2011.09.010.

[217] J. R. Espinosa, M. Quiros, The Electroweak phase transition with a singlet, Phys. Lett. B 305 (1993) 98–105. arXiv:hep-ph/9301285, doi:10.1016/0370-2693(93)91111-Y.

[218] E. Fernández-Martínez, J. López-Pavón, J. M. No, T. Ota, S. Rosauro-Alcaraz, ν Electroweak baryogenesis: the scalar singlet strikes back, Eur. Phys. J. C 83 (8) (2023) 715. arXiv:2210.16279, doi:10.1140/epjc/s10052-023-11887-z.

[219] J. M. No, M. Ramsey-Musolf, Probing the Higgs Portal at the LHC Through Resonant di-Higgs Production, Phys. Rev. D 89 (9) (2014) 095031. arXiv:1310.6035, doi:10.1103/PhysRevD.89.095031.

[220] V. Barger, P. Langacker, M. McCaskey, M. J. Ramsey-Musolf, G. Shaughnessy, LHC Phenomenology of an Extended Standard Model with a Real Scalar Singlet, Phys. Rev. D 77 (2008) 035005. arXiv:0706.4311, doi:10.1103/PhysRevD.77.035005.

[221] T. Huang, J. M. No, L. Pernié, M. Ramsey-Musolf, A. Safonov, M. Spannowsky, P. Winslow, Resonant di-Higgs boson production in the $b\bar{b}WW$ channel: Probing the electroweak phase transition at the LHC, Phys. Rev. D 96 (3) (2017) 035007. arXiv:1701.04442, doi:10.1103/PhysRevD.96.035007.

[222] S. Profumo, M. J. Ramsey-Musolf, C. L. Wainwright, P. Winslow, Singlet-catalyzed electroweak phase transitions and precision Higgs boson studies, Phys. Rev. D 91 (3) (2015) 035018. arXiv:1407.5342, doi:10.1103/PhysRevD.91.035018.

[223] C.-Y. Chen, J. Kozaczuk, I. M. Lewis, Non-resonant Collider Signatures of a Singlet-Driven Electroweak Phase Transition, JHEP 08 (2017) 096. arXiv:1704.05844, doi:10.1007/JHEP08(2017)096.

[224] K. Hashino, M. Kakizaki, S. Kanemura, P. Ko, T. Matsui, Gravitational waves and Higgs boson couplings for exploring first order phase transition in the model with a singlet scalar field, Phys. Lett. B 766 (2017) 49–54. arXiv:1609.00297, doi:10.1016/j.physletb.2016.12.052.

[225] J. Ellis, M. Lewicki, M. Merchand, J. M. No, M. Zych, The scalar singlet extension of the Standard Model: gravitational waves versus baryogenesis, JHEP 01 (2023) 093. arXiv:2210.16305, doi:10.1007/JHEP01(2023)093.

[226] M. Gonderinger, Y. Li, H. Patel, M. J. Ramsey-Musolf, Vacuum Stability, Perturbativity, and Scalar Singlet Dark Matter, JHEP 01 (2010) 053. arXiv:0910.3167, doi:10.1007/JHEP01(2010)053.

[227] J. M. Cline, K. Kainulainen, P. Scott, C. Weniger, Update on scalar singlet dark matter, Phys. Rev. D 88 (2013) 055025, [Erratum: Phys.Rev.D 92, 039906 (2015)]. arXiv:1306.4710, doi:10.1103/PhysRevD.88.055025.

[228] X.-G. He, T. Li, X.-Q. Li, J. Tandean, H.-C. Tsai, The Simplest Dark-Matter Model, CDMS II Results, and Higgs Detection at LHC, Phys. Lett. B 688 (2010) 332–336. arXiv:0912.4722, doi:10.1016/j.physletb.2010.04.026.

[229] D. Buttazzo, G. Degrassi, P. P. Giardino, G. F. Giudice, F. Sala, A. Salvio, A. Strumia, Investigating the near-criticality of the Higgs boson, JHEP 12 (2013) 089. arXiv:1307.3536, doi:10.1007/JHEP12(2013)089.

[230] F. Staub, SARAH 4 : A tool for (not only SUSY) model builders, Comput. Phys. Commun. 185 (2014) 1773–1790. arXiv:1309.7223, doi:10.1016/j.cpc.2014.02.018.

[231] A. E. Thomsen, Introducing RGBeta: a Mathematica package for the evaluation of renormalization group β-functions, Eur. Phys. J. C 81 (5) (2021) 408. arXiv:2101.08265, doi:10.1140/epjc/s10052-021-09142-4.

[232] G. G. Ross, GRAND UNIFIED THEORIES, 1985.

[233] P. Langacker, M.-x. Luo, Implications of precision electroweak experiments for M_t, ρ_0, $\sin^2\theta_W$ and grand unification, Phys. Rev. D 44 (1991) 817–822. doi:10.1103/PhysRevD.44.817.

[234] J. R. Ellis, S. Kelley, D. V. Nanopoulos, Probing the desert using gauge coupling unification, Phys. Lett. B 260 (1991) 131–137. doi:10.1016/0370-2693(91)90980-5.

[235] U. Amaldi, W. de Boer, H. Furstenau, Comparison of grand unified theories with electroweak and strong coupling constants measured at LEP, Phys. Lett. B 260 (1991) 447–455. doi:10.1016/0370-2693(91)91641-8.

[236] J. Ellis, TikZ-Feynman: Feynman diagrams with TikZ, Comput. Phys. Commun. 210 (2017) 103–123. arXiv:1601.05437, doi:10.1016/j.cpc.2016.08.019.

[237] S. Kanemura, Y. Okada, E. Senaha, C. P. Yuan, Higgs coupling constants as a probe of new physics, Phys. Rev. D 70 (2004) 115002. arXiv:hep-ph/0408364, doi:10.1103/PhysRevD.70.115002.

[238] S.-P. He, S.-h. Zhu, One-loop radiative correction to the triple Higgs coupling in the Higgs singlet model, Phys. Lett. B 764 (2017) 31–37, [Erratum: Phys.Lett.B 797, 134782 (2019)]. arXiv:1607.04497, doi:10.1016/j.physletb.2016.11.007.

[239] A. Dobado, M. J. Herrero, W. Hollik, S. Penaranda, Selfinteractions of the lightest MSSM Higgs boson in the large pseudoscalar mass limit, Phys. Rev. D 66 (2002) 095016. arXiv:hep-ph/0208014, doi:10.1103/PhysRevD.66.095016.

[240] M. E. Peskin, T. Takeuchi, A New constraint on a strongly interacting Higgs sector, Phys. Rev. Lett. 65 (1990) 964–967. doi:10.1103/PhysRevLett.65.964.

[241] M. E. Peskin, T. Takeuchi, Estimation of oblique electroweak corrections, Phys. Rev. D 46 (1992) 381–409. doi:10.1103/PhysRevD.46.381.

[242] T. Takeuchi, W. Loinaz, A. K. Grant, Precision tests of electroweak physics, in: 13th Topical Conference on Hadron Collider Physics, 1999, pp. 60–67. arXiv:hep-ph/9904207.

[243] B. Grinstein, M. B. Wise, Operator analysis for precision electroweak physics, Phys. Lett. B 265 (1991) 326–334. doi:10.1016/0370-2693(91)90061-T.

[244] D. E. Morrissey, M. J. Ramsey-Musolf, Electroweak baryogenesis, New J. Phys. 14 (2012) 125003. arXiv:1206.2942, doi:10.1088/1367-2630/14/12/125003.

[245] D. J. Weir, Gravitational waves from a first order electroweak phase transition: a brief review, Phil. Trans. Roy. Soc. Lond. A 376 (2114) (2018) 20170126, [Erratum: Phil.Trans.Roy.Soc.Lond.A 381, 20230212 (2023)]. arXiv:1705.01783, doi:10.1098/rsta.2017.0126.

[246] A. D. Sakharov, Violation of CP Invariance, C asymmetry, and baryon asymmetry of the universe, Pisma Zh. Eksp. Teor. Fiz. 5 (1967) 32–35. doi:10.1070/PU1991v034n05ABEH002497.

[247] G. W. Anderson, L. J. Hall, The Electroweak phase transition and baryogenesis, Phys. Rev. D 45 (1992) 2685–2698. doi:10.1103/PhysRevD.45.2685.

[248] M. Quiros, Finite temperature field theory and phase transitions, ICTP Summer School in High-Energy Physics and Cosmology, 1999, pp. 187–259. arXiv:hep-ph/9901312.

[249] E. J. Weinberg, Radiative corrections as the origin of spontaneous symmetry breaking (1973). arXiv:hep-th/0507214.

[250] J. de Blas, J. C. Criado, M. Perez-Victoria, J. Santiago, Effective description of general extensions of the Standard Model: the complete tree-level dictionary, JHEP 03 (2018) 109. arXiv:1711.10391, doi:10.1007/JHEP03(2018)109.

[251] B. Henning, X. Lu, H. Murayama, How to use the Standard Model effective field theory, JHEP 01 (2016) 023. arXiv:1412.1837, doi:10.1007/JHEP01(2016)023.

[252] J. Aebischer, A. Crivellin, M. Fael, C. Greub, Matching of gauge invariant dimension-six operators for $b \to s$ and $b \to c$ transitions, JHEP 05 (2016) 037. arXiv:1512.02830, doi:10.1007/JHEP05(2016)037.

[253] S. Weinberg, Gauge and Global Symmetries at High Temperature, Phys. Rev. D 9 (1974) 3357–3378. doi:10.1103/PhysRevD.9.3357.

[254] D. Curtin, P. Meade, H. Ramani, Thermal Resummation and Phase Transitions, Eur. Phys. J. C 78 (9) (2018) 787. arXiv:1612.00466, doi:10.1140/epjc/s10052-018-6268-0.